Compression Moulding of Hybrid Carbon Fibre Composites for Structural Applications

By: David Michael Corbridge, Meng

Thesis submitted to the University of Nottingham for the degree of Doctor of Philosophy

May 2017

Abstract

Automotive manufacturers are receiving pressure from customers and regulators to reduce emissions. Reducing the weight of the vehicle through the use of carbon fibre is seen as one of these mechanisms. The challenge is to develop suitable manufacturing processes that can offer appropriate cycle times to meet demand and deliver materials with adequate mechanical properties for structural applications. Compression moulding of discontinuous fibre moulding compounds with local continuous fibre inserts provide better production rates and part complexity compared to the autoclave components and higher performances than injection moulding. However, combining a unidirectional carbon fibre (UD) material with a random short fibre orientation sheet moulding compound (SMC) that flows heterogeneously will lead to degradation in the properties of the continuous reinforcement. This work aims to demonstrate a hybrid of continuous and discontinuous fibre compounds in a single moulding operation with increased stiffness and determine if the surface distortion of the reinforcement can be used to predict local stiffness.

A benchmarking study was carried out with UD and the SMC followed by hybridisation. This was non-destructively tested for flexural moduli providing a localised map of stiffness which was compared with a theoretical value. This work demonstrated that simply placing unidirectional (UD) prepreg with the SMC caused significant distortion and migration of the reinforcement in a one-dimensional flow scenario. Resin tended to bleed out of the hybrid reinforcement, causing a resin rich area at the UD ply drop off point. This resin bleed was more prominent at the ends of the UD fibres.

The resin system in the UD was staged by partially curing it to a controlled level through the measurement of the storage modulus, and showed that flow could be dramatically reduced. This was determined by rheology and inter-laminar shear tests to measure material degradation from staging to improve flow control. It was found that for flow control of the reinforcement staging beyond gelation was required. The inter-laminar shear strength of UD is significantly higher than the SMC, and found that even with 50% staging properties were still higher.

Where there were high levels of flow resistance in compression moulding, staged hybrids resulted in to two moulding defects; a dry region on the SMC under the reinforcement and rippling outside the reinforcement, which reduced the stiffness by nearly 50% in the affected areas.

Staging accompanied with charge layout design of the UD to $90_2/0$ showed markedly reduced flow in one, two and three dimensional scenarios, almost completely resisting the flow of the SMC. In the 2D flow scenario where the SMC charge coverage was 60% compared to the manufacturers' recommended 80%, flow was limited to 3% and the stiffness could be locally predicted to an accuracy of 16%.

By controlling the level of staging and careful consideration of the charge design, hybrid components can be manufactured repeatedly with increased accuracy in stiffness prediction and demonstrated an improved flexural strength and modulus increase of >44%, increasing the potential use to a wider range of complex geometry structural applications.

Acknowledgements

I would like to thank my supervisors, Lee Harper and Davide De Focatiis, for the guidance, support and patience throughout my PhD. The technical team: Paul, Ben and Harry, for the time spent in the laboratory dealing with the unforeseeable as well the Composites Group, notably Oliver, Gabriel, Kishen and Hannah, for perspective and humour. Lastly, a special thank you to Sarah for her patience and support in all my years of studying.

Table of Contents

1. Nomenclature

Autoclave	A pressurised oven
B-staged	Used in prepreg the resin is partially cured to increase viscosity, improving handling
Cavity	A space between the two halves of the mould, where the material is placed and can flow in to
Charge	The material is placed in the tool
Charge coverage	The ratio of the tool covered by the material when placed
Closure speed	The rate at which the press closes to the halves of the mould
Co-moulding	Moulding two different materials together in a single operation
Compression moulding	A method manufacturing method where two mould halves come together to form a component
Debulking	Manufacturing operation where uncured composite material is placed in a vacuum to remove air and consolidate
Delamination	Common in continuous fibre composites made from sheets, the material fails between each layer
Dry-spot/blister	a region where there is no resin, this can cause blisters below the surface
Dwell	Where a temperature is reached and the equipment maintains that temperature
Fibre volume fraction (Vf)	Ratio by volume of fibre to matrix
Fibre-matrix separation	The event where matrix flows without the fibre, leaving it behind
Flash gap	a small space between the 2 halves of a mould that is wide enough for air and resin but not fibre
Flowability	The ability of a material to move while under pressure
Fountain flow	A type of flow exhibited where the surface is resistant and the core/centre readily flows

Glass transition temperature	the temperature where the material changes from ductile to brittle,
Hybrid composite	A material that is made up of two or more materials, within the composite family
Inter laminar shear strength (ILSS)	A very short 3 point bending test to determine the adhesion between plies
Laddering	Where fibres under stress, separate leaving gaps in the material
Lay-up	The sequence and orientation in which the plies of material are placed
Lubricating layer	A thin layer of thermoset resin which has reduced in viscosity and readily allows the material to slide across the tool face
Migration	A a layer or section of composite flows together as a group instead of spreading
Net-shape	The material placed in mould is the same shape as the final product
Over-moulding	A component or material is placed in a mould and resin is injected around it
Photogrammetry	Method to obtain numerical measurements from images
Preferential flow/transverse flow	A type of material flow where the surface which is in contact with the tool flows faster than the centre/core
Prepreg	A composite material that has been impregnated with resin prior moulding
Race tracking	Where a resin or section of the material, has accelerated flow compared to the bulk of the material
Resin bleed	Often in the flash gap, but observed when the resin flows without the fibre
Resin rich	An area of very low fibre volume fraction

Sheet moulding compound (SMC)	A material designed for compression moulding, typically short random fibers and resin
Sink marks	After curing and cooling, local regions shrink more than the rest of the component leaving small depressions
Staging	A thermoset resin that has been partially cured
Tack	The sickness of the uncured composite material
Unidirectional (UD)	A type of composite where all the fibres are aligned in the same direction held together by resin

2. Introduction

This introduction has three objectives: firstly to explain the automotive industry's interest in lightweight materials due to the pressures they face from consumers and legislation to create more fuel efficient and lower emission vehicles. Secondly, to justify the potential replacement of steel with carbon fibre rather than aluminium, which is cheaper, readily recyclable and has a more proven manufacturing method. In contrast, carbon fibre has higher mechanical performance, notably stiffness and energy absorption properties, and a lower density[1]. Although the manufacturing cost is still relatively high, the cost of carbon fibre is likely to decrease through future technological advances. Finally, provide a brief introduction into the different continuous and discontinuous composite materials and the hybridisation methods.

2.1. Materials in the automotive sector

Steel is currently the material of choice in the automotive industry, predominantly due to manufacturability, material and manufacturing costs. New materials are increasingly being used; Figure 1 shows a growth in high performance steels, plastics, composites and aluminium in vehicles in America. In contrast in Europe, consumers and EU legislation are driving improvements in fuel efficiency and in reducing emissions. An option for delivering these improvements is to make vehicles lighter. Since steel is the largest contributor of weight, it can be substituted for an alternative material, as seen in Figure 1. However, lighter materials also have limitations and are not as widely used as a result.

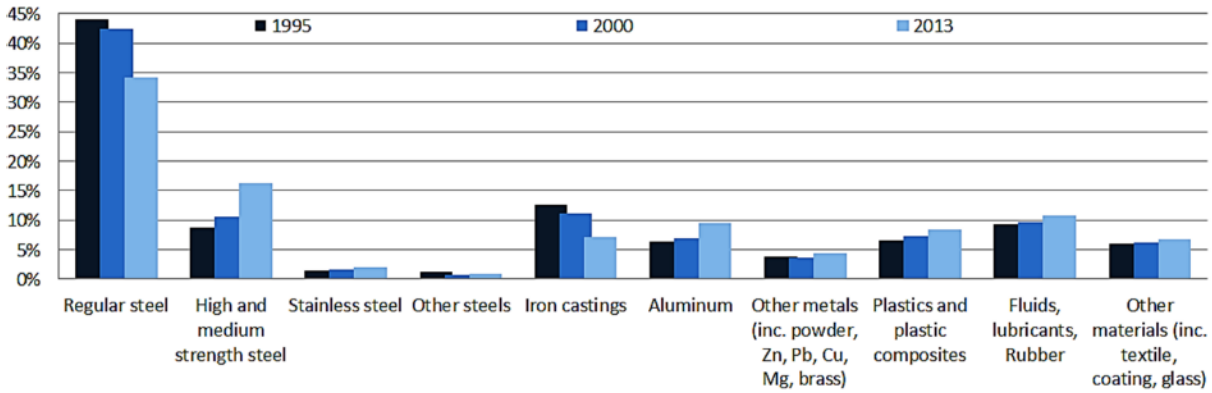

Figure 1: Average car material composition by percentage weight, adapted from [2]

The average weight of a passenger vehicle has increased from 964kg in 2006 to 1025kg in 2015[3] and will continue to increase due to the addition of safety features and luxury items, such as on-board entertainment. However, there have been previous attempts to reduce weight in consumer vehicles, such as the carbon fibre chassis on the BMW i3. Comparing the weight of a BMW i3 and a Nissan leaf, whose chassis is made from steel, they are approximately 1195kg and 1494kg respectively[4]. The use of carbon fibre contributes to a 20% weight reduction over the comparable steel chassis. This is an encouraging step forward to breaking the monopoly held by steel in the consumer automotive market, but more research is required for alternative materials to be considered in high volume applications.

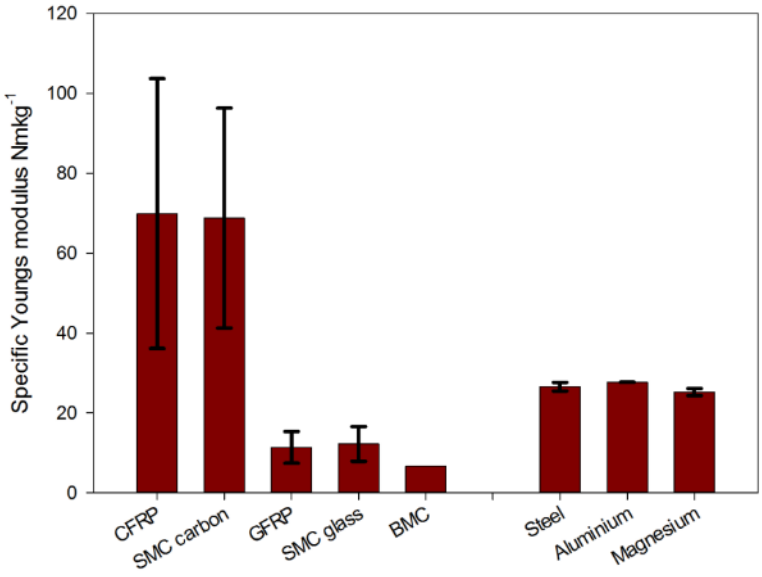

Figure 2: Comparison of potential automotive materials, adapted from [5]

Figure 2 shows that carbon fibre composites are >2.5 times stiffer per kilogram compared to alternative metals, glass fibre reinforced plastics (GFRP) or bulk moulding compounds (BMC), highlighting the potential for significant weight reductions. Switching to a composite material reduces the weight, which enables a smaller and lighter engine to achieve similar performance. For example [6], in a like-for-like comparison, replacing aluminium with carbon fibre prepreg (PCM) on the decklid of a Nissan demonstrated the potential by reducing the mass of the decklid by 40% compared to a steel counterpart. Furthermore, as the decklid weight was reduced, lighter struts and mounting hardware could be substituted. Also, with a cure rate of 3 minutes, 50,000 components per annum are possible,

making this competitive for medium-high volumes. However, these materials are generally more expensive and manufacturers do not want to make their vehicles less desirable, so a gradual change to lighter materials is occurring, as shown in Figure 1.

Although manufacturers are trying to keep their costs low, legislation is driving innovation. Emissions for passenger vehicles on average have fallen from 161 gkm^{-1} in 2006 to 132 gkm^{-1} in 2012, and the European Union has agreed to set the new CO_2 emissions target to $95gkm^{-1}$ by the end of 2020 [7]. Meeting targets like these will continue to push manufacturers to innovate through new fuel sources, increased efficiencies and lightweight materials.

2.2. Cost of materials

The price of steel is almost 30 times lower than CFRP (carbon fibre reinforced plastics) as shown in Figure 3, but the specific Young's modulus is more than 50% lower than that of CFRP. Aluminium and magnesium have lower densities at 2.9 kg m^{-3} and 1.91 kg m^{-3} respectively, but are two and four times more expensive than steel, making these materials highly attractive for non-structural applications.

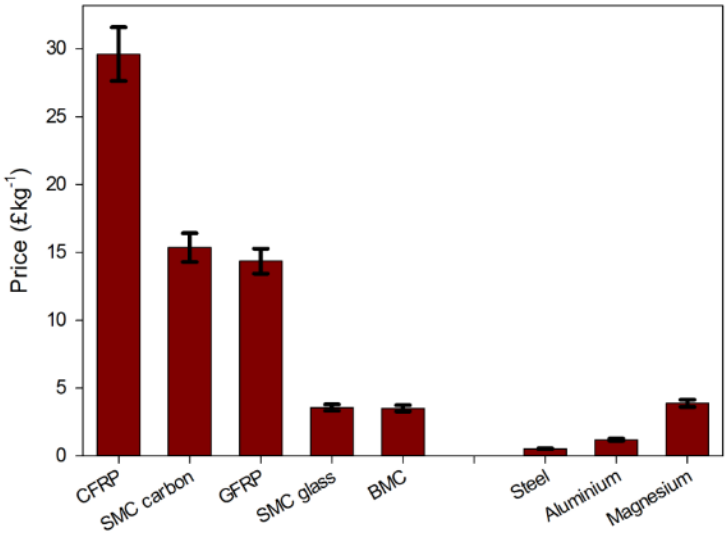

Figure 3: Cost per kg of common replacements for steel in the automotive industry plotted, adapted from [5].

Although Aluminium is far more established in terms of characterisation and manufacturing, the market opportunity for composites is in applications where

vehicle performance is desired, or where stiffness and energy absorption properties are critical. This is where there is the opportunity for composite materials to have a significant role.

Although raw carbon fibre costs ~$15-20/kg [8, 9] this varies depending on grade and source. Most carbon fibre is produced from polyacrylonitrile (PAN) which is derived from oil and therefore tied to the price of crude. Although oil exhibited a price crash in 2014-2016, PAN still constitutes 50% of the carbon fibre manufacturing costs [10].

The cost of carbon fibre is still limiting its adoption in some industries, but if costs were to fall below $11/kg [11] due to innovation, such as microwave [12] or plasma [13] processing methods, or alternative precursors to PAN, such as polyolefins that have a 15% higher yield [14], then this would further increase the opportunities for carbon fibre, notably in the automotive industry.

Aluminium is an attractive alternative to steel because it has a significantly lower density, uses a similar infrastructure for processing and is readily recyclable. Conversely, composites are complex to recycle, since separating the resin from the fibres is expensive and many processes damage the individual filaments, which decreases their recycled value. This creates a challenge, as at the start of 2000, vehicle reuse and recycling was 75%. In 2006 the End-of-Life Vehicles (ELV) directive set a target for 85% and 80% [15] for recovery and recycling respectively, and 95% for both combined in 2015 [16], requiring automotive producers to consider the recyclability of their vehicles.

2.3. Composites

A composite is made from two parts: the matrix, which holds the material in shape, and the reinforcement, primarily for mechanical performance enhancement. There are a wide range of fibres used in the composites industry that come in a variety of forms, but the most common types are glass, carbon and Kevlar™. After the filaments are manufactured from their precursors, they are wound on bobbins and collected in tows. A tow is a cluster of filaments which typically contains thousands of individual filaments.

2.3.1. Continuous fibre composites

Fibres can be woven into different fabrics that have their own specific attributes. A low crimp fabric has less tow crossover, allowing it to be more easily formed into shape; this is referred to as drapability. The reduced number of crossovers between the warp and weft result in less shear between the tows, and less resistance to deformation during forming. With increasingly less crimp, the mechanical properties are enhanced as the fibres are less wavy. However, increased crimp improves stability and prevents tows from slipping out of the woven structure. Less crimp provides better mechanical properties and drapability, and improves wetting, but this benefit comes at the expense of stability, which can make low crimped fabrics difficult to handle. A fabric with a higher stability is likely to be more flow resistant, which might be an important factor when trying to reduce the flow of the reinforcement caused by the SMC.

Carbon fibre can be supplied pre-impregnated with a resin. This is called a prepreg and has a very uniform resin distribution. It also allows easy handling of unidirectional (UD) fibres as the resin holds the fibres in place and prevents the fibres slipping out of the fabric. However, once thermoset prepregs have been impregnated, the resin will slowly cure in storage, requiring the material to be used promptly or frozen to prolong the lifespan.

2.3.2. Discontinuous fibre composites

Fibres can be chopped into various lengths and deposited at random orientations before being impregnated. This type of prepreg is known as a sheet moulding compound (SMC). There is a wide range of SMCs, ranging from predominately matrix and filler with a low fibre weight fraction ~30%[17], to high value products that can be ~50% fibre. Figure 4 illustrates a common SMC manufacturing process where the tows (rovings) are chopped, deposited on a film of resin and compressed between another film of resin. Alternatively, high performance SMCs, such as HexMC are impregnated prior to chopping to ensure full wetting of the fibres[18] .

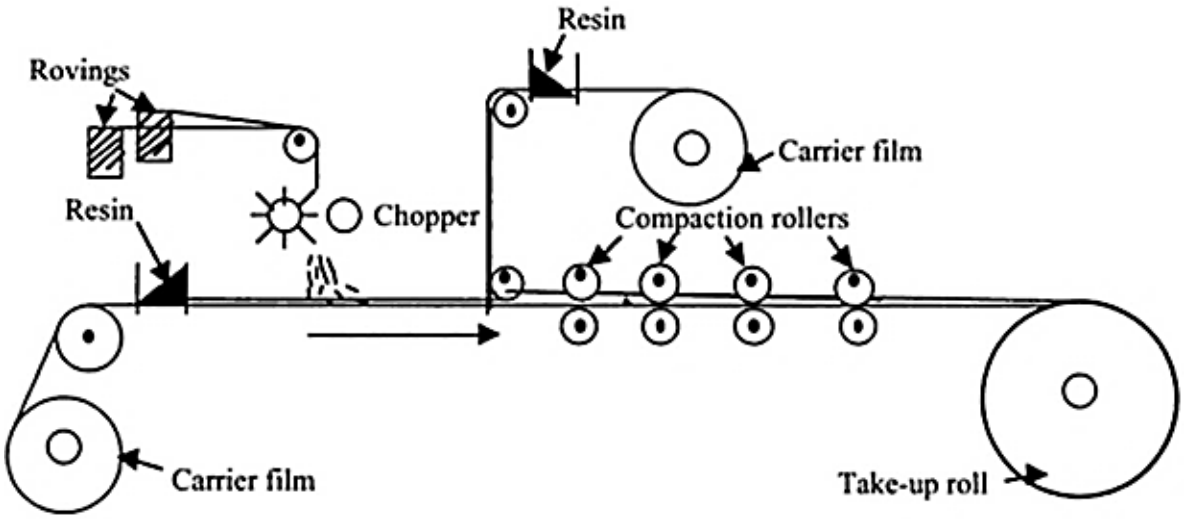

Figure 4: Schematic of the manufacturing method for SMCs[19]

SMCs are designed to flow to fill complex geometries, unlike prepreg which needs to be placed in the tool net-shape. The ratio of SMC covering the surface area of the cavity is called charge coverage. Typically, lower fibre volume fraction materials such as bulk moulding compounds can have a smaller charge coverage as they flow more readily when pressure and heat are applied during tool closure [20]. The smaller and less detailed the charge, the less labour intensive the lay-up is, reducing production costs. Ideally, SMCs are homogenous, but flow tends to create heterogeneity through flow-induced alignment and fibre-matrix separation. This can create issues, or be an opportunity to enhance the component properties in the flow direction.

Carbon fibre SMCs have twice the stiffness to weight ratio of aluminium alloys and can be cast or forged into similar shapes. They are also essentially an enhanced alternative to glass SMCs. However, a problem with this material has given it the nickname "black metal", used when designers simply switch a metal component for a carbon fibre SMC. The problem with this is that, like all materials, they have their own moulding and material nuances. Using carbon SMC as a direct replacement for metals can cause issues with the moulding, as the geometry may not always be appropriate. Another issue is that it is difficult to fully utilise the benefits of the material if it is used in this way, resulting in conservatively designed parts with thick sections that fail to offer a significant weight reduction over aluminium.

Figure 5: Replacement of aluminium with carbon fibre SMC in a front lower control arm of the Lamborghini Sesto Elemento [21]

SMCs have two major benefits over continuous fibre composites: firstly they are able to fill complex geometries, and secondly, they can be produced at higher volumes through compression moulding compared to processes that require meticulous layups. This targets SMCs at markets where labour intensive lay-up is not economically justifiable, such as the automotive suspension arms shown in Figure 5 [21], or in the aerospace industry, where there are many duplicate parts such as the Boeing 787 window frames, shown in Figure 6. The latter are currently made from an SMC [22]. The wide range of potential applications for carbon SMC is one of the factors why it is predicted to have an annual compound growth rate of 5.5% from 2014-2019 [23].

Figure 6: Boeing 787 window frame from carbon fibre sheet moulding compound [24]

2.3.1. Hybrid composites

Hybrid composites are two or more composite materials that have been manufactured together. The motivations for hybridising composites are to enhance the properties of less expensive materials to improve performance, to improve the manufacturability of high performance materials or to increase parts integration through a material that provides a secondary function, such as an embedded wire mesh for heating applications. There are two main methods to hybridise a composite materials component:

Interply: This could be called a sandwich structure. This structure involves discrete layers or sections, such as plywood or GLARE (glass laminate aluminium reinforced epoxy).

Intraply: This involves the weaving or arrangement of different fibres in a ply in a regular or tailored manner, such as the use of carbon and glass fibre in the warp and weft directions respectively.

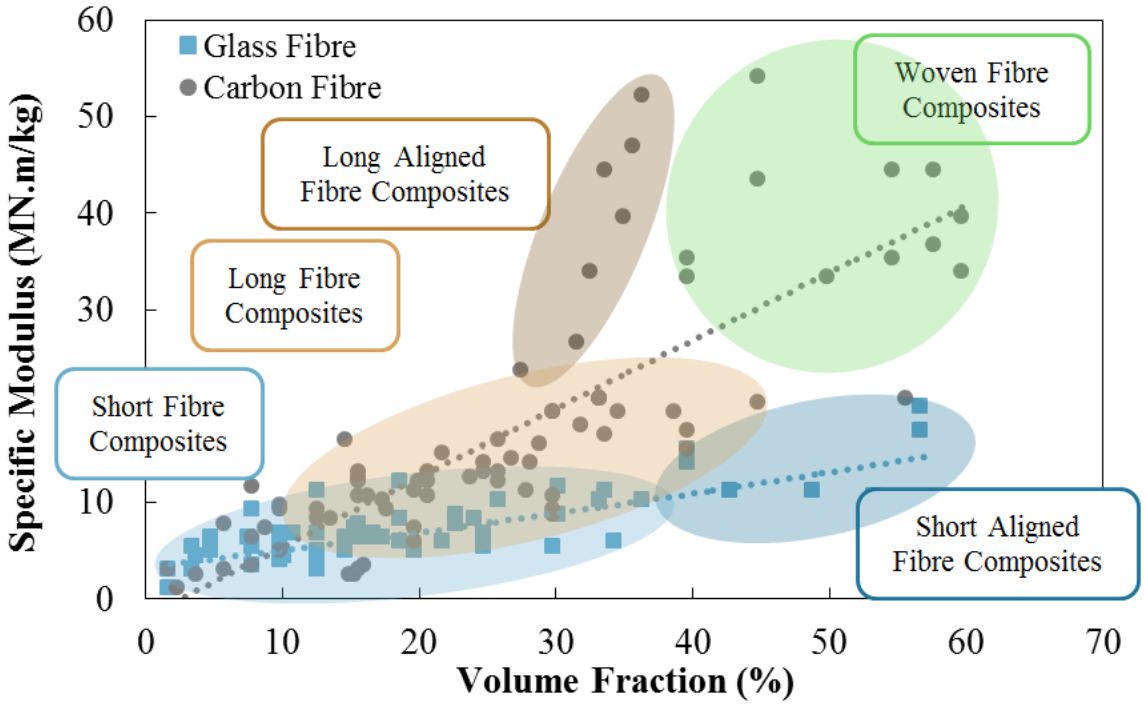

Figure 7: Relationship between Specific modulus and V_f in different types of carbon and glass composites[25]

Continuous fibre composites are stiffer than short fibre composites as shown in Figure 7. This is caused by a series of factors such as fibre critical length and higher potential fibre volume fractions, although short fibre materials are often purposefully manufactured with low volume fractions to decrease cost and increase flowability. Increasing the length of discontinuous fibres and aligning them enhances properties but at the cost of decreased flowability. The contrast between short and continuous fibre composites leads to an opportunity: to exploit the use of aligned long fibres which have high performance and combine them with short fibre composites that have better flowability.

This work aims to explore the feasibility of manufacturing hybrid composite components where continuous fibre reinforcement can provide enhancing properties and short fibre material the flowability. One such example is, the Hyundai's front crash beam, was made from 26 steel components that can now be made from three composite parts; through a continuous glass and carbon fibre pultrusion overmoulded with thermoplastic, providing a 43% weight reduction at similar performance [26]. Co-moulding an SMC with continuous fibre composites provides a solution that can produce areas of complex detail, providing a similar solution to over-moulded thermoplastics but with superior mechanical properties. Components like these could be manufactured as a single operation, removing the need for multiple part handling, storage and assembly processes, and creating an increasingly lean manufacturing operation. This can be achieved by a single compression moulding operation which can produce ribs, local thickness variations and in-moulding of metallic inserts if required, giving designers enhanced flexibility.

2.4. Manufacturing methods

There are many well-established manufacturing methods for thermosetting composites that are capable of manufacturing high quality components, and each have their own individual strengths and limitations. Common manufacturing methods and cycle times are shown in Table 1, with steel stamping used as a comparison representing the main manufacturing method currently used in the automotive industry.

Moulding process	Pressure (MPa)	Cycle time (min)
Autoclave	0.3-0.7	300-600
Resin transfer moulding (RTM)	0.1–6	3-30
Compression moulding	3–20	1-15
Injection moulding	10–100	1-2
Steel stamping	140-200	0.16

Table 1: Comparison of commonly used manufacturing methods[20, 27-31]

Autoclaves are heavily used in the aerospace sector and are viewed as the standard process for high quality composites, due to the low volumes and high levels of component quality required. The process involves manually laminating prepreg plies onto a rigid tool, increasing the ply count to build the thickness of the final component. This is then placed in a bag where a vacuum is created and maintained, which is then placed in a pressurised oven that consolidates and cures the part. The benefits of this method are that the process is highly repeatable and part quality is excellent, although due to cycle time this method is prohibitively slow for medium-high volume markets such as the automotive industry.

There is a wide range of resin transfer moulding methods, and the common aspects involve infiltrating a dry fabric with a liquid resin before curing. This process has lower pressure requirements than compression moulding, allowing cheaper tooling. Production rates are competitive for the automotive industry.

In thermoset compression moulding the material is placed in a hot mould cavity with two halves which is then closed as shown in Figure 8, squeezing the material into the profile of the tool; pressure is maintained during flow of the material and until the part is cured. This process is very similar to injection moulding, shown in Figure 9 but the material is placed directly in the tool and not injected, making the process slower. However, since fibres do not need to flow through an injection gate, fibre lengths can be considerably longer, enhancing mechanical performance.

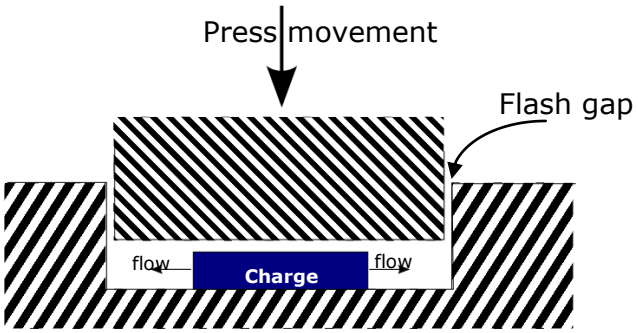

Figure 8: Diagram of typical compression moulding tooling and material

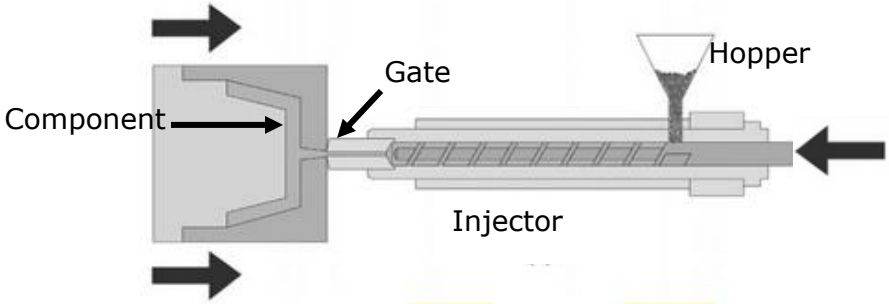

Figure 9: Injection moulding set-up[32]

Sheet and bulk moulding compounds are designed to be placed in a compression moulding tool and compacted. This is a quick process compared to the extremely labour intensive autoclave layup where plies of prepreg have to be precisely stacked and positioned to their near net-shape. This research aims to add prepreg to the moulding compounds in regions where enhanced properties are required.

Thermoset injection mouldings can have production rates as low as 1-2 minutes, but require significant initial investment as the pressure is only slightly less than for steel stamping. Autoclave components have poor mechanical properties compared to compression moulding; that said, it is possible to produce complex components.

This body of research will focus on compression moulding, but autoclave specimens will be manufactured as a benchmark. These components have low

void content and minimal flow and are generally viewed as the process that will yield the optimum results. Because of this, the autoclave provides a suitable benchmark manufacturing technology against compression moulding.

2.5. Aims and objectives

Composites in the passenger automotive industry have had intermittent use since their introduction. However, the use of carbon and glass fibre composites is slowly increasing in medium volume niche vehicles, such as the BMW i3. There are numerous manufacturing technologies suitable for the medium to high production volumes that are demanded by the passenger automotive market. This research aims to demonstrate the potential of composite compression moulding to meet this demand, by locally enhancing the performance of carbon fibre moulding compounds, thus broadening the potential applications of carbon fibre components in the automotive industry.

Compression moulding, with fast curing resin systems, is attractive to the automotive industry. However, localised hybridisation of composites has a wider range of applications such as aerospace and sport, where the properties of short fibre moulding compounds alone are not sufficient to meet the mechanical performance requirements.

Understanding the effect of the flow of the moulding compound on prepreg is critical in the evaluation of the achievable mechanical properties, since flow is likely to cause a decline in the performance of the prepreg. Flow could cause waviness of the continuous fibres, fibre distortion, and buckling, which will all lead to degradation in mechanical properties. The filling capability of moulding compounds to produce detail and complex 3D geometry is the primary advantage of SMCs. Because of this, it is unrealistic to manufacture these materials with no flow, as continuous fibre prepreg could be processed more effectively in this way yielding superior mechanical properties.

The overall aim of this research is to demonstrate the degree of mechanical enhancement that is achievable by the addition of localised reinforcement. This work also aims to understand the effect of localised SMC flow on the overall mechanical properties of prepreg, using image analysis techniques. An investigation to explore different ways to minimise flow-induced disruption of the

reinforcement will be conducted, considering the relative positioning of the continuous fibre material within the tool and staging (semi-curing) of the reinforcement prior to hybridisation.

3. Literature review

This chapter presents a review of the limited current literature relating to the field of compression moulding of hybrid composites, focusing on particular cases where thermoset matrices reinforced with both continuous and discontinuous fibres are compression moulded together. Testing methods relevant to the characterisation of compression moulded composites will also be discussed.

The aim of this literature review is to provide a broad understanding of the potential effects and issues that may arise during the moulding of thermoset hybrid composites; through the consideration of the behaviour of thermoset SMCs and the effects other researchers have identified by hybridising dissimilar fibre architectures.

3.1. Compression moulding of SMCs

This research will discuss the key features of SMCs, namely the moulding nuances of the material that may have an effect on the co-moulding with continuous fibre reinforcements. The main benefit of SMCs over conventional prepreg is the reduced layup time for complex components, as the positioning of the SMC in the tool requires less precision, as shown in Figure 8. In-mould flow of the charge is used to fill complex areas of the geometry, however this is often the cause of component defects.

3.1.1. Flow mechanisms

There are two different types of flow that can occur during compression moulding: fountain and preferential (transverse) flow. Although an equal flow velocity through the charge thickness would be preferable in SMCs, this is not likely in thermoset resins and instead preferential flow commonly occurs which causes the core to be more susceptible to fracture and fibre matrix separation[33]. During the moulding process individual or combinations of different types of flow can also occur in a single cycle[34].

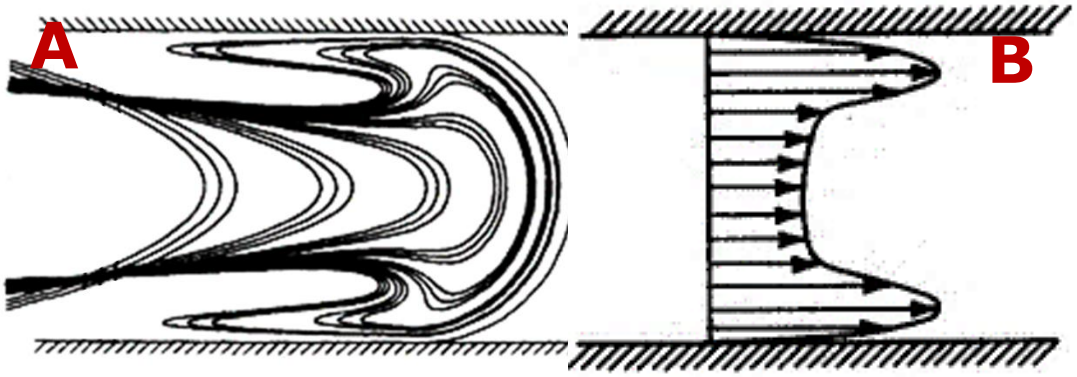

Figure 10: The two different flow mechanisms: (A) is fountain flow typically in thermoplastic moulding [35] where the material flows from the core and deposits on the tool face. (B) Transverse/preferential flow during compression moulding; the arrows depict velocity through the thickness of the charge, a greater velocity towards the edge and a relatively slow core [36]

Fountain flow, illustrated in Figure 10 (A), results in no sliding along the tool surface due to high friction or solidification. Therefore, the core of the charge flows and deposits on the outside, which causes alignment of fibres on the surface and misalignment in the core [37]. This is more prominent in filled thermoplastics, which is processed in cold tools as the outside of the charge solidifies from contact with the cold tool surface and the lower viscosity hot core flows.

Preferential flow, shown in Figure 10 (B), is dominant in thermoset resins. This is where the hot tool decreases the surface viscosity, creating a lubricating layer effect that has a greater flow velocity. This has been observed in SMCs, which can lead to the collapse of the surface layer in front of the charge creating a new entangled flow front [38]. Preferential flow can be minimised by allowing the charge temperature to be homogenised through a dwell time, where the tool surfaces touch the charge with negligible force; however, this can increase the likelihood of fibre matrix separation (FMS), since a lower viscosity can increase the likelihood of resin bleed from the fibres, or pre-gelation. Alternatively decreasing the time of the charge in the tool prior to compaction, by increasing closure speed [39] or simplifying charge placement[40], can reduce the available time for the charge to heat up which decreases the viscosity.

If the top and bottom temperature of the tool are equal, the charge receives longer heating on the bottom surface, due to the time required to close the tool. This creates an uneven preferential flow between the top and the bottom of the charge [38, 41]. This effect can be mitigated by minimising the time the charge is in the tool prior to compaction, and having a higher closure speed [42]. In hybrid composites with thermoset resin, preferential flow may cause problems if the reinforcement is on the outside, as the lubricating layer may enhance the reinforcement migration.

3.1.2. Fibre matrix separation

Fibre matrix separation (FMS) occurs when the resin is squeezed out from the SMC, causing regions of low fibre content, locally affecting the mechanical properties. FMS can occur due to many factors including: closure speed, charge design and coverage, temperature, pressure and mould design.

The flow of SMCs within the tool is important for removing defects and homogenising the material. However, issues can arise from poor parameter control. Olson et al. [41] qualitatively demonstrated that fibre distribution was more uniform with an increased mould closure speed of 250 mm/min compared with 45 mm/min, because the slow closure speed gives time for the resin to decrease in viscosity and bleed out of the fibres. Schmachtenberg et al. [43] measured a >25% reduction in fibre volume fraction (V_f) from the starting V_f in the region outside the initial charge coverage area at a closure speed of 60mm/min compared to <5% at 300 mm/min. 'Reverse-fountain flow' was observed at slow closure speeds, where the edges in preferential flow collapse in front of the flow front, this causes a resin rich flow front as the resin is more prone to collapse in front than the fibres [36]. During a one dimensional weld line test, where two charges flowed into each other, a slow closure speed caused a gradual reduction in V_f up to the weld. A high closure speed caused a dramatic reduction in fibre volume fraction at the weld line, and the V_f was comparatively uniform in the remainder of the component [43].

A high V_f and fibre aspect ratio can both lead to an increase in the likelihood of FMS since both contribute to fibre entanglement. This is where fibres become sufficiently mixed that they become knotted and resist flow, which can cause resin to bleed out of the fibres. The further the charge has to flow, the greater the opportunity for FMS; but, an increased closure speed can decrease the rate at which FMS occurs [44].

3.1.3. Layup and charge construction

Charge construction plays a pivotal role in the manufacture of defect free and uniform V_f components. Improper charge construction can have a detrimental effect on quality by causing high levels of localised flow and numerous defects; for example, the construction of a charge should be pyramidal to prevent top layers enveloping lower layers and trapping air [45]. Race tracking is also present in compression moulding as in resin transfer moulding, where one section of the cavity fills quicker than the other, causing weld lines and voids where two parts of the material meet. This is common where the material flows around in-mould holes, forming a component weakness as the fibres rotate as depicted in Figure 11 [46]. To prevent this, the material needs to be placed around the feature as to avoid two flow fronts flowing around a feature and welding, especially if it's a region of high stress.

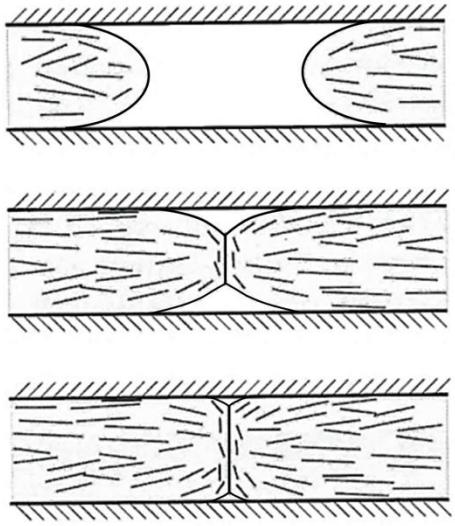

Figure 11: Flow fronts creating a weld line[46]

3.1.4. Rib formation

Ribs are a common feature in components manufactured from SMCs as the material can readily flow, compared to structures made from continuous fibres where they have to be meticulously laid up. Creating ribs allows designers to locally stiffen components by increasing the second moment of area. This is of particular interest to the automotive industry where bending, impact resistance and torsional stiffness are important.

The filling of ribs with SMC has a higher likelihood of FMS as the material is flowing out of plane, which can be exacerbated by fibres bridging the rib and prevent filling [47]. A break in the SMC ply at the entrance of ribs has been shown to enhance filling by preventing fibre entanglement [46], as shown in Figure 12. As fibre aspect ratio increases, the likelihood of fibre entanglement increases, which can cause jamming of the fibres and a resin-rich rib [48]. These regions due to their high resin content can also cause sink marks and are more common in complex geometries. Smith et al. observed that placement of highly flow-resistant continuous fabrics can be used to prevent sink marks [49]. This could be employed in improving surface finish on hybrid composites by ensuring the reinforcement does not flow.

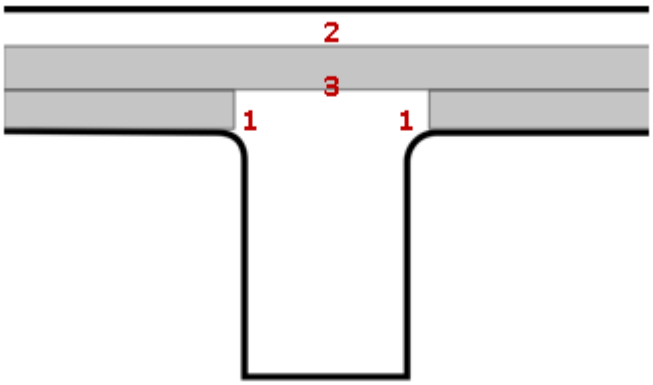

Figure 12: Diagram of charge design at a rib with material break to encourage flow, numbers represents regions in the rib. The numbers 1-3 represent the corners, top and the centre of the rib.

Increased pressure can increase the flow of an SMC, but increasing the fibre volume fraction decreases the flowability. In a spiral study of a glass SMC, it was observed that increasing the V_f from 19.7% to 36.5% decreased the flow length from 35% to 15% around the spiral [50]. Carbon fibre sheet moulding

compounds are more abrasive than glass alternatives and are more resistant to flow [51]. Traditionally SMCs have low V_f <30% and require a charge coverage of 50-70%. With V_f >50% charge coverage needs to be approximately 80%, or higher in complex geometries [52].

FMS is exacerbated during the formation of ribs, but high closure speeds can be used to minimise these effects [53]. There has been a great deal of research into the limitations of SMCs when moulding ribs. There is a high degree of flow as fibres are forced into the rib, causing fibre alignment [54]. Kim [55] observed the tendency of fibres to congregate at the rib corners in region (1) of Figure 12, causing resin-rich regions at the centre of the joint (3). Changes to tool and charge design can be used to aid the effective filling of ribs. Increasing the friction at the rib edges, by a rough tool finish (1) prevents slip and encourages earlier rib filling [56], which additionally reduces the impact and likelihood of sink marks. Increasing the friction in (1) can prevent fibres being bent out of plane and dragged into the cavity from Region 2 [57]. However, a decrease in pressure at the rib entrance from viscous friction can result in FMS separation [58].

The centre of the rib (**3**) is thicker than the rest of the component, which can lead to a resin rich pocket. This region is also susceptible to sink marks and residual stress because it is typically the last region to solidify [59]. However, this can be mitigated by increasing the radii at (**1**), as larger radii aid in rib filling but at the expense of creating a larger region of non-uniform thickness, which can lead to residual stresses as it will cure slower (**3**).

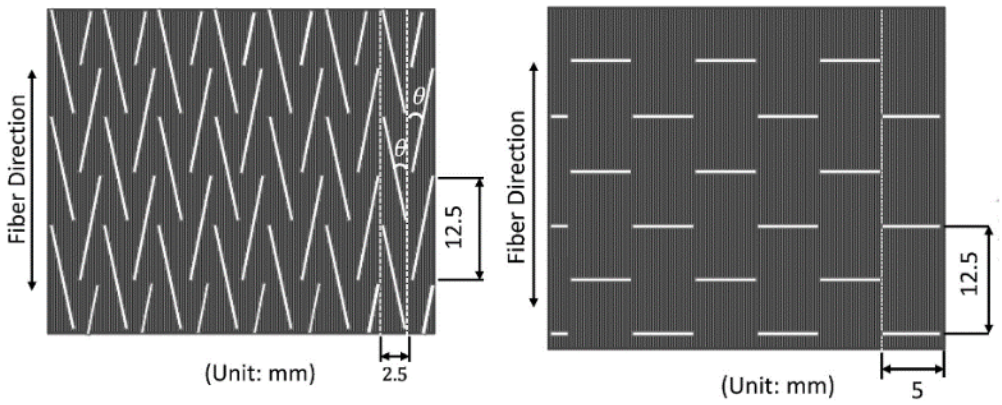

Figure 13: Different slit patterns in unidirectional prepreg, adopted from[60]

Unidirectional array chopped strands (UACS), similar to Cytec Dform®, is prepreg that has regular slits cut into the fabric to improve flow of the material, illustrated in Figure 13. Taketa et al. [61] demonstrated the use of UACS in a rib construction on a flat plate consisting of 15 translucent glass fibre plies and one UD carbon fibre ply. Fibres on the surface opposite the rib (**2**) were not pulled into the feature, Taketa does not state the reason for this, however the UACS inter-layer slip does allow the layers near the rib entrance to readily fill the feature. The outer layers not being pulled into the feature is important when designing the charge strategy to prevent the continuous reinforcement from being drawn into features by the SMC.

3.2. Curing of epoxy resin prepreg

To produce accurate curing profiles of the resin pure resin samples would be required in a differential scanning calorimeter (DSC), however the sample size is small and so obtaining a representative sample with carbon fibre involved would be difficult. It is not always possible to obtain neat resin samples from prepreg suppliers due to intellectual property protection. It can be challenging to extract the resin from the prepreg, as it has already been partially cured, B-staged. As a result, the resin has a high viscosity at room temperature, which resists flow and remains adhered to the fibres. This removes the possibility of cold pressing prepreg. Heating the prepreg to decrease the viscosity is a possibility, but adding heat to the system progresses the curing reaction and, as a result, the resin extracted by this process will not be the same as the original resin in the prepreg. A final option is to use prepreg directly in the analysis, and attempt to

subtract the contribution of the fibres. This has its challenges in determining and understanding the extent to which the fibres affect the resin.

There are alternative methods for testing the level of cure depending on the nature of the material. Parallel plates in a rheometer can be used for ”soft” samples, or dynamic mechanical analysis (DMA) in a 3 point bend or single cantilever setup can be used for ”solid” samples. As the sample warms, the viscosity of the resin changes due to temperature and later due to degree of cure. It is assumed that during heating the fibres are inert and do not affect the level of cure of the epoxy resin.

3.2.1. Rheometry

An epoxy resin goes through multiple state stages during a curing cycle. These stages can be identified using a rheometer, by linking the degree of cross-linking with the viscosity. When the resin storage modulus or viscosity is measured at room temperature (RT) it exhibits a RT value as shown in Figure 14 at (1), which can be liquid or solid as the epoxy molecular weight varies from an average of 350 to 3500 g/mol [62].

When the sample begins to warm up the resin viscosity decreases (2), this is caused by the effect of temperature on viscosity. The material then goes through a stage called ‘pot life’ (3) where the resin viscosity is only marginally changing [63]. This is an important step as the resin is curing by chains lengthening, which does not cause a significant rise in viscosity. All prepreg is partially cured to this stage (3), called B-staging, to improve handling, by altering the viscosity to control tack and ply stiffness [1]. Once impregnated, the material has a use-by-date, but freezing can prolong this period.

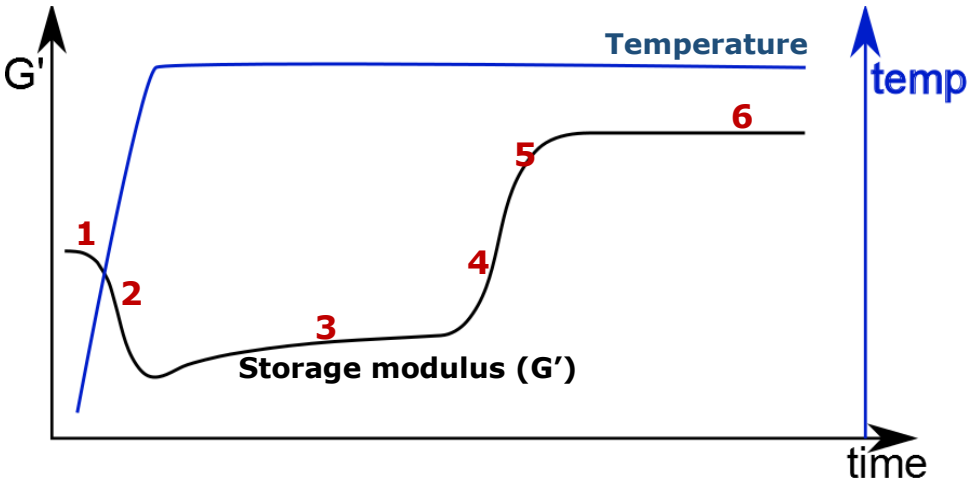

Figure 14: Typical epoxy resin cure cycle of storage modulus (G') against time

In region (4) the resin begins to cross-link and form a three-dimensional network of chains [64]. This rapidly increases the viscosity of the composite; however, the resin remains in a liquid state, allowing particles to move freely. During this stage tan δ, or the loss factor, will peak, signifying the gelation point where tan δ is the ratio of the viscous and the elastic portion of the material [63]. During gelation there is a mixture of gelled and non-gelled molecules slowing the reaction by reducing mobility as the crosslink density increases. Following this rapid change, the systems become vitrified (5), and the reaction slows as it becomes diffusion controlled [65]. This prevents rapid curing rates as the reaction is diffusion dominated at the end [66]. After the reaction has completed (6), there is no further cross-linking and the resin should be completely cured, and no further increases in stiffness will be achieved.

3.2.2. Dynamic mechanical analysis

It was shown by Costa et al. [66] that during the isothermal dwell in a DMA test the specimen will undergo significant cure, but will only show a slight increase in stiffness. This was demonstrated for Carbon/epoxy 8552, where a 34% degree of cure resulted in no significant increase in storage modulus (E') [65], compared to expected values from simulations. This shows the disparity between stiffness and degree of cure. Figure 15 shows the change in storage modulus (E') during a ramp and dwell cycle with different frequencies. Higher frequencies increased the curing rate and consequently increased the storage modulus, whereas a lower frequency of 0.01Hz provided a cure profile comparable to DSC, as shown in Figure 15 .

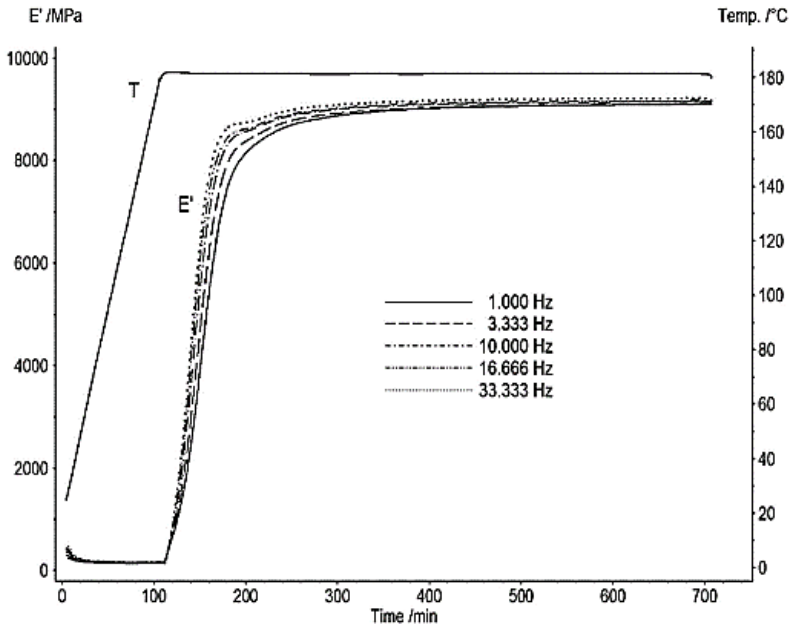

Figure 15: DMA analysis of the change in storage modulus (E') for 5 frequencies in a ramp and dwell process[66]

When testing the rheometry of fibre reinforced prepreg the presence of fibres can cause variation in the results, such as fibre alignment, volume fraction and distribution and air entrapment. In rheometry the cure profile in grooved oscillating parallel plates had no effect on the cure rate and improved the repeatability [67].

There can be a difference in cure rates between differential scanning calorimeter (DSC) and a rheometer; this is because the stiffness of the specimen changes over a longer period of time (rheometer) than the release of heat. As a result, the stiffness of prepreg does not reflect the degree of cure that has been measured. This was observed by Hayaty et al. [68], who showed that the peak tan δ (gelation position) is independent of temperature and frequency in parallel plate rheometry with a variation of just 2.3%.

3.2.3. Prepreg defects

There are numerous variations and defects that can occur in prepreg and these have been outlined by Potter et al. [69]. The main flaws are fibre misalignment through lay-up, flow-induced residual stress and voids. Compression moulding of prepreg is an alternative method to the traditional autoclave and is increasingly being used in high volume applications[6, 70, 71]. However, this process does not extract voids like an autoclave and the prepreg plies needs to be smaller than the cavity for it to be easily placed inside; which increases the likelihood of flow which can lead to misalignment. The different levels of shrinkage caused by the anisotropic properties of continuous prepreg, composites are designed where layers of ply shrinkage is symmetric through the thickness preventing warp.

3.3. Hybrid Composites

Due to limited research in hybrid composites, this section will highlight a range of different hybrid composite examples and draw experience from other examples that are relevant to compression moulding of thermoset continuous and discontinuous fibres. Controlling the straightness of continuous fibres in a hybrid structure is difficult when hybridising with an SMC, as there could be variations in the SMC sheet thickness which is causing waviness, even before flow occurs. This can cause the continuous fibres to become wavy, which was observed in the production of hybrid flax and carbon laminates [72]. It was evident from cross-sections that the carbon fibres plies were irregularly spaced due to the variable UD flax fibres, as shown in Figure 16. This research highlighted that the failure mode can change if the fibre architecture is significantly disrupted. The delamination resistance was improved and the plaques generally failed due to matrix cracking and fibre pull-out. Similarly, a hybrid of carbon fibre UD combined with short Kevlar fibres exhibited a wavy structure of the UD plies because of variations in thickness of the Kevlar [73]. Again, interply delamination was improved as the short Kevlar fibres created bridges between the UD plies, increasing the inter-laminar shear strength.

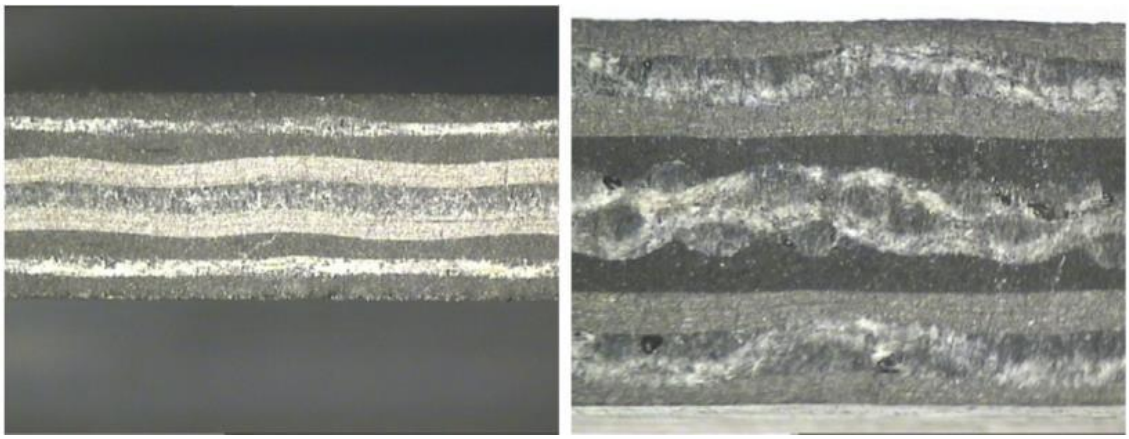

Figure 16: Cross section of UD flax and carbon fibre (left) and flax cross ply with UD carbon (right)[72]

Hybrid fibre architectures can be used for reducing cost, Hitchen et al. [74] controlled the stacking sequence of expensive carbon fibres for the primary load case with cheaper fibres for the secondary load cases. This demonstrated that the hybrid material performed similarly in flexural and compression strength as the high cost carbon fibres, but with a 12% cost reduction.

Fu et al. studied the effect of different ratio compositions of glass and carbon fibre injection moulded components [37]. They observed that with the same processing method carbon-glass hybrids, in comparison to pure carbon or glass systems, produced a randomly orientated core with flow induced alignment on the surface. As a result, this improved the mechanical properties of the specimens above the hybrid rule of mixtures. The fracture toughness of the random fibres was higher, as oblique fibres would impede crack propagation more than transverse only fibres.

Li et al. [75] found that hybrid composites with hybrid fibre architectures could provide improved ductility and flexural properties compared to pure UD carbon fibre plaques. This was demonstrated by interleaving UD carbon fibre plies with ultra-high-modulus polyethylene fibre (UHMPEF) plies. This produced synergistic effects as the ductile UHMPEF acted as a crack arrester and prevented crack propagation.

Sheet moulding compound/continuous-random (SMC/C-R), are continuous fibres that have a layer of chopped fibres deposited on top. Nunes et al. [76] conducted a trial comparing the mechanical performance of circular plaques of glass and carbon SMC/C-R. A 3-point non-destructive bend test was conducted at different orientations of the disk. The results indicated that the SMC/C-R generally provided higher flexural stiffness compared to continuous fibre disks in the direction of the continuous fibres. It was noted that the results were skewed because they were unable to prevent the SMC/C-R from warping due to an orientation bias. This was likely due to a poorly balanced component, because the continuous fibres used in the trial have in-plane heterogeneous coefficients of thermal expansion causing the continuous fibre reinforcement transverse to the fibre direction to shrink and warp the disk SMCs are less likely to distort than SMC/C-R due to their homogeneity. However, balancing a hybrid composite could be an issue in future studies, as there may be conflict between design for performance and distortion prevention.

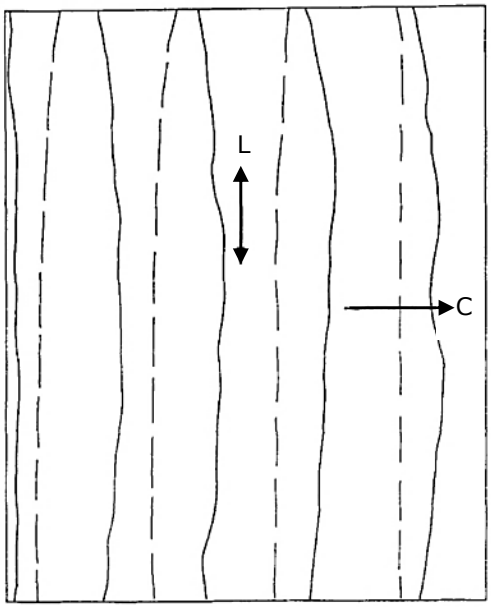

Figure 17: Flow induced distortion of SMC/C-R in a 1D flow scenario with tracer fibres. Continuous lines represent surface tracers and the dotted lines represent the fibre orientations beneath. Fibre direction(L), flow direction(C) [77]

Compression moulding is likely to distort the continuous plies when moulded with short fibres, which can result in a reduction of the mechanical properties of the UD fibres. Mallick demonstrated with four plies of SMC/C-R that the level of distortion on the UD fibres was less on the inner plies, as shown in Figure 17 by the position of the continuous red tracer fibres, solid being on the surface and dashed in the centre. It was concluded that increasing the number of SMC/C-R plies decreased the distortion on the inner plies, thus providing increasingly more predictable mechanical properties [77]. Noting that the charge design has an effect on the final component, the placement of the continuous fibres in Mallick's demonstration caused significant distortion on the continuous fibres as they were placed on the outside (C-R)/(C-R)/(R-C)/(R-C).

The addition of continuous reinforcement to discontinuous fibres is aimed at improving mechanical properties. Wulfserg et al. [78] demonstrated that the flexural and tensile moduli and tensile strength doubled through hybridisation, but there was a negligible effect on flexural strength. The reinforcement was used as the internal layer, encapsulated with SMC on either side and the samples were taken from an area that was within the initial charge coverage, which negates the benefits of using SMCs. The improvements in flexural and tensile moduli are encouraging for automotive applications where stiffness is a strong driving factor for composite use.

In summary, hybridisation of composites can have a range of benefits, such as Kevlar or UHMPEF can be used to tailor mechanical performance to increase inter-laminar shear strength or ductility. Low cost fibres can be added to high strength carbon fibres to reduce overall cost without compromising performance. However, short and natural fibres tend to have thickness variations causing waviness in the reinforcing fibres. The flow of short fibres then causes further waviness in the continuous fibres, which is more significant on the surface than in the core.

The drilling of holes in continuous fibres composites is undesirable as it can lead to localised stress concentrators, as shown in Figure 18[79], leading to regions of notable mechanical weakness. Random discontinuous fibres do not exhibit this issue and have been proven to be notch insensitive [80]. The open hole, or notch strength of continuous fibre composites in tensile testing decreased as

much as 50% compared to SMCs, which showed depending on their fibre length and filamentisation decreased by between 0% and 25% [79]. Hybrid composites have the potential to enhance damage tolerance; as SMCs are notch insensitive they can be moulded on exposed areas more prone to damage, protecting the continuous reinforcement within [81].

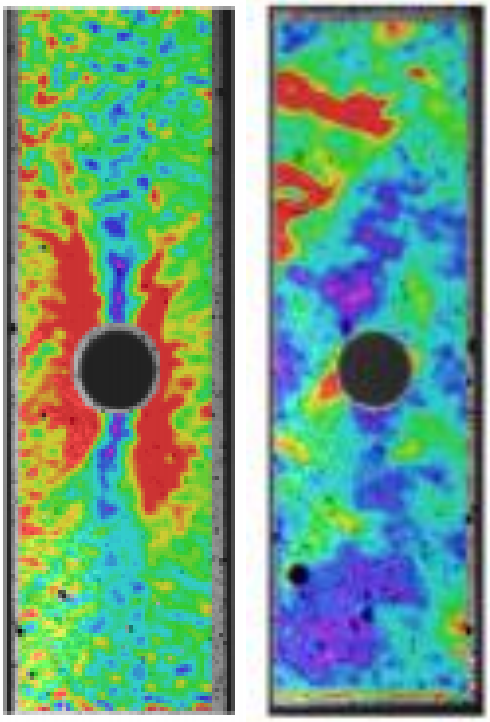

Figure 18: stress distribution difference between random SMCs (right) and continuous prepreg(left), with red to purple showing regions of high to low stress

3.4. Industrial research in hybrid composites

3.4.1. Thermoset hybrids

Mitsubishi demonstrated a manufacturing method that was capable of hybridising continuous and discontinuous fibres, involving a two-stage process [71]: Firstly, continuous prepreg was heated and preformed to a net shape; secondly, the net shape preform was placed in a mould with the SMC charge and compression moulded together. The first step significantly increases the rigidity of the continuous fibre reinforcement, reducing the likelihood of fibre distortion in the continuous insert by increasing the viscosity of the resin. As a result of this partial or complete curing, which was not stated, the strength of the bonding at the UD/SMC interface was shown to be comparable to using an adhesive during elevated temperature testing at up to 80 °C in a flat-wise

adhesion test. However, staging needs to be executed carefully, as over-staging may limit the level of cross-linking between the two materials and potentially weaken the join.

Figure 19: Mitsubishi Rayon prepreg compression moulding demonstrator component [71]

The demonstrator component highlighted the potential of hybridisation through the use of continuous fibre plies along the length of the component and SMC producing features such as ribs, gussets and inserts, as shown in Figure 19.

Wet compression moulding is similar to the traditional process, but eliminates the need for B-staging and prepreg material. The dry fabric is cut, stacked into a laminate and sprayed with liquid resin before being consolidated in a heated tool. The resin flows under pressure, impregnating the fibres before curing [82]. This process has been used to produce carbon-steel hybrid components in the BMW 7 series B-pillar [83].

3.4.2. Thermoplastic hybrids

3.4.2.1. Compression moulding

Hangs et al. [84] produced a demonstrator component shown in Figure 20 with blue thermoplastic bulk moulding compound, black continuous fabric and yellow local tape laminate reinforcement. There were significant problems as the flowing material pushed through the reinforcement during compression, causing damage to the continuous fibre reinforcement.

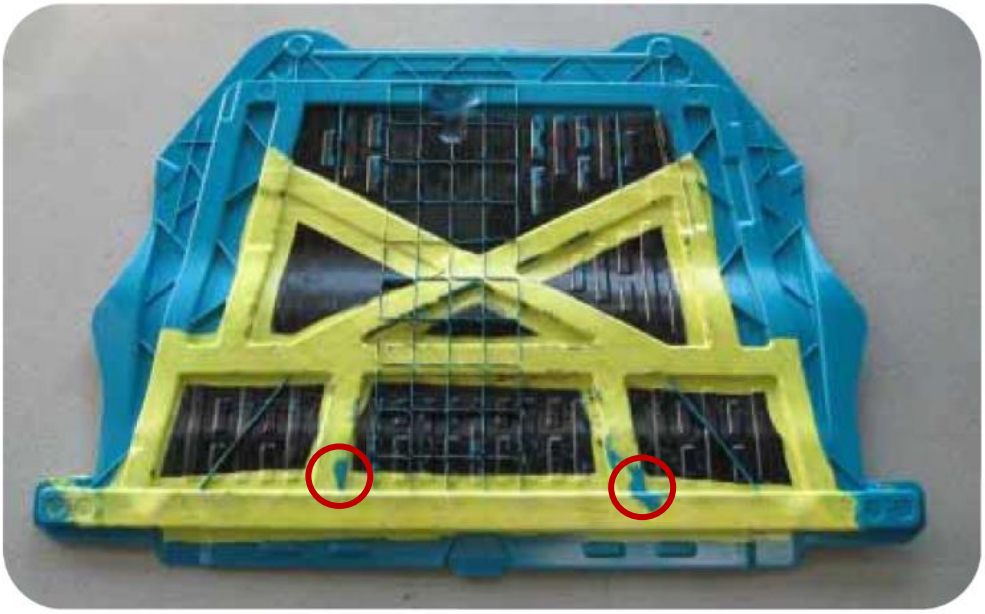

Figure 20: Fraunhofer thermoplastic hybrid demonstrator component with a black continuous fabric, yellow tape laminate and a blue BMC, highlighting the BMC pushing through the inserts[84]

The research continued and investigated the effects of charge arrangement as seen in Figure 21. When the bulk moulding compound was placed on top off the insert there was less disruption than when placed to the side (Figure 21). The report does not attempt to explain why this is the case, but it could be from fountain flow caused by the bulk compound solidifying on tool contact and flowing around the insert preventing significant disruption. This effect is unlikely in thermosets due to the lubricating layer effect as the material is prone to have increased flow at the tool face.

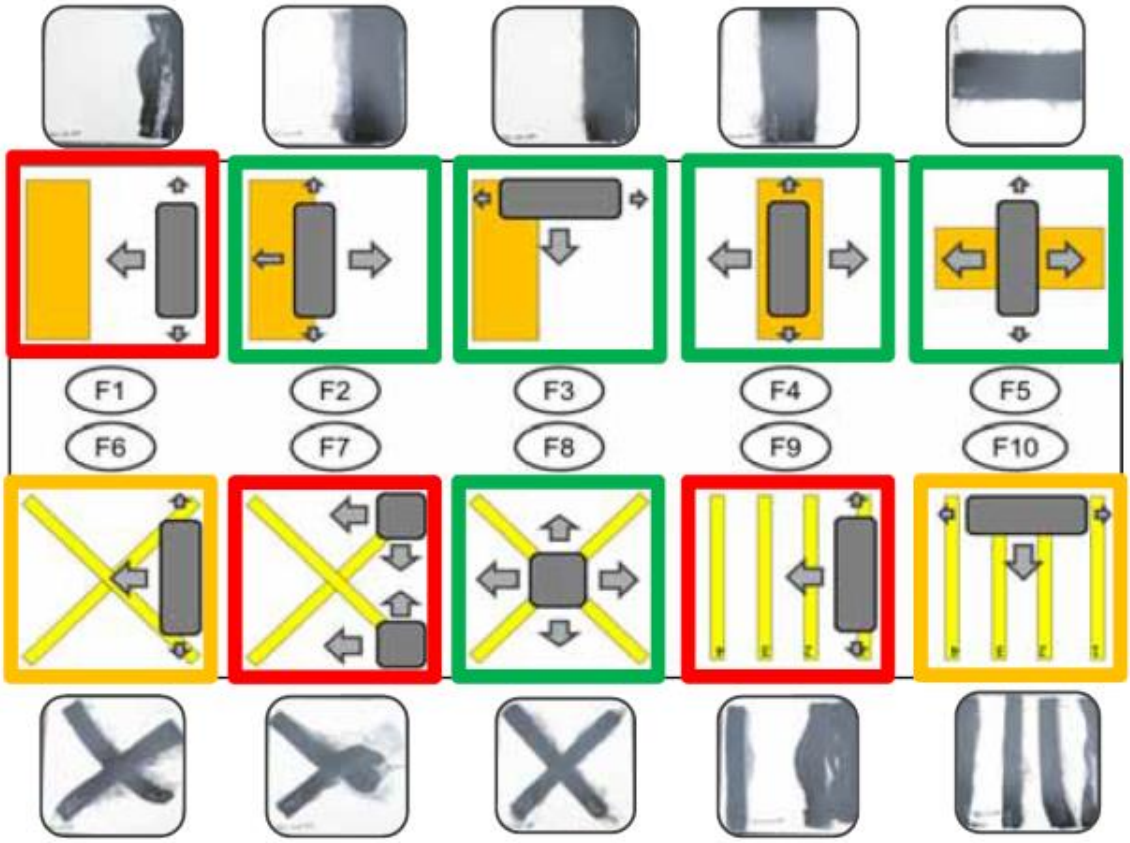

Figure 21: Effect of different thermoplastic moulding compound charge placement over continuous reinforcement with images showing tape distortion [84]

Hybridising thermoplastics has its unique challenges compared to thermosets. Mitsubishi Rayon demonstrated that using discontinuous carbon fibre with a polypropylene matrix in a hat-shaped hollow structure with internal ribs did not enhance the flexural stiffness in relation to weight. However, a hybrid composite comprising UD and discontinuous fibres with ribs exhibited a 22% increase in modulus compared with an all discontinuous fibre component [85]. For automotive applications a hat-shaped hollow beam of polypropylene carbon fibre hybrid with UD in the top and bottom outer flat sections demonstrated improved energy absorption and strength compared to steel due to the increased ductility [86].

3.4.2.2. Over-moulding

Over-moulding is an established technology used to encapsulate metallic inserts in an injection moulding cavity with a polymer. This process has been adapted to incorporate continuous fibre reinforcements into the component. The polymer is filled with short fibres and the continuous sheet fabric is preformed into shape prior to injection as shown by the process in Figure 22.

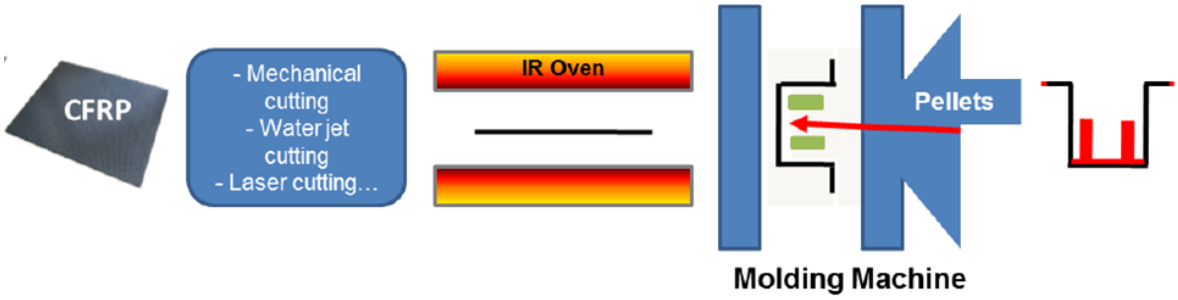

Figure 22: Thermoplastic hybrid over-moulding process[87]

Although over-moulding is in use commercially, it cannot achieve the same mechanical performance of SMCs, as the fibre length for injection moulding is significantly shorter. However, there are significant developments taking place in this field, as over-moulding is making hybridisation more cost effective [88]. Several issues have been identified in hybrid over-moulding. These include forming a good interface as there is a different shrinkage level for each of the constituent materials, maintaining the integrity after preforming, and preventing reinforcement distortion [89].

The benefit of manufacturing hybrid composites by compression rather than injection moulding is that fibres can be significantly longer. As a result, compression moulding components tend to have better properties.

3.5. Testing Techniques

3.5.1. Photogrammetry

The flow of prepreg or continuous fibre fabrics has not had much academic research, and photogrammetry of prepreg during flow is a new field. Photogrammetry is common in sheet metal forming [90-92] for experimentally depicting localised flow using a range of surface marking methods, such as screen printing (serigraphy), laser or chemical etching. Digital image correlation (DIC) cannot be used to track flow in this situation, as the cameras need to monitor the movement of patterns throughout the moulding process and the charge is typically obscured by the tool. Markings on the surface to obtain localised strain fields can be used in a wide range of applications, including to analyse the location and variation of strain in human amnion (a random mat of collagen fibres used to house the embryo) during tensile testing [93]. That said, every method has their own distinct benefits and surface marking techniques , which was described by Ozturk et al. [94]. There are three generic type of grids which is shown in Figure 23: circular, square and speckled. Speckle grids are generally used in the continuous monitoring of deformation. Whereas circle and square grids are often used where the deformation process obscures the part and only before and after images are possible, such as compression moulding. Circle grids create deformation co-ordinates by determining the centre of each the circle; this has its limitations, if the circle centres do not form square like shapes or if circles are smudged sufficiently to blur the circularity. Similarly square grids are prone to false positive or missing lines which lead to failure in creating the digital grid.

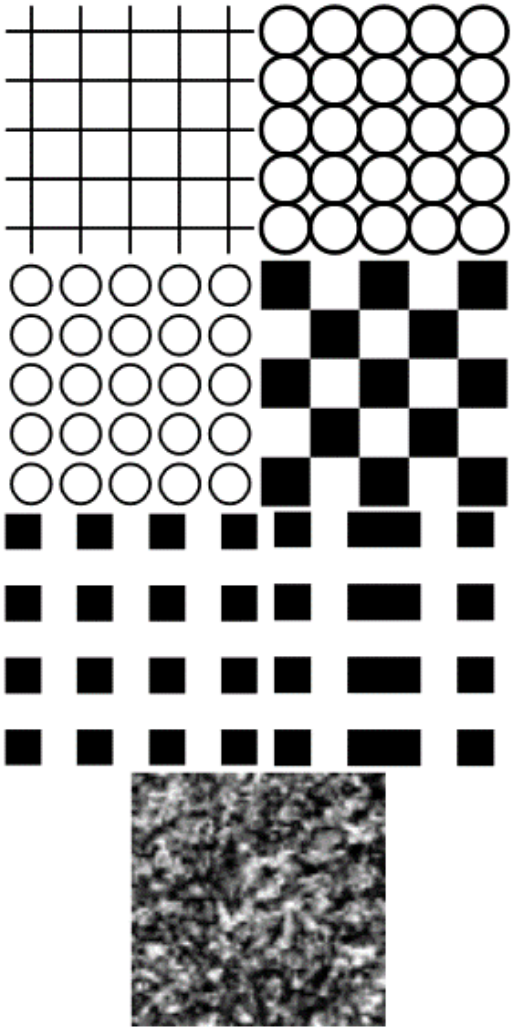

Figure 23: Different grid types[68]

Imaging techniques are difficult to apply to fibre reinforced composites because of poor contrast between the fibres and matrix. It is particularly difficult for anisotropic materials such as SMC, as surface based grids become easily distorted [95]. This was demonstrated by Olsson et al. [40] when internal layers of SMC broke through to the surface and erased the grid. Tracking the flow of internal plies has been done in glass composites using tracer fibres with minimal effect to the flow properties [77]. Metallic fibres or mesh can be used during moulding, as shown in Figure 24 However, this also creates problems since they might have an effect on the flow of the material and alter mechanical properties.

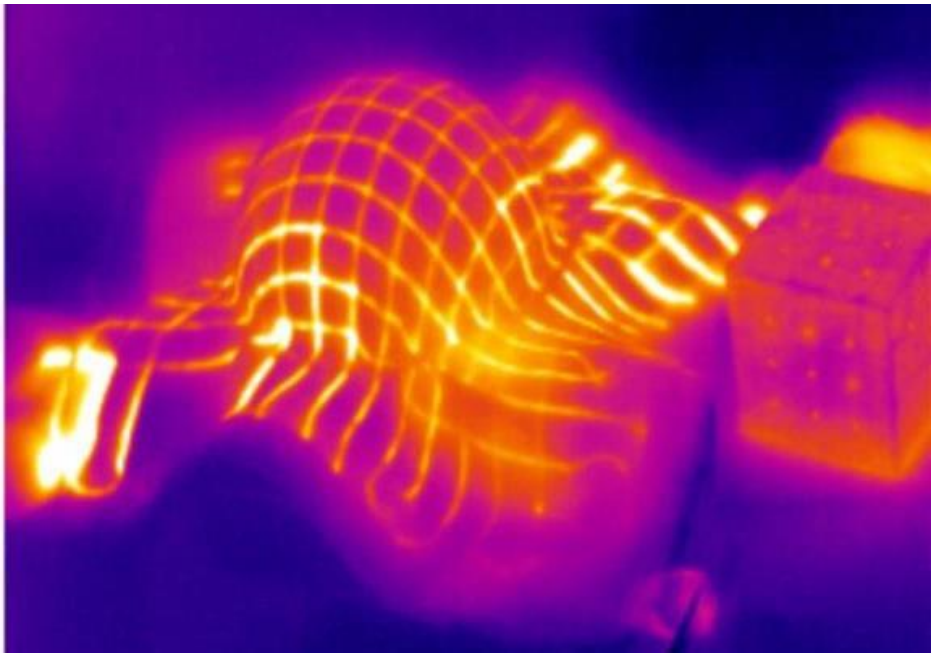

Figure 24: Infrared picture of a heated metallic internal ply[96]

There has been limited use of grids for strain analysis in compression moulding of composites; however, the use in drape forming of textiles has been extensive [96-101]. Two issues with grid markings were recorded by Lomov et al. [102]on dry fabrics, which are also common with the metal forming industry. Firstly, shear and friction at the tool surface and the inter-fabric shear erodes the grid. Secondly, there is an assumption that the grid is aligned perfectly with the fibre direction and that the fibres within the fabric are aligned with each other. These issues may be exacerbated by a comparatively high pressure, and the addition of resin that may flow and engulf the markings.

A novel methodology measuring the surface in-plane fibre waviness was developed by Sutcliffe et al [103] where the fibre angle of small sections (5x5mm) can be analysed without the use of a grid. The method is effective for highly localised areas as it would be laborious for large regions. The method takes samples of RTM CFRP polished to P3200 and uses an optical microscope to detect the fibres. This is similar to Apodius GmbH, where a camera at close proximity can detect the fibre angle and small defects in dry and prepreg fabrics and moulded parts if surface finish is good [104]. This system detects the angle instantly; however, requires being close to the surface which may involve long scanning times for an entire component.

3.5.2. Fibre Orientation

The measurement of the fibre angles through the thickness of the laminate, void content and fibre distribution is commonly conducted by taking cross sections and using optical microscopy. The preparation and processing time for this method limits it to localised testing. Nevertheless, there is merit in closely investigating regions of interest. With cylindrical fibres the angle of the fibre is calculated by measuring the length of the minor and major diameter as shown in Figure 25 [105]. This is comparatively simple and quick compared to kidney shaped fibres.

$$\theta = \cos^{-1}\sqrt{\frac{b}{a}} \tag{1}$$

Where

θ = fibre angle (°)

b = minor diameter

a = major diameter

However, the method uses the eccentricity of elliptical cross sections of fibres when cut at a known angle, and assumes that the fibres have a circular cross section. Ideally the samples are cut at 45° to the fibre orientation to enhance the eccentricity and reduce the effects of pixel noise error, producing a more accurate measurement.

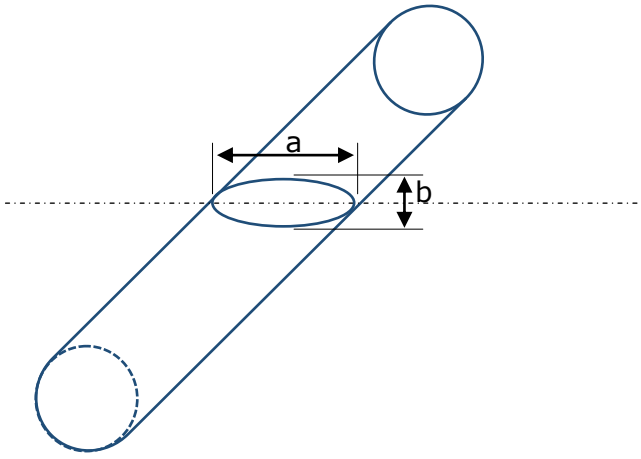

Figure 25: Fibre cross-section creating the ellipse, with *a* and *b* being the major and minor axis respectively

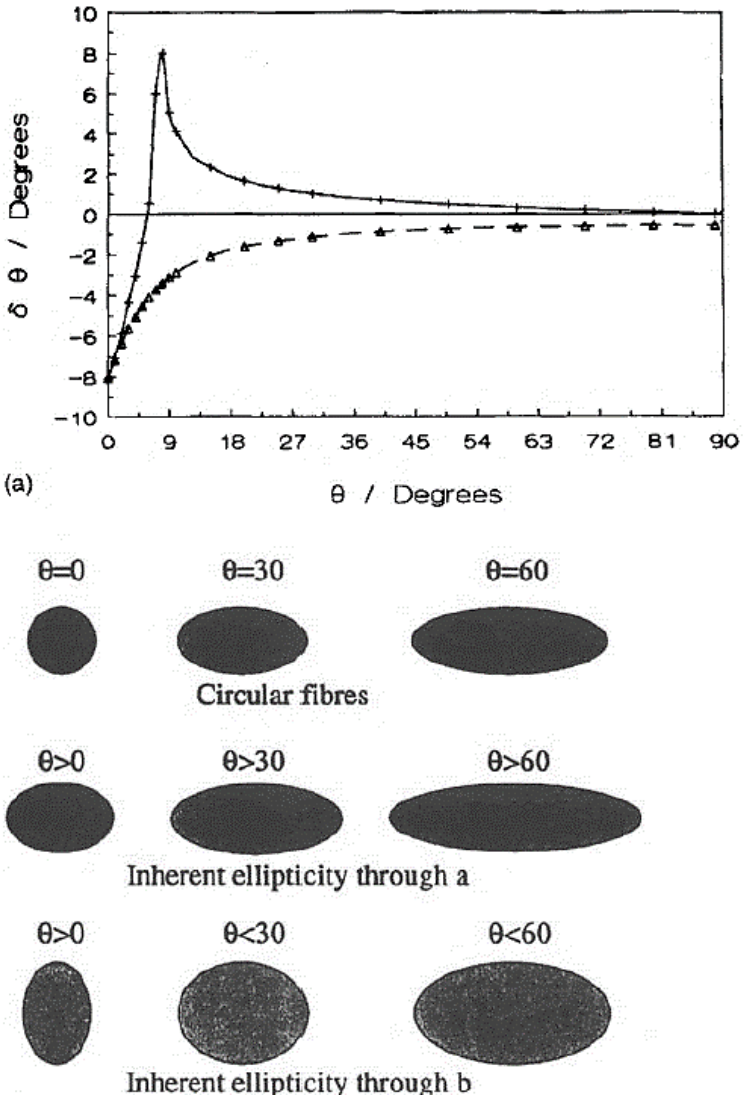

Figure 26: Effect of elliptical fibres on fibre angle calculation when the ellipse is in the major axis + or in the minor axis Δ[35]

Fibre angles can also be calculated for elliptical fibres, but two sets of images are required. This enables the rotation of the fibre from the two images to be calculated from the change in the centroids of each fibre $x \,\&\, y$, as well as the distance between the two images z, allows the calculation of the fibre angle of elliptical fibres [35].

$$\theta = \tan^{-1}\sqrt{\frac{\delta x^2 + \delta y^2}{\delta z}} \quad (2)$$

Where

θ = fibre angle (°)

x, y, z = Cartesian co-ordinates

The elliptical fibres create an error in calculating the fibre angle which is shown in Figure 26 where the fibre angle in the major axis (a) or the minor (b), affects the error to a maximum of 8°, decreasing as the fibre angle increases. Figure 26 illustrates the difference in fibre appearance if the fibre angle is in the major or minor axis between 0° and 60° of circular and elliptical fibres. This highlighted the complexity of the issue, especially if the fibres are not all the same shape. The issue with this method is the increased time it takes in adding an additional image, especially where the V_f can be >50%, meaning identifying individual fibres from clusters can be challenging.

This method works well, but becomes increasingly complex when the fibres are non-circular, such as kidney bean shaped fibres which can occur due to the fibre manufacturing process. The solvent used to dissolve the polymer precursor diffuses out of the centre of the fibre, which causes the core density to decrease. This results in the outer surface layer of the fibre which has coagulated to collapse into a kidney bean shape [106].

3.5.3. Flexural modulus testing

Flexural testing traditionally involves placing a specimen on two supports and applying a load, with the main types being 3 and 4 point bending; 3 point bending has one loading point compared to 4 point bending, which is shown in Figure 27.

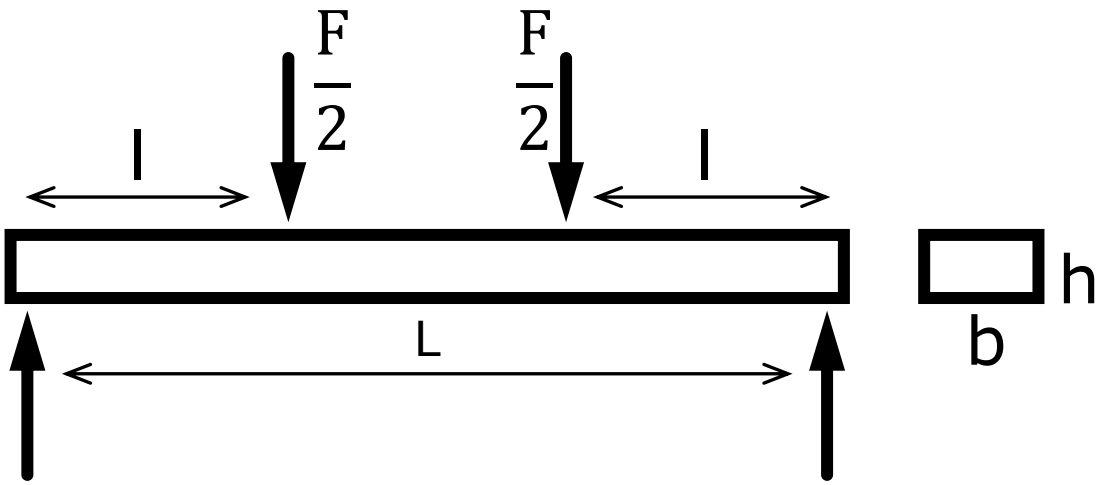

Figure 27: 4-point bending diagram

The deflection was measured using a linear variable displacement transducer (LVDT) in the centre of the specimen. The flexural modulus (E_f) from four point bending was taken from *BS EN ISO 14125:1998+A1:2011, Fibre-reinforced plastic composites — Determination of flexural properties*[107], stating the change in force (ΔF) over the change in deflection (Δs), where the support span length (L), the sample width (b) and thickness (h) are constants. The constant 0.21 provided by the testing standard is accurate as long as the ratio between the loading members(l) to support members (L) is a third. The width was measured with Vernier callipers to an accuracy of 0.01mm and the thickness was measured using a micrometer to an accuracy of 0.001mm.

$$E_f = \frac{0.21L^3}{bh^3}\left(\frac{\Delta F}{\Delta s}\right) \tag{5}$$

Where

E_f = Flexural modulus (GPa)
L = span length (mm)
b = specimen width (mm)
h = specimen thickness (mm)
ΔF = change in force (N)
Δs = deflection (mm)

The primary difference between 3 and 4-point bending is the stress distribution. As shown in Figure 28, a 3-point bending test has a triangular stress distribution, compared to 4-point bending, where there is a trapezoidal stress distribution. The latter could be considered favourable if an average stress over a particular area is preferred; however, 4-point bending requires a larger span to prevent shear distorting the results. It was observed when comparing 3- and 4-point bending tests that 4-point bending provides a 5% higher flexural modulus caused by the bending rotation at the supports changing the loading span[108].

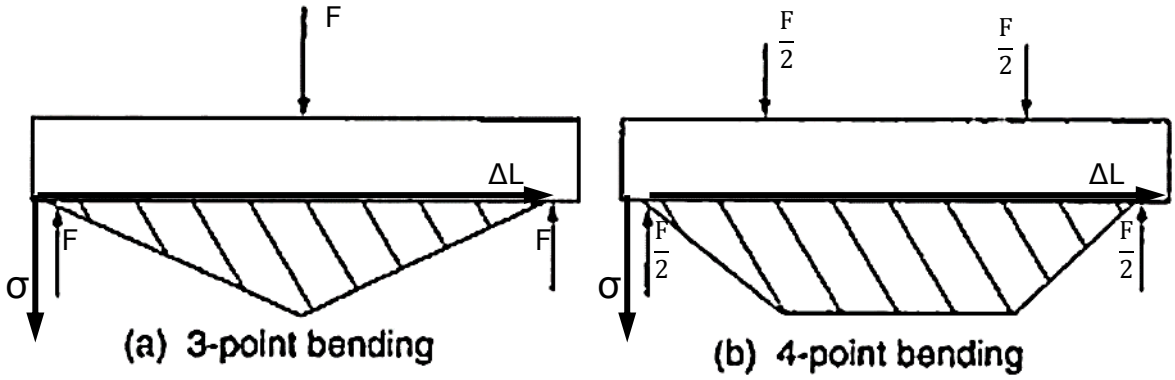

Figure 28: Stress distribution of 3 and 4 point bending, adapted from [109]

3.5.4. Properties of Off-Axis Anisotropic Composites

The rule of mixtures (RoM) employs the volume ratio of matrix to reinforcement to predict the stiffness of composites.

$$E = E_f V_f + E_m V_m \quad (3)$$

Where

E = flexural modulus (GPa)
E_f = flexural modulus of fibres (GPa)
E_m = flexural modulus of matrix (GPa)
V_f = fibre volume fraction (%)
V_m = matrix volume fraction (%)

For a RoM to be applied to hybrid composites one can assume that there is no interaction between the two systems and iso-strain can be applied to both materials.

$$E = E_1V_1 + E_2V_2 + \ldots \quad (4)$$

Where

E_n = flexural modulus (GPa) of n material in composite

V_n = volume fraction (%) of n material in composite

Rule of hybrid mixtures (RoHM) calculates the properties of a hybrid composite by volume proportion adding the properties of each material within the hybrid together as shown in equation (4). Authors [110, 111] have identified a strong relationship between RoHM and experimental values on a range of different properties and materials, but with a bias. As some have shown a slight over estimation of the RoHM, others have observed this in strength only and not moduli [112] while another stated the opposite to be true [113]. It was considered that an over prediction was caused by internal compressive strains arising during curing and different elongation properties of the constituents acting as crack arrestors; [114] or by the differing fibre orientation of the two hybrid materials preventing crack propagation [37].

If the fibres are not aligned with the loading direction, the Krenchel efficiency factor (Equation (6)) is added to the ROM to take into account misalignment. An efficiency factor of 0.375 is used where fibres are randomly dispersed in-plane which is equivalent to a quasi-isotropic laminate[115].

$$\eta_0 = \sum \alpha_i \cos^4(\theta_i) \quad (6)$$

$$E = \eta_0 E_f V_f + E_m V_m \quad (7)$$

Where

η_0 = Krenchel efficiency factor

α_i = properties of plies in the composite aligned in θ_i

θ_i = ply fibre angle (°)

In a unidirectional composite where all fibres are aligned parallel to the fibre direction, the longitudinal and transverse mechanical properties can be accurately calculated using the RoM. There are multiple methods for calculating

degradation in performance from fibre misalignment, such as classical laminate analysis (CLA). This allows the calculation of properties in thin plates as transverse stresses are omitted, however require more variables than RoM, such as Poisson's ratio and the shear modulus [116], which are not always available as inputs when calculating the properties of a material. Figure 29 shows the difference in theoretical properties of CLA and ROM. As shown by experimental data, the RoM tends to over-estimate, as the fibres become less aligned in the loading direction, shown in [117] and [118].

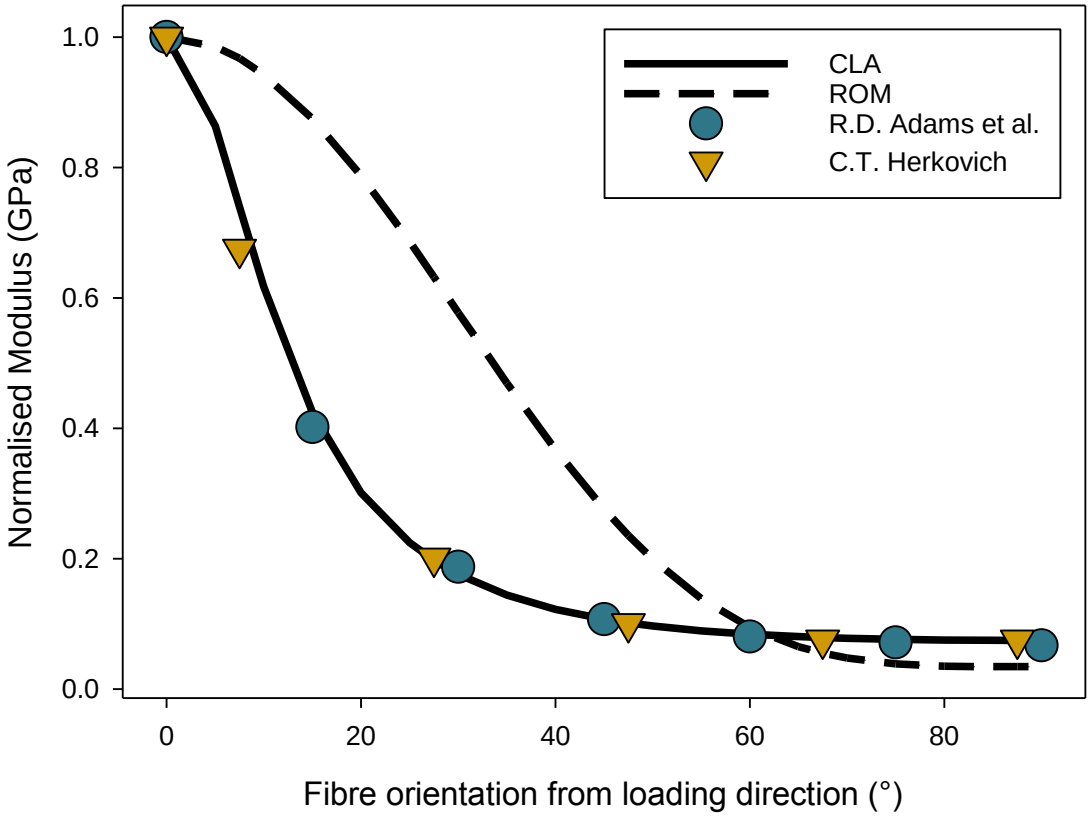

Figure 29: CLA and RoM of off-axis flexural testing with experimental data[117] [118]

3.6. Summary

There are many motivations for hybridisation such as cost reduction, enhanced functionality and mechanical performance. The literature is limited on compression moulded thermoset hybrid composites, but it is possible to draw conclusions from different hybrid scenarios which are relevant to the hybrid study of continuous and discontinuous carbon fibre composites.

Using discrete sections of continuous fibre localised reinforcement has numerous challenges in that the randomness of the other constituents being natural or discontinuous fibres are likely to cause distortive flow damage or penetrate the reinforcement. Therefore investigations to control or minimise this will be beneficial.

Research has been conducted where layers of different materials, such as chopped Kevlar and natural fibres, are combined with continuous fibres to form a hybrid composite. This research highlighted that variations in thickness of one of the materials can lead to the primary reinforcement fibres becoming wavy, which reduces their effective performance. This indicates the susceptibility of continuous fibres to distortion from local thickness variations.

Thermoplastic hybrid composites have been successful manufactured by clamping a prepreg and injection moulding the detail of the component around the reinforcement, essentially fibre filled over-moulding. This technology showed that the reinforcement can be held in place while the detail is produced. However, injection moulded fibres have to be short to enable flow, reducing the performance of the features.

Limited research has investigated moulding SMCs with continuous fibres to demonstrate enhanced properties. Whilst most observed distortion of the continuous fibres in the hybrid composite, none went as far as investigating methods for measuring the distortion effects or attempted to minimise the flow of the discontinuous SMC.

This literature review has highlighted research that has been conducted for hybrid composites; notably in thermoset compression moulding. In addition, the literature review has drawn attention to relevant testing methods such as four-point bending, photogrammetry and epoxy resin characterisation which will be used in the hybrid study to supplement and provide context to the research in later chapters.

4. Materials and Methods

This chapter describes the materials and methods used to manufacture and characterise the hybrid fibre composites. This includes material data, compression, out-of-autoclave and autoclave moulding and material characterisation testing methods: four-point bending, density measurements, interlaminar shear strength test (ILSS) and rheometry. Finally photogrammetric methods are described for measuring the distortion of the unidirectional fibres caused during the compression moulding process.

4.1. Materials

The materials used in this research have been provided by Hexcel. These are a carbon fibre sheet moulding compound: HexMC®/C/2000/M77 and unidirectional prepreg: HexPly® M77/38%/UD300/SGL-50K, shown in Figure 30.

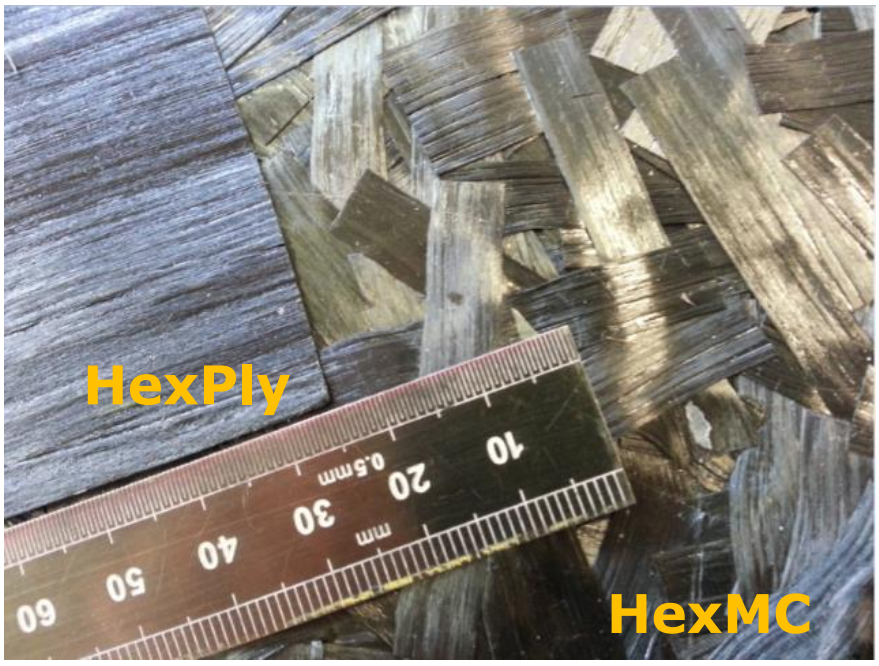

Figure 30: Image of HexPly® M77/38%/UD300/SGL-50K and HexMC®/C/2000/M77

4.1.1. Resin

The resin used in this study is a commercial epoxy resin, M77, which is designed for compression moulding with a long shelf life and a fast cure rate. Properties of the resin are provided in Table 2. However, mechanical properties were not and the materials were only provided in impregnated form.

Resin properties		
Shelf life	-18 °C	18 months
	23 °C	6 weeks
T_g	130 °C	
Tack	Low	
Density	1.22 g/cm^3	

Table 2: Resin properties of M77

4.1.2. Unidirectional prepreg

The recommended processing conditions and material properties of the UD, HexPly® M77/38%/UD300/SGL-50K used in this study are shown in Table 3. This material is a 50k high strength unidirectional carbon fibre supplied by the SGL Group with a 300g/m^2 areal mass and density of 1.8 g/cm^3. This is impregnated with 184 g/m^2 of M77 resin to provide a prepreg weight, fibre weight fraction and volume fraction of 484 g/m^2, 62% and 52.5% respectively.

Processing Conditions		
Heat rate range	1-20 °C/min	
Pressure range	1-30 bar	
Cure cycle	110 °C	18 min
	120 °C	7 min
	150 °C	2 min
Material Properties*		
Flexural strength	0°	1550 MPa
Flexural modulus		113 GPa
Prepreg density	1.52 g/cm^3	

Table 3: Processing conditions and mechanical properties of HexPly, *mechanical properties are normalised to 60% fibre volume fraction and press cured at 150 °C for 2 min at 30 bar[119]

4.1.3. Sheet moulding compound

The carbon fibre sheet moulding compound has an areal weight of 2000 g/m^2. This is produced by cutting prepreg into 10 mm strips, chopping to 50 mm lengths, randomly dispersing the chips to form a sheet and then consolidating

between carrier films. The fibre volume fraction is 57%, as supplied. Table 4 shows the manufacturers' recommended processing parameters and material properties of the SMC.

Processing Conditions		
Heat rate	1-20 °C/min	
Pressure	>80 bar	
Cure cycle	100 °C	40 min
	120 °C	8 min
	130 °C	6 min
	140 °C	4 min
	150 °C	3 min
Material Properties		
Flexural strength	0°	500 MPa
Flexural modulus		30 GPa
Short beam shear strength (ILSS)	70 MPa	
Prepreg density	1.55 g/cm^3	

Table 4: Processing conditions and mechanical properties of HexMC, 4mm press cured plaque at 150 °C for 3 min[120]

4.2. Manufacturing methods

4.2.1. Autoclave

A series of plaques were produced using the manufacturers' recommended material processing parameters, as shown in Table 5. This provided a comparison between autoclave moulding, the most common processing method for continuous fibre pregregs, and compression moulding. It was expected that the material properties would be lower as a result of the less controllable compression moulding manufacturing process.

Autoclave moulding parameters	
Plaque size	300x300 mm
Ramp	2 °C/min
Temperature	110 °C
Dwell time	18 min
Cool rate	2 °C/min
Pressure	7 bar

Table 5: Autoclave moulding parameters for benchmarking against compression moulded prepreg

4.2.2. Compression moulding

A Daniels upstroke press was used to manufacture the plaques in the study, providing up to 150 bar pressure over a 32 inch diameter piston. There are two sets of four 1 kW heater cartridges to provide the curing for the plaques, as shown in Figure 31. Inserted in the centre of the male tool is a Kistler 6162AA mould cavity pressure sensor. This is suitable for low viscosity crosslinking moulding compounds for temperatures of up to 200 °C.

Figure 31: Daniels upstroke press with heaters and pressure transducer labelled

4.2.2.1. Tooling

The compression moulding tool is intended to manufacture square plaques with the dimensions of 406x406 mm, with 18 mm radii corners and a flash gap of 0.15mm.The plaque thickness can be controlled by stops. The tool is fitted with a 100x100mm ejector plate in the centre that can be seen in Figure 32, which is connected to an 8 bar pressure airline to assist in part ejection.

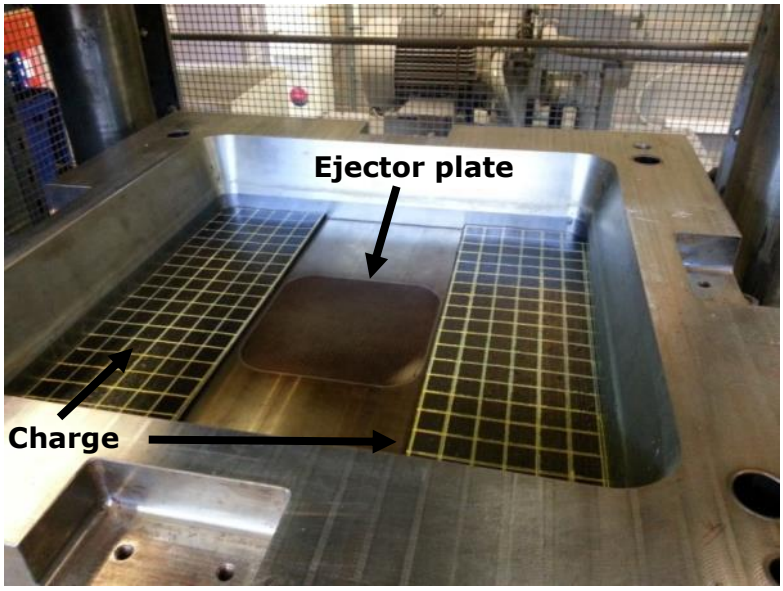

Figure 32: Charge location within compression moulding tool cavity with square central pneumatic ejector plate

Physical contact between the two metal halves, called matched tooling was not used during moulding to ensure a constant pressure was applied to the charge. This meant that the male and female parts of the tooling do not make contact and pressure is completely transferred through the part. Consequently, the mass of the charge determines the final part thickness.

4.2.2.2. Mould release agent

The mould release agent used to aid component removal from the tool was Frekote 700-NC, which is designed for thermosets and prepregs [121]. The release agent was applied at a tool temperature of 50 °C, which aids the evaporation of the solvent. Prior to a series of mouldings, seven layers of Frekote are applied, waiting for evaporation between each application. This is sufficient for multiple mouldings, however if the part begins to stick to the tool further layers of Frekote are applied at temperature (130 °C).

4.2.3. Charge construction and positioning

4.2.3.1. One dimensional study

The notation used to describe a charge and plaque construction is shown in Figure 33. To provide an example, U3 90° H2 60% is shown in Figure 34, consisting of three plies of UD aligned at 90 degrees to the flow direction placed on top of two plies of HexMC, with a tool charge coverage of 60%. As it is a one-dimensional flow scenario, the two charges are 122x405mm^2 each.

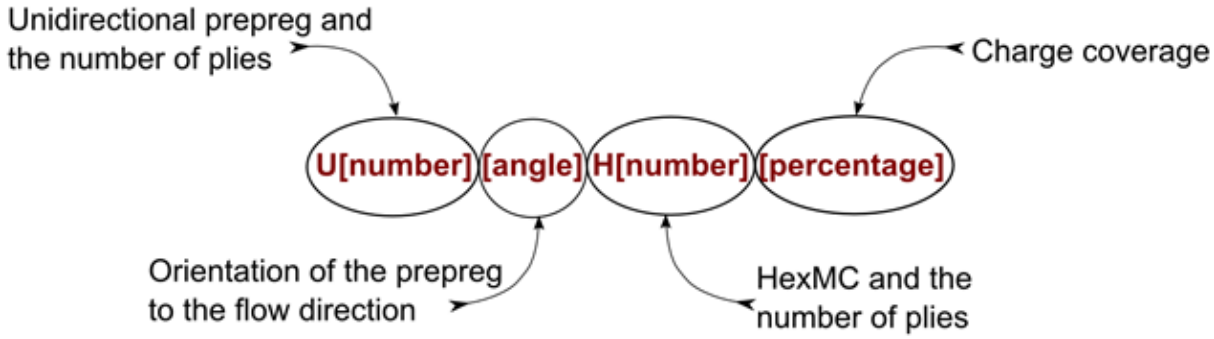

Figure 33: Explanation of charge construction notation

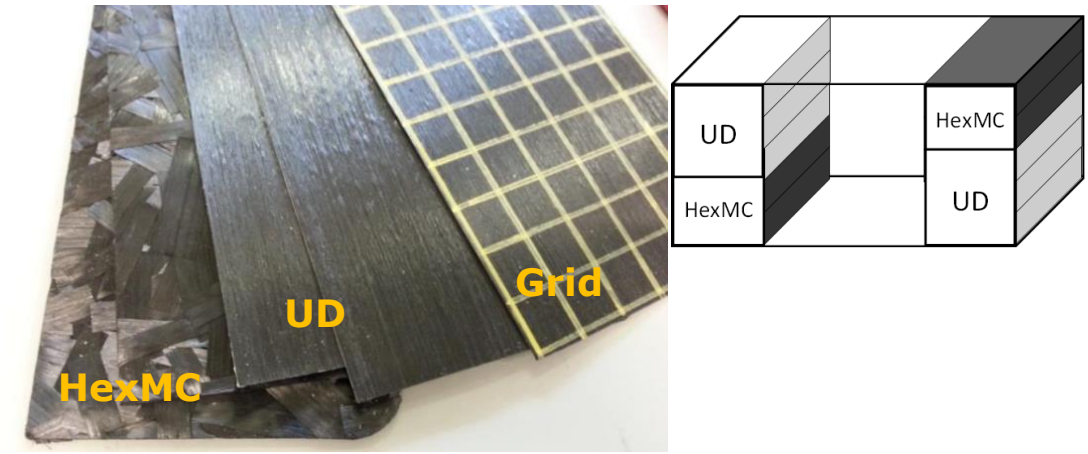

Figure 34: U3 90° H2 60% charge (122x405mm^2), spread out so each ply is visible, with a 20x20mm grid, drawn on the upper UD ply, with diagram to show charge layup within the cavity

Prior to moulding the material is first allowed to defrost from storage before it is cut into the required dimensions, assembled into a charge and placed in the tool. If debulking or staging is required, the reinforcement is debulked for 15 minutes or staged in an oven for the required duration prior to charge assembly.

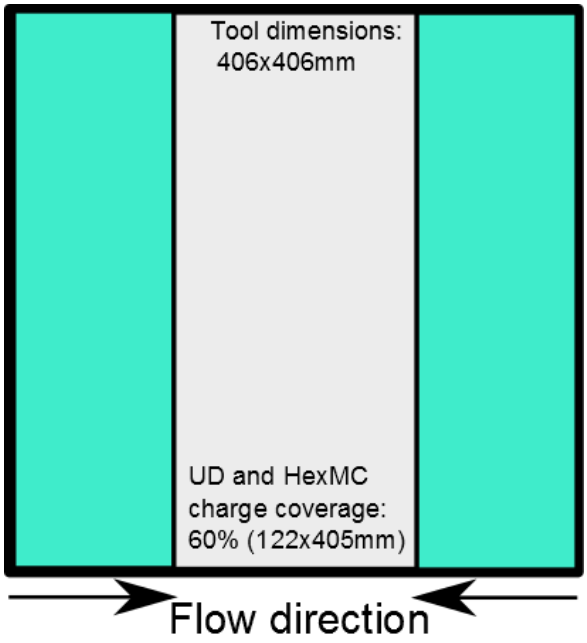

Figure 35: Two charges of UD and HexMC placed on either end of the tool, flowing to the centre in a one dimensional flow scenario

The moving lower platen of the press is floating and uses locating pins to guide into the male tool, which ensures a constant flash gap. If the charge is placed

off-centre within the cavity, this can cause the floating platen to tilt, resulting in an irregular plaque thickness. To ensure plaques manufactured during the flow studies had a constant thickness; two identical charges were placed at either end of the tool, as shown in Figure 35. Both charges flow at approximately the same rate towards the centre of the tool, where a weld line might occur. This was considered to be acceptable for this study because testing would be conducted away from this region. However, this would be undesirable in practice, as weld lines are well known to produce planes of weakness. .

4.2.3.2. Two dimensional study

A separate study was conducted to increase the complexity of the charge flow by adding flow in both the *x* and *y* direction. This was conducted to utilise the lessons learned in the one dimensional flow scenario to a more complex study and to determine if they were still applicable. For repeatability, the moulding parameters were kept constant as in the one dimensional study

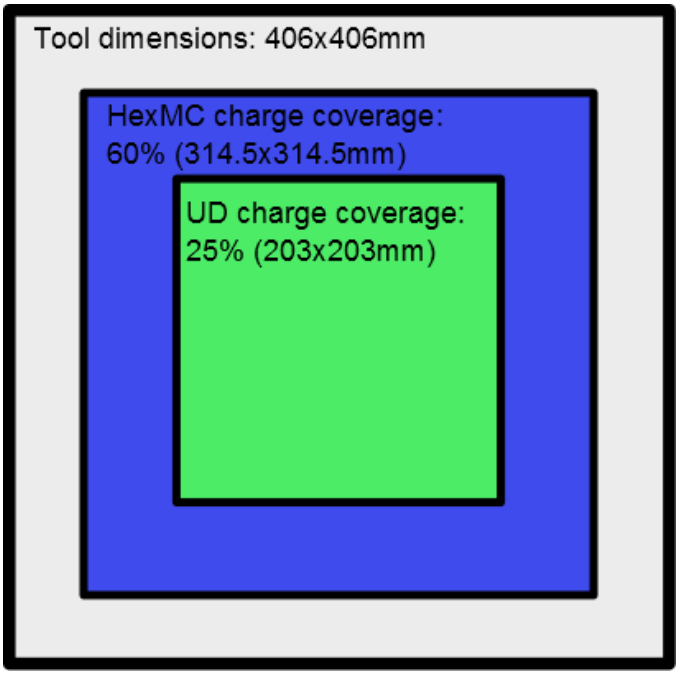

Figure 36: Diagram of 2D flow scenarios charge design and location

In the 2D hybrid study, the UD was placed on top of the HexMC, with a charge coverage of 25% and 60% respectively. This assembly was then placed in the centre of the cavity as illustrated in Figure 36. The smaller charge coverage of the UD reinforcement was to prevent voids, by using a pyramidal charge. It has also been observed in the literature [38] that the charge front is chaotic;

therefore, it may be desirable to keep the reinforcement away from the flow front to prevent disruption.

4.2.3.3. Three dimensional study

A three dimensional demonstrator was made to investigate the effect of flow in the *z* axis. For cost effectiveness the female cavity did not change and the male section was replaced as shown in Figure 37. Four pneumatic ejector pins were added around the centre to aid part removal, and an optional metallic insert could also be added. The profile of the tool was chosen to provide the opportunity to demonstrate a series of features not possible with a flat plaque. This male tooling included ribs and a changing thickness throughout the plaque, being thickest at the edge (20mm) decreasing towards the centre (1.8mm). Incorporating ribs of 10 mm deep and 5 mm wide at the base is important as it is the main method designers use to add stiffness to a component, but creates flow in the *z* axis. This complexity was investigated as it is possible that the HexMC will pull the continuous UD fibres into the ribs.

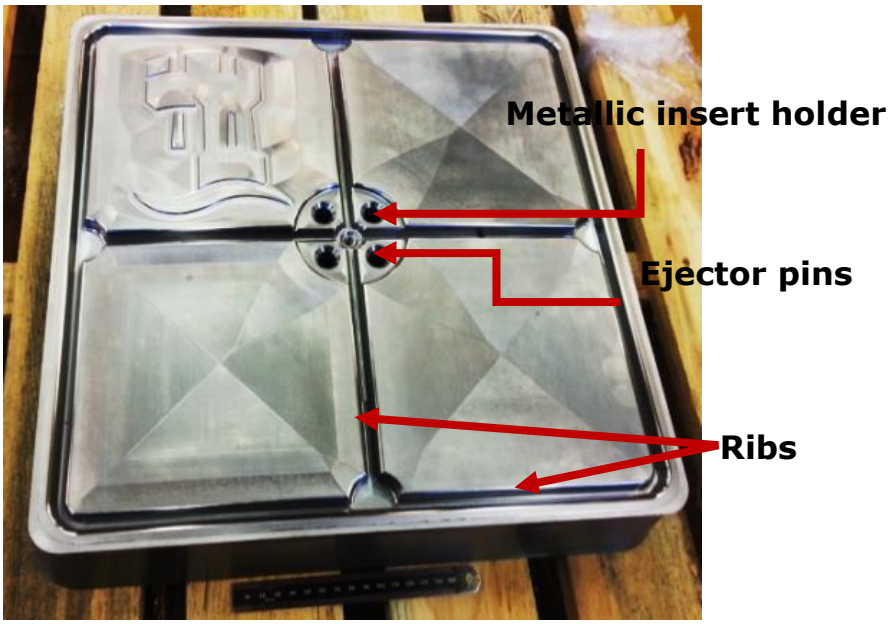

Figure 37: Male section of compression moulding tool

Specifically designed M8 metallic inserts were provided by bigHead™, as shown in Figure 38. The large flange with holes allows resin and fibres to flow into them, locking the insert in place. These were pushed onto a holder in the male tool prior to moulding, using a spring to hold the insert in place.

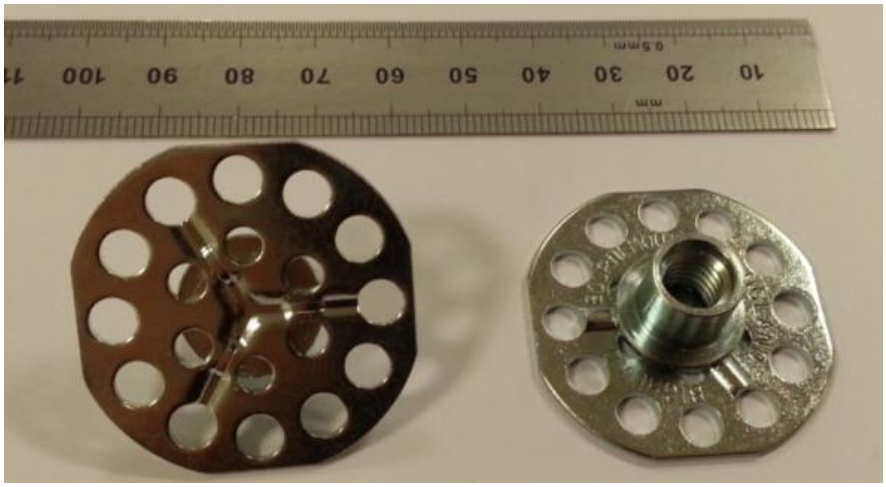

Figure 38: M8 bigHead insert with machine recess for in mould insertion

The tool was initially commissioned with a high filler-content polyester/glass SMC (Menzolit SMC 0390 47-5317) supplied by Oxford Plastics, as shown in Figure 39. The glass SMC was the initial attempt to test the feasibility of the tool to ascertain if a quality component was possible on a material that flows more readily and has a higher shrinkage. After a series of successful trials a HexMC component was produced, with a few minor defects. These initial trials highlighted the importance of charge design which was carried forward in the hybrid study.

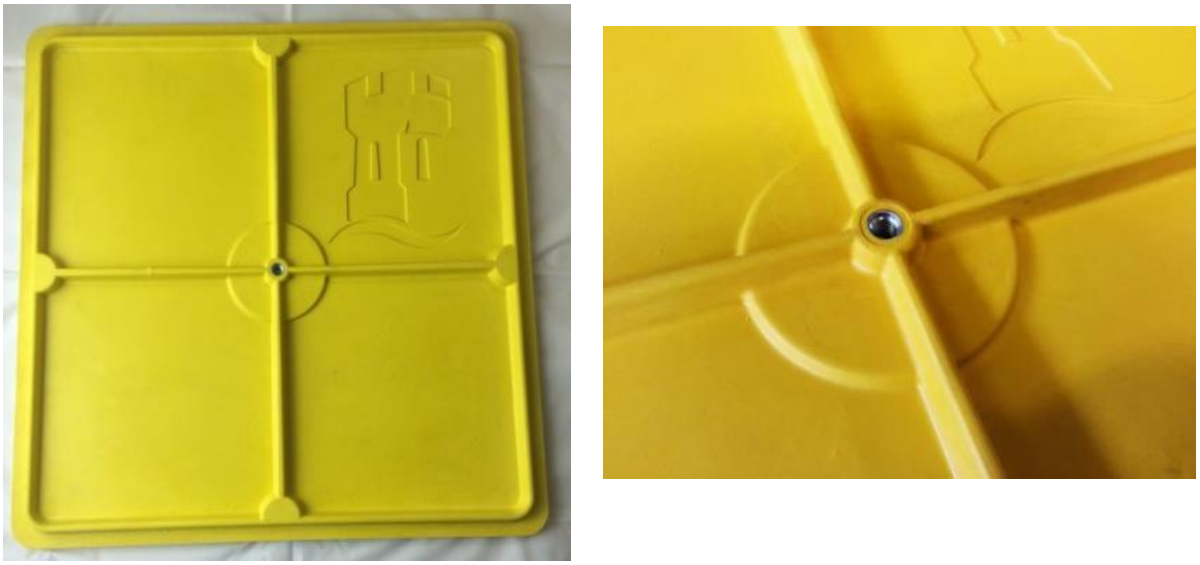

Figure 39: Heavily filled glass SMC with bighead™ insert, Oxford Plastics Verkid PG25-H350, colour RAL 1023.

Figure 40: HexMC M77 3D component without metallic insert

Three dimensional components were initially manufactured from HexMC, using two different charge designs. A simple net-shape charge of 8 plies of 405x405mm squares did not produce encouraging results as there were an increased number of voids. Instead, a charge with the lower half being net-shape and four towers of HexMC with the split at the ribs, shown in Figure 41 was used. This prevents fibres bridging at the rib entrance and encourages flow into the feature[46]; this alternative arrangement was successful.

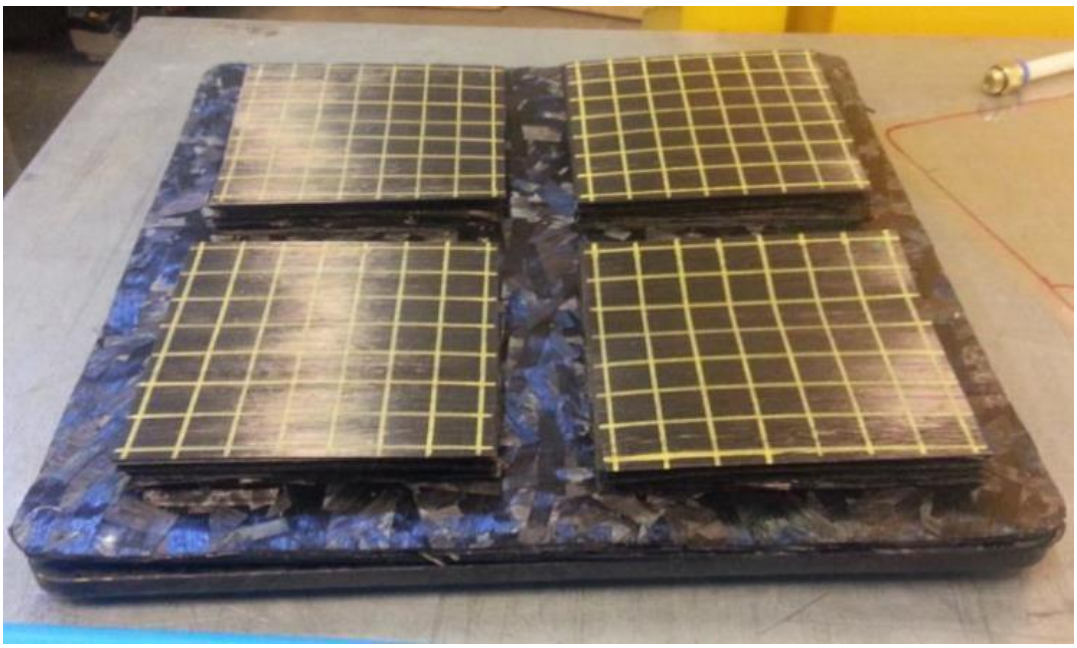

Figure 41: Tower type hybrid charge construction

As the UD prepreg had no tack, an adhesive (Airtac 2E Airtech) was used. This was because the UD placed on the towers and under the charge as shown in

Figure 41 were prone to slipping when being placed quickly in a hot cavity that has limited access.

4.2.3.4. Compression moulding parameters

The moulding parameters used in the one and two dimensional trials are shown in Table 6. The temperature was set to 130 °C to prevent gelation creating drag marks on the HexMC during closure. The manufacturer recommends a 6 minute cure at 130 °C; however, an extra 2 minutes was added as the material was still pliable. There was warpage if there was difficulty in getting the plaque out of the tool, this was because the plaque was above the glass transition temperature of 125 °C.

The material was placed in the hot cavity (130°C), which was then promptly closed. After the dwell of 8 minutes the press is then opened at the part is removed. The press maintains temperature throughout the process. This kept to ensure the die's do not stick due to difference in heating rates of each half and to prevent hot/cold spots.

Parameters	
Pressure	84.5 Bar
Temperature	130 °C
Closure Speed	2.5 mm/s
Dwell	8 minutes

Table 6: Compression moulding parameters for all compression moulding trials

The moulding parameters are different from the manufacturer's recommendations for HexMC and UD, as there needs to be a compromise between the two materials. Whilst the resins were matched to allow for the same cure time, the applied pressures need to be different, as HexMC requires flow for homogenisation and consolidation, whereas high pressure on UD could lead to fibre fracture and distortion. Moulding HexMC below 80 bar leads to a range of defects, such as fibre matrix separation and blistering. The solution was to mould the UD at the same pressure as the HexMC. It was advised that higher

pressures were beneficial for HexMC, and 84.5 bar was found to be sufficient for this study.

4.2.4. Out-of-autoclave (OOA)

An out-of-autoclave manufacturing method was used to evaluate the bonding between staged and non-staged pregreg. This process was preferred as it produced minimal material flow and a closer temperature profile to compression moulding. Additionally, it allowed smaller plaques to be manufactured.

The manufacturing sequence and parameters are shown in the flow diagram in Table 7 and Figure 42. Three plies of UD were stacked together if the staged UD was to be debulked. Corking was placed around the prepreg to prevent flow and excessive resin bleed during curing and a 5mm aluminium plate was placed on top to ensure a good surface finish. This arrangement, shown in Figure 43, was debulked for 15 minutes, before being placed in a Heraeus Function Line oven and staged for the required duration. If the prepreg was not debulked prior to staging, then the UD was stacked loosely together and placed directly in the oven.

Parameters	
No. of plies	6 (3 staged on top of 3 non-staged)
ply orientation	0°
Sample size	150x150mm
Temperature	Preheated to 130°C
Cure time	1 hour
Weight placed on prepreg during cure cycle	50kg (equivalent to: 0.218 bar)
Cork edge damn	
Vacuum held throughout cure cycle	
Debulking every 3 plies	

Table 7: Out of autoclave moulding parameters for inter laminar adhesion testing

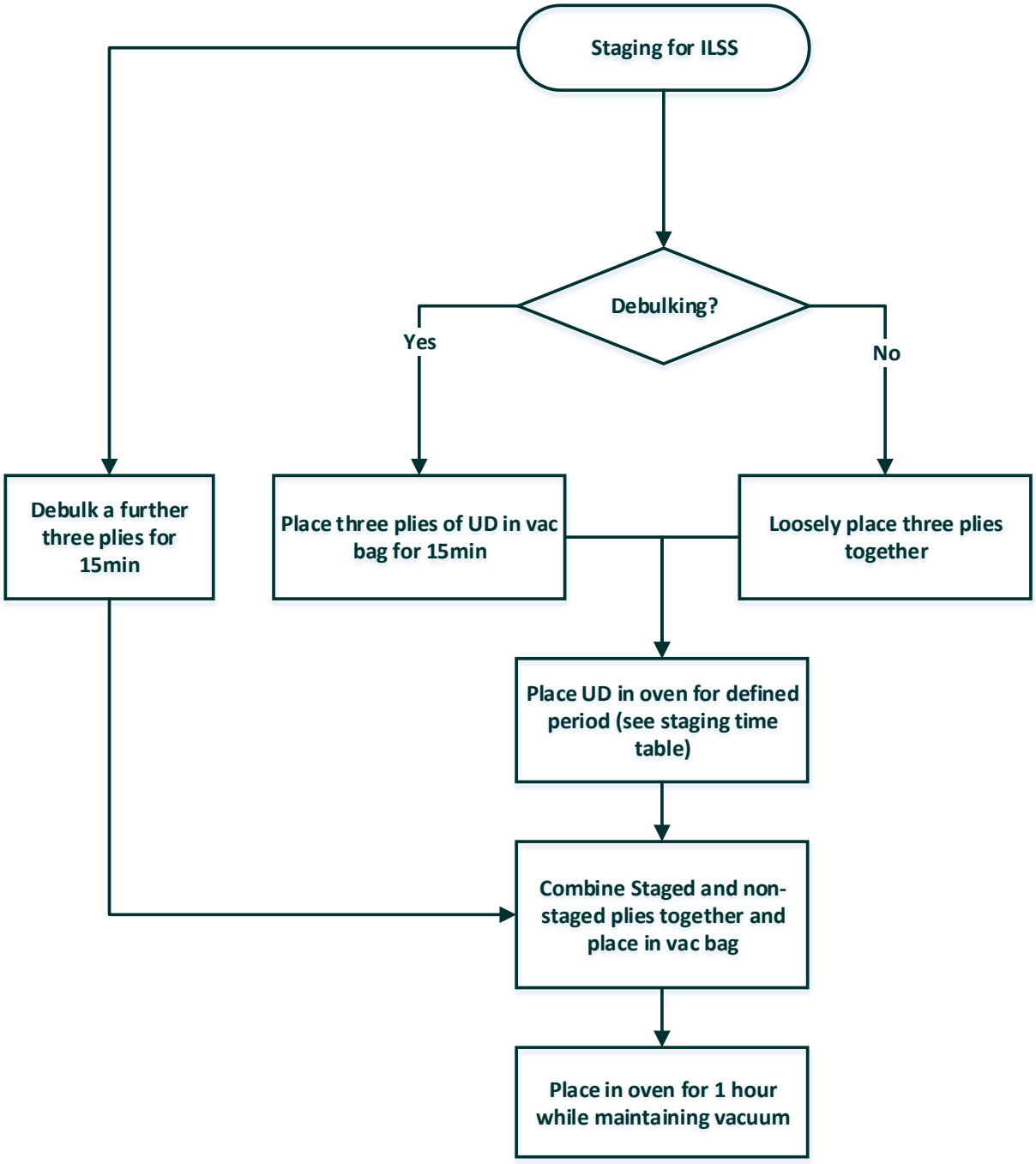

Figure 42: Process of staging for ILSS tests

Another three plies of UD were then placed in the vac bag and debulked for 15 minutes. The staged stack was then added to the other three plies in the vac bag and debulked again. This was then placed in the oven for 1 hour with a 50kg mass placed on top to aid consolidation. A vacuum was maintained throughout curing.

Figure 43: Bagging for out-of-autoclave with corking for staging trials

4.3. Testing Methods

4.3.1. Flexural modulus testing

The flexural testing method is based on *BS EN ISO 14125:1998+A1:2011, Fibre-reinforced plastic composites — Determination of flexural properties*[107]. For pure HexMC and UD specimens, the span-to-thickness ratio was kept at 40.5 as shown in Table 8. During the hybrid studies, a shorter span of 25 inner to 75 outer was used and was kept constant to improve testing resolution. The flexural testing was conducted within the elastic limit of 0.2% strain. This enabled multiple tests to be performed along a single flexural specimen as illustrated in Figure 44 producing a plaque stiffness map. This was conducted through non-destructive flexural 4 point bending test, within the elastic limit on one section of a specimen, after the test the specimen was slid across to a new section of the same specimen to be between the loading members and retested, as shown by F_1,F_2 & F_n in Figure 44.

Four point bending			
	Constituent material		**Hybrid**
Span ratio	40.5	**Outer span**	75 mm
Roller diameter	5 mm	**Inner span**	25 mm
Testing velocity	1 mm/min		
Load cell	5 kN (100N for UD transverse)		
Specimen width	15 mm		

Table 8: Pure scenarios and hybrid study four point bending parameters

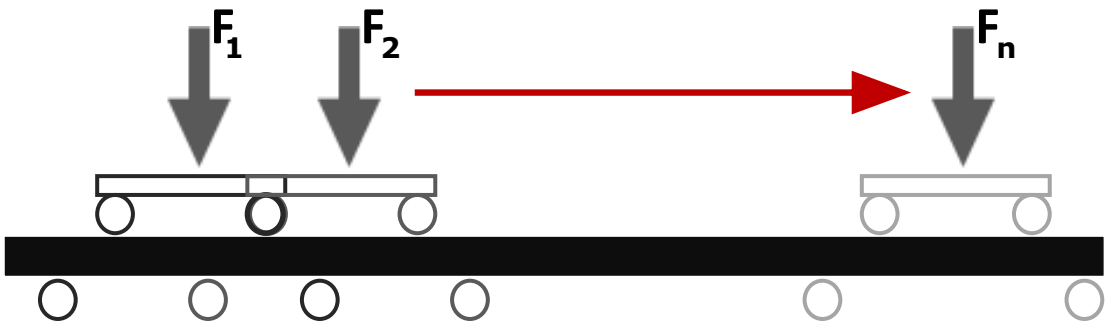

Figure 44: Incremental flexural testing along a single specimen,

4.3.2. Flexural strength testing

There is no hybrid composite mechanical testing standard available for SMC and continuous fibre hybrid composites. For UD it is recommended [107] to have a 40.5 span to thickness ratio and 16.5 for SMC, to prevent shear failure. For testing the flexural strength i.e. to failure, a 40.5 ratio was used to ensure deformation due to shear was not affecting the flexural properties of the specimen.

The testing for flexural strength was conducted using a very similar process, with the same load cell, specimen dimensions, span-to-thickness ratio and roller diameter. The testing speed was increased to 5mm/min, which was still within the recommended testing standard (*BS EN ISO 14130:1998 Fibre-reinforced plastic composites — Determination of apparent interlaminar shear strength by short-beam method)*. Each set of samples were split in two, testing half with the

UD under compression (UD face up) and half with the UD under tension (UD face down). Each specimen was first marked to ensure the same testing location was used and a modulus was taken using an LVDT, similar to the flexural modulus testing. After all the moduli were recorded, the LVDT was removed to avoid damaging the equipment during the sample fracturing.

4.3.3. Interlaminar shear strength

Interlaminar shear strength was measured to understand the level of adhesion between the staged and the non-staged prepreg,. This allowed an understanding on the effect the degree of staging has on the bonding between the reinforcement and the moulding compound.

The interlaminar shear strength (ILSS), or short beam shear test, of carbon fibre composites is a simple method to determine the adhesion between the individual plies of prepreg, which is essentially a 3 point bending test with a small span-to-thickness ratio, as shown in Figure 45. This is done by measuring the maximum load required for the specimen to fail (Figure 45), which is calculated as the maximum shear stress. There are other methods, such as double lap shear and double cantilever beam test, but these require more complex setups and larger specimens.

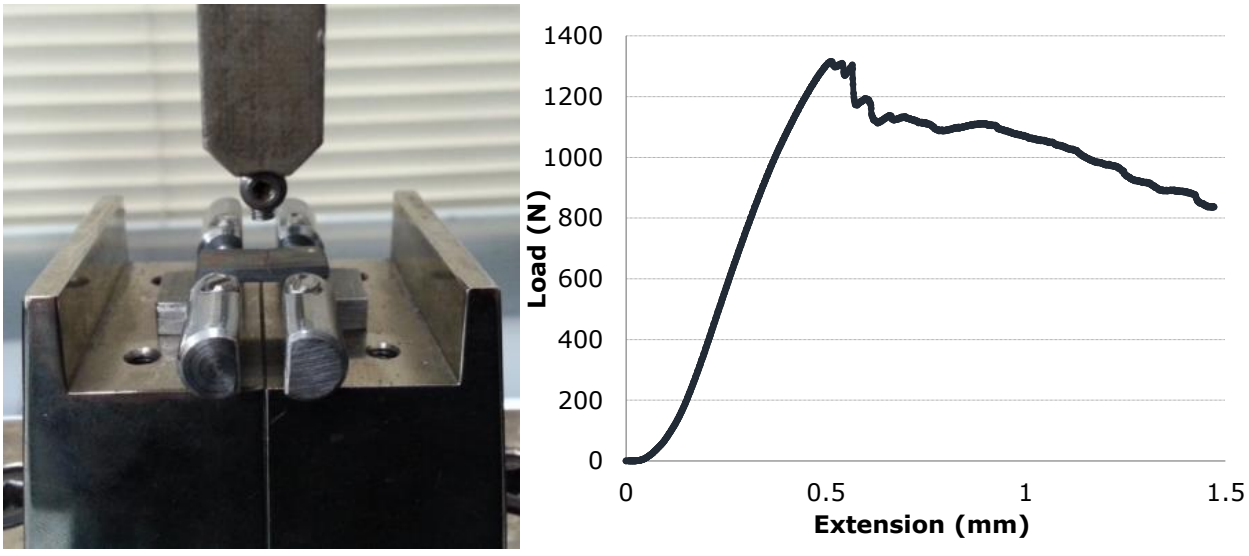

Figure 45: setup of ILSS, with 5 mm and 2 mm diameter loading and support rollers respectively with representative ILSS data of 50% staged

The ILSS tests used the standard: *BS EN ISO 14130:1998 Fibre-reinforced plastic composites — Determination of apparent interlaminar shear strength by short-beam*. The only deviation from the standard is where a 2mm specimen thickness is not possible, since the individual ply thickness is predefined. The standard was followed by applying the appropriate thickness correction factor.

ILSS testing was undertaken on symmetric UD composites, consisting of three plies of staged UD on three plies of unstaged UD. The symmetric layup was to ensure that there was no bias between the two materials and the shear stress through the thickness was symmetric. This would not have been possible with HexMC because of the localised thickness variability, which would have led to a bias on the stress distribution.

Due to the ply-by-ply construction, there tends to be resin concentrations between each layer which allows cracks to propagate in the ILSS test. It has been found by multiple authors [122, 123] that void content dominates the degradation of ILSS properties. This is because pockets of air tend to get trapped in between the plies, in the resin-rich region [124]. This enhances the weakness between the two materials, as the staged material will have reduced flow and this will create more voids between the staged plies.

4.3.4. Density measurement

After flexural testing, the specimens where cut on a diamond saw between the loading spans to provide a localised fibre volume fraction (V_f) measurement to correspond to the flexural modulus test location. The samples ranged in length from 12mm to 24 mm, 15 mm wide, and ranged in thickness from 0.6 mm for a UD plaque up to 3.5mm for a hybrid plaque. After cutting with a diamond wheel, the carbon fibre specimens were deburred with P600 abrasive paper to remove splinters from the edges. This was done to prevent bubbles adhering to rough sections or getting trapped, which would increase buoyancy and provide incorrectly high resin content (low V_f).

To identify the V_f, a Mettler Toledo XS105 Dual Range scale with a repeatability of 0.02 mg was used to measure the sample density (S_ρ), with the set-up shown in Figure 46. Assuming a known density of the constituents: the fibres (F_ρ) and resin (R_ρ), the V_f was calculated. A wetting agent was used to prevent bubbles

adhering to the surface of the specimen (Pervitro 75%). Three drops where added per 250ml of de-ionised water.

$$V_f = \frac{\rho_s - \rho_r}{\rho_f - \rho_r} \quad (8)$$

Where

V_f = Fibre volume fraction (%)

ρ_s = Sample density (g/cm^3)

ρ_f = Density of fibre (g/cm^3)

ρ_r = Density of resin (g/cm^3)

Figure 46: Mettler Toledo XS105 Dual range scale

4.3.4.1. Flexural modulus normalisation

The flexural modulus is often normalised to a constant fibre volume fraction of 55%. This is done to remove the effect of fibre content on the material properties and allow the comparison of other properties[125, 126]. This normalisation is done by:

$$E_{nf} = E_f \times \frac{0.55}{V_f} \quad (9)$$

Where

E_{nf} = Normalised flexural modulus (GPa)

E_f = Flexural modulus (GPa)

V_f = Fibre volume fraction (%)

4.3.5. Rheology

A rheometer was used to measure the change in storage modulus with respect to time at a fixed temperature. As it was not possible to obtain pure resin samples of M77 to determine the curing characteristics, prepreg was used instead. This is problematic, since it is not possible to know how much resin is present in the sample and to what extent the fibre influenced the results. The purpose of this study was to investigate the flowability of the prepreg, therefore measuring the prepreg properties during curing rather than the resin would have provided a closer representative analysis to carry forward into the hybrid scenarios.

An Anton Paar Modulus Compact Rheometer (MCR) 302, fitted with a convection temperature device CTD 450 was used in the study. A small 25 mm diameter disk of a single ply of UD prepreg was placed between oscillating parallel platens as shown in Figure 47, and run to the program defined in Figure 48.

A ramp and dwell temperature profile was used, as it could be replicated in an oven. This would allow the time measured to achieve specific cure in the rheometer be transferable to large plies of UD for staging. The storage modulus was recorded as a measure of determining the material transition from liquid to solid, so that UD would increase in stiffness sufficiently to potentially resist the flow of the HexMC.

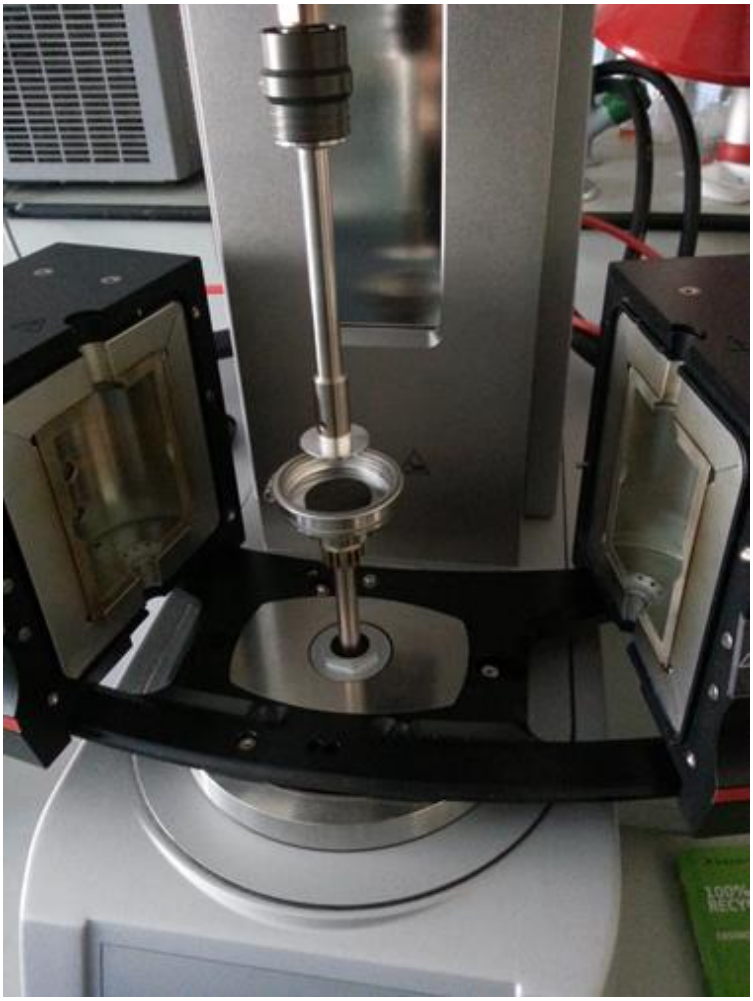

Figure 47: Rheometer setup for measuring change in prepreg storage modulus

A flat oscillating plate was used at a low strain to measure the change in the composite properties. This was to avoid the plate sliding over the surface, potentially dragging the fibres over each other, which could artificially affect the storage modulus. A low frequency was chosen as it was noted in the literature that higher frequencies may increase the rate of cure; which would be problematic as the staging in the oven would have no agitation. This would mean the oven staged UD would be less cured than intended. A nominal load of 1N was applied to ensure that during the initial stage, when the resin was liquid and able to flow, contact between the oscillating plates remained constant.

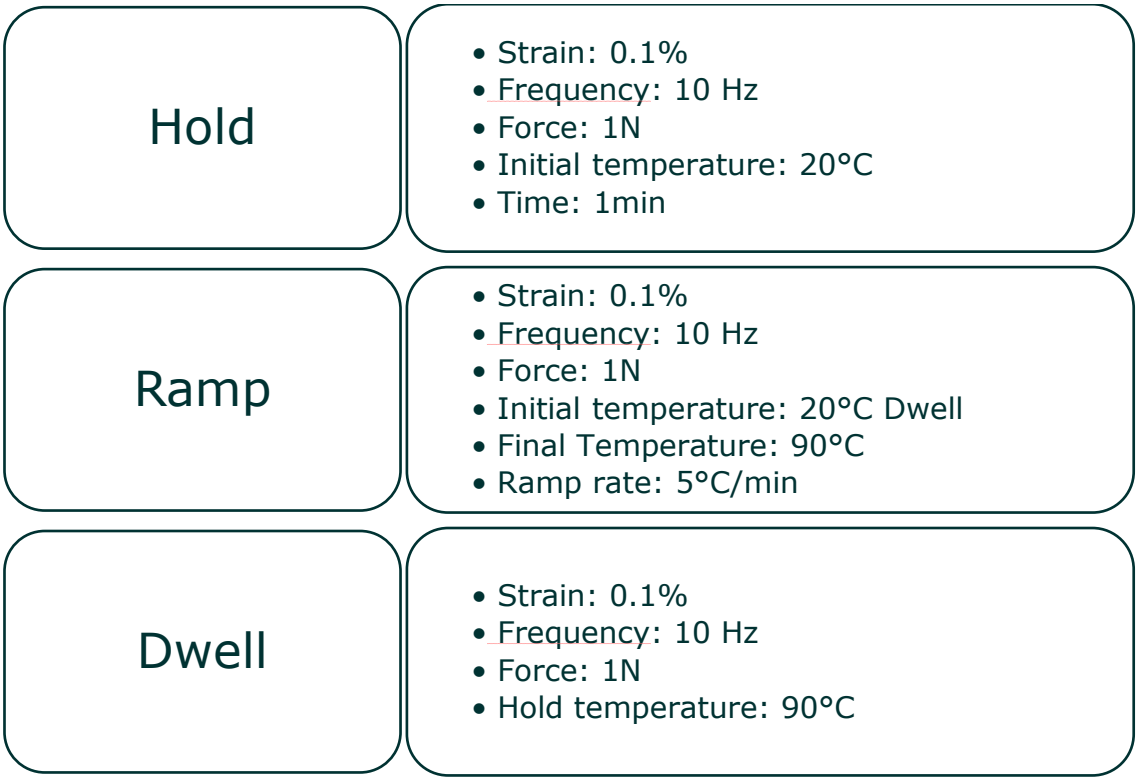

Figure 48: Diagram to show the sequence of the rheometer

4.3.5.1. Prepreg staging

When staging of the UD prepreg was required prior to moulding, the material was placed in an oven at the same ramp rate as the rheometer. The heating ramp rate was kept constant at 5°C/min and then held at 90°C for the times stated in Table 9, to achieve the desired degree of cure. Five minutes was subtracted from the staging duration due to a time delay in the initiation of the ramp in the rheometer.

Percentage cure	Time
0.5%	27 min 15 s
25%	57 min 54 s
50%	63 min 45s
75%	69 min 31 s
99%	107 min 57 s

Table 9: Staging times for prepreg for specific degree of cure

4.4. Fibre angle variation

Using surface markings to measure the distortion of the UD reinforcement is a feasible technique, as the markings generally stay with the fibres even when there is significant resin bleed out. However, there are concerns that the distortion and flow on the surface is not representative of the plies and fibres underneath. Micrographs were locally taken to asses if this was the case. The study compared the distortion in a no flow scenario, U3 100% and the UD within a hybrid, U3 90° H2 60%, which were cut at various locations using a diamond saw, cast in epoxy resin and polished to a surface finish of 5 µm. The specimen cross-sections were captured using a Nikon Eclipse LV 100ND microscope with Nikon Digital sight DS-Ri1 camera.

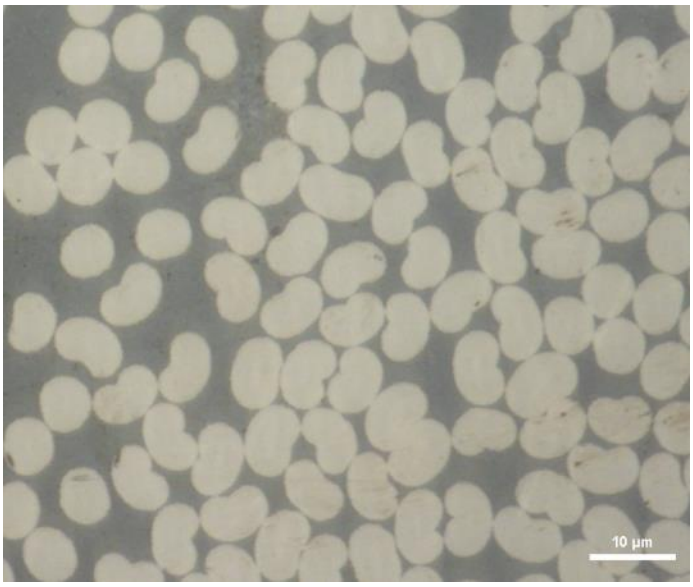

Figure 49: Micrograph of kidney bean shaped fibres, from U3 100%

Using microscopy to identify fibre angles relies on repeatable and consistent filament shapes to provide a reference orientation. After a series of micrographs had been taken, it became evident that the fibres varied in shape, being round, elliptical and kidney bean shaped, as shown in Figure 49. This was not thought to be an effect of the polishing, as the ellipses were not biased in a specific direction; the reasons for different shaped fibres have been covered in the literature review.

The ratio of the major to minor axis was used to determine the fibre angle even though there were a variety of differently shaped fibres. This section is not focusing on the absolute fibre angle value, rather the change in angle because of

the high degree of scatter seen Figure 50. A locally weighted scatterplot smoothing (LOWESS) or local regression (LOESS) of the samples was used to show the change through the thickness at different locations within the plaque, as presented in Figure 51. This showed the change in angle from the surface of the plate through the thickness in U3 100%, in a zero flow scenario where it can be assumed the fibres are aligned.

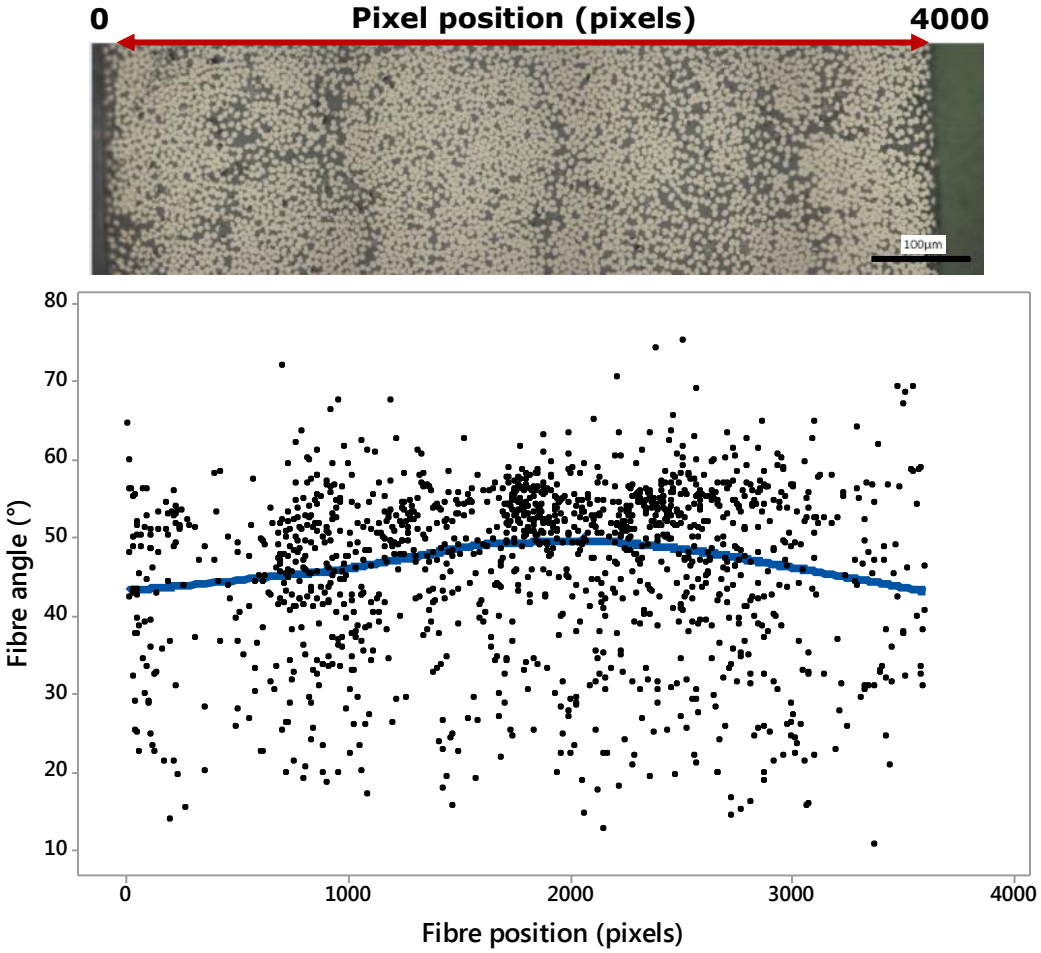

Figure 50: Fibre angle distribution of U3 100%, with LOWESS smoothing (0.5, 1), at position C1 from the diagram in Figure 51

There are difficulties in measuring the fibre angle of hybrids, due to the fibre shape, and also in distinguishing between the end of the UD reinforcement and the beginning of the SMC.

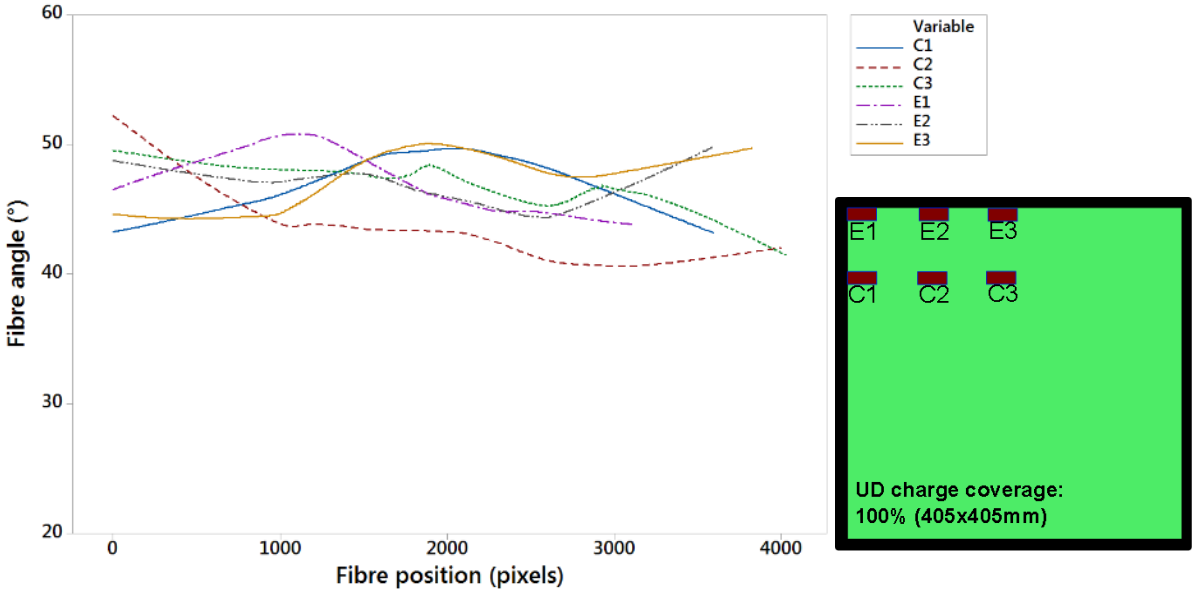

Figure 51: Fibre angle distribution of U3 100% at different positions within the plate, shown by the diagram inserted, with LOWESS smoothing parameters of (0.5, 1)

In the high flow scenario hybrid, U3 90° H2 which is shown in Figure 52, with samples taken from various places within the plaque, only 6.1 shows a discernible change in fibre angle. The other locations do not show a change in angle through the thickness from the surface to the centre of the plaque. The variations in the lengths of the lines in Figure 52 are due to local variations in UD thickness and error when locating the UD-SMC interface.

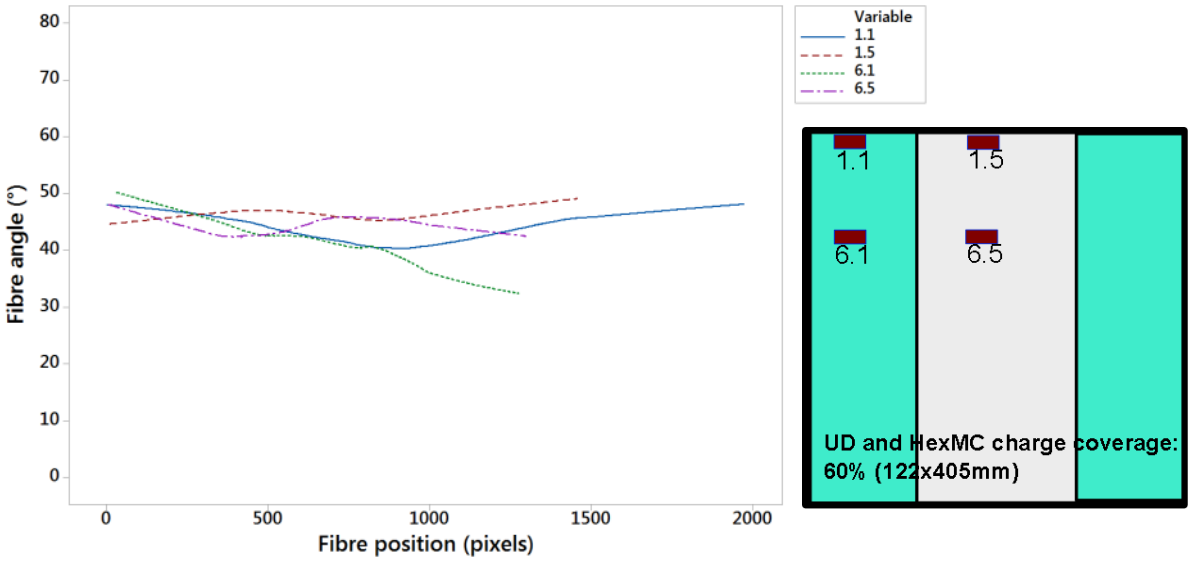

Figure 52: Fibre angle distribution of U3 90° H2, at different positions within the plate, shown by the diagram, with LOWESS smoothing (0.5, 1)

It was first observed that the reinforcement moves as a single element in U3 0° H2 migrating with the SMC. In the high and low flow regions, the reinforcement moves as a single element and there is very little discernible difference between the fibre angle on the surface and that which is in contact with the SMC. The scatter is high and it is not possible to measure the fibre angle reliably to determine with certainty there is no difference between the surface and the inner plies; however, it appears the difference is negligible. This led to the conclusion that the surface grid on the plaque is representative of the flow through the thickness on the UD reinforcement.

4.5. Image analysis methodology

4.5.1. Photogrammetry

Image analysis was used to determine the localised flow of the prepreg in UD and hybrid trials. An initial study was run on a relatively high flow scenario, U3 90° (Figure 54) plaque, to determine which colour and whether a grid or dots were optimum. This is because, high levels of localised flow could result in loss of a point, whereas a grid could be more easily extrapolated to bridge any lost markings.

The grid was drawn and then scanned to record a pre-moulding grid. It was then rescanned after moulding. The time between marking the surface and moulding was kept to at least one hour to ensure the paint had completely dried. In the instances where staging was involved, the markings where applied prior to staging.

4.5.1.1. Paint marker

A 1.2 mm Artline 440XF solvent paint marker by Shachitata Ltd was used to mark the prepreg prior to moulding, in order to measure the degree of flow. This is a fast drying and fade resistant paint marker and is stable at high temperatures, which did not appear to react with the resin. This marker was chosen above other methods, as permanent markers were washed out during the moulding and UV powder was absorbed into the resin, leaving no visible trace. Metallic filaments were considered, but these could have an impact on the mechanical properties which could distort the mechanical tests. Furthermore the

paint marker did not appear to penetrate below the top layer of the plaque, as shown in the micrograph in Figure 53.

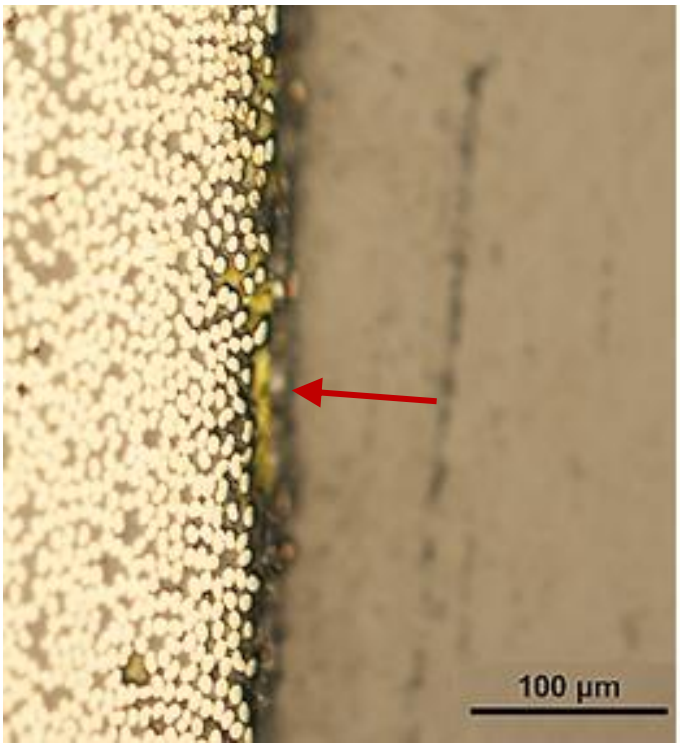

Figure 53: micrograph to show the yellow paint marker penetration into UD

Different colours were trialled as shown in Figure 54; green and blue were too dark to obtain a reliable result, especially when the markings were faint. White was clear but a bold line was difficult to produce due to the quality of the paint pen. White paint was also prone to wash-out and could not be distinguished when reflections of light were present, which created false positives. Red and yellow paint gave the best lines, and using filters during image analysis it was found that yellow was marginally better. Dots were also trialled however with the level of flow a single missing point would lead to 4 grids squares to be erased; where a line would allow interpolation between missing data.

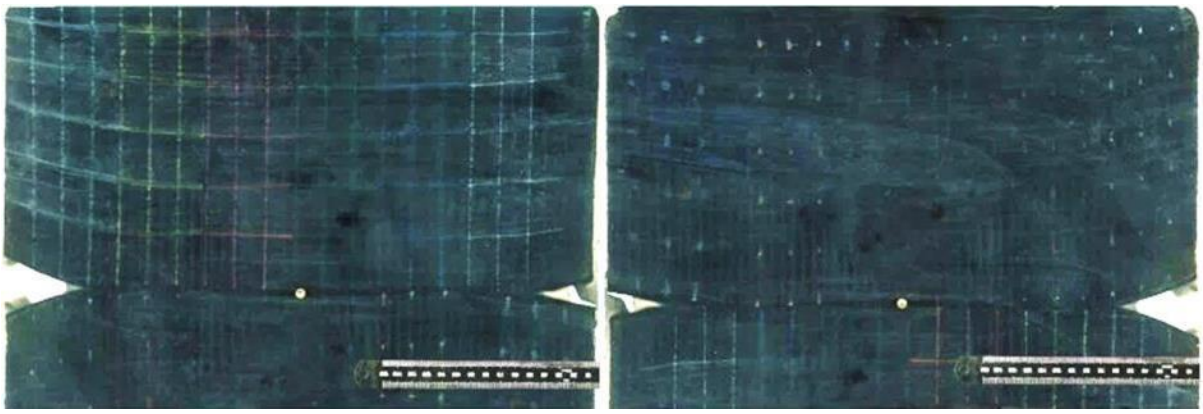

Figure 54: different colour Paint marker trials on a U3 90° plaque and determining is lines or dots were preferable.

Initially a digital camera was used to take images, however a scanner was later preferred as this had the advantage of removing the perspective correction. The random fibres in HexMC created a mat of tows, each with their own reflective properties depending on the angle to the camera. Consequently, it was impossible to take a photo of HexMC without glare. A Xerox WorkCentre 7556 scanner removed glare from the plaques, however it was only possible to take a picture of half a plaque at a time due to the size of the scanning bed. This was acceptable, as the plaques were symmetric through the centre.

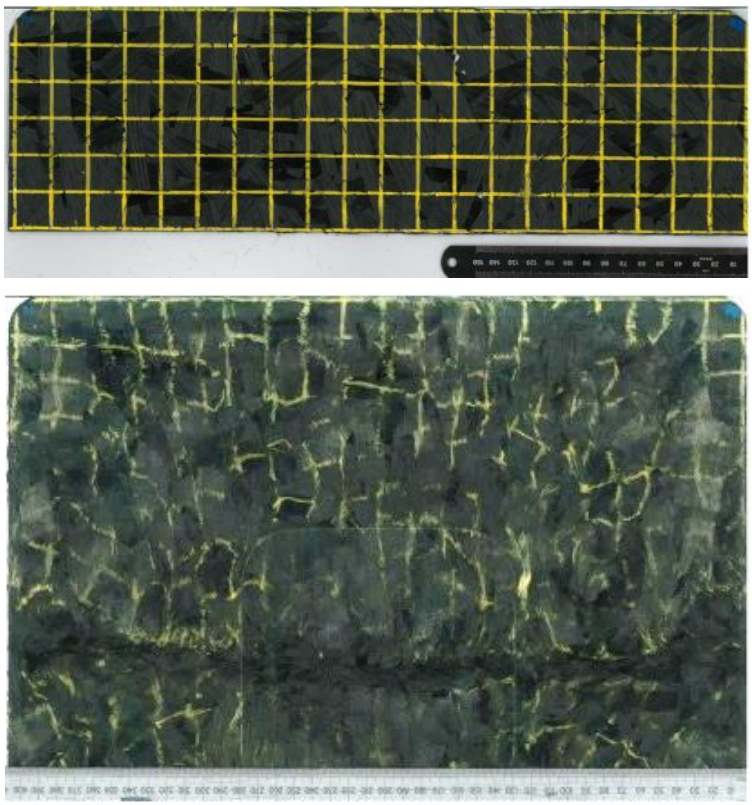

Figure 55: Grid on SMC before and after deformation

A paint grid was used to monitor the flow of the SMC, as shown in Figure 55. Due to the random nature of the flow, the internal tows were exposed to the surface and external tows were covered, this was also observed by Olsson et al.[41]. Additionally, the high level of localised flow also caused erosion of the markings. Loss of paint marking came from four factors:

1. Friction on the tool surface erasing the line
2. Deposition of the line on to the tool
3. The grid being overlapped by the resin or fibre
4. Colour bleed into the resin

As a result of the trial, it was concluded that it was not possible to effectively track the flow of the SMC using this method. The decision not to monitor the flow of the SMC was considered acceptable, as the UD is intended to dominate the mechanical properties. This work aims to investigate the performance enhancement of SMC by the addition of continuous fibres; therefore it is more important to monitor the UD than the SMC. However, it would have been advantageous to be able to monitor the SMC in the future as it would determine where the areas of high flow are occurring.

4.5.2. Node displacement capture

The images are processed in Matlab 2014b with the Image Processing Toolbox. Figure 56 shows the series of steps to obtain the coordinates of intersection points of the grid

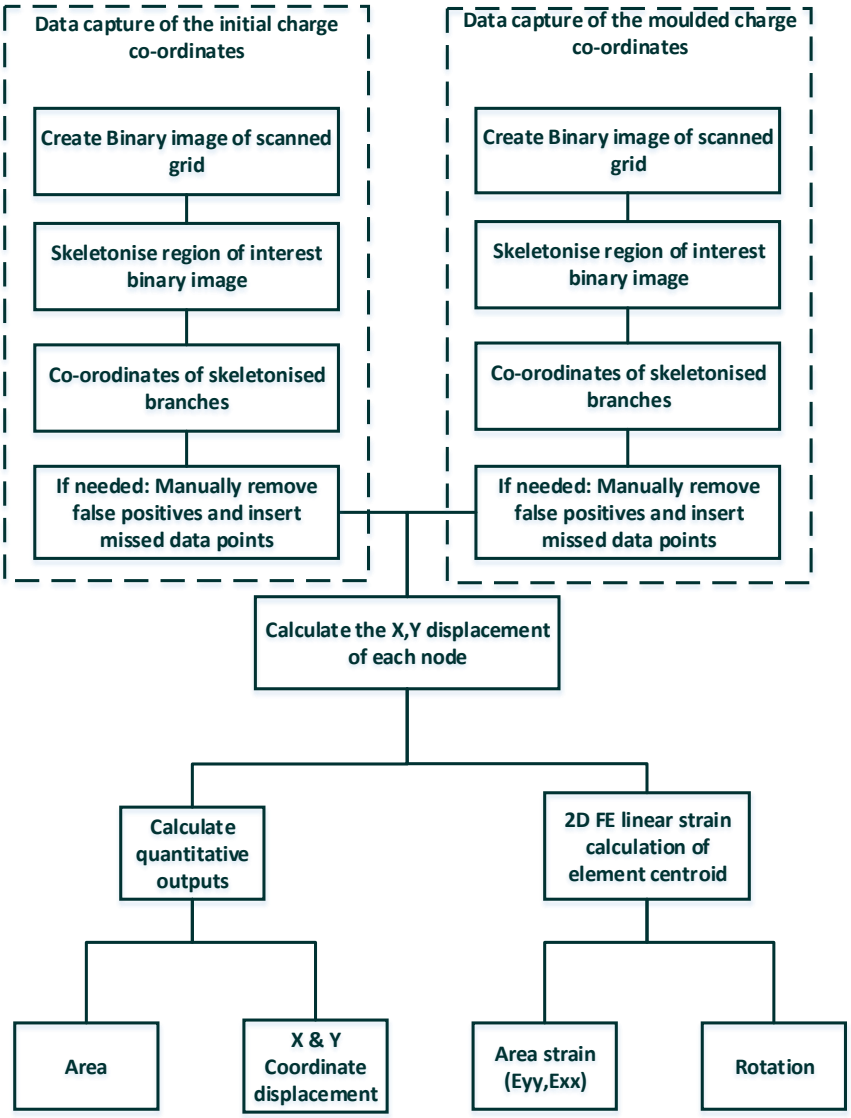

Figure 56: The flow chart of the steps taken in obtaining quantitative analysis for the grid deformation

4.5.2.1. Binary image

Once the images of the pre and post moulded plates have been scanned a binary image of each plate is created as shown in Figure 57, by setting a threshold brightness value. The lighting of the scanned images was highly repeatable; however, the moulding can cause a degree of destruction of the marked grid and change the reflective properties of the plate, as seen in the bottom of Figure 57. The thresholding level may need to be adjusted in high flow scenarios.

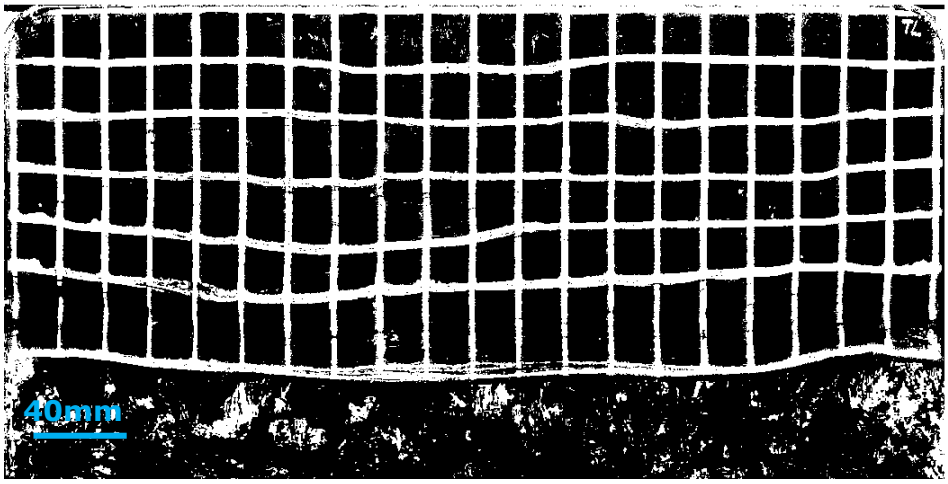

Figure 57: Binary image of plate, U3 90° H2 s25%

4.5.2.2. Skeletonisation

Skeletonisation is an inbuilt Matlab function where the binary image is eroded; however, the grid is maintained by preventing the white pixels from separating, creating a single pixel width chain. This method was chosen over other techniques as it removed the decision about the exact position of the line, and removed pixels equally from each side of the drawn line without bias.

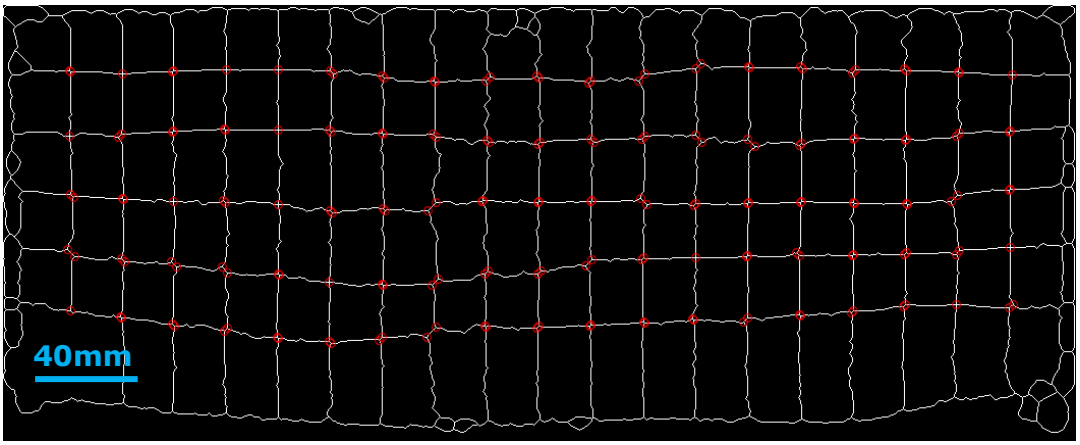

Figure 58: Skeletonised image of grid with intersection points, U3 90° H2 s25%

This was particularly relevant where a grid line would split, essentially causing a double line. A number of short spurious branch points are removed to reduce the number of false positives of the grid intersection points. The intersection points are then located as shown in Figure 58. If needed, false positives and missed points are then manually added. Figure 59 shows the plotting of the coordinates on the image of the plaque after skeletisation.

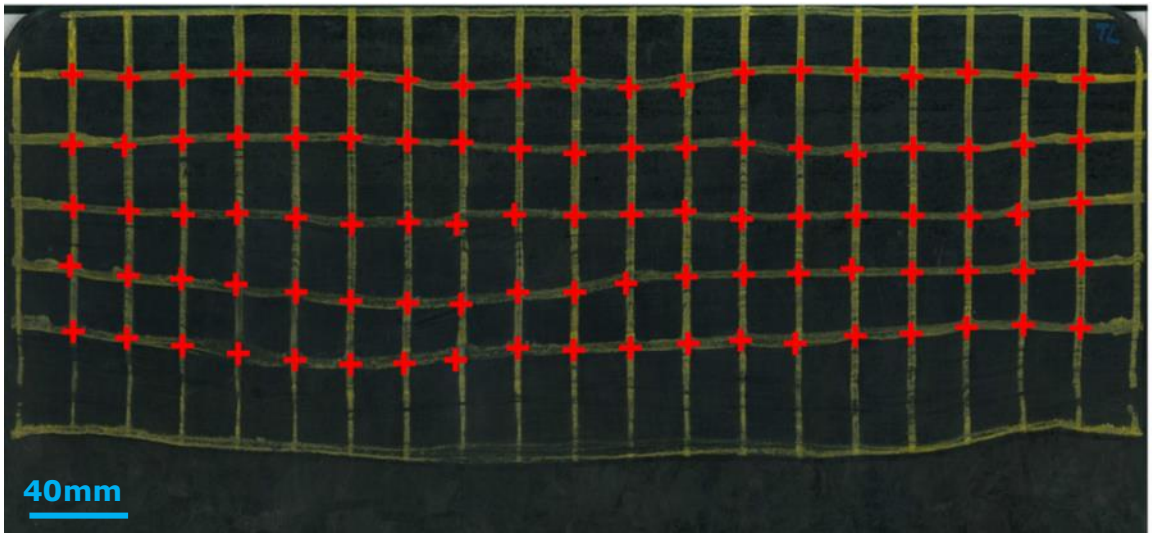

Figure 59: Intersection points of grid replotted on plate, with red crosses representing the grid intersection points. (U3H2 s25%)

This step is repeated for both the pre and post moulded plaques. This gives two sets of co-ordinates that allow the displacement of each node to be calculated.

4.5.2.3. Quantitative outputs

The grid on the surface of the reinforcement allows quantitative analysis of the deformation. This permanent deformation could be called a strain, as the material has been plastically deformed into a new shape. However, there is no residual elastic strain and the material will not recover back to the original position.

Some basic measures of deformation can be calculated by taking each node and plotting the distance travelled from position of the node in the pre and post moulded plaques. The area of each square is a measure of the deformation of the element, but does not provide information about in which axis the deformation has occurred. However, it does provide the combined *x* and *y* axis expansion/contraction of each element.

4.5.3. Four node 2D finite element analysis

The movement of the nodes between the pre and post moulded plates enables a displacement field to be calculated using four noded elements, similar to the approach of Buerzle et al. [93]. As the flow has been obstructed from view, it is assumed that the deformation within each element is linear. This permits a 2D linear four node element to be constructed from the isoparametric coordinates

r and s, the displacement u and v, and the initial co-ordinates $\mathrm{X_n}$, $\mathrm{Y_n}$ from[127], enable the calculation of the in plane element rotation and extension, as show in Figure 60.

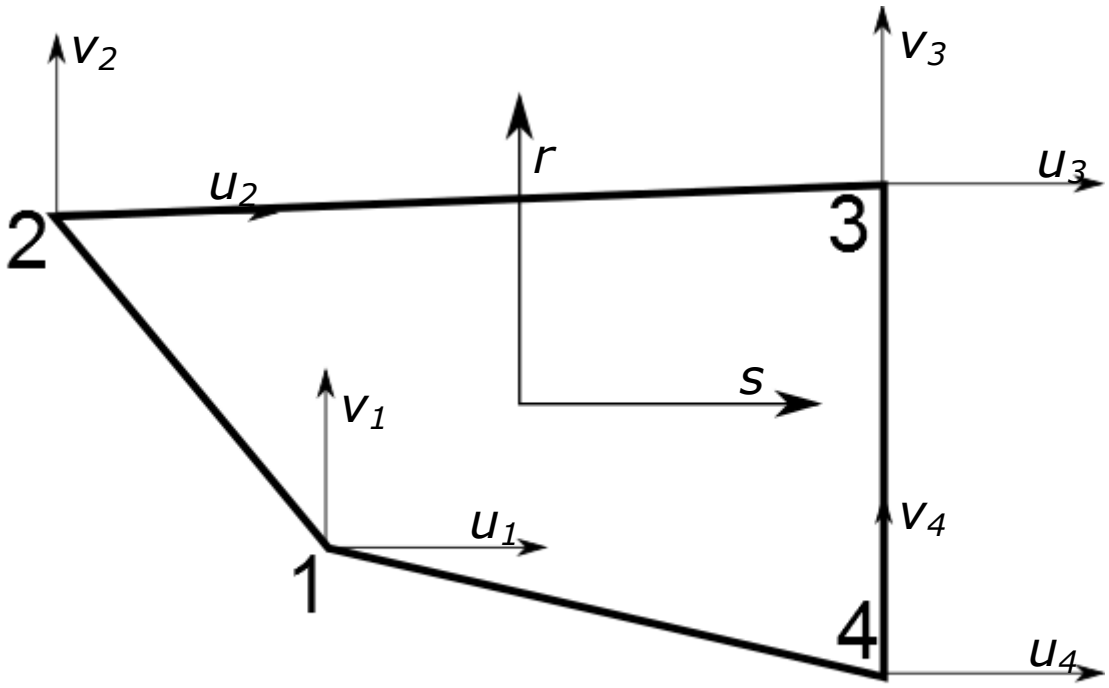

Figure 60: Isoparametric 4 node element, with the local co-ordinates (*r,s*) and the displacement functions (*u,v*)

$$\mathrm{X(r,s)} = 0.25(1-\mathrm{r})(1-\mathrm{s})\mathrm{X_1} + 0.25(1+\mathrm{r})(1-\mathrm{s})\mathrm{X_2} + 0.25(1+\mathrm{r})(1+\mathrm{s})\mathrm{X_3} + 0.25(1-\mathrm{r})(1+\mathrm{s})\mathrm{X_4} \quad (10)$$

$$\mathrm{Y(r,s)} = 0.25(1-\mathrm{r})(1-\mathrm{s})\mathrm{Y_1} + 0.25(1+\mathrm{r})(1-\mathrm{s})\mathrm{Y_2} + 0.25(1+\mathrm{r})(1+\mathrm{s})\mathrm{Y_3} + 0.25(1-\mathrm{r})(1+\mathrm{s})\mathrm{Y_4} \quad (11)$$

$$\mathrm{u(r,s)} = 0.25(1-\mathrm{r})(1-\mathrm{s})\mathrm{u_1} + 0.25(1+\mathrm{r})(1-\mathrm{s})\mathrm{u_2} + 0.25(1+\mathrm{r})(1+\mathrm{s})\mathrm{u_3} + 0.25(1-\mathrm{r})(1+\mathrm{s})\mathrm{u_4} \quad (12)$$

$$\mathrm{v(r,s)} = 0.25(1-\mathrm{r})(1-\mathrm{s})\mathrm{v_1} + 0.25(1+\mathrm{r})(1-\mathrm{s})\mathrm{v_2} + 0.25(1+\mathrm{r})(1+\mathrm{s})\mathrm{v_3} + 0.25(1-\mathrm{r})(1+\mathrm{s})\mathrm{v_4} \quad (13)$$

Where

X_n = Initial element corner co-ordinates in the X axis

Y_n = Initial element corner co-ordinates in the Y axis

X = Initial central element co-ordinates in the X axis

Y = Initial central element co-ordinates in the Y axis

r = Isoparametric coordinates

s = Isoparametric coordinates

u_n = Change in X corner co-ordinates from original position

v_n = Change in Y corner co-ordinates from original position

u = Displacement in central X co-ordinate from original position

v = Displacement in central Y co-ordinate from original position

Using the linear shape function enables the element rotation and engineering strains ε_{yy} and ε_{xx} to be calculated:

$$\begin{bmatrix} \frac{\partial u}{\partial X} & \frac{\partial u}{\partial Y} \\ \frac{\partial v}{\partial X} & \frac{\partial v}{\partial Y} \end{bmatrix} = \begin{bmatrix} \frac{\partial u}{\partial r} & \frac{\partial u}{\partial s} \\ \frac{\partial v}{\partial r} & \frac{\partial v}{\partial s} \end{bmatrix} \begin{bmatrix} \frac{\partial X}{\partial r} & \frac{\partial X}{\partial s} \\ \frac{\partial Y}{\partial r} & \frac{\partial Y}{\partial s} \end{bmatrix}^{-1} \tag{14}$$

$$\varepsilon_{xx} = \frac{\partial u}{\partial X} \tag{15}$$

$$\varepsilon_{yy} = \frac{\partial v}{\partial Y} \tag{16}$$

Where

ε_{xx} = Element extension in the X axis

ε_{yy} = Element extension in the Y axis

The shape functions are used to calculate the deformation gradient **F**. Polar decomposition gives the element rotation, **R**, and element stretch and compression, **U**. The centre of each element was considered for the average rotation, similar to the average four point bending method used to extract localised stiffness.

$$\mathbf{F} = \begin{bmatrix} \frac{\partial u}{\partial X} & \frac{\partial u}{\partial Y} \\ \frac{\partial v}{\partial X} & \frac{\partial v}{\partial Y} \end{bmatrix} + I \tag{17}$$

$$\mathbf{F} = \mathbf{RU} \tag{18}$$

Where

F = deformation gradient

R = Element rotation

U = Element extension

With four node isoparametric elements it is possible to calculate the strain across each element, since the rotation within each element is not constant at each corner. However, this increased resolution does not benefit the analysis, as the resolution of the flexural tests is limited to 15x25 mm; which is similar to the resolution of the grid itself. Therefore, central strain and rotation are considered appropriate.

4.5.4. Theoretical flexural modulus

The image analysis and density testing are done in order to be able to predict the stiffness of a given area, without the time consuming and costly method of mechanically testing each section. By measuring the surface deformation of the UD it was possible to predict the stiffness of the hybrid composite, even though the SMC underneath has undergone a significant amount of non-homogenous and disruptive flow.

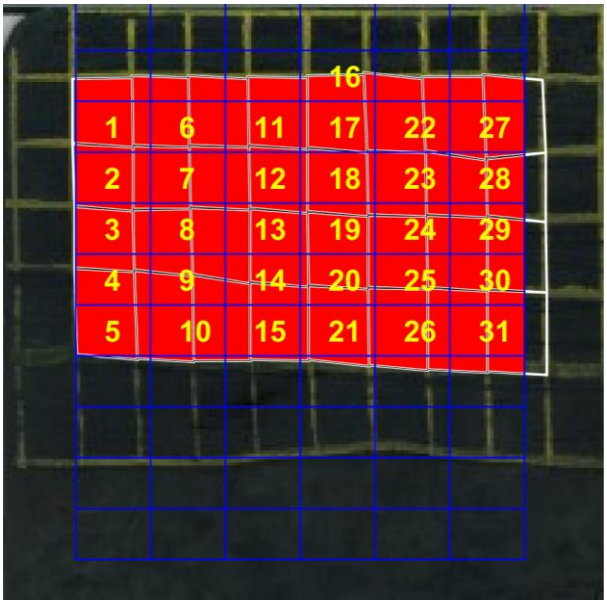

Figure 61: The overlapping of the image analysis grid with the testing specimens. The numbers correspond to the used specimens in the theoretical calculation

As a flexural modulus specimen spans across the photogrammetric grid, a weighted average was used to assign a rotation and extension to each experimental flexural modulus. This was done by interpolating the different measurements taken during the process. Figure 61 illustrates the overlapping of the test specimens (blue) with the image analysis grid (white). Where the ink grid, (white) in Figure 61 covered ≥50% of a flexural specimen area (blue grid), this value was incorporated in the theoretical stiffness calculation of a testing specimen, which can be seen in location **16**.

When $$A_s \geq 0.5 \quad (19)$$

$$\bar{x} = \sum_{i}^{n} \frac{A_i}{A_s} \times X_i \quad (20)$$

Where

A_i = Ratio of the ith grid element under the flexural specimen

A_s = Total ratio of grid elements under flexural specimen

X_i = Rotation or extension of ith element

$\bar{x}_n$ = Mean Rotation or extension of flexural specimen

n = flexural specimens

A number of assumptions were made in this model. There was a preservation of volume (no material loss). However, this is not true as there is 4-6% weight loss due to resin flash. The distortion on the surface of the UD is representative of the distortion on the UD inner plies.

A modified rule of mixtures formula was used to calculate the theoretical flexural modulus. This can be compared with the local experimental flexural modulus which was then plotted against the theoretical value, to determine if there is a correlation between the surface deformation and the component stiffness. Constants for measuring the theoretical flexural modulus were the thickness of the plaque, the thickness of the UD prior to moulding and the UD flexural modulus. The flexural modulus was taken from the normalised UD net-shape compression moulded plaque. The rotation, extension for fibre misalignment and reinforcement thinning caused by flow was captured by photogrammetry. Finally due to the high degree of flow induced alignment caused by the SMC, experimental values were used in the theoretical calculation; however, with

minimal flow this value could be removed to a single flexural modulus average for the plaque. All flexural moduli were normalised to 55% V_f to account for variations caused by the edge effect.

$$\mathrm{E_{tf}} = \cos^4\theta \times \mathrm{U_t} \times \varepsilon_{yy} \times \mathrm{U_{fm}} + \mathrm{S_t} \times \mathrm{S_{fm}} \quad (21)$$

Where

$\mathrm{E_{tf}}$	=	Theoretical flexural modulus (GPa)
θ	=	Fibre angle (°)
$\mathrm{U_t}$	=	UD thickness ratio
ε_{yy}	=	Engineering strain
$\mathrm{U_{fm}}$.	=	Normalised UD flexural modulus to 55% V_f (GPa)
$\mathrm{S_{fm}}$	=	Normalised UD flexural modulus to 55% V_f (GPa)
S_t.	=	SMC thickness ratio

The strain measurement ε_{yy} was used to determine the degree of thinning that occurs on the UD thickness ratio $\mathrm{U_t}$ (i.e. a strain of 0.2 will cause a reduction in the thickness of the UD by 20%). A Krenchel type efficiency factor is included if the layup is not unidirectional, to account for the fibre misalignment in the ply layup. The SMC thickness ratio $\mathrm{S_t}$ is calculated from the UD reinforcement subtracted from the total thickness. An experimental flexural modulus of the SMC is used for $\mathrm{S_{fm}}$ which is interpolated from HexMC scenarios that have the same charge design as the hybrid trial.

The root mean square error was used as a means to measure the accuracy of the theoretical flexural modulus with the experimental value:

$$\mathrm{RMSE} = \sqrt{\frac{1}{n}\sum_{i=1}^{n}\left(E_{f_i} - E_{tf_i}\right)^2} \quad (22)$$

Where

$RMSE$	=	Root mean square error (GPa)
E_f	=	Experimental flexural modulus (GPa)
E_{tf}	=	Theoretical flexural modulus (GPa)

5. Constituent Materials

The comparison of properties of the constituent materials, the sheet moulding compound HexMC and UD prepreg used for hybrid composite are detailed in this chapter. The purpose of this chapter is to provide a comparison of these materials as a benchmark for the hybrid study; this is particularly important where the properties of the UD are designed for low pressure press moulding conditions to minimise distortion cause by excessive pressure. This chapter will first investigate the properties of UD parallel and transverse to the fibre direction in a near zero flow scenario, with comparison drawn from an autoclave manufactured plaque and secondly the flow of UD prepreg in different fibre configurations. Finally the properties of HexMC are investigated with and without flow.

5.1. Unidirectional prepreg (UD)

5.1.1. Net-shape properties

Unidirectional carbon fibre prepreg was compression moulded net-shape to test whether increasing the number of plies affected the properties and creating a thickness bias. It is possible that the enhanced consolidation on the thinner plaques would improve the properties, especially when moulding at a higher pressure than that recommended by the manufacture.

The Flexural modulus was measured on plaques consisting of 2, 4, 6 and 8 UD plies moulded at 84.5 bar pressure, compared to 30 bar recommended by the manufacturer. Five samples were tested per plaque to testing parameters outlined in the methodology flexural modulus four point bending section 4.3.1.

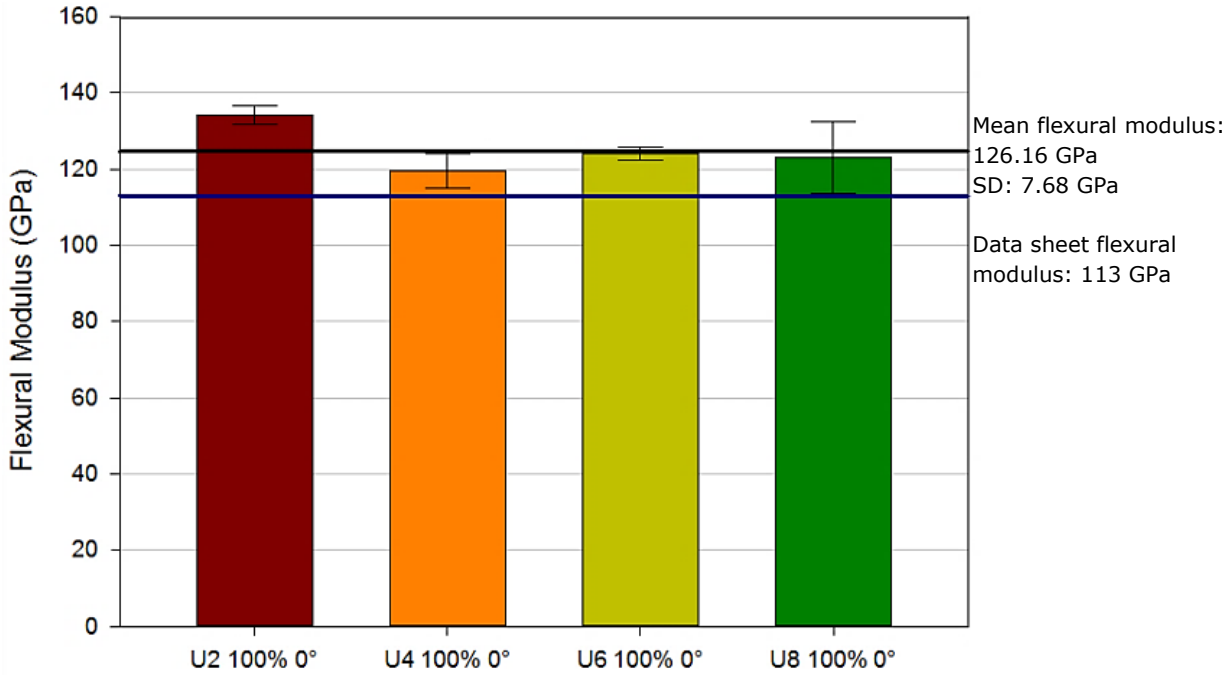

Figure 62: The effect of increasing number of plies of UD prepreg on flexural modulus parallel to the fibre orientation

The flexural modulus measured on plaques with an increasing number of UD plies is shown in Figure 62. The mechanical properties were all greater than the manufacturer's datasheet value for a compression moulding UD prepreg; this is attributed to the increased pressure squeezing excess resin out through the flash gap. It was observed that thin plaques of <0.8 mm (<3 plies) had abnormally high properties, as shown in Figure 62.

The different number of UD plies flexural moduli are normalised to 55% V_f and are shown in Table 10. U2 is between 5.58% and 10.74% higher than the other scenarios, indicating this effect is not solely related to V_f. This is caused by several factors including minor movement in thicker charges and increased shear as the charge is compacted causing misalignment. There is an increased error of the measured span and thickness as the samples become increasingly thin, because both are cubed in the flexural modulus calculation.

	U2	U4	U6	U8
Mean flexural modulus (GPa)	134.11 (10.73)	118.37 (6.05)	124.03 (7.47)	122.14 (8.02)
Mean fibre volume fraction (%)	56.52 (52.06)	55.24 (52.87)	55.28 (54.66)	54.34 (52.37)
Normalised to V_f 55% (GPa)	130.51 (11.34)	117.85 (6.29)	123.41 (7.52)	123.61 (8.42)

Table 10: The effect of changing number of plies of UD on the mean flexural modulus and fibre volume fraction parallel and (transverse).

The effect of increasing the number of plies on the transverse flexural modulus is shown in Figure 63. An average of 8.07 GPa was found, corresponding to a decrease of 93.6% compared to testing in the fibre direction. The manufacturer did not provide the transverse flexural properties of UD. This property is important because it gives a large contrast when the fibres are no longer aligned to the primary loading case, which is likely to happen when the flow of the SMC has distorted the UD reinforcement. The stiffness transverse to the fibre direction follows a similar trend to the parallel fibre properties, with U2 and U4 being the highest and lowest respectively, while U6 and U8 were very similar to each other.

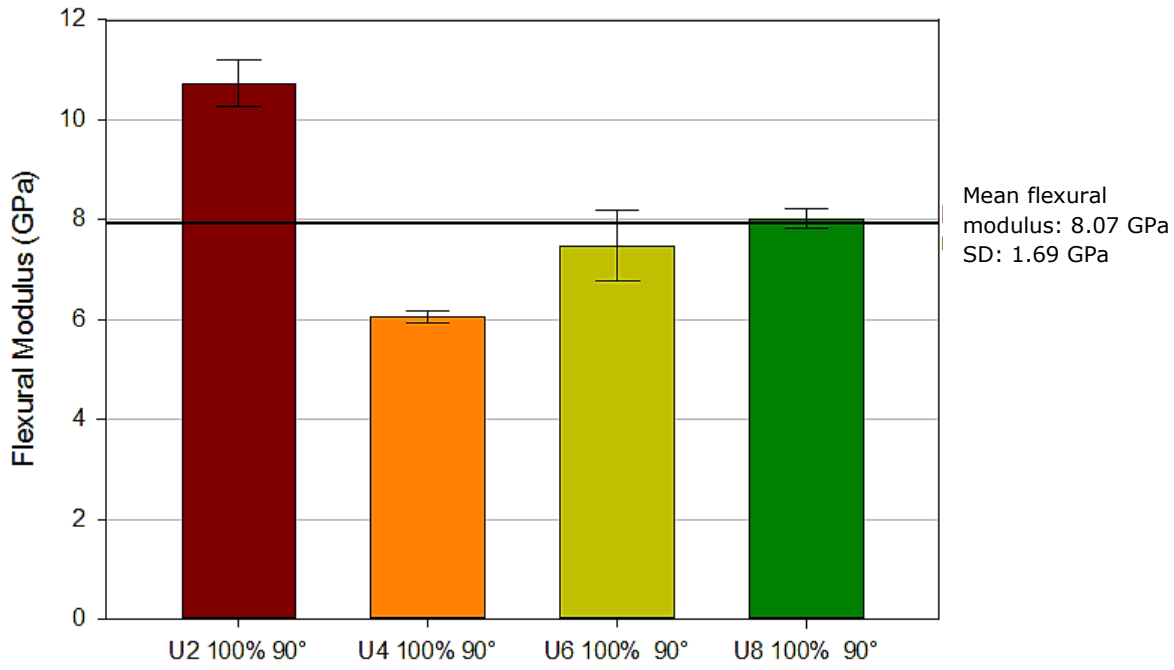

Figure 63: The effect of increasing number of plies of UD prepreg on flexural modulus parallel to the fibre orientation

5.1.2. Flow effects on unidirectional prepreg

During the hybridisation of UD with an SMC, it is expected that there will be a degree of flow; therefore, a study on the flow properties of UD will provide an understanding needed to interpret the hybridisation results.

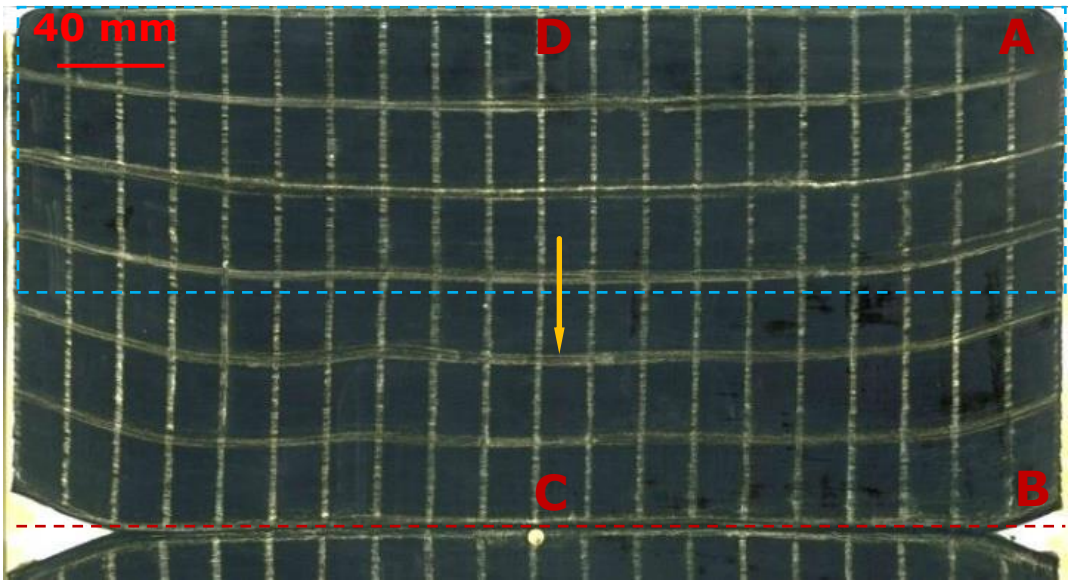

Figure 64: 3 plies of UD aligned in the flow direction (yellow arrow) compression moulded (U3 90°) with a charge coverage of 60% (blue hatched line square), forming a weld line at the centre without another identical charge (red hatched line)

Figures 64 and 65 show the effect of placing two charges of three plies of UD symmetrically at either end of the tool, with each charge covering 30% of the tool coverage (total=60%). Figure 64 shows the effects of flow on plies aligned transverse to the flow direction. When this is the case, the fibres exhibited significant flow and almost completely filled the cavity. There is curvature on the outer four squares and an almost even fibre flow in the centre of the plaque. Figure 65 shows the effects of flow on, plies aligned parallel to the flow direction. It can be seen that the carbon fibres did not break and as a result there is <3 mm of flow and significant resin bleed. The grid in both instances is largely preserved, with minor erosion, smudging and laddering. Laddering is where the fibres flow, spreading the grid and revealing lower fibres that are not marked. This shows that flow can be avoided by charge configuration in UD composites, an effect which may be transferable to hybrid composites. There are side effects caused by this control of fibre flow as the resin bleeds out of the fibres causing a thick resin band which may weaken the SMC-UD interface.

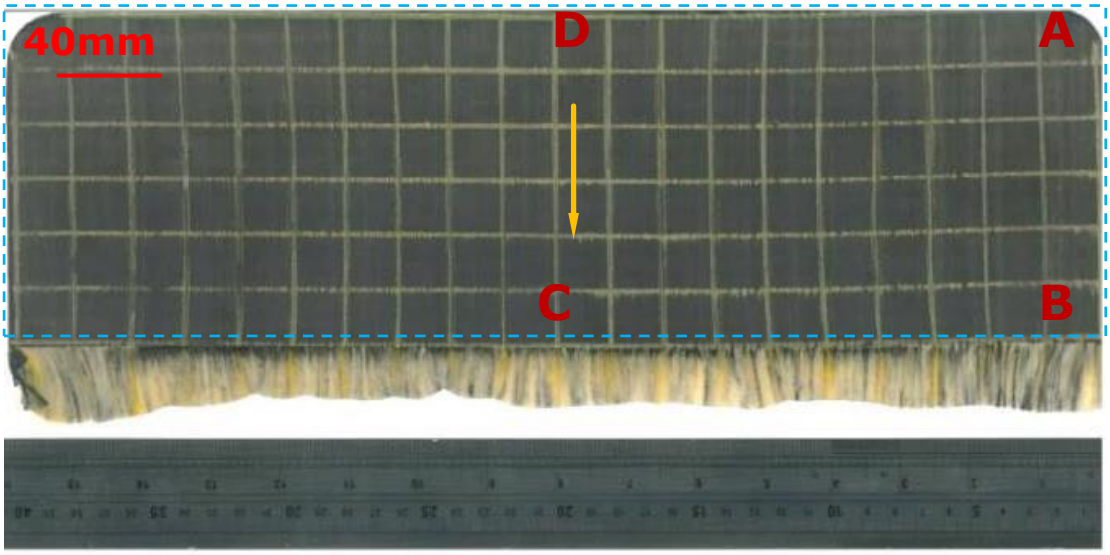

Figure 65: 3 plies of UD aligned in the flow direction (yellow arrow) compression moulded (U3 0°) with a charge coverage of 60% (blue hatched square)

5.1.3. Localised effects of flow U3 90°

To provide understanding on the effects of flow on the UD material, incremental four-point bending tests allowed geospatial measurement of stiffness, and density measurements allowed fibre volume fraction to be determined within a manufactured plaque. Figure 66 shows the flexural modulus and fibre volume fraction for each four-point bending location, plotted on the surface of the plaque to show their original location; **A**, **B**, **C** & **D** provide a cross-reference to Figure 64. It would be expected that the edge of the plaque would yield a poor stiffness because of the fibre curvature. However, when testing, it was found not to be necessarily the case as the stiffness was highest in the region of the greatest distortion. This was probably caused by the elevated V_f and visually evident by the dry plaque edge is shown in Figure 66.

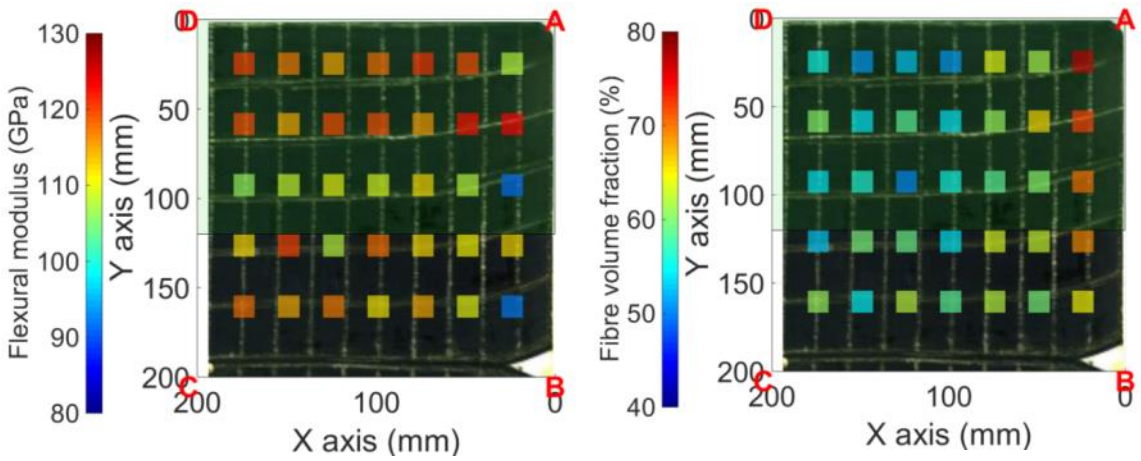

Figure 66: U3 90° flexural modulus parallel to the fibre direction and fibre volume fraction surface plot

As the resin flows more at the fibre ends there is an increase in V_f along the edge **A-B** of the tool. This was caused by the higher permeability in the fibre direction compared to the transverse direction, enabling the resin to be squeezed out through the flash gap[128].

The flexural modulus from Figure 66 was normalised to 55% V_f and is shown in Figure 67. The standard deviation (SD) of the mean within the plaque increased from 7.15 GPa to 13.14 GPa. This indicates the influence the V_f and rotation has on the flexural properties as the samples near side **A-B** in Figure 67 changed from being the highest in the plaque to the lowest. This plaque was encouraging as U3 90° flowed readily and did not cause drastic reduction in stiffness. In a hybrid composite the reinforcement will likely be distorted by the flow of the HexMC and this plaque demonstrates that in 1D flow the properties are still near the manufacturer's recommended stiffness.

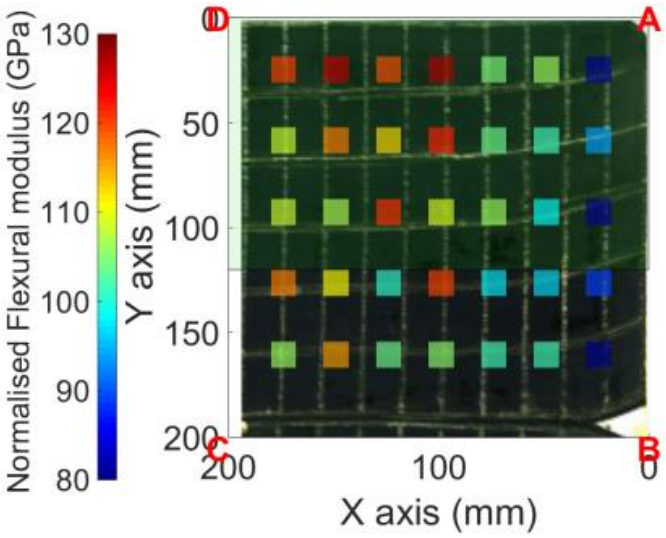

Figure 67: Flexural modulus parallel to the fibre direction of U3 90°, normalised to 55% V_f

5.1.4. Image analysis of U3 90°

By using the grid drawn on the surface it is possible to measure the local rotation and deformation of the UD, allowing the plotting of surface maps on the plaque to show trends and regions of high distortion. As this was a one dimensional flow scenario where the charge width was 405 mm in a tool cavity of 406mm, negligible flow in the *x*-direction was expected. The flow in the *x*-direction was primarily from fibre waviness causing a slight shrinkage. There was no obvious trend in the location of the shrinkage within the grid; the average strain in each element (ε_{xx}) was -1.12%, meaning each square on average contracted to 19.78mm compared to the 20 mm original width.

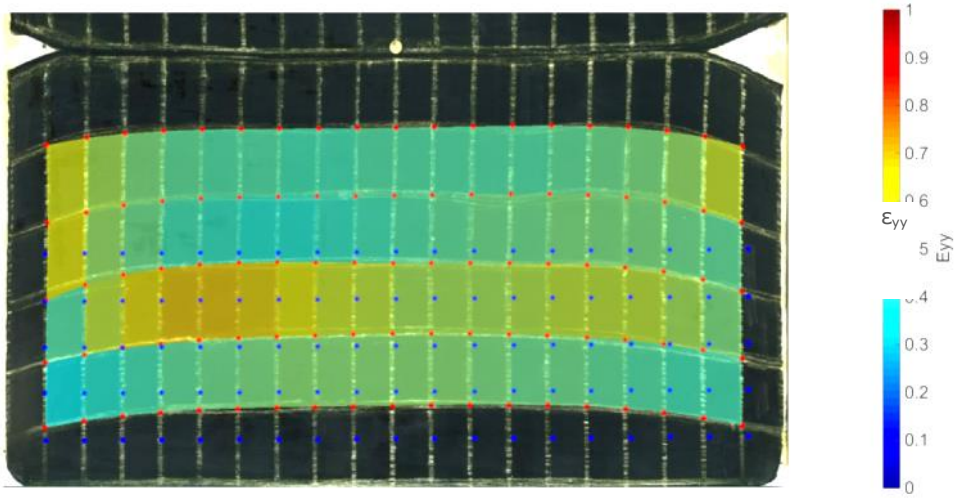

Figure 68: Element extension (ε_{yy}) in the y direction of U3 90°

In comparison, element extension in the flow direction ε_{yy}, as shown in Figure 68 plotted over the original plate, indicates that each element has expanded, on average by 49.53%. The mean element rotation, shown in Figure 69, was unsurprisingly restricted to the fibre ends which exhibited rotations >3°, steadily decreasing to <1° in the centre of the plaque. In Figure 66, properties generally increase from **D→A**; however, once normalised, the reverse occurs. Therefore the increase in flexural modulus is driven by the V_f increase, but the rotation has an effect on the degradation of the V_f-normalised properties at the edge.

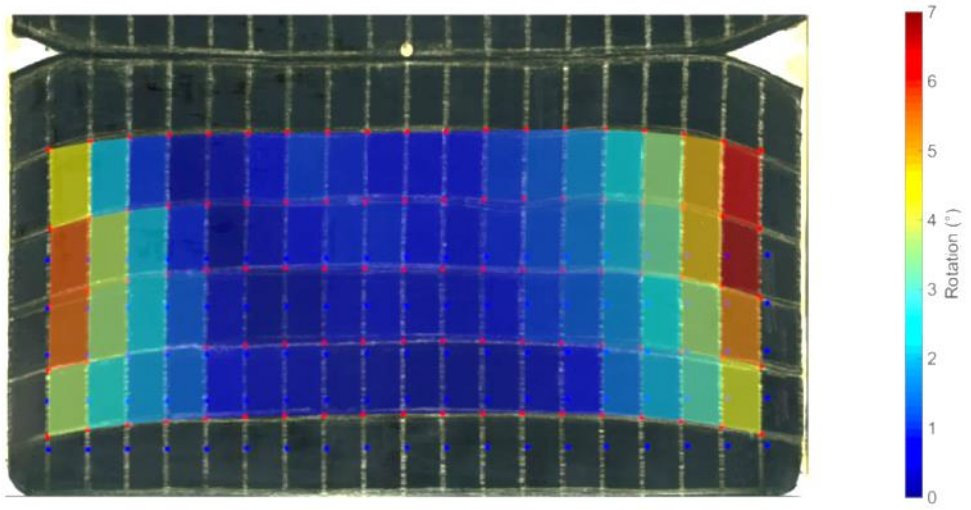

Figure 69: Rotation (°) at the centre of each element of U3 90°

The fibre volume fraction and orientation, taken from the element rotation, were used to calculate the theoretical flexural modulus expected within the UD plaques. The root mean square error (RMSE) of the mean is a measure of the average deviation from the regression line. This measure describes how close the theoretical values are to the experimental data.

Using the element rotation and a measure of fibre misalignment to the testing direction a theoretical flexural modulus was calculated, as discussed in the methodology 4.5.4 using a modified RoM, approach and presented in Figure 70, which compares the theoretical and experimental flexural moduli. For clarity a plot of where the theoretical values have come from within the plaque is added. The RMSE was 16.44%, which is significantly high in a scenario where it should be relatively straight-forward to predict the flexural modulus. The theoretical calculation only has three variables: fibre volume fraction, fibre orientation and fibre stiffness. Regions of high distortion (**1, 5 & 15**) shown in Figure 70 are not being accounted for sufficiently. This was caused by two factors: the rotation of

8° does not cause a large decline in properties and so the rotation consideration is not having a large effect; the element rotation is an average at the centre so local corners of an element may have higher rotation, which will not be accounted for.

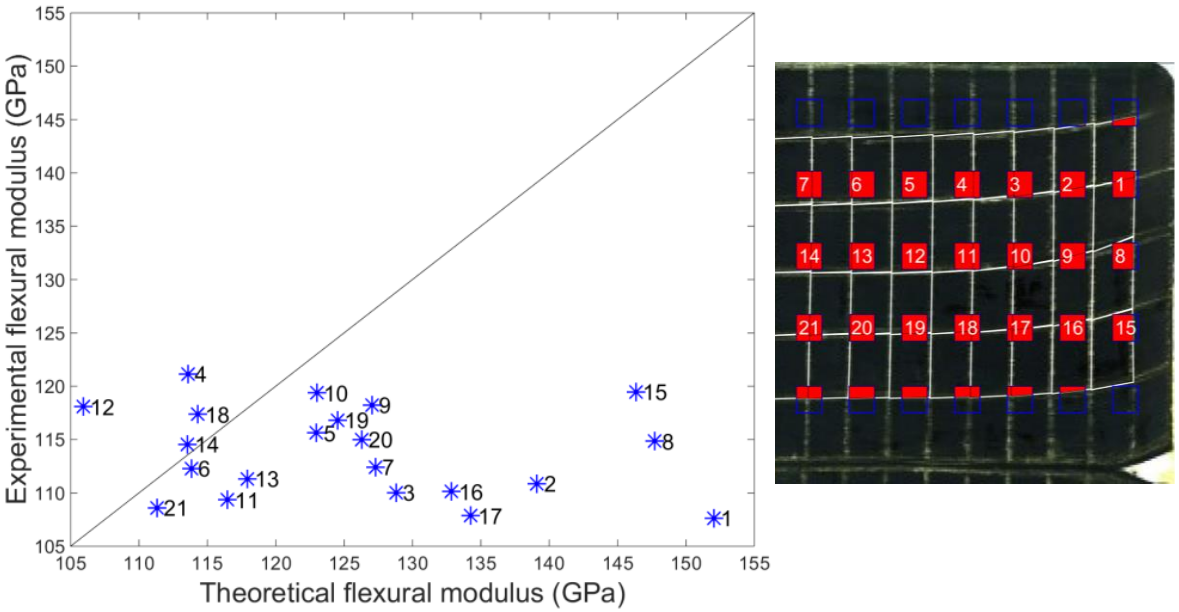

Figure 70: Theoretical calculation of U3 90° (left) with position location

5.1.5. Localised effects of flow in U3 0°

Significant resin bleed occurred when the fibres were aligned parallel to the flow direction. However, the flexural properties of the specimen were enhanced by an increase in V_f the spatial relationship between V_f and flexural modulus is shown in Figure 71. There was an incremental mean increase of 1.53 GPa in stiffness as the specimens became closer to the flow front. This was caused by resin readily bleeding out of the fibres at the flow front compared to the flash gap. Notably, as there has been minimal distortion and flow of the fibres, there is relatively small scatter in flexural stiffness and V_f. Although the properties of U3 90° 60% analysed in the previous section were generally high, a range of 88.81 GPa and a standard deviation of 15.77 GPa would create a design challenge with such high localised variation, compared to 17.02 GPa and 4.59 GPa in U3 0° 60%. U3 0° 60% was encouraging as there was minimal flow, low fibre distortion and limited variation in flexural modulus and V_f across the plaque.

Fibre volume fractions >70% cause practical concern because there is difficult in sufficient wetting the fibres to produce a composite material, as theoretical

perfect packing is 78.5% for square packing and 90.7% for hexagonal packing. This high values (>70%) may be caused by a compounding of errors in the experimental setup. Being: bubbles attached to the surface and internal voids artificially affecting the bouyance of the component, rounding errors in the supplied resin and fibre densities and due to the sample thickness these samples were very light and so small errors in weight will cause large deviations in the fibre volume fraction calculation

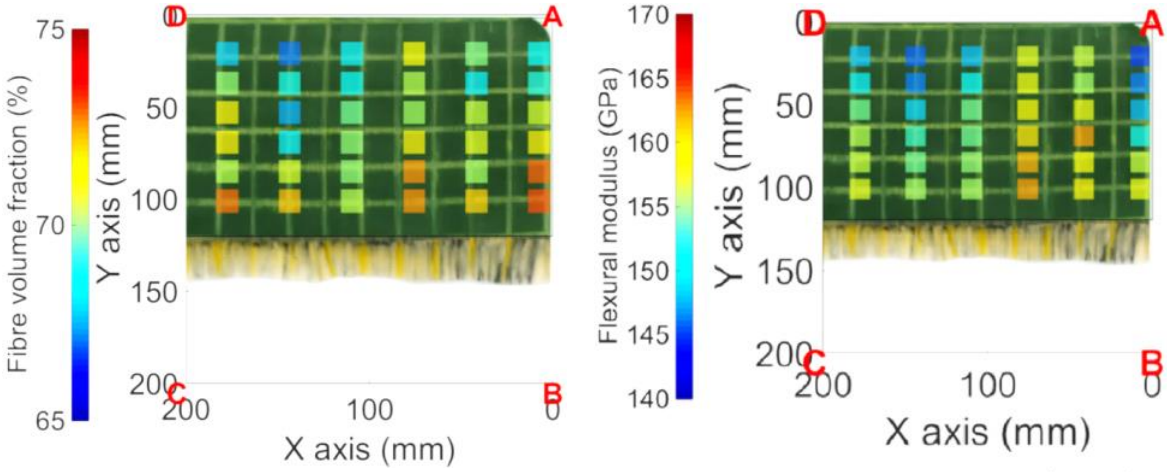

Figure 71: Fibre volume fraction and flexural modulus parallel to the fibre direction of U3 0° 60%

5.1.6. Image analysis of U3 0° 60%

In the flow scenario U3 0° 60% where the UD fibres were all aligned parallel to the flow direction, there was a large degree of resin bleed but very little fibre movement. This was quantified from the ε_{xx} mean value of 0.51%, corresponding to an average extension of 0.102 mm for each grid element, with a maximum of 13.27% and minimum of -6.2%. There was a mean rotation of 0.55° ranging from a maximum of 1.79° to a minimum of 0.01°, an extension (ε_{yy}) mean of 0.78% with a maximum of 3.37%, and a minimum of -2.67% in the flow direction but with no discernible trend. This was expected as there was very little fibre movement. There was a trend for the highest ε_{xx} to be observed at the plaque edge, due to a small degree of flow because the charge is slightly smaller than the tool, resulting in the charge width expanding from 405 mm to 406 mm.

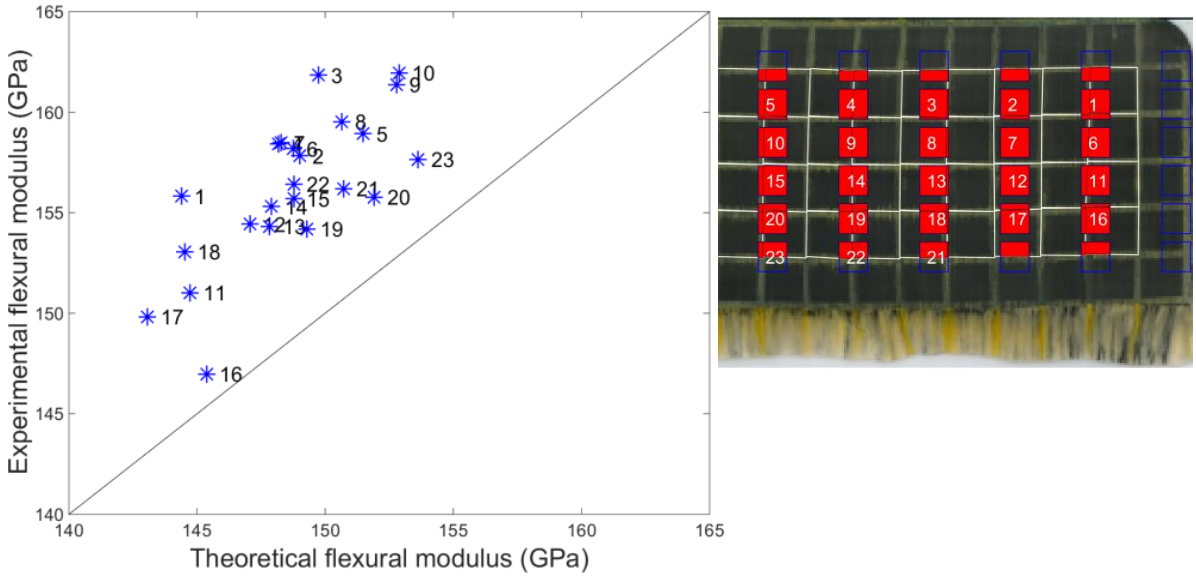

Figure 72: Theoretical flexural modulus calculation of U3 0° 60% with specimen location

The experimental vs theoretical flexural moduli of U3 0° 60% are shown in Figure 72,highlighting a theoretical value underprediction with a RMSE of 5.19%. This is 1.03% lower than the RMSE in the autoclave scenario that was also underpredicting the flexural modulus by 3.9%. The autoclave scenario was similar to U3 0° 60% since the theoretical fit was slightly under the experimental values by a mean of 5.07%; this highlighted the accuracy of the method.

5.2. Comparison of UD scenarios

Table 11 compares the summarised photogrammetric data of the two grid strain analysises, U3 0° 60% and U3 90° 60%. The rotation and V_f changes U3 90° 60% led to a prediction of a higher flexural modulus, 125.68 GPa compared to the experimental values measured as of 113.86 GPa; this was probably caused by the distortion of the fibres. Conversely, U3 0° 60% experimentally was higher than the theoretical value, but with a reduced difference of 5.07%. Figure 73 shows the relationship between flexural modulus and V_f for different UD plaques, manufactured through autoclave and compression moulding, with different charge coverages and varying ply numbers. When comparing the flow scenarios to other UD compression moulding scenarios in Figure 73, the results appear similar to other compression moulding scenarios. The standard deviations (SD) of U3 90° 60% (Table 11) show that there is significant variation in the local extension and rotation, and where distortion occurs in the UD. Predicting the

properties is challenging as the RMSE was 16.44% compared to 5.19% in U3 0° 60%. This distortion of U3 90° 60% did degrade the properties, compared to all the other UD plaques tested.

	Within the grid strain analysis area (SD)		RMSE (%)	Mean (SD)		
	Exp mean (GPa)	Theo mean (Gpa)		θ (°)	ε_{yy} (%)	ε_{xx} (%)
U3 90° 60%	113.86 (4.19)	125.68 (12.74)	16.44	1.78 (1.68)	49.53 (6.74)	-1.12 (1.02)
U3 0° 60%	156.23 (3.71)	148.69 (2.90)	5.19	0.55 (0.4)	0.78 (1.29)	0.51 (4.7)

Table 11: Comparison of the photogrammetry data of U3 0° 60% and U3 90° 60%, including the experimental mean of the data within the grid strain analysis and standard deviation (SD)

U3 90° and U3 0° were compared with benchmarks of different net-shape UD with increasing number plies, and with an autoclave moulded plaque, which can be viewed as the best performance this material will be able to achieve. These properties were plotted against the manufacturer's stated stiffness (blue) and a theoretical RoM stiffness (black). The autoclave (orange) in Figure 73 produced the lowest mean stiffness, as the low pressure did not squeeze the resin out, causing the lowest fibre volume fraction. U3 0° 60% (blue) has the highest properties, evident by the thick band of resin bleed in Figure 65. This was caused by flow resistance of fibres when aligned parallel to the flow direction.

Data from an autoclave moulded plaque (U3 autoclave), compression moulding net-shape and U3 0° 60% plaques are all between the two manufacturers' data sets in Figure 73. U3 90° (Figure 64) had the highest level of flow causing the highest level of variability in stiffness and V_f and is only partially sitting within the black and blue bounds. This can be expected as the flow caused fibre distortion and misalignment leading to a decline in properties and resulting in the plaque performing worse than the others as the fibres are no longer in the loading direction. The resin bleed at the fibre ends prevented stiffness degradation as V_f was higher despite local misalignment of the fibres.

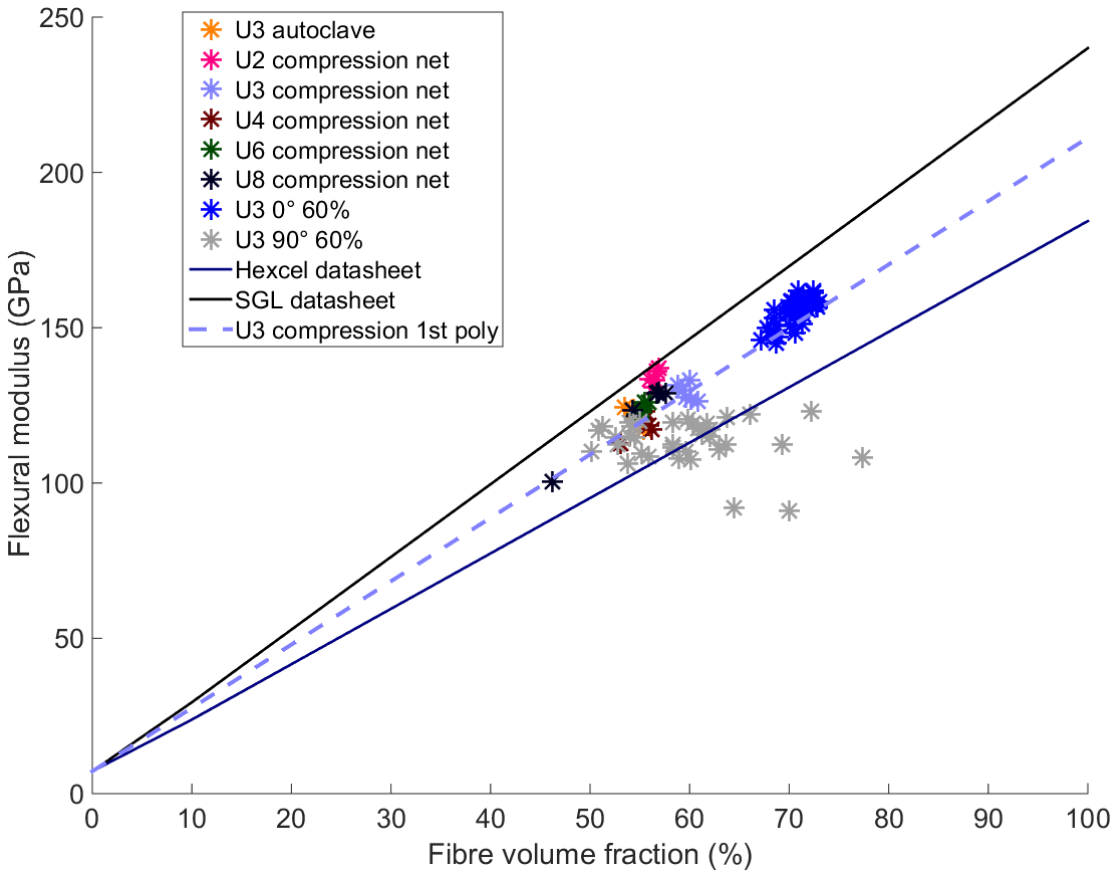

Figure 73: Flexural modulus plotted against fibre volume fraction of UD scenarios. Theoretical manufacturers' values and a least squares polynomial of U3 net compression as a basis for theoretical calculation (at 100% V_f, flexural modulus is 211.15 GPa; at 55% 116.13 GPa)

The least squares fit () polynomial is determined for through U3 net and is shown on Figure 73, with the same *y*-intercept as 7.2 GPa, the resin flexural modulus of. This was used in the theoretical calculation of the UD and hybrid plaques because the two manufacturers' datasheet values were not representative of the experimental properties. Using this to calculate a theoretical value of the autoclave scenario produced a normalised mean of 117.23 GPa compared to 122.24 GPa, 4.28% lower, with a RMSE of 6.22%. This assumed no flow induced fibre misorientation as grid strain analysis was not available, and does show the variation in an optimum moulding method.

5.3. Sheet moulding compound

The SMC was characterised prior to the hybrid study to give insight into the properties of the moulding compound for different charge designs. Since the material is anisotropic in and out of plane, an initial test was conducted to determine if there was an in-plane bias on the SMC. It was observed when testing H4 60% that the mean flexural modulus was 40.40 GPa and 40.70 GPa with a standard deviations of 5.42 Gpa and 5.74 GPa respectively for the two test orientations. The minor differences between the values are likely caused by the difficulty in repeatedly placing the specimens in exactly the same position.

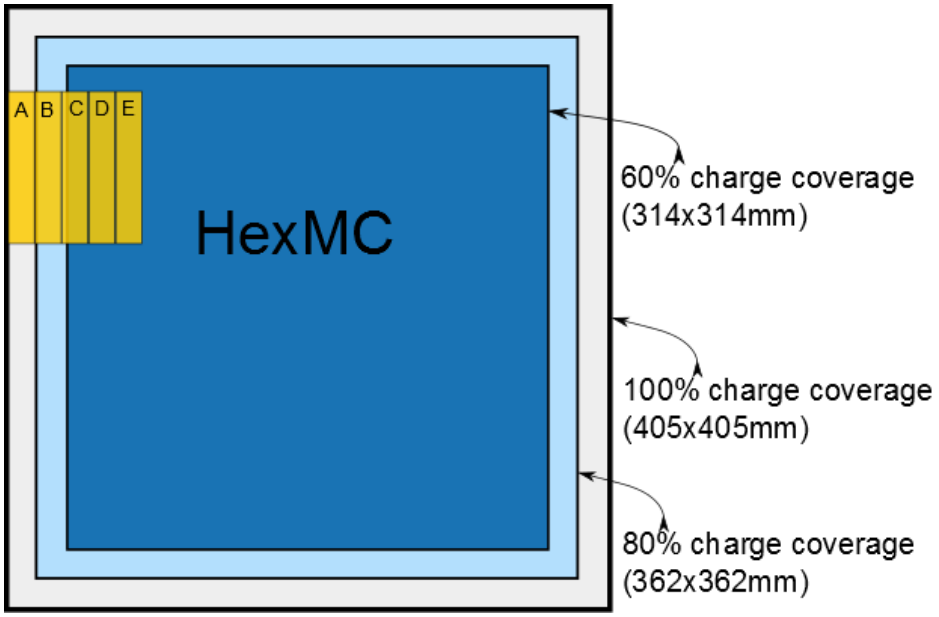

Figure 74: Charge coverage diagram for the 2D flow studies of SMC with locations of flexural specimens

The effect the tool edge and flash gap has on SMC plaques was demonstrated by plotting the flexural modulus and V_f of different SMC charge configurations at specific locations. Figure 74 shows the charge coverage and flexural specimen locations in the HexMC study for the results presented in Figure 75. It was observed the V_f is typically higher towards the flash gap, and there was a gradual decline from **A→E**.

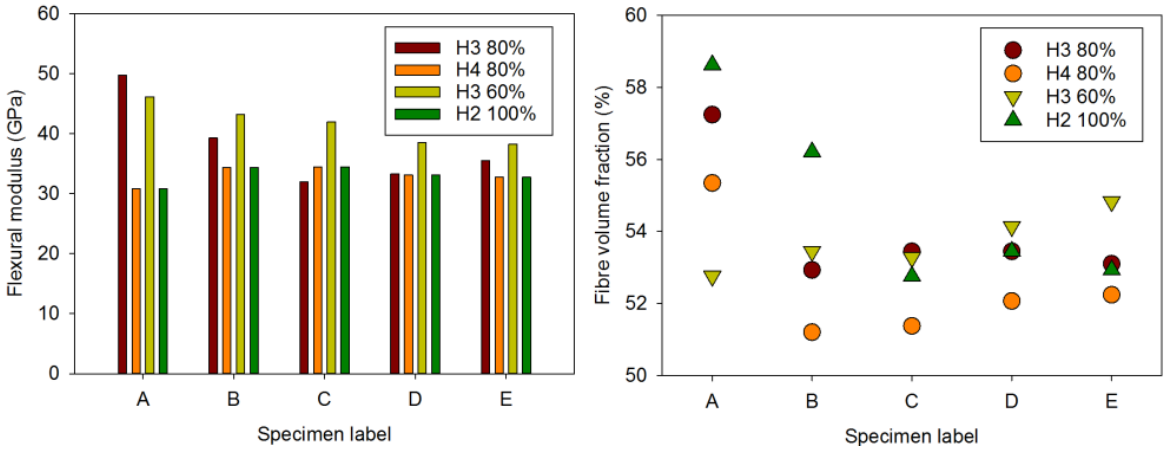

Figure 75: Variation of stiffness and fibre volume fraction of different SMC ply and charge coverage scenarios described in Figure 74.

For SMC scenarios with 3 plies (H3 80% and H3 60%), an increased stiffness was observed at the tool edge; however, this was not the case for 4 plies (H4 80%) and the 2 ply net shape scenarios (H2 100%). In some scenarios, the peak in V_f is likely caused by fibres stacking at the tool edge and the resin bleeding out, which results in a higher stiffness at the tool edge. This effect has been observed in the literature, notably in Davis et al. [46], where fibres rotate as flow fronts meet. This can happen when meeting a tool wall as the fibres simultaneously attempt to flow along the side of the tool, receive pressure from the bulk material behind, and resin is flowing through the fibres and out of the flash gap.

This enhanced stiffness was not observed in the net-shape charge (H2 100%) as the fibres underwent significantly less flow and did not cause consolidation of fibre bundles at the edge. Due to the variability of SMC, it is expected to have regions of high and low fibre content. There will be regions of high fibre alignment in the testing directions, and resin rich regions caused by multiple fibre ends. As this material is heterogeneous there will be a large range of properties, especially when the testing region decreases in size.

5.3.1. Localised effects of flow H2 60%

A grid was drawn on the surface of two identical charges consisting of two plies of HexMC which flowed into the centre with a coverage of 60%, as shown in Figure 76. Due to the chaotic flow it is not possible to analyse the grid; however, near the tool edge there has been less flow and the grid is partially visible. This shows that there is both fountain and preferential flow as the grid stretches and flows from the core; along **A-E** there has been very little surface flow, meaning the centre of the charge has flowed. It is also evident in the flow of SMCs that tow spreading and overlapping causes the erosion of the grid.

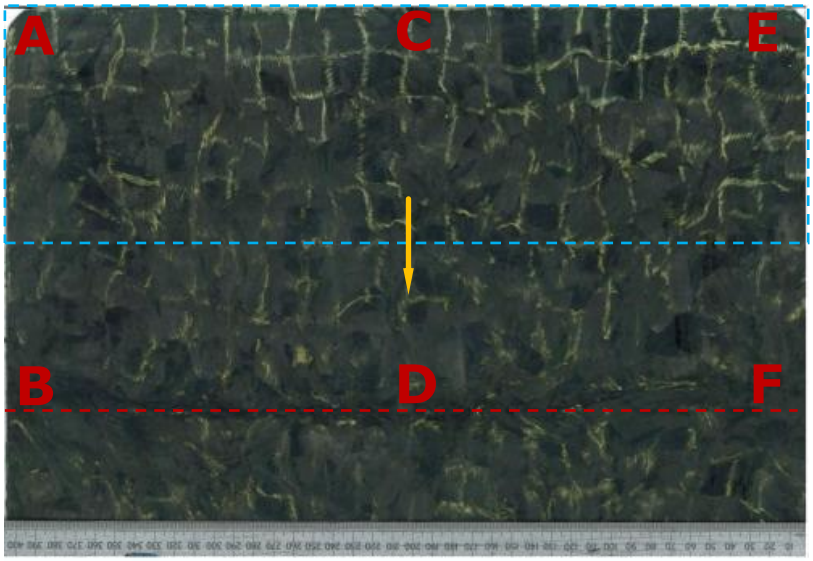

Figure 76: 2 plies of SMC in each half of the cavity of 406x406 mm, with charge coverage(blue), flow direction (yellow) and weld line (red) of 60% (H2 60%)

With a charge coverage of 60%, significant fibre alignment was observed. The V_f and flexural modulus parallel and transverse to the flow direction are shown in Figure 77 and Figure 78, which are plotted over the region where the specimens were taken from; the green square shows the original charge location. The fibre alignment resulted in a mean flexural modulus of 22.67 GPa and V_f of 55.03% in the transverse direction, and 45.81 GPa and V_f 54.01% in the longitudinal direction. The normalisation of the flexural modulus with respect to V_f did not show a relationship between the values; this is because in SMCs the effect of fibre orientation is significant. Figure 77 shows the fibre volume fraction of two plies of HexMC in a 1D flow scenario in samples cut parallel and transverse to the flow direction. There was no discernible trend for V_f, which exhibited a low range of 8.62%.

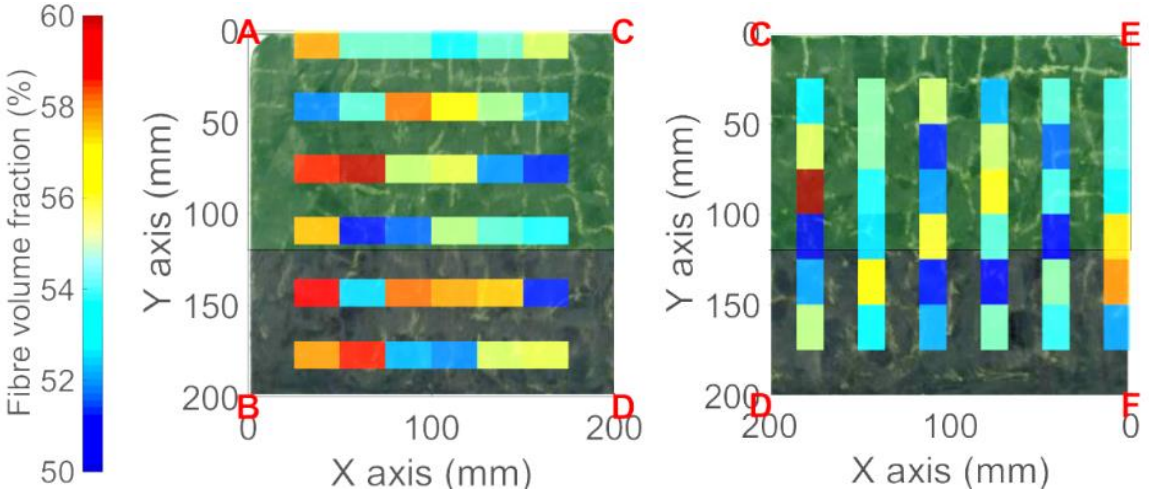

Figure 77: Fibre volume fraction modulus of H2 60% transverse (left) and parallel (right) to the flow direction, the translucent green area ending between 100 and 150 is the original charge edge.

An increased V_f at the tool edge can be observed in Figure 77; this is only evident parallel to the flow direction and is comparable to Figure 75 where similar charge constructions did not necessarily cause a peak in flexural modulus or V_f at the tool edge. This result highlights the inhomogeneity of the SMC, as there are large variations from location to location. Between two adjacent loading spans of 15mm there can be as much as >5% change in V_f. Transverse to the flow direction, the properties are highest on average on the edge **A-C** depicted in Figure 78, due to reduced flow-induced alignment. When testing transverse to the flow direction, 100mm from tool edge (**A-B**) the flexural properties are >20 GPa and then decline towards the centre of the plaque. This is likely from fibres aligning in the flow direction and the tool edge reducing the flow induced alignment. This was also observed parallel to the flow direction as the flexural modulus of the specimens increased from **C&E→D&F**, from37.05 GPa to 40.5 GPa respectively, as the fibres have flowed and become increasingly aligned.

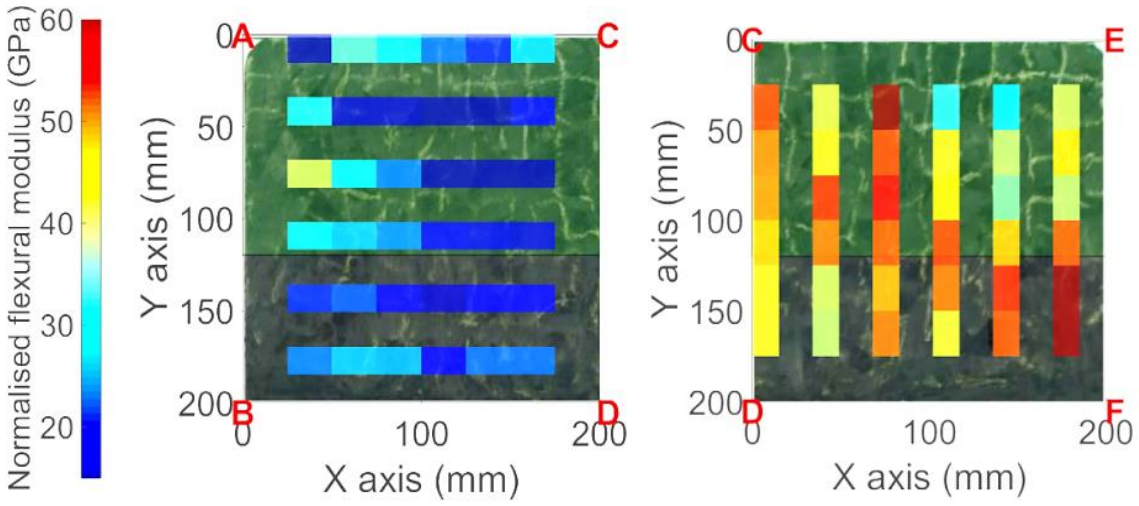

Figure 78: Flexural modulus of H2 60% transverse (left) and parallel (right) to the flow direction

At edge **B→F** it was observed that flow induced alignment diminishes. This is due to the two charges creating a weld line and entangling the fibres. Similarly to when a charge flows into the tool edge, the fibres align parallel with the weld line.

5.4. Summary

This chapter reported the mechanical properties of compression moulded UD prepreg and HexMC, which will provide a benchmark for the hybridised materials. Additionally, research was carried out on the flow of high V_f carbon fibre SMCs and prepreg in compression moulding, as there is limited literature on their performance under significant flow.

UD was manufactured in the traditional autoclave process and by compression moulding, with the same moulding parameters that will be used in the hybrid study. It was shown that there was no decline in flexural properties when compression moulding UD compared to the autoclave process. A 6.4% increase in stiffness was reported, which was caused by an increase in V_f. Although the normalised flexural modulus of the compression moulded plaque is 3.02% lower than the autoclave, this is likely caused by minor degrees of flow and by the debulking process in the autoclave evacuating voids.

In the flow scenarios, UD aligned parallel to the flow direction exhibited significant resin bleed and negligible fibre flow. In contrast, fibres aligned

transversely flowed significantly without fibre breakage, resin pockets or blistering. It was shown that mechanical properties were not dramatically degraded by the flow of the UD, which is encouraging as flow of the HexMC is inevitable.

Compression moulding HexMC highlighted that in 2D low flow scenarios, flow induced alignment was difficult to detect as the distance travelled was limited in a centrally placed charge. However, in a 1D flow scenario there was significant flow induced alignment and the flexural stiffness was affected accordingly. The stiffness was 45.81 GPa and 22.67 GPa parallel and transverse to the flow direction respectively. It was not possible to track the distortion of the HexMC using the same method as the prepreg because of the chaotic flow which erased the grid. This will not be an issue as the hybrid study will investigate the performance enhancement the prepreg can provide to the SMC. Therefore, for the purpose of the study, tracking the prepreg will suffice, but tracking the SMC would have provided helpful insight into the flow during hybridisation.

There was a notable edge effect observed when the HexMC flowed into the tool edge, where the flexural properties increased. It was primarily seen in the first specimen, **A**, at approximately 30 mm from the border of the plaque before returning to a base value, this was primarily from a peak in the V_f fraction. Although the inhomogeneity of HexMC causes high variation within the plaque, it was observed that the flexural modulus and V_f could be significantly different within a small distance of 15mm.

6. Hybrid Composites

This chapter introduces the initial trials of co-moulding UD with HexMC in a one step process. Firstly UD is manufactured with HexMC in an autoclave to provide a co-moulding scenario where minimal flow occurs. This is then compared with the compression co-moulding of a net-shape hybrid and two hybrid scenarios where the UD is aligned transverse and then parallel to the flow direction in a one dimensional flow scenario. This chapter will also investigate the localised flexural modulus, V_f and reinforcement distortion, that was introduced in the previous chapter. Finally, photogrammetric data in the hybrid scenarios is used to provide a theoretical stiffness prediction and then compared to experimental stiffness. This is to determine if adding UD to HexMC in a one step process produces stiffness enhancement without any processing of the reinforcement.

6.1. Hybrid Composites - Autoclave

The low resin flow from the autoclave allows an opportunity to test whether hybridisation can enhance the stiffness of the HexMC. This can be viewed as the least disruptive method for hybridisation, as there is minimal flow of the HexMC resulting in the lowest distortion of the UD reinforcement. However, distortion of the UD fibres was observed following the autoclave cure cycle which was caused by local flow from consolidation and thickness variations in the HexMC.

Two flexural tests were conducted on the same specimen of U3 H2 autoclave to determine if there was a significant difference between the UD reinforcement stiffness when the sample was rotated by 180° about the beam axis; i.e. with UD either under tension or compression, as shown in Figure 79. The results show no preference could be observed in the stiffness as a result of the rotation. The mean flexural modulus of the specimens with UD under compression and tension was 60.08 GPa and 60.89 GPa respectively, a difference of 1.32%. This was likely caused by the difficulty in placing the test specimen in exactly the same position for the two tests.

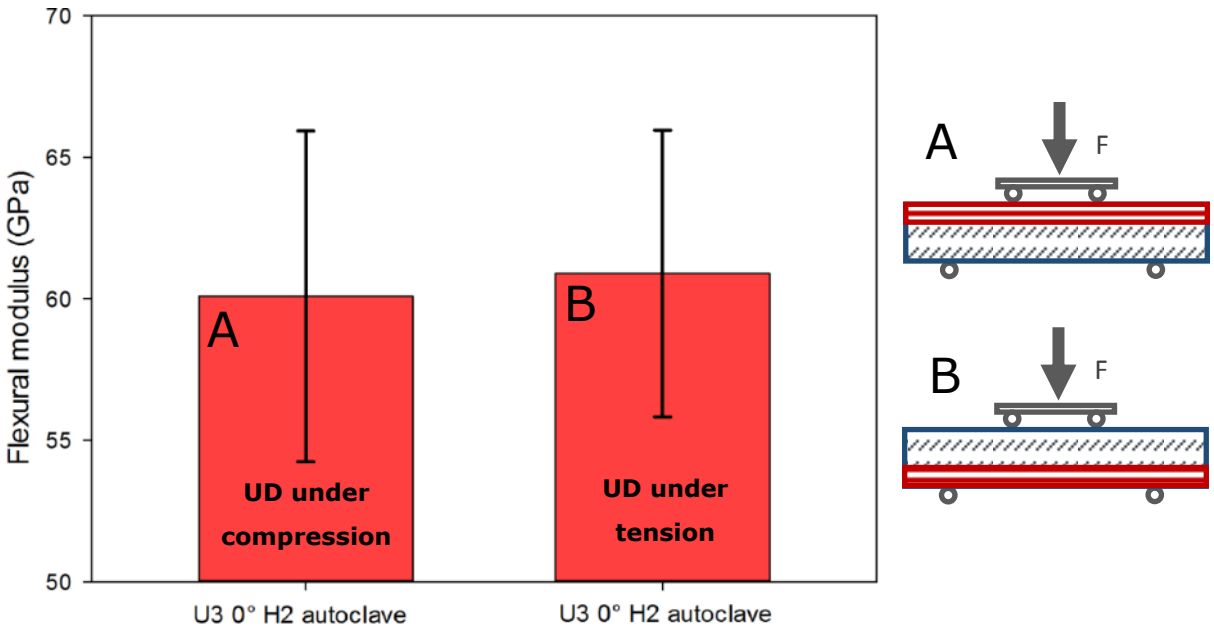

Figure 79: Flexural modulus of hybrid plaque of U3 H2 manufactured in the autoclave, tested with (A) UD on top, under compression and (B) UD on bottom of sample, under tension

Autoclave stiffness measurements shown in Figure 80 were taken from a hybrid U3 H2 transverse and parallel to the UD fibre direction. The flexural modulus varied from 60.49 GPa to 19.92 GPa respectively. This is approximately a 45.08% reduction in the transverse UD direction, but a 66.78% increase in the UD fibre direction compared with two plies of HexMC produced in the autoclave. This increase highlights the potential effect hybridisation can have on improving the stiffness of SMC components.

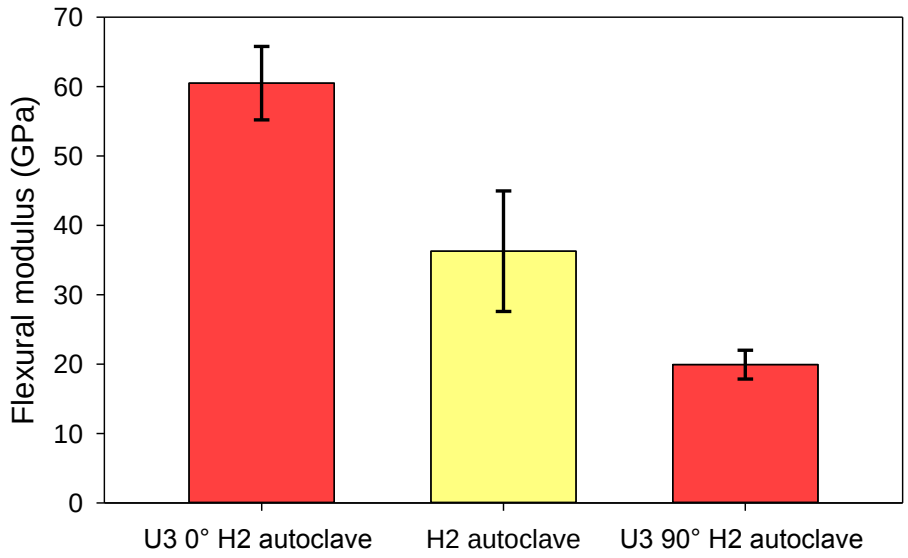

Figure 80: Flexural modulus of U3 H2 autoclave specimens with the bending axis parallel (0°) and perpendicular (90°) to the fibre direction. For comparison the flexural modulus of H2 autoclave plaque is shown.

The theoretical mean flexural modulus of 61.52 GPa for the parallel autoclave scenario was similar to the experimental value of 60.49 GPa, a difference of 1.68%. In the autoclave manufacturing process, the low pressure causes minimal material flow, ensuring the UD fibres maintain their alignment and little resin is removed from the material, yielding a mean V_f of 54.76% and a low V_f variability of 1.90%.

6.2. Hybrids Composites – net-shape (U3 H2 net)

A hybrid plaque with three UD and two HexMC plies was manufactured net-shape. This was to provide a scenario with the least distortion through compression moulding as the HexMC would flow as little as possible preventing the distortion of the UD. This was not the case, as the U3 H2 net-shape plaque exhibited the worst quality. The heterogeneous flow of the HexMC created voids and resin pockets on the surface of the UD, and creases where the UD had partially overlapped itself. Since there was no primary flow direction unlike the other hybrid scenarios, the HexMC flowed in all directions. This is apparent from the grid distortion in Figure 81, showing the UD surface of the hybrid plaque with ply layup construction. The regions where the flexural modulus was measured are shown in Figure 82.

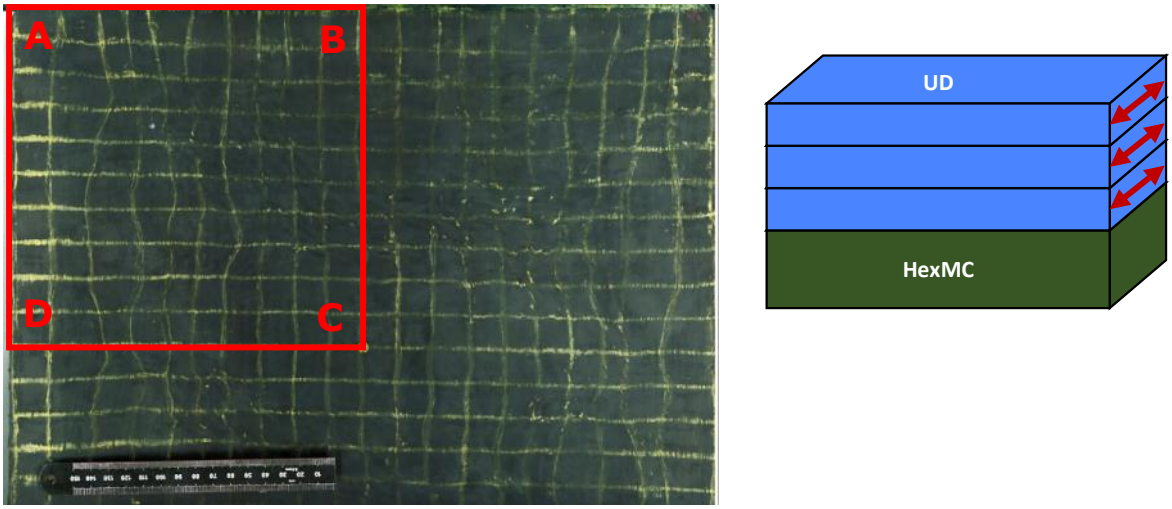

Figure 81: U3 H2 net shaped plaque with the testing region shown as a red square. Charge construction diagram (red arrows indicate UD fibre direction). A through D represents plate locations reference in Figure 82.

Figure 82 shows measurements of the flexural modulus and V_f of U3 H2 net at their respective positions on the plaque. The UD fibre direction is from **A&B→D&C** in Figure 82. The flexural modulus was a maximum at the fibre ends where the resin is able to travel along the fibres and escape through the flash gap showing a peak in V_f. The properties were on average, better than H2 100%. However, four stiffness measurements were within or lower than one SD of H2 100%, reaching a minimum of 27.98 GPa. This suggests that the reinforcement was not enhancing the properties of the material significantly.

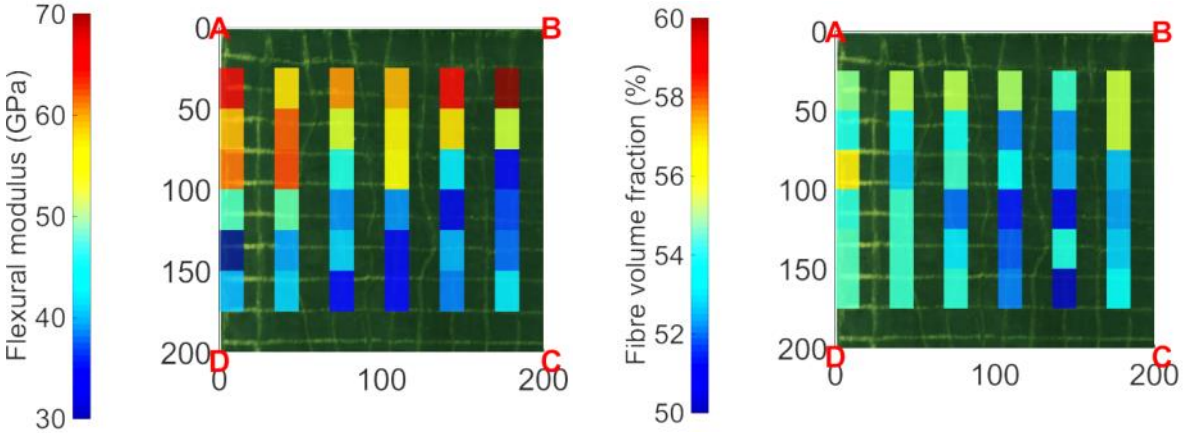

Figure 82: Flexural modulus and fibre volume fraction of U3 H2 hybrid plaques shown at the respective position

6.2.1. Flow distortion of a net-shape hybrid

Using the grid the element rotation and strain in the *x* and *y* axes were obtained for U3 H2 net, and is shown in Figure 83 with the blue and red plotted points representing the pre and post moulding co-ordinates respectively. The heterogeneous flow of HexMC caused a trend in the flow of the reinforcement. There was greater extension (ε_{xx}) in the grid elements on the edge to the left and right of the plaque; this was caused by the charge being smaller than the cavity. The flow resulted in a mean rotation of 2.42°, and a small element strain ε_{xx} and ε_{yy} of 0.18% and -2.69% respectively; this was expected as there should be minimal flow.

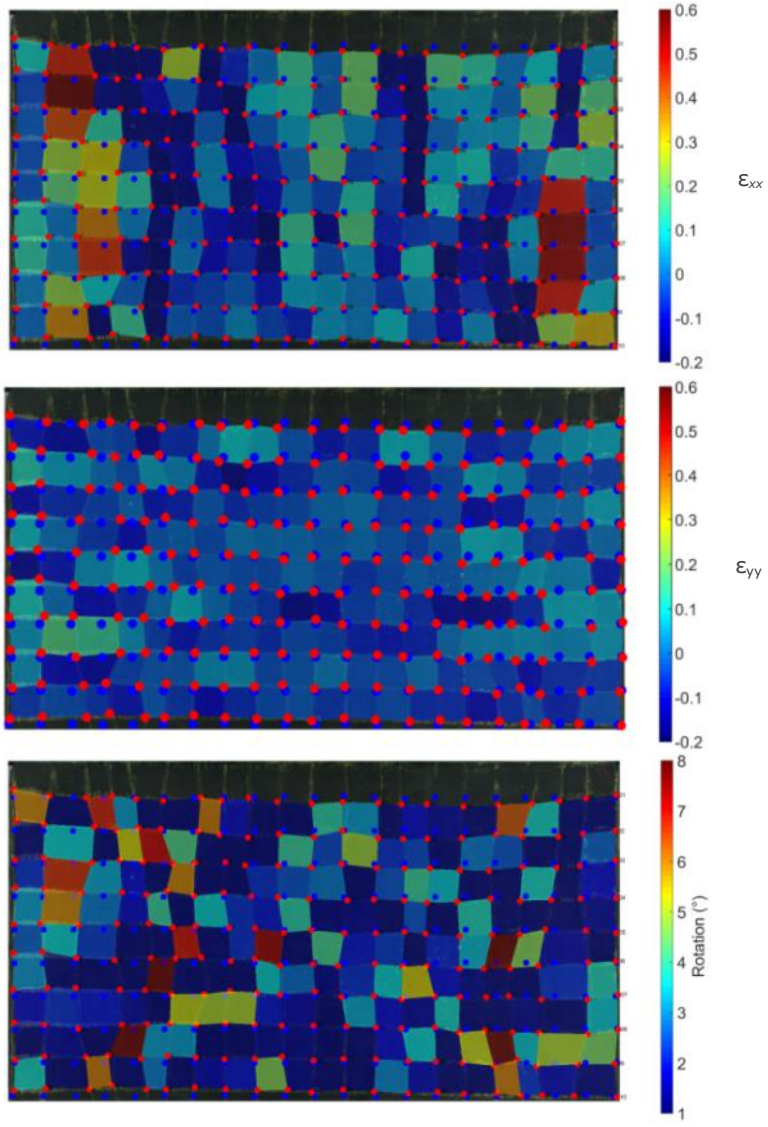

Figure 83: U3 H2 net element extension ε_{xx}, ε_{yy} and rotation

Using photogrammetry and density measurements a theoretical flexural modulus was calculated based on the ε_{xx}, the rotation at each grid element and the localised V_f. Figure 84 shows this theoretical modulus compared to the measured experimental values. There was a clear trend in the areas near the UD fibre ends (samples **1-12**), of a higher experimental flexural modulus than the theoretical. A mean value for the SMC was in the theoretical stiffness used since there were no localised flexural properties of H2 100% were available. This was considered appropriate as no significant flow induced alignment could be observed.

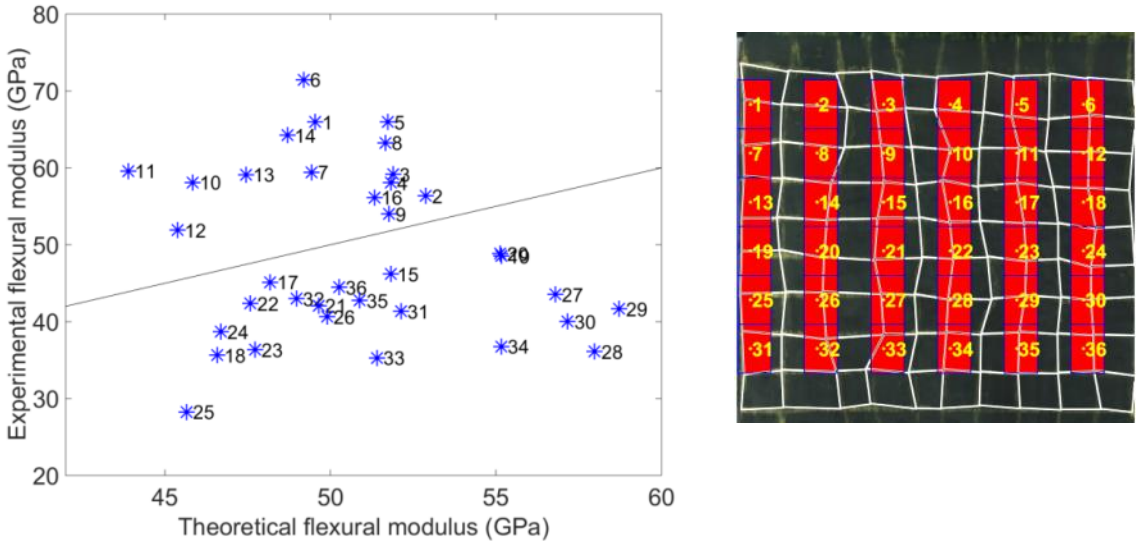

Figure 84: Comparison of U3 H2 net experimental and theoretical flexural modulus with point location

6.3. Hybrids Composites – UD transverse to flow direction (U3 90° H2 60%)

The three plies of UD, aligned perpendicular to the flow direction (90°) was placed on top of two plies of HexMC with a 60% charge coverage, providing a large region in the U3 90° H2 60%. The plaque had no discernible defects, such as blistering, fibre-matrix separation plaque that was outside the charge coverage area. This was done to exaggerate the flow on the UD. A number of visual observations were made from the one dimensional flow scenario of the hybridised plaque, or resin pockets. As shown in Figure 85, the UD appeared intact without any tearing, apart from the significant distortion of the reinforcement. This can be observed from the grid lines where the fibres become wavy and the reinforcement shortened and pulled away from the tool edge.

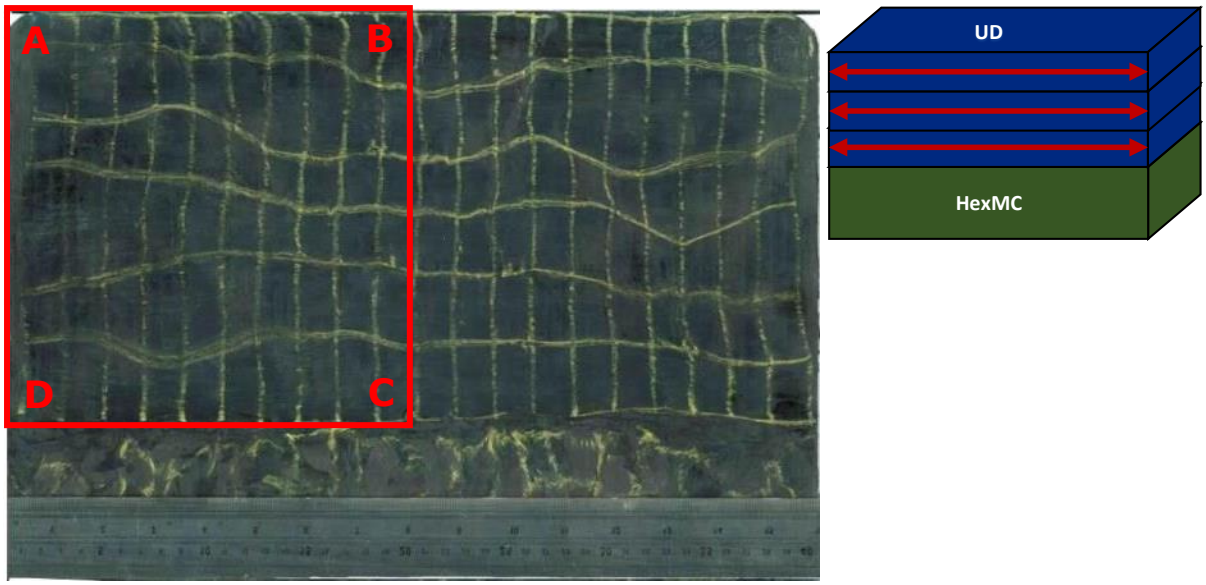

Figure 85: U3 90° H2 60% plaque with the testing region shown as a red square. Charge construction diagram (red arrows indicate UD fibre direction). A to D represent plate locations for Figure 86

There appeared to be no resistance to flow of the UD as it filled the same proportion of the cavity as that filled by the HexMC. The heterogeneous flow of the UD was caused by the HexMC, as seen in H2 60% in the previous chapter. This is due to local thickness variations and fibre orientations in the HexMC material.

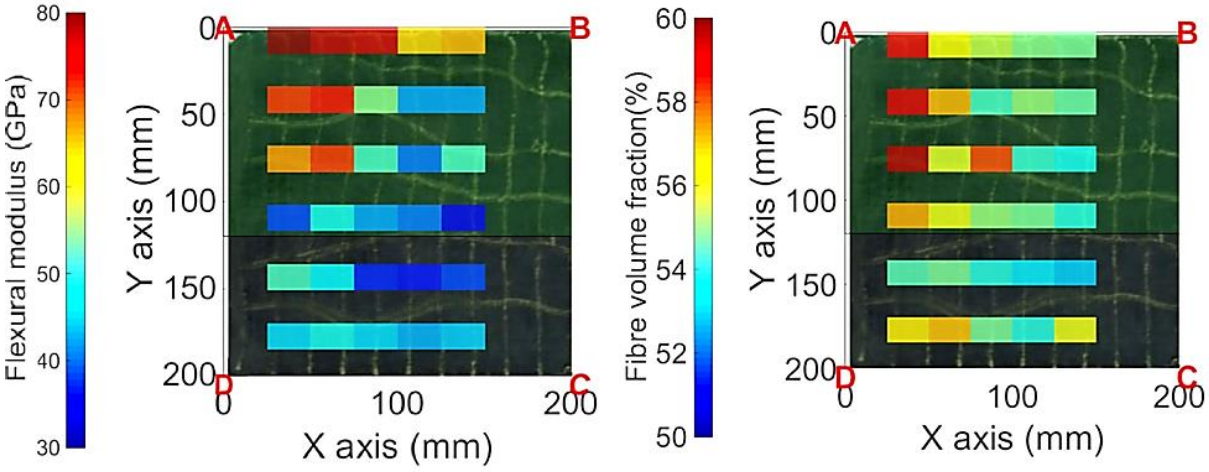

Figure 86: Flexural modulus (GPa) and fibre volume fraction of U3 90° H2 60%

Similarly to U3 90°, the flexural modulus and V_f in hybrid U3 90° H2 60% have a comparable trend and is shown in Figure 86. The maximum flexural modulus and V_f can be observed along the tool edge, **A→B** and at the fibre ends **A→D**. This is

likely caused by similar mechanisms in U3 90° as the resin readily flows along the fibres and out through the flash gap, increasing the V_f.

There was also a peak in the flexural modulus near the weld line **D→C**, which is caused by the HexMC packing and changing orientation when it met the other charge. It is encouraging that V_f peaks there, indicating that the resin is not bleeding out of the material. With this charge configuration and level of charge coverage hybridisation has little benefit compared to pure HexMC since properties range from 83.67 GPa to 35.52 GPa, with such a very large range would be impractical to design a component.

6.3.1. Flow distortion of transverse UD hybrid, U3 90° H2 60%

Using image analysis, the localised strain of the UD reinforcement was measured for U3 90° H2 60% and is shown in Figure 87. There was significant flow in the UD; with 75% of the elements extending by over 50%, and ~24% extending over 100% with an average ε_{yy} extension of 76.59%. There were no cases where the UD had completely split to reveal the HexMC underneath, which indicates that there must be significant thinning of the UD to flow to such a degree.

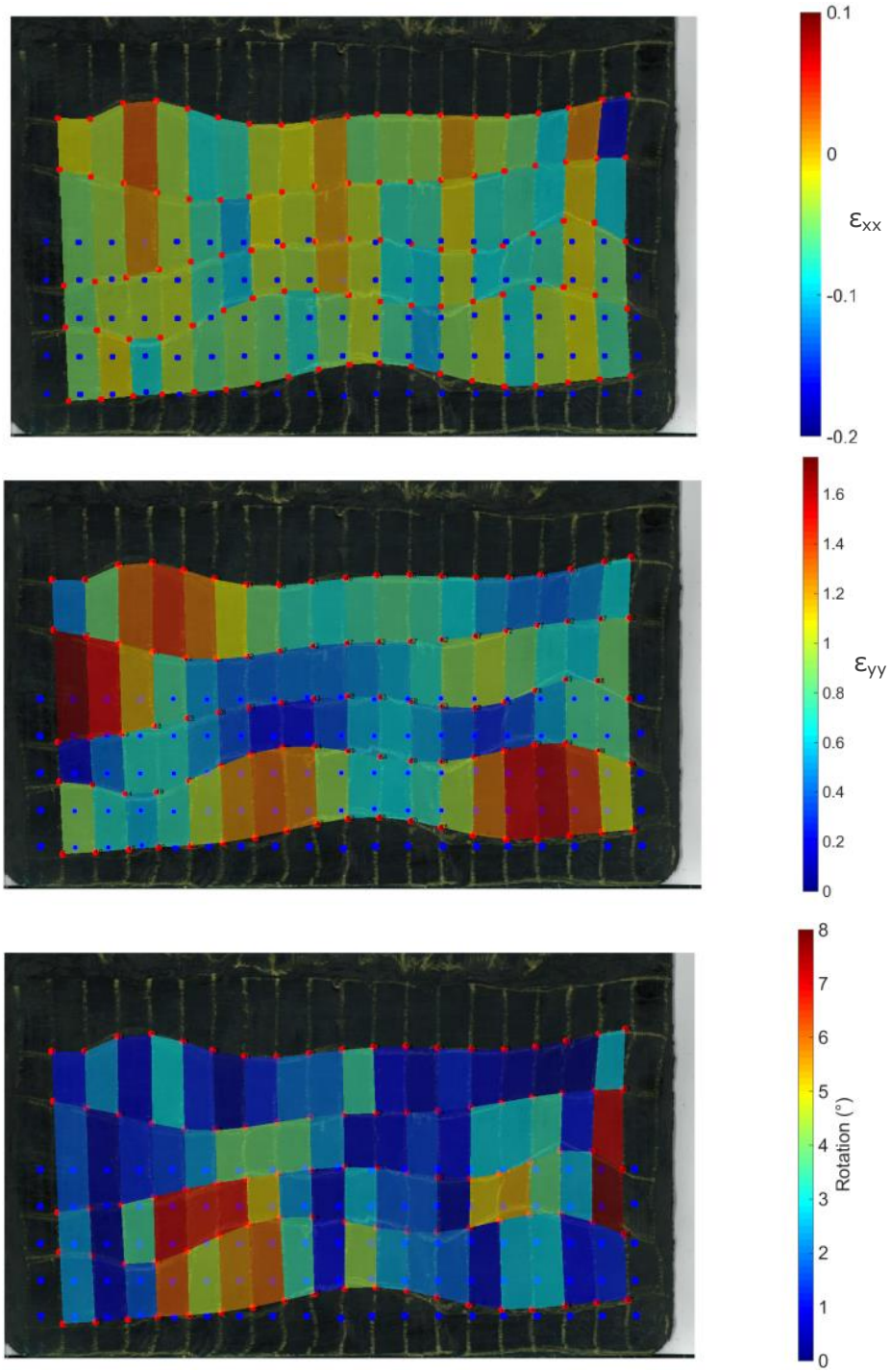

Figure 87: U3 90° H2 60% element extension in the x and y axis and the absolute rotation (°)

The absolute element rotation was on average 2.51° with a maximum of 8.21°, but with no discernible geospatial trend. There was a high degree of rotation within each element which is seen from the original (blue) and the deformed (red) positions of the nodes. This caused the grid to decrease in overall width and pull away from the tool edge.

There was difficulty in measuring the average mean thickness of the UD in a hybridised scenario since a true picture would require numerous destructive micrographs, and even so it can be difficult to distinguish between the UD and the HexMC. A theoretical RoM approach can be used to estimate the extent to which the UD has enhanced the properties of the HexMC, including the degradation in stiffness caused by fibre distortion.

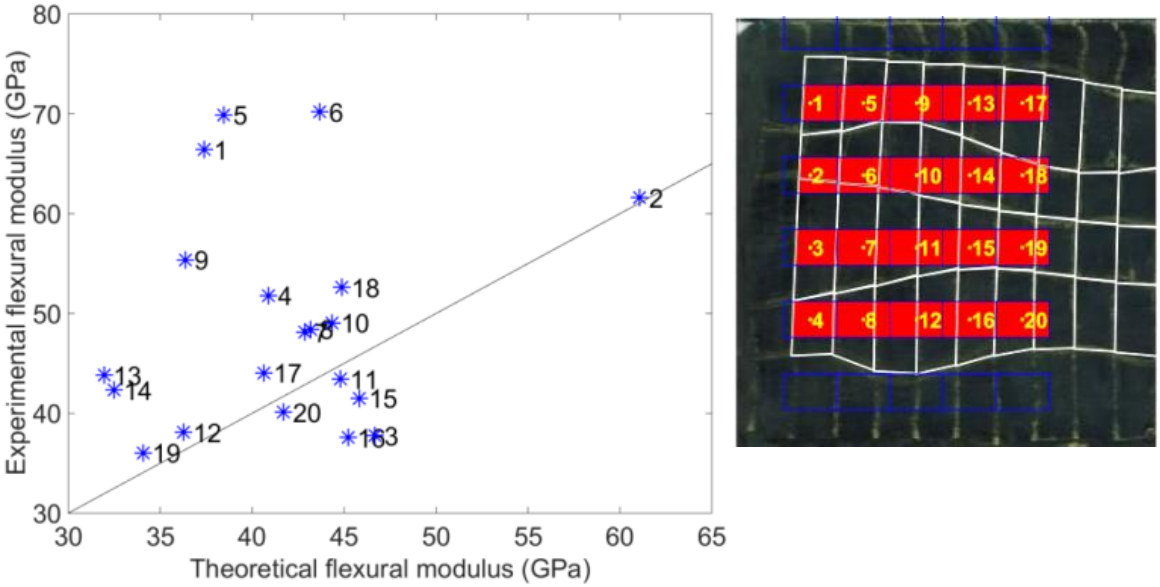

Figure 88: Comparison of U3 90° H2 60% experimental and theoretical flexural modulus with point location

The theoretical stiffness against the measured experimental values for U3 90° H2 60 are shown in Figure 88. The RMSE is 27.84% which is considerably higher than in the UD scenarios, this is from the specimens in the corners of the plaque, exhibit a higher V_f (Figure 86), notably samples **1, 5 & 6**. Sample **2** had a good agreement as the grid element predominately within **2** did not expand leaving the ratio of UD to HexMC locally theoretically unchanged, elevating the flexural properties compared to the other elements, as seen in Figure 88 point location image comparing **1,2 & 3** .

6.4. Hybrids Composites - UD parallel to flow direction (U3 0° H2 60%)

Placing the UD reinforcement parallel to the flow direction in a hybrid fibre architecture was analysed for localised stiffness, fibre volume fraction and photogrammetric data. This ply orientation was done as it was considered that having the reinforcement fibres parallel to the flow direction might resist migration of the HexMC, similarly to U3 0° 60%. This was not the case, as the thermoset resins created a lubricating layer which caused migration of the reinforcement on the hot tool surface. Figure 89 shows the moulded plaque of U3 0° H2 60% which is comprised of three plies of UD and two plies of HexMC, as demonstrated by the diagram to the right of the moulded plaque. The red area refers the region that has undergone flexural testing. There was significant migration of the UD but the UD stayed as a single reinforcement patch with minor shearing along the fibres. Looking closely at the fibre ends of the reinforcement, there was a resin band along the entire interface; this was highlighted by a micrograph of the edge of the UD-HexMC interface which is shown in Figure 90. The flow of the HexMC carried the bottom ply of the UD more than the top ply, creating a stepped region which then filled with resin.

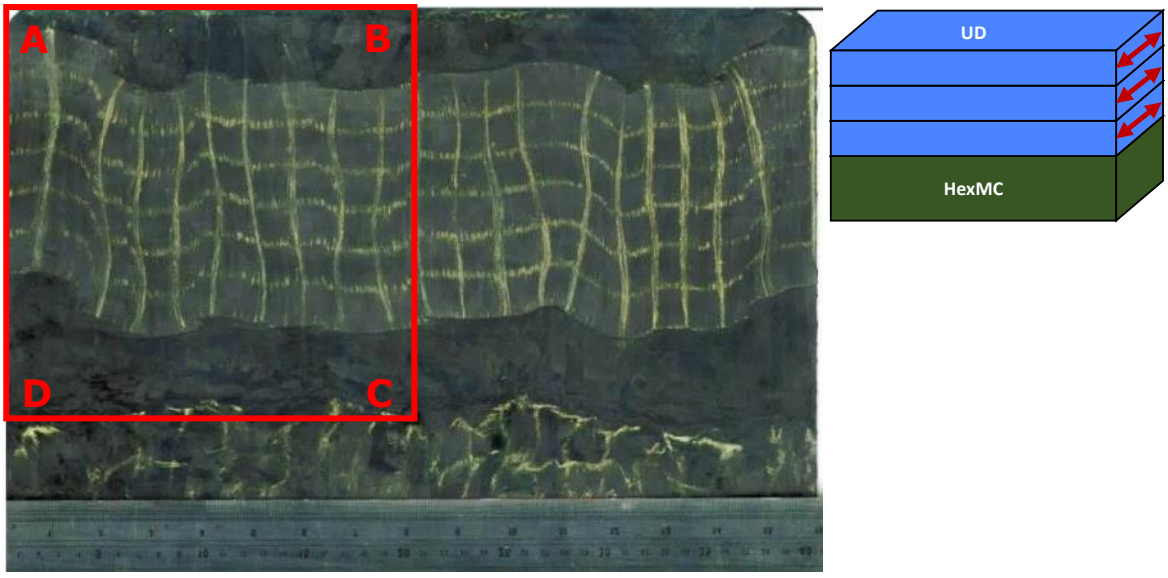

Figure 89: U3 0° H2 60% plaque with the testing region shown as a red square. Charge construction diagram (red arrows indicate UD fibre direction). A to D represent plate locations for Figure 91

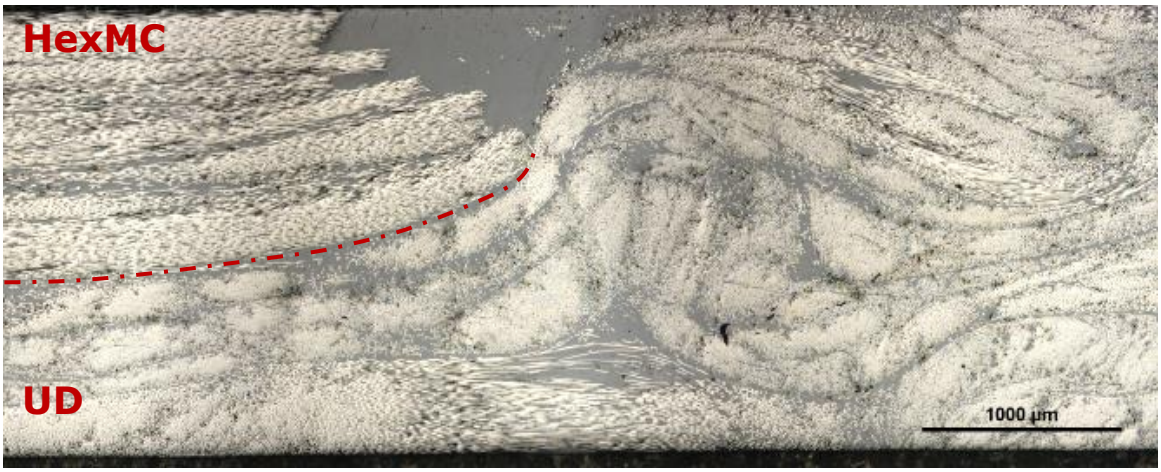

Figure 90: U3 0° H2 60% micrograph of UD reinforcement - HexMC interface

When testing the flexural properties only within the hybridised UD section parallel to the UD fibre direction as shown in Figure 91, the flexural stiffness was 72.82 GPa. This is compared to a mean of 45.81 GPa in H2 60% for samples taken within the flow direction. However, as expected when testing regions that include partial or whole sections of HexMC, the stiffness dramatically declined. There was no discernible trend in the spatial distribution of V_f or between the flexural properties and the V_f.

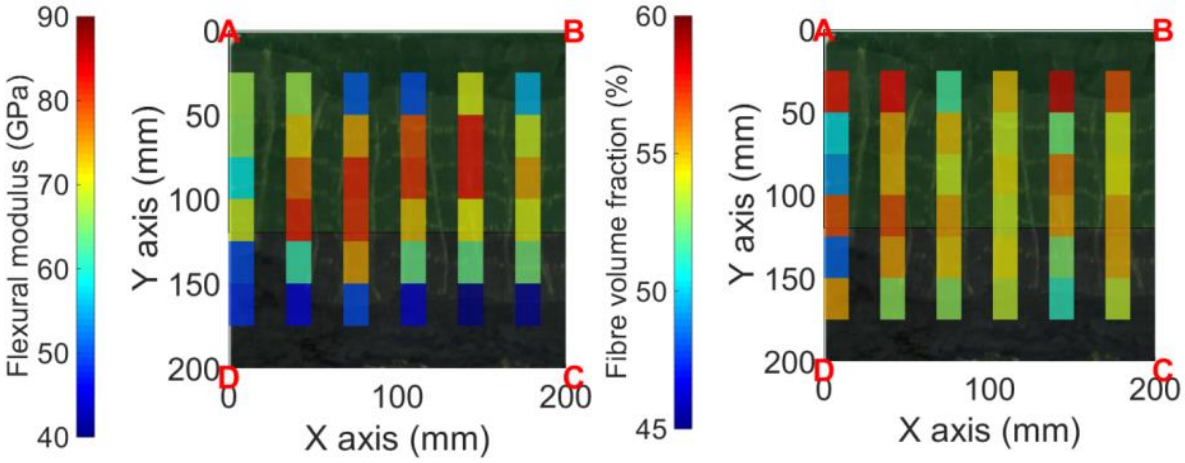

Figure 91: Flexural modulus (GPa) and fibre volume fraction of U3 0° H2 60%

6.4.1. Flow distortion of UD parallel hybrid, U3 0° H2 60%

In U3 °0 H2 60% where the fibres migrated with the HexMC, the rotation was predominately restricted to the edges of the UD, exhibiting rotation of over 18° and up to a maximum of 32°, as shown in Figure 92. The UD material in the centre of the tool flowed more than the material at the edges, causing extensive reinforcement curvature. This was also observed in U3 90° 60%, where there was a similar curvature of the reinforcement UD.

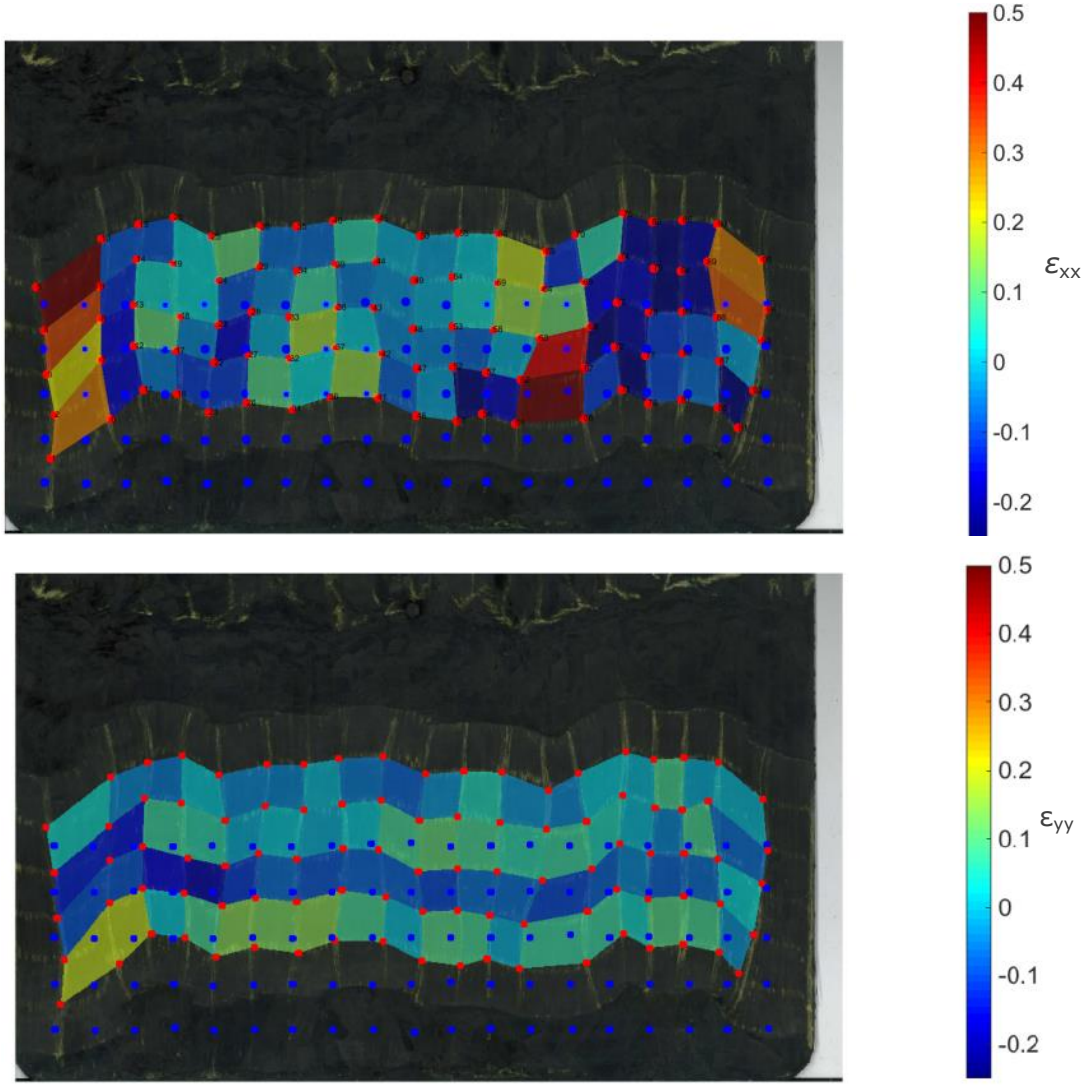

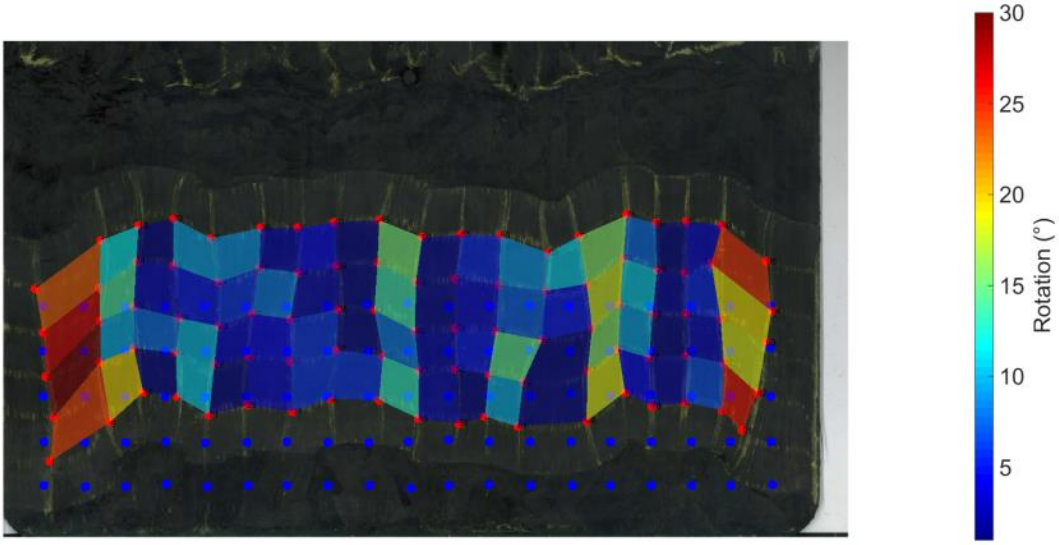

Figure 92: U3 0° H2 60% element strain in the x and y axis and the absolute rotation (°)

Curvature caused the grid elements to reduce in thickness (ε_{xx}), notably seen at the edges in Figure 92; however on average there was a contraction by 1.59%. It was observed that the fibres did not fracture and the elements contracted in the flow (ε_{yy}) direction as well by 0.07%, equating to a reduction of 0.013 mm, however there was no trend in the spatial distribution.

The flexural samples were taken in the flow direction which caused the modulus to be enhanced by both the HexMC flow induced fibre alignment and the UD reinforcement. Although the rotation and the migration look detrimental to the hybrid, at close inspection of the flexural specimens the UD was relatively straight. U3 0° H2 60% in Figure 93, can be used to show that regions towards the flow front of the reinforcement (**10, 15, 16 & 17**) exhibited some of the largest errors from the theoretical flexural modulus. Although the scatter by comparison to the other staged scenarios was small. The RMSE was halved, approximately 12.48% compared to >24.84% in the other hybrids.

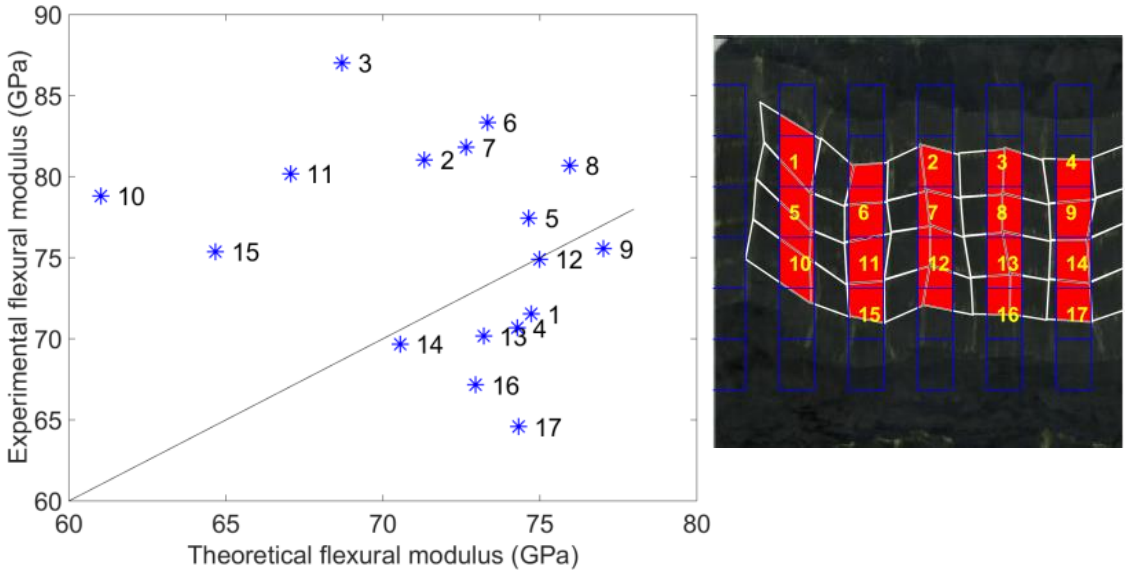

Figure 93: Comparison of U3 0° H2 60% experimental and theoretical flexural modulus with point location

6.5. Hybrids Composites - Comparison

Figure 94 shows the mean flexural modulus of UD, hybrids and HexMC normalised to a V_f of 55%. The mean measured V_f is noted above each bar. The addition of UD in the hybrid plaques all enhanced the stiffness compared to pure SMC; Scenario **3**, U3 H2 100% compared to H2 100% is 43.54% stiffer. The samples in **2** were cut transverse to the flow direction which is comparable to H2 60% transverse and was enhanced by 135.45%. Scenario **1** is comparable with H2 60% parallel and is 56.88% better. Region **β** had similar stiffness as the H2 60% parallel indicating that the reinforcement HexMC interface properties were maintained.

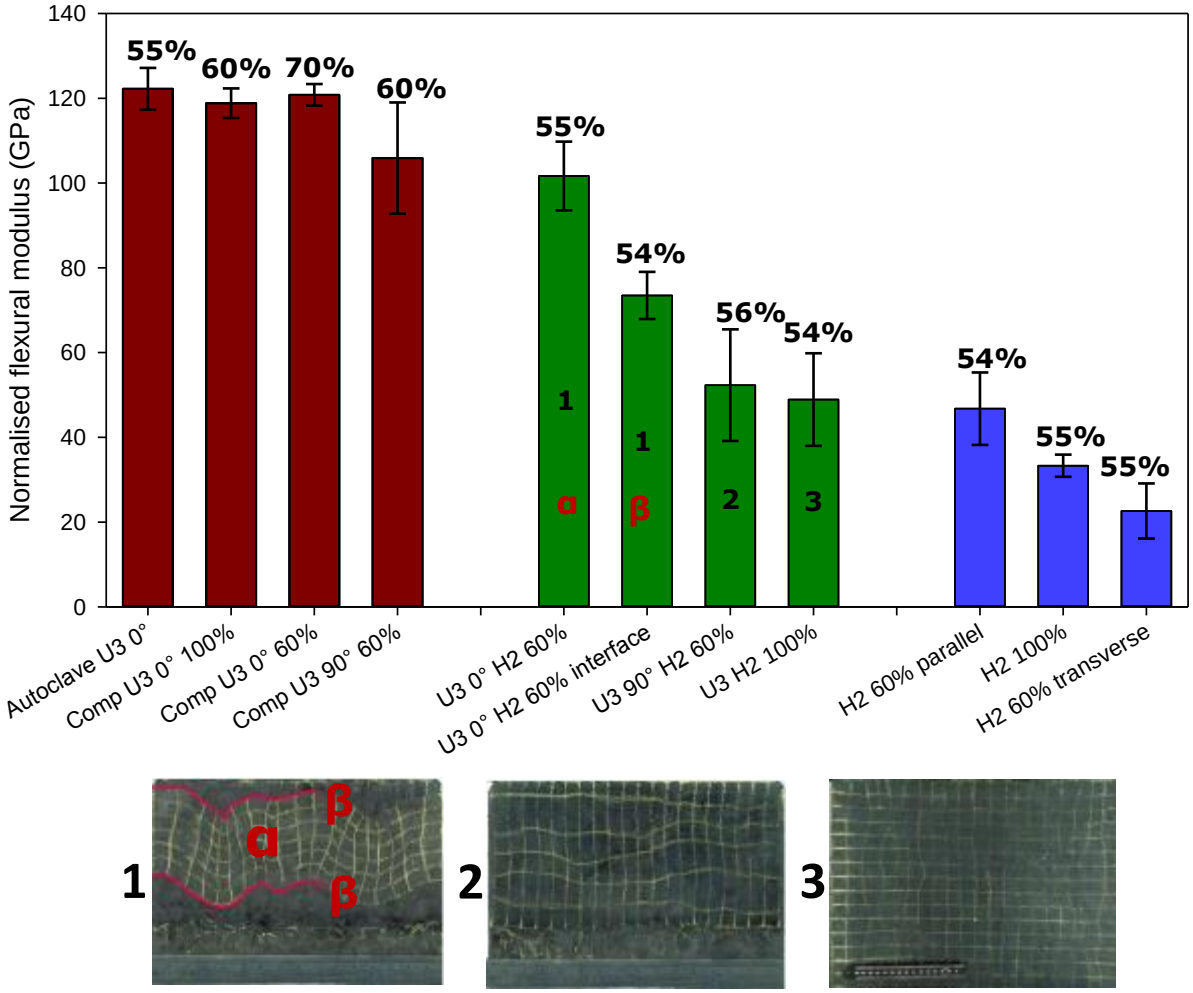

Figure 94: Comparison of the mean flexural modulus normalised to V_f 55% compression and autoclave moulded UD with hybrids and HexMC in differing charge construction. The percentages above the bars are the V_f.

Although compression moulded UD had a higher stiffness then the autoclave plaque, when normalised to 55% V_f the autoclave plaque was 3.1% (3.7 GPa) greater as shown in Figure 94. H2 60% was tested parallel and transverse to the flow direction (blue bars), this showed the stark contrast in normalised stiffness of 46.77 GPa and 22.62 GPa respectively. Almost half way between these results is H2 100%, where there is no flow induced alignment. This demonstrates the effect that flow induced alignment has on the modulus parallel and transverse to the flow direction.

6.5.1. Theoretical flexural modulus

Considering the scatter between the experimental and theoretical modulus, there is a clear pattern that the theoretical calculation does not sufficiently account for the edge effect. Normalising to 55% to account for the V_f increase does improve the accuracy but does not remove the edge effect as the trend is still apparent in Figure 88 and Figure 84. Table 12 shows the mean hybrid experimental and theoretical flexural moduli, the mean error between the values, and the difference between the mean of the experimental and theoretical values as a percentage. Although the mean RMSE of the scenarios were large, between 12-28%, the scatter caused by the large degree of flow created difficulty in predicting stiffness reliably. The net-shape plaque, even with its numerous defects, had a mean theoretical stiffness 3.59% lower than the experimental; however, the flow scenarios with the UD transverse and parallel to the flow direction were underestimated in the theoretical prediction by 17.46% and 5.61% respectively. This may have been caused by increased flow alignment above that observed in the H2 60% scenario.

	GSA Hybrid mean (GPa)	GSA HexMC mean (GPa)	Theoretical mean (GPa)	RMSE	$\frac{\text{Exp}}{\text{Theo}} \times 100$
U3 90° H2 60%	48.91	21.47	41.64	27.84%	117.46%
U3 0° H2 60%	75.88	47.35	71.85	12.38%	105.61%
U3 H2 100%	48.90	33.31	50.72	24.84%	96.41%

Table 12: Comparison of mean grid strain analysis (GSA) flexural modulus of hybrid composite with theoretical, including the flexural specimens related to the same position; all normalised to 55% V_f.

6.6. Summary

The hybrid plaques exhibited a larger stiffness than the corresponding pure HexMC counterpart, demonstrating that hybridisation can enhance the SMCs stiffness.

In contrast with the image analysis of the UD composites from the previous chapter, the hybridised composites had a larger RMSE, 5%-16% compared to 12% - 28%. The flow scenarios tended to over predict and the net-shape under predict but numerous defects were visible. The large RMSE was likely caused by the variability of the HexMC causing localised variations in flow.

There are significant challenges in hybridisation, mainly arising from large localised variations in flexural properties due to the HexMC which can migrate and distort the reinforcement. The resin permeability of the reinforcement causes local variation in V_f, even in a zero flow scenario, and increases the stiffness at the fibre ends.

Controlling this distortion is critical for two reasons. Firstly, it is undesirable to manufacture a component where it is not possible to predict the location of the reinforcement post-moulding. Secondly, limiting the flow of the reinforcement and resin may also aid in reducing the variability and enhance the performance of the hybrid. Preventing large deformation of the reinforcement will minimise localised thinning and fibre misalignment that was demonstrated in the hybrid plaques. Preventing resin flow may also reduce the resin band along the entire UD-HexMC interface that was observed in U3 0° H2 60%, but this could increase void content as trapped air will not be able to escape.

The next chapter will minimise distortion and migration using two approaches: by varying reinforcement ply construction and by partially curing the UD in order to increase the viscosity of the resin to prevent flow.

7. Hybridised Composites – Staged

This chapter is divided into two parts: to determine the optimum staging parameters for the UD prepreg to minimise flow-induced distortion during the processing of hybrid architectures, whilst maintaining inter-laminar properties. The second part is a charge flow study to quantify the influence of the staging and evaluate the resulting stiffness of the hybrid panels.

7.1. Prepreg Staging Determination

As pure resin samples were not available, prepreg was used instead which was considered acceptable as this analysis was to determine the change in flowability of the UD. As the epoxy resin cures, the degree of cross-linking increases as it begins to solidify; this change can be measured by the storage modulus. This change in elasticity can be used as a means of quantifying the degree of cure. The greater the level of cure, the stiffer the resin becomes, and therefore the more resistant to flow.

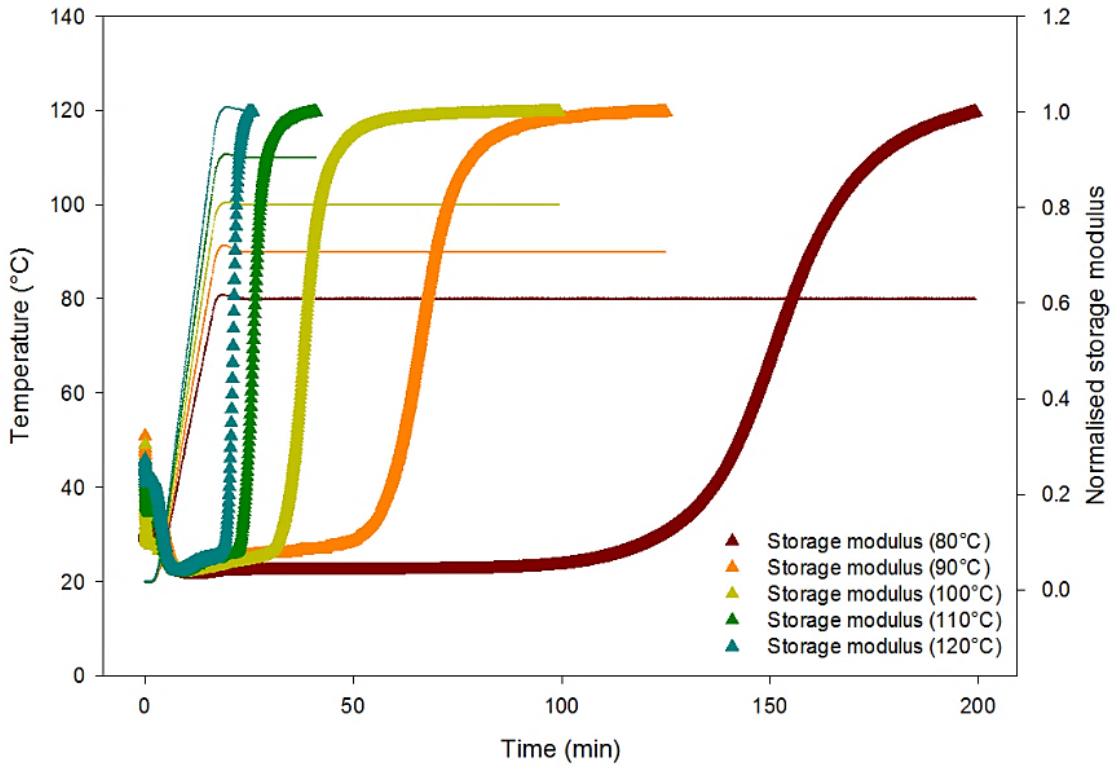

Figure 95: Effect of different temperature dwells on storage modulus

Figure 95 shows the change in normalised storage modulus at a given time for different temperature dwells. The data was normalised to the maximum storage modulus recorded for each temperature. Prepreg was placed in a rheometer chamber at room temperature, at a relatively high viscosity. This is then warmed, causing a temporary decrease in storage modulus, followed by a plateau. Eventually the resin starts to cure by cross-linking and the storage modulus rapidly increases. These results correspond to the changes in epoxy resin storage modulus described in the literature review. The dwell temperature significantly affects the duration of the plateau; which is where curing is occurring but not significant enough to affect the storage modulus, as there is only chain lengthening[63], which is later followed by cross-linking leading to a rapid rise in the storage modulus.

This worked investigated staging to minimise flow. The initial horizontal region, will be considered to have negligible curing (near 0%) as the change in material behaviour, flowability, has not been significant. 100% cured will be measured at the final plateau in the storage modulus in Figure 95. Most of the reaction happens very quickly and as a result, this makes it difficult to stage to specific levels. For example, at 120°C the time to change from 25% to 75% staged is 0.83 minutes, leaving a high margin for error. However at 90°C there is a large enough window of ~11min for practical extraction of samples during staging between 25% and 75% staging. The duration of >60min for staging is not a realistic industrial solution to match the processing time of compression moulding. However, resin formulation or increased temperature curing with strong process parameter control would result in similar effects and make this process viable.

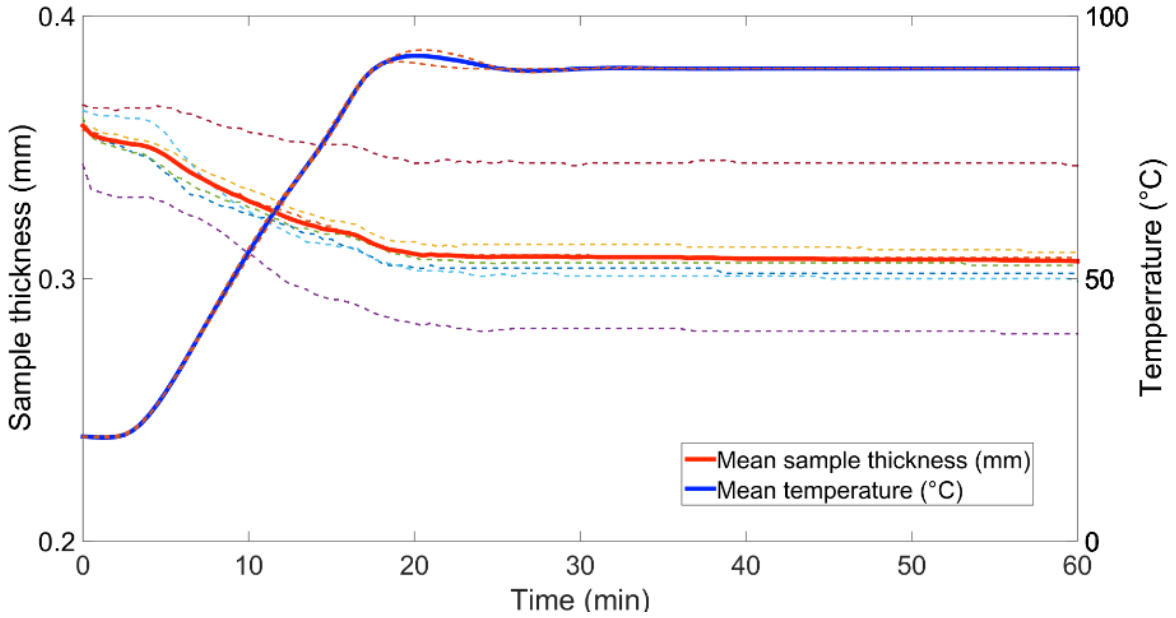

Figure 96: Mean change of sample thickness and temperature over time. Dotted lines show raw data, highlighting prepreg variability.

As the prepreg has a resin-rich side (lower) and a dry side (upper), full contact with the upper or lower platens of the rheometer is a challenge as the samples are not smooth. A small normal load (1 N) was maintained to ensure contact was kept throughout the test. Notably, after heating, there was a degree of flow as the viscosity decreased. This is shown in Figure 96, when the prepreg compacted, becoming thinner during the initial stages of the test. However, no resin or fibres were squeezed out from under the parallel platens. This demonstrates that the resin did not leave the material and is representative of the prepreg during moulding. Additionally, during the bulk of the staging time the material was not changing thickness, so the storage modulus data is measuring flow when the material is not consolidating.

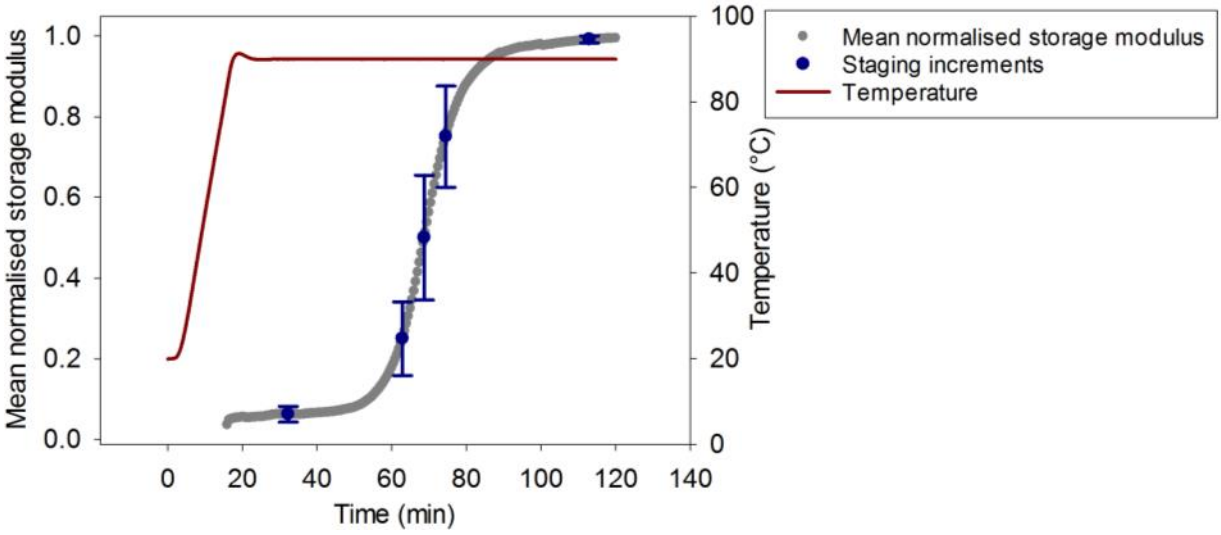

Figure 97: storage modulus of UD during at 5°C/min ramp and 90°C dwell

The storage modulus was averaged between five tests. Figure 97 shows the mean normalised storage modulus for a dwell at 90°C. The results show that there is very little change in the mean normalised storage modulus between 16-50 min, but the reaction accelerates between 60-80 min and is almost complete after 90 min. The tests averaged with locations plotted at 0.5%, 25%, 50%, 75% and 99%. These times are presented in Table 13 and were used for the staging durations.

Staging value	Time (min)	Standard deviation of normalised storage modulus (%)
0.5%	32.25	1.8
25%	62.91	8.4
50%	68.75	14.3
75%	74.53	11.6
99%	112.96	0.8

Table 13: Time corresponding to desired staging level, and standard deviation of the normalised storage modulus

Staging is a potential option to prevent flow of the reinforcement by affecting two factors. The staging of the prepreg increases the viscosity of the resin, reducing its ability to flow. Staging may also reduce the effect of the lubricating layer, preventing the reinforcement from readily sliding across the tool face during flow of the SMC. Figure 98 shows the loss factor with the gelation point (loss factor = 1) between 0.5% and 25% staging at 52.25 min. The mean value

was calculated by taking the average from the same tests presented in Figure 97. This shows that the resin has gelled and will no longer be acting as a lubricating layer in staged hybrid composite which aided in the migration of the reinforcement when there was no staging. This means that to have any practical degree of staging for flow mitigation gelation must occur.

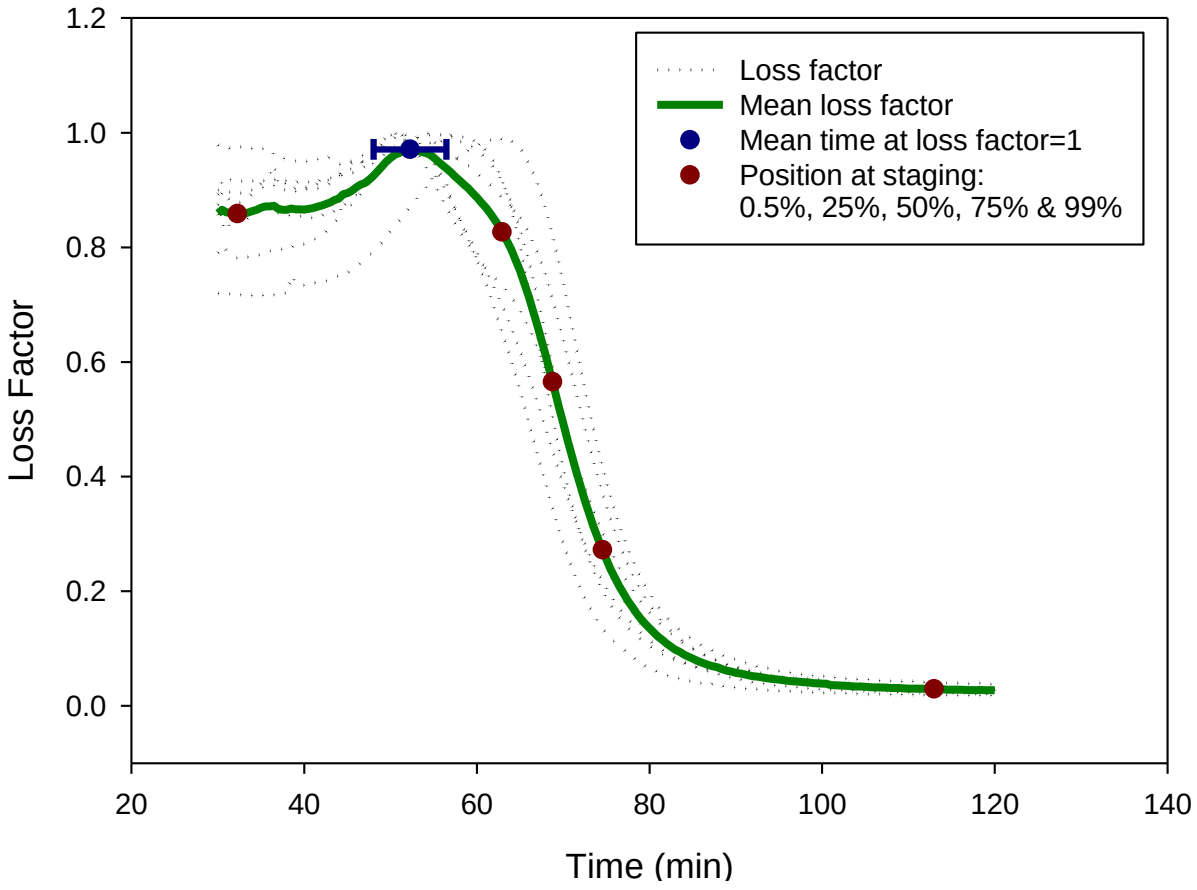

Figure 98: The gelation point, tan δ (blue) at 90°C, with staging positions times (red), increasing from 0.5% to 99%

The variability in Figure 97 can be attribued to the deviation in the contact area between the prepreg and the parallel platens of the rheometer, variation in the V_f in a single ply of prepreg and stray fibres. Stacking multiple plies, using a roughened or ribbed parallel platen and a lower frequency may all reduce the variability between the samples. This data was used to estimate the staging time of large plies of prepreg; therefore, five samples were deemed sufficient to account for the sample-sample variability.

7.2. Inter-laminar shear strength

Inter-laminar shear strength tests were conducted to evaluate the quality of the interfacial adhesion between the staged UD prepreg and the non-staged HexMC in hybrid laminates. For the purpose of this study, UD prepreg was used for both the staged and non-staged materials to provide greater control over material variability. ILSS is essentially a short spanned 3-point bending test where the top of the specimen undergoes compression and the bottom surface is in tension. Each scenario was tested ten times in order to determine if there was an orientation bias. Five were tested with the staged side face up and five facing down as seen from the results in Figure 99.

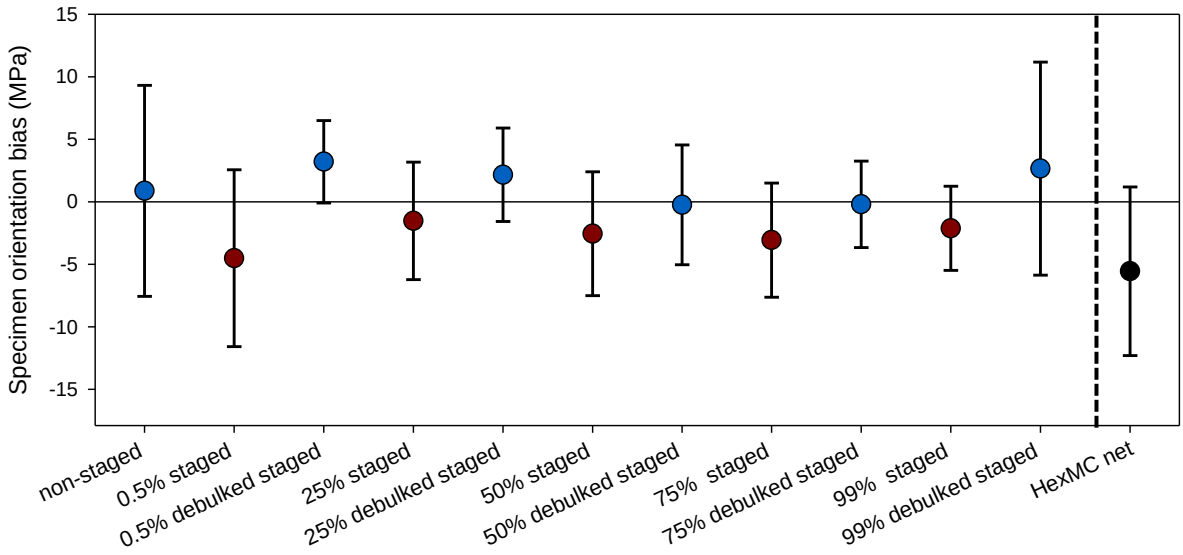

Figure 99: ILSS tests on staged UD, under compression bias (-ve) or under tension bias (+ve), with HexMC as a comparison, Debulked in blue and not debulked in red.

On average, excluding the HexMC, there is a bias of the non-debulked staged UD under compression to yield artificially higher results of 4.93 MPa. However there was a tendency for the debulked UD to have tension bias. This was caused by the UD section under tension dominates the composite properties, so if the weaker section was under compression the properties would be higher.

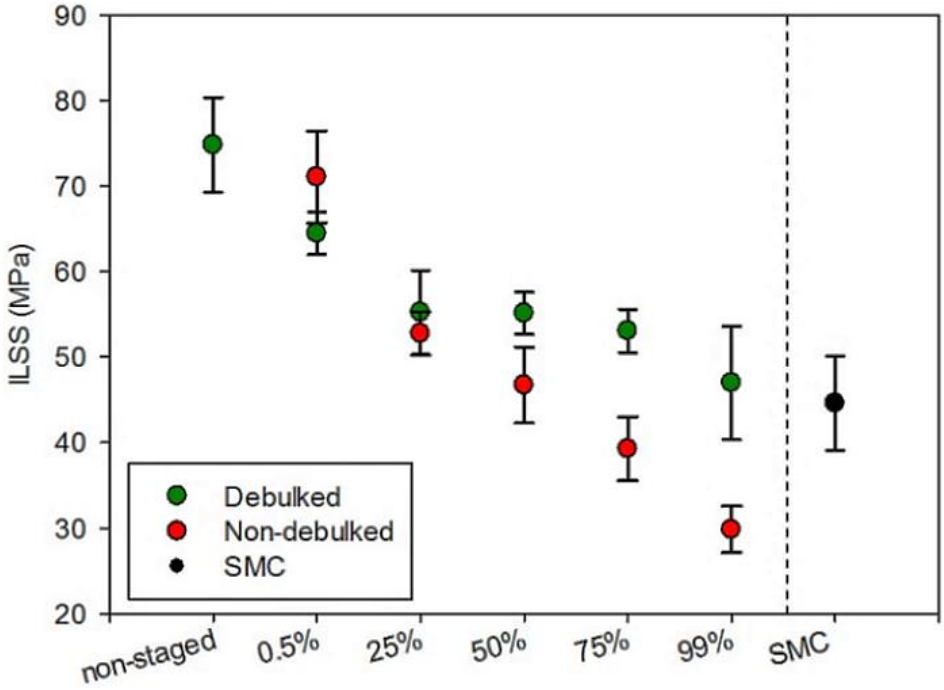

Figure 100: Influencing of staging on the ILSS of UD prepreg samples. Staged samples consisted of 3 plies of staged UD and 3 plies of non-staged UD OOA moulded. SMC is included for comparison.

The testing of the staged side under compression and tension were averaged together to provide a comparison between the non-staged, staged and debulked-staged samples in Figure 100. The ILSS decreases linearly with increasing levels of staging. Debulking the UD plies prior to moulding had a negligible effect on the ILSS up to staging levels of 25%. However, debulking and staging past 25% improves the laminate consolidation and removes entrapped air, as the increasing ratio of voids has a detrimental effect on the ILSS [124]. Material staging reduces the resin viscosity and decreases the opportunity for void evacuation during debulking and curing, which is likely to be a cause of the degradation in ILSS. Compression moulding these staged plaques may have enhanced the adhesion, since the pressure is 84.5 bar compared to 1.22 bar in out-of-autoclave, though there is no vacuum in compression moulding to extract voids.

7.2.1. ILSS Failure in OOA staged UD

Figure 101 shows typical through-thickness fracture locations for a range of ILSS samples with different levels of staging. From 0% to 25%, failure occurred between all plies. For staging levels greater than 50%, failure was concentrated at the interface between the non-staged UD plies or only within the staged UD.

The observed failure modes in ILSS help determine an appropriate degree of staging.

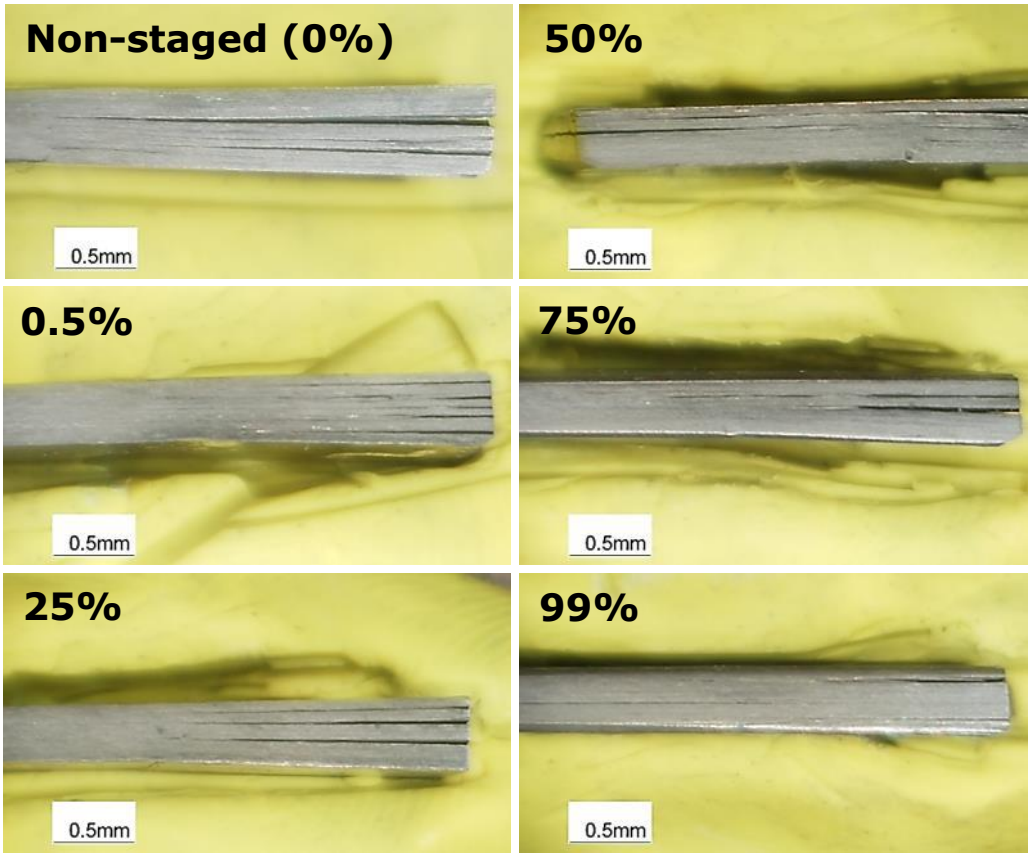

Figure 101: Side image of failed ILSS specimens. Three plies of staged UD are at the top of each sample as shown, and three plies of non-staged UD are at the bottom. All samples were moulded out of autoclave, in a vac bag.

The images in Figure 102 show the end of an ILSS specimen staged to 0%, 50% and 75%. In the 75% specimen delamination occurred between each of three staged plies, with no signs of failure in the non-staged half of the specimen. Failure in the 0% and 50% staged samples was more random throughout the thickness. This demonstrated that staging to 75% caused improper adhesion to the non-staged plies. This, together with the ILSS data, shows that staging past 50% is detrimental to the adhesion properties between the staged and the non-staged UD and should be avoided.

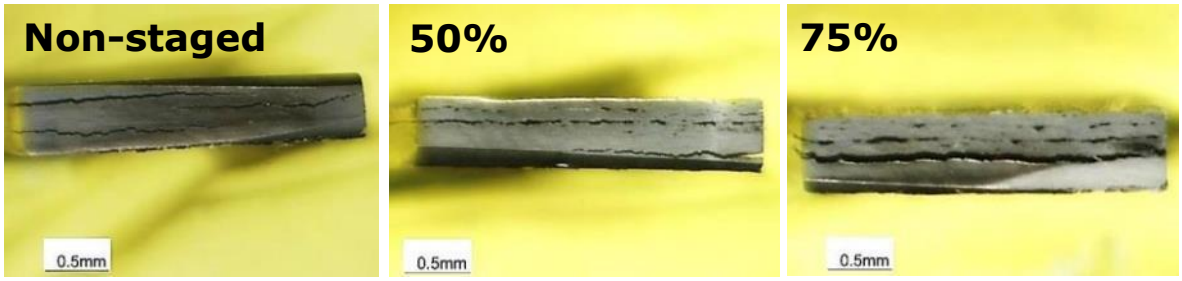

Figure 102: ILSS failure for samples constructed from 3 plies of staged UD (top half) and 3 plies of non-staged UD (bottom half). All specimens moulded out-of-autoclave and percentage values indicate degree of staging.

7.2.2. Failure of compression moulded HexMC

Although SMCs are not a laminar material with discrete plies, the fibres tend to remain in-plane. This tendency causes ILSS tests to fail in a range of modes, as well as inter-tow shearing as shown in the acceptable inter-ply failure image in Figure 103. The ILSS of HexMC was 44.6 MPa with a mixture of acceptable failure modes. There was no trend in strength to failure mode type. The failure is unlikely to be linear since the crack propagates through the weakest regions of the heterogeneous specimen.

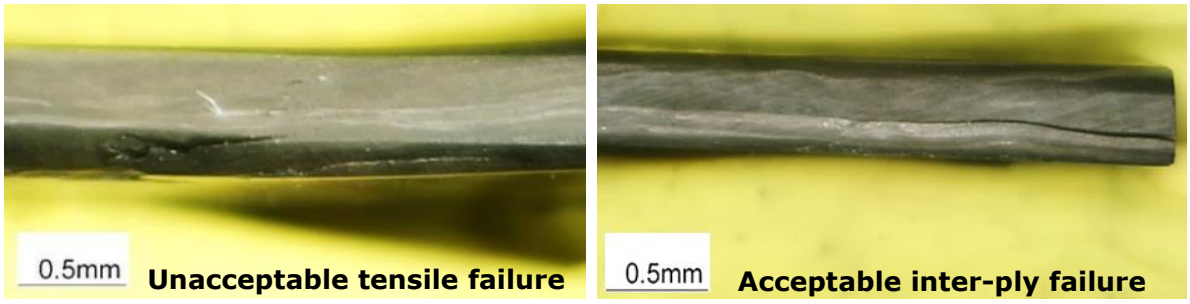

Figure 103: H2 60% specimens parallel to the flow direction

Inter-laminar shear is the dominant failure mode for specimens manufactured from UD prepreg. The failure modes for SMCs were a mixture of acceptable shear and unacceptable compressive or tensile failure according to the failure modes listed in the standard (see BS EN ISO 14130:1998), as shown Figure 103 and Figure 104. For HexMC, inter ply, or more accurately inter-tow crack failure would propagate through the specimen; however, due to the heterogeneity the failure was not as straight as a UD material. Figure 104 shows the occurrence of a vertical step.

Figure 104: H2 60% specimen's perpendicular to the flow direction

During ILSS testing it was observed that when the specimen was left to develop failure on the underside (tension) past the initial maximum ILSS, there was a tendency for the failure to step and travel along the specimen to a fibre end, as illustrated in Figure 105. This type of localised strain was also observed by Johanson et al. [129] during tensile testing of discontinuous fibre composites. Localised higher strains were observed when a bundle end coincided with a transverse fibre, causing a large stress concentration on the surface.

On the underside of a specimen it was observed that failure would follow either tow boundaries or travel in the fibre direction of a surface tow. In Figure 105 the blue line indicates a tow edge and the red line indicates the fracture. Notice in image **A** that the path matches the tow edge exactly, but in **B** the path follows the fibre direction steps diagonally and briefly follows the underlying tow boundary and then along the surface tow fibre direction. This shows the heterogeneity of the material and crack propagation in SMCs.

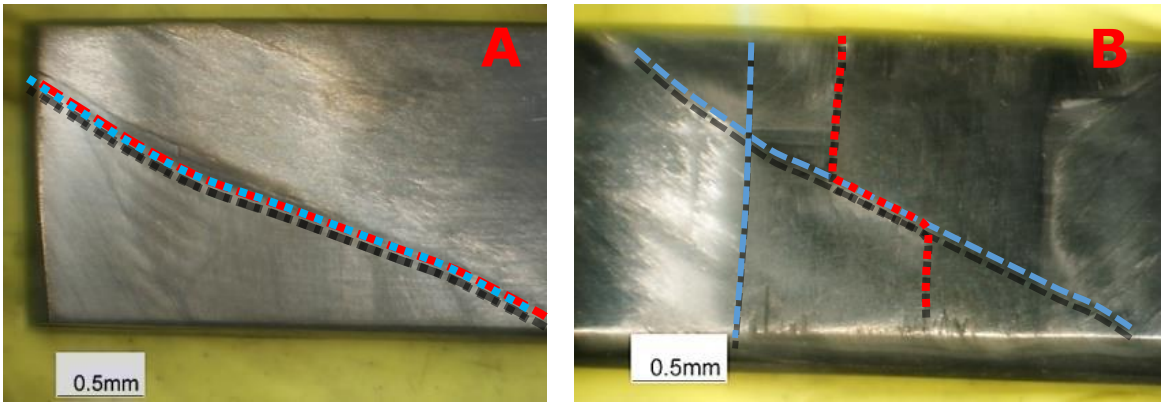

Figure 105: HexMC P2 100% ILSS underside, failure path (red), surface tow boundaries (blue)

7.2.3. Summary

This work was conducted with the aim of using material staging as a means to restrict the flow of the UD reinforcement when moulded with an SMC, without excessively degrading the reinforcement properties. This was done by determining a method to consistently stage the material to a required degree and to measure the extent of the staging on the adhesion between staged and non-staged materials. This can then be applied to the compression moulding of hybrid composites.

This research is to determine and demonstrate a suitable staging of UD to be used in the hybrid study. Staging of <25% is the point where debulking has little benefit, but does aid consolidation at 50% staging and onwards. Debulking improves the ILSS of staged prepreg; however, the added operation time to bag and debulk prepreg is not commercially viable at the production volume comparable with compression moulding. A series of platens where the prepreg could be heated and consolidated might provide similar conditions to debulking while achieving higher production rates.

Non-debulked UD plies staged to 50% should be used to produce plaques with hybrid architectures to enhance the SMC, as the ILSS staged UD was shown to be comparable to the ILSS of the SMC. Additionally the failure locations of ≤50% staged plaques were within the staged and non-staged plies within the specimen, and only in the staged regions at ≥75%. Therefore 50% staging was the limit to prevent degradation past the ILSS of the SMC. Staging to 50% is the maximum staging that should be used to limit the flowability of the UD in compression moulding. This will be applied to the flow of the reinforcement in the study.

7.3. Reinforcement staging effects on hybrid composites

Using staging of the UD prepreg to limit the flowability, Figure 106 shows the effect of the increased staging on reinforcement. All scenarios had a charge dimension of 405x122mm and coverage of 60%. While 0% staging produced a reinforcement flow of approximately 203mm and an extension of 66% measured from the initial width (122mm) to the maximum width after moulding. It is likely the UD would have flowed further but it stopped at the weld line, indicating that the flow of the reinforcement was not restricted.

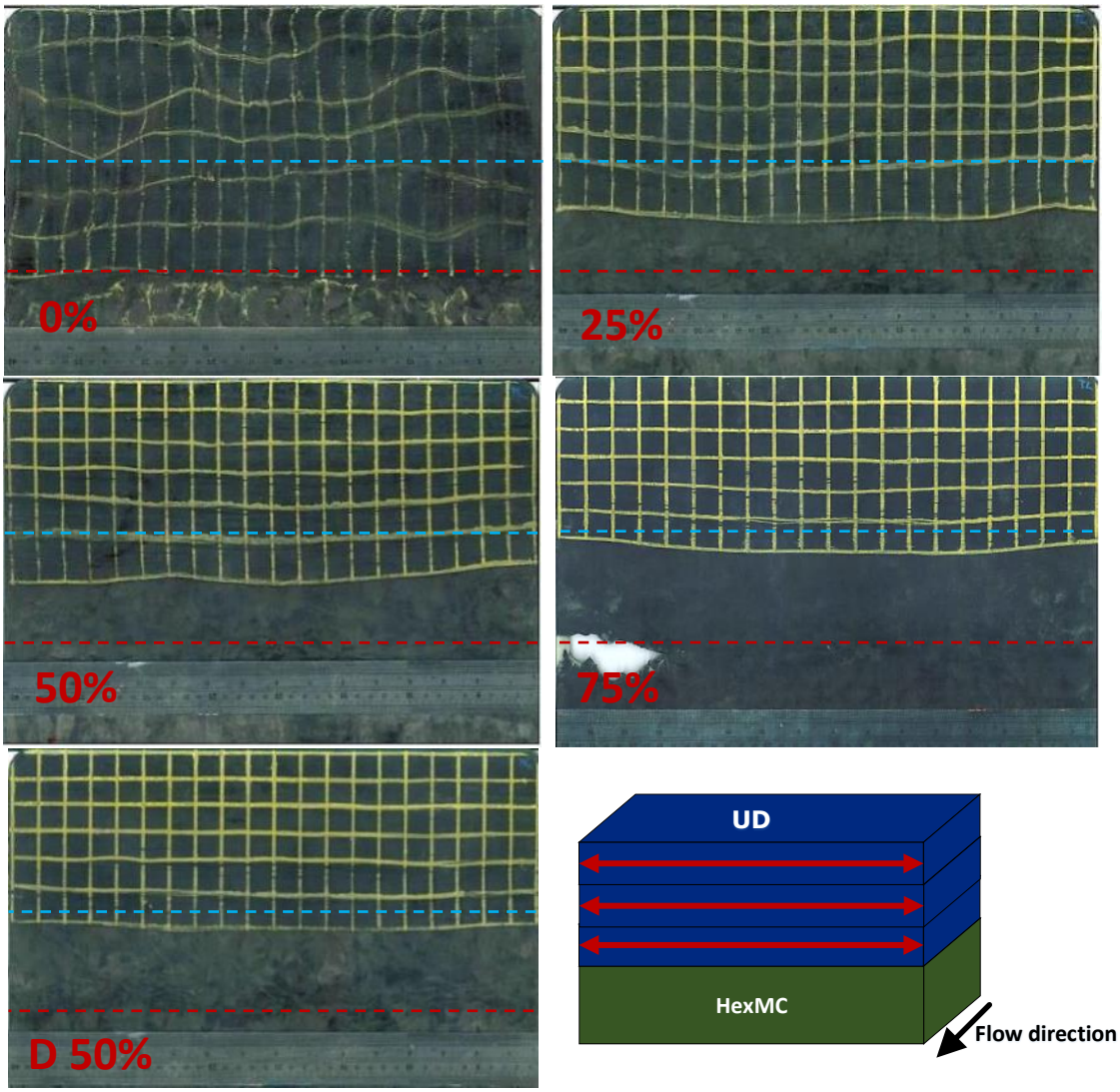

Figure 106: Image of three plies of staged UD with two plies of SMC at various stagings with a debulked 50% scenario (D). The dashed lines are the initial charge local (blue) and the centre weld line (red).

Staging from 25 to 75% reduced the flow to between 34.4% and 9.08% respectively, as shown in Table 14. Debulking with 50% staging had a marked effect on the flow of the material, reducing it from 28.7% to 13.9%. Although this is encouraging, the aim of this process was to provide a fast method for preventing flow, by matching the process step time with the compression moulding curing cycle time. Placing the charge in a vac bag for 15 minutes prior staging is not practical.

Charge configuration	Staged	Distance flowed in mm (extension %)
U3 90° H2	0%	203mm (66.4%)
	25%	164mm (34.4%)
	50%	157mm (28.7%)
	75%	134mm (9.08%)
U3 90° H2 Debulked	50%	139mm (13.9%)
U3 0° H2	50%	129mm (5.7%)
U2 90° U1 0° H2	50%	133mm (9%)

Table 14: Distanced flowed of the reinforcement in increasing staging and charge design

For the 75% staged scenario, the reinforcement limited the flowability of the SMC, as it was the only scenario where there was not a complete weld line, which indicates that the staged reinforcement may reduce the flowability of the SMC.

With the staging being past the gelation point, there was no lubricating layer so changing the UD configuration to be parallel to the flow direction increased the resistance to migration. This configuration, with 50% staging, reduced the migration of the reinforcement from 28.7% to 5.7%, as shown in Figure 107. This high level of flow resistance was from the fibre resisting migration as carbon fibres do not elongate.

Using a single ply parallel to the flow direction at the HexMC interface was succesful as this allowed the entire reinforcement to resist the flow of the SMC,

as it protected the transverse fibres. This is shown by the charge configuration illustration in Figure 107. In this charge construction the maximum flow was 9%, with one ply in contact in the SMC parallel to the flow direction and the the other two transverse. This highlights that charge design has a significant role in limiting the flowability of the material.

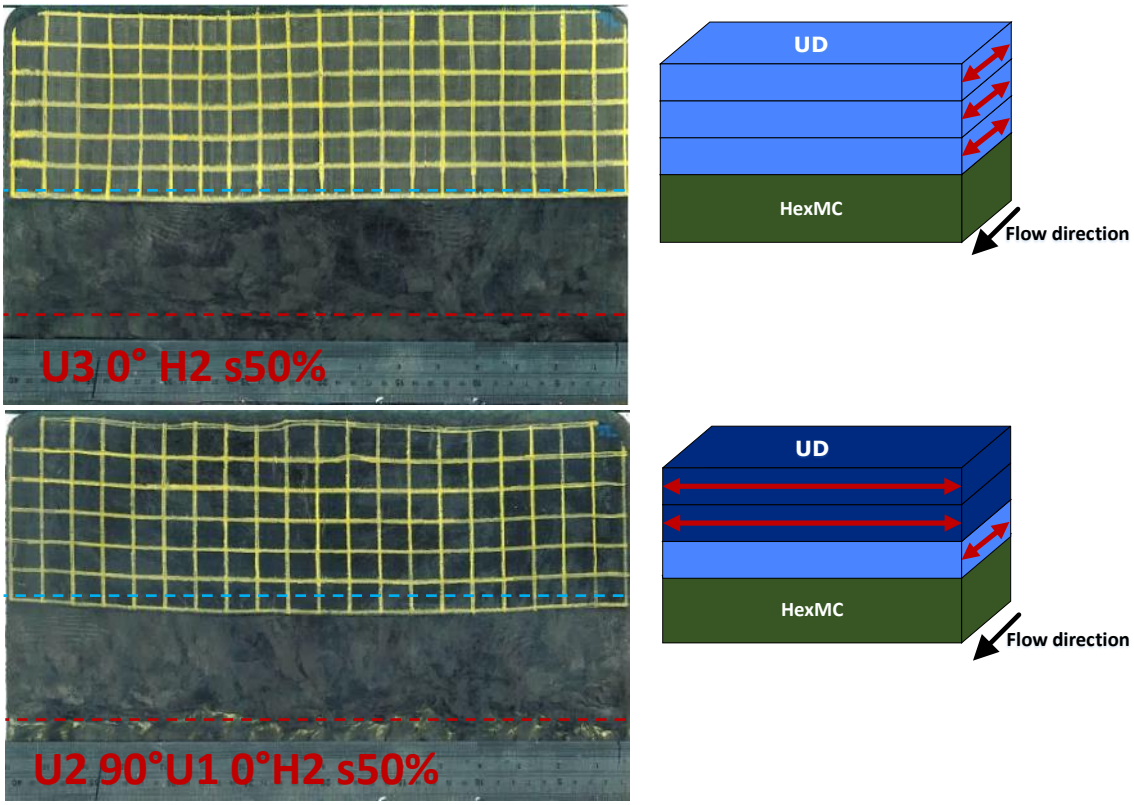

Figure 107: Different charge design of three plies of 50% staged UD moulded on top of 2 plies of SMC. The dashed lines are the initial charge local (blue) and the centre weld line (red).

7.3.1. Defects caused by staging

In U3 90° H2 where no staging occurred, spreading of the UD occurred, similar to the laddering observed during the flow of the SMC. In comparison, the staged scenarios exhibited less laddering but more tearing where the UD split, shown in Figure 104 . This was confirmed the micrograph Figure 108, which shows a resin band in the UD reinforcement Figure 108. This was observed in all U3 90° H2 staged scenarios at multiple locations.

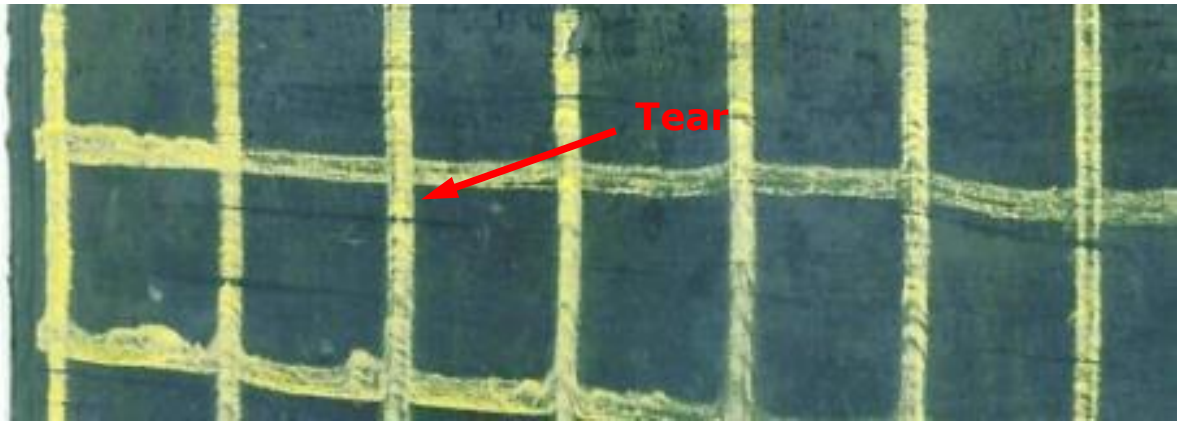

Figure 108: Close-up section of image U3 90° H2 s25%, micrograph E1 in Figure 109

The resin band example in Figure 109 is of U3 90° H2 s25%, which shows the effect of the reinforcement tearing. The UD has completely split, filling with resin. This effect can be felt on the surface of the plaque, in the form of a sink mark.

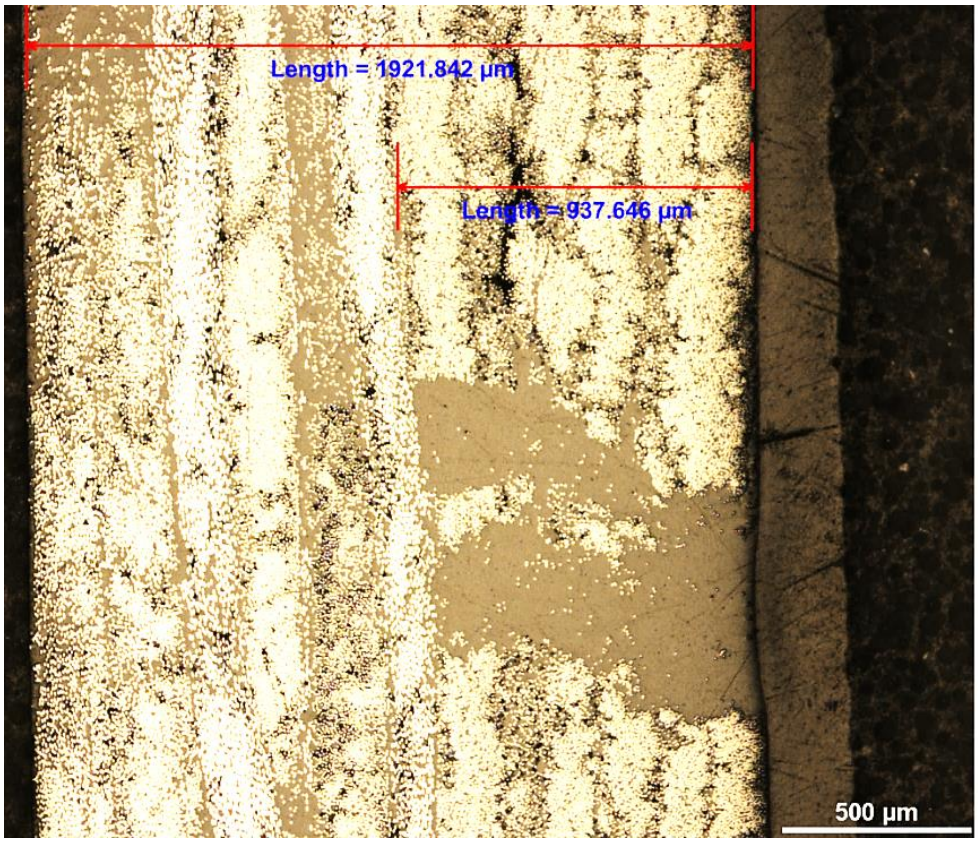

Figure 109: Micrograph E1, U3 90° H2 s25%, depicting tearing of the UD reinforcement, location shown in Figure 108

The opposite surface to where the UD is placed in the hybrid plaque has a distinct area of dry fibres. Figure 110 shows U3 90° H2 s50% where the dry region mimics the reinforcement edge contour on the other side; this was observed on all the other staged plaques. There is a ~5% decrease in V_f in these areas for ≥50% staged samples; however, no apparent decline was observed in V_f on 25% staging, and although the marks are still present they are more faint. The cause for this dry region is likely from high flow coupled with the initial pressure on the stiffened reinforcement, which is not as compressible as non-staged UD. This created a locally higher pressure which caused abrasion on the SMC surface in contact with the tool exposing fibres.

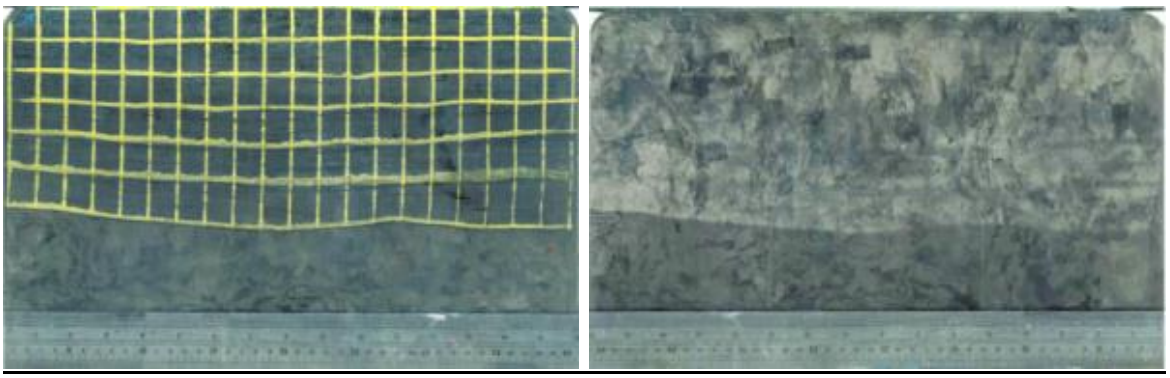

Figure 110: Images of U3 90° H2 s50%, the top and bottom of the left side of the plaque

A micrograph of a section where the reinforcement ends, spanning the dry region, was taken to determine if this dryness was a surface effect or evident through the thickness. A micrograph was taken of the dry fibre region on the underside of the reinforcement in Figure 110 and the V_f was measure in Figure 111. This shows the change in vertical V_f within the red box as a means to determine the effect of this dry region. At <2000 and >6000 pixels there is a region of relative flatness, between 5000-6000 there is the beginning of a downward trend as the UD begins to thin and the HexMC region expands causing a reduction in V_f. This then continues as the reinforcement ends with a resin rich joint. An investigation into the micrographs shows that there is a V_f effect of the HexMC on the underside. Although there is not a dramatic change such as shown in Figure 110 where there is a clear line between the UD drop off and the HexMC, the graph in Figure 111 shows a gradual decline between the two.

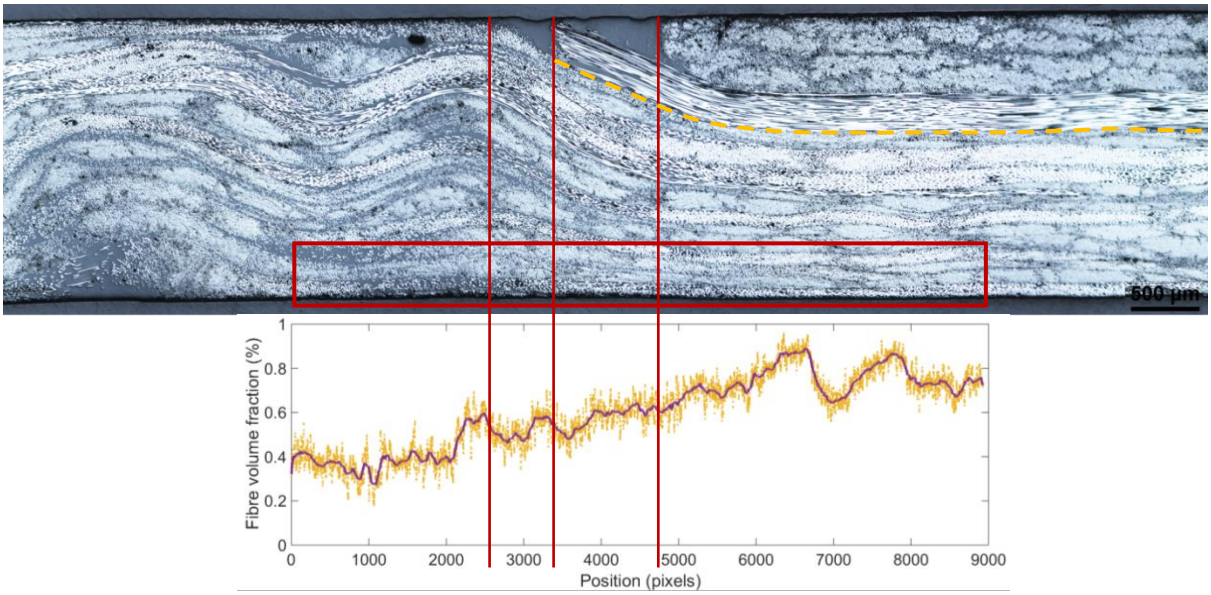

Figure 111: Measurement of the change in V_f along the lower edge of U2 90° U1 0° H2 s50%

7.3.2. The effect of staging on void content

Figure 112 shows the mean void content of plaques, with standard deviation error bars, taken from within only the UD section of each plaque.

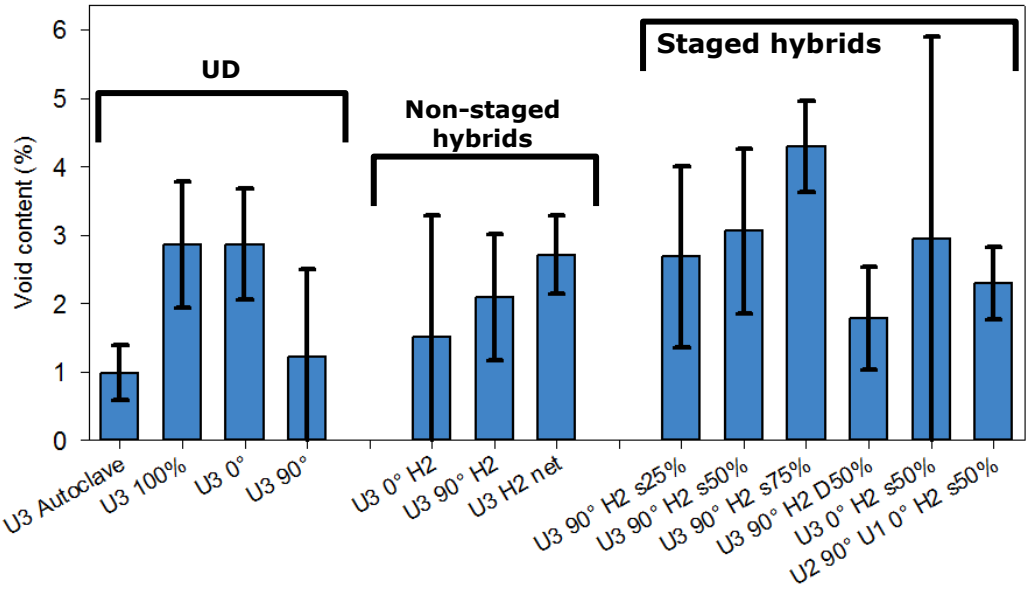

Figure 112: Void content of different charge configurations, taken from a range of locations within the plaque of only the UD element

Figure 112 confirms that debulking aids void removal. For example, U3 autoclave and U3 90° H2 D50% both have lower void contents than their respective counter parts. Increasing material flow, including fibres and resin,

also improved void reduction. Flow of the resin only does not reduce the void content as much as both resin and fibres, such as in U3 0° where there was significant resin flow but minimal fibre movement and in the non-staged scenarios where high levels of fibre flow or migration lead to lower void content. Similarly, in U3 H2 net very little flow occurred, preventing entrapped air to be removed. Increased levels of staging also reduced flow, hence reducing entrapped air removal.

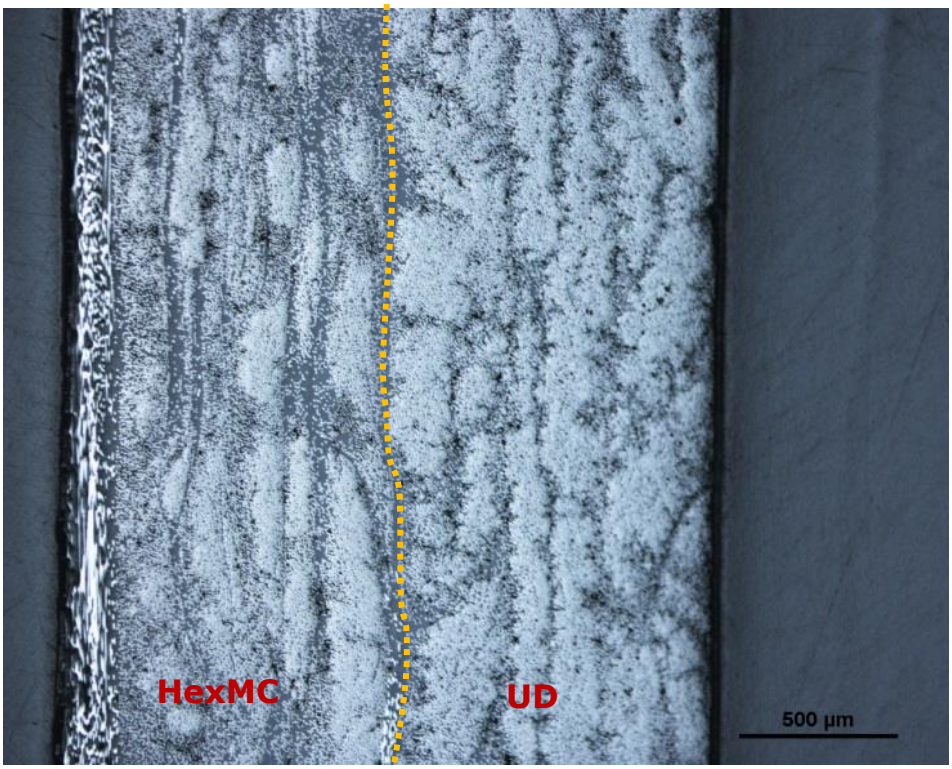

Figure 113: Effect of fibre flow induced alignment in U3 0° H2 s50% on the left HexMC and right UD

It was commonly observed in the HexMC with high levels of flow, that there was notably higher fibre alignment on the outer surface, as shown on the left of the sample in Figure 113 was more often parallel to the flow direction, with the rest of the sample randomly orientated. This is possibly due to the friction on the tool surface limiting flow and rotation of the surface layer of the SMC. This would provide an explanation to the dry surface on the underside as this layer is sliding along the surface exposing the fibres, creating a dry layer.

7.4. Effect of reinforcement staging and charge design on local properties

Four hybrid plaques of three plies of UD aligned transverse to the flow direction with 25%, 50% and 75% staged and a plaque of debulked and then staged to 50%. This was locally flexural tested and density measurements were taken, which was plotted over the original image as shown in Figures 114 and 115. There was a 0.40% decrease in V_f as shown in Figure 114 from the fibre ends (**A & D**) to the centre of the reinforcement (**B & C**), and a 5.30% decrease in flexural modulus along the same path as shown in Figure 115. The V_f declined at the reinforcement edge near region **C;** however, the V_f and flexural modulus did increase near the flash gap at **D** as the resin was able to leave the plaque.

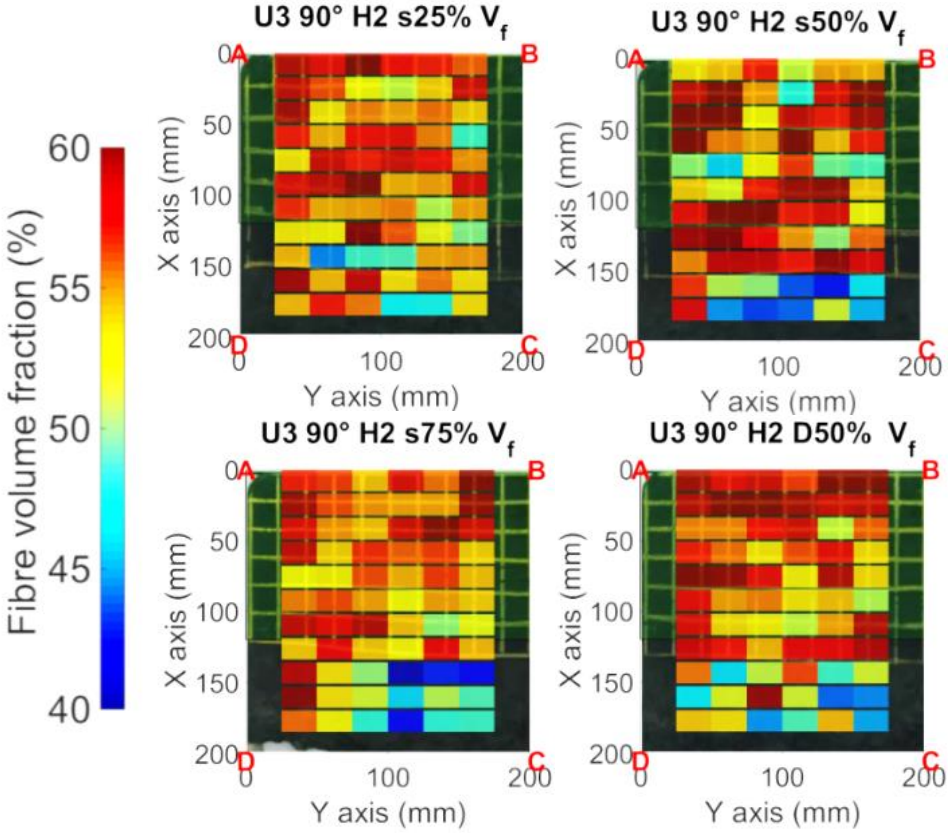

Figure 114: Fibre volume fraction of U3 90 H2 s25% - s75% and debulked staged to 50%

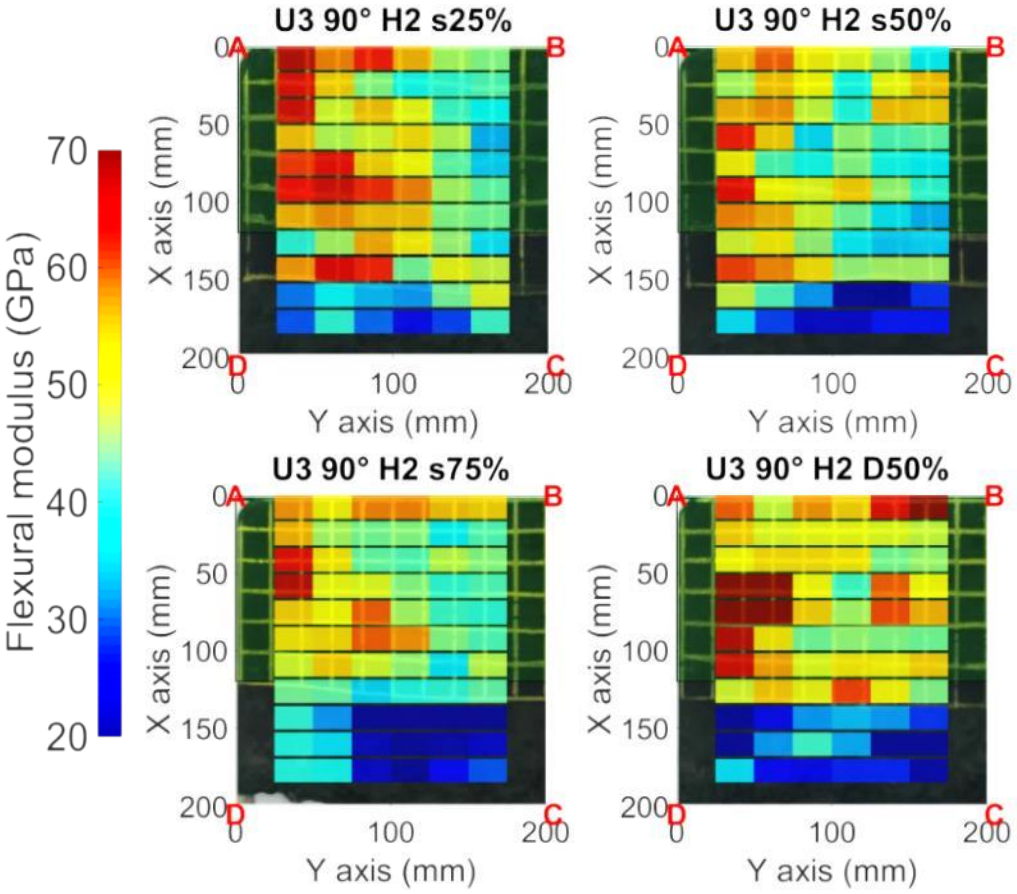

Figure 115: Flexural modulus of U3 90 H2 s25% - s75% and debulked staged to 50%

7.4.1. Reinforcement flow control through charge design

When there was no staging in U3 0° H2, the HexMC dragged the UD reinforcement and distorted it; in contrast, when the reinforcement was staged to 50% there was only 7 mm of migration, as shown in Figure 116 (a). This is from the staging passing the gelation point and reducing the lubricating layer effect, meaning the friction at the reinforcement to tool interface dramatically increases. In these flow scenarios (a & b), there was very little migration, however there were regions of SMC rippling, as shown in Figures 116 and 117, where the SMC had swirled making the tows effectively very short.

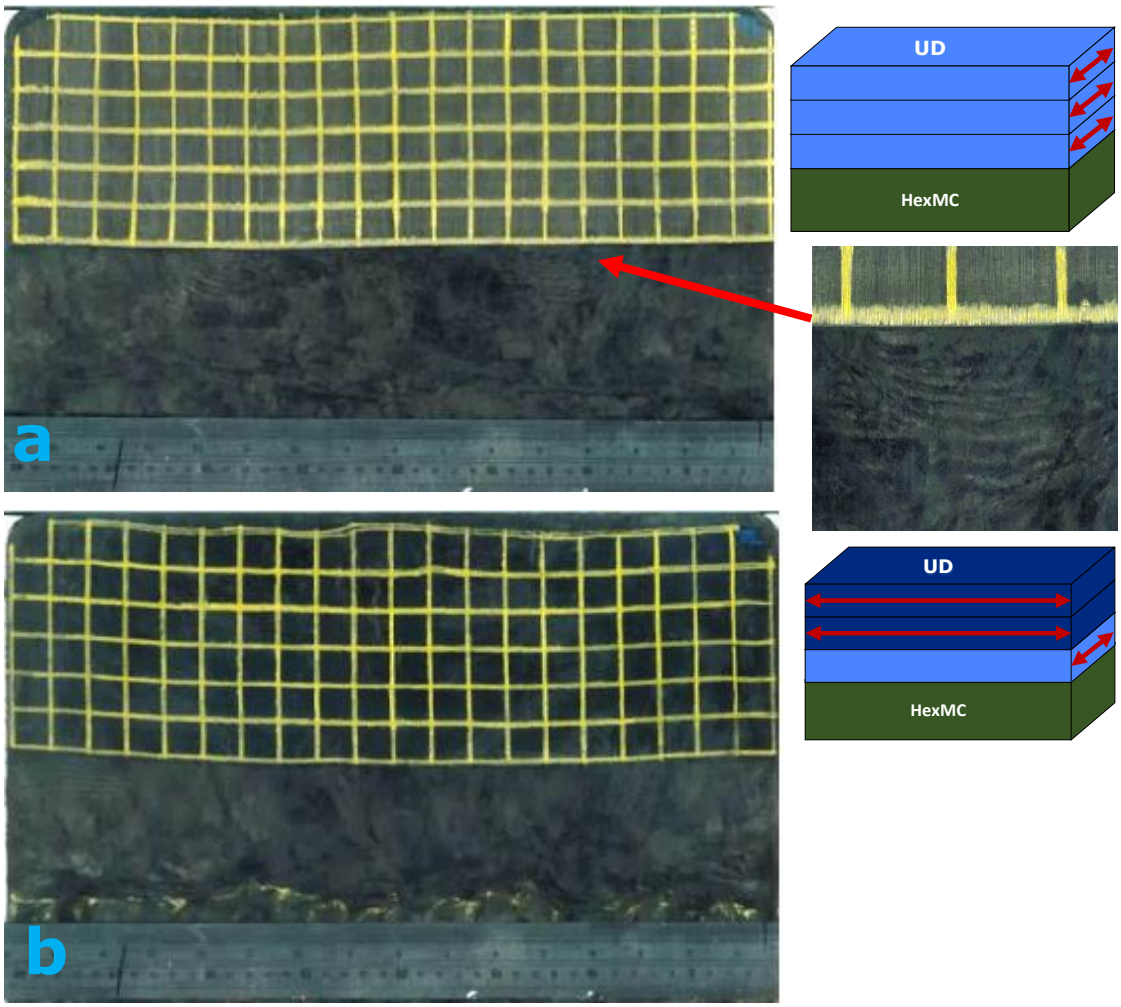

Figure 116: Image of moulded plaque, U3 0° H2 s50% (a) and U2 90° U1 0° H2 s50% (b) and image of rippled region

Figure 117: Micrograph of U3 0° H2 s50%, showing a rippled region.

To utilise the restricted flow exhibited by U3 0° H2 s50%, the ply that was in contact with the HexMC was aligned parallel to the flow direction and other two were aligned transverse to the flow direction, as shown in Figure 116 (b). This arrangement exhibited less flow compared to U3 90° H2 s50%, as shown in Table 14. There was slight migration of the UD with some of the transverse fibres separating from the reinforcement.

With the reinforcement in the flow direction, it was expected that the properties would be higher than those in a scenario where the UD was aligned transversely. There was a decline in flexural stiffness at the edge (**A→D**) caused by the reinforcement being slightly smaller than the tool width and the flow of the reinforcement causing the UD to pull away from the edge. This slight migration made the edge to be a mixture of reinforcement and SMC causing the stiffness to be on average, 32.41 GPa.

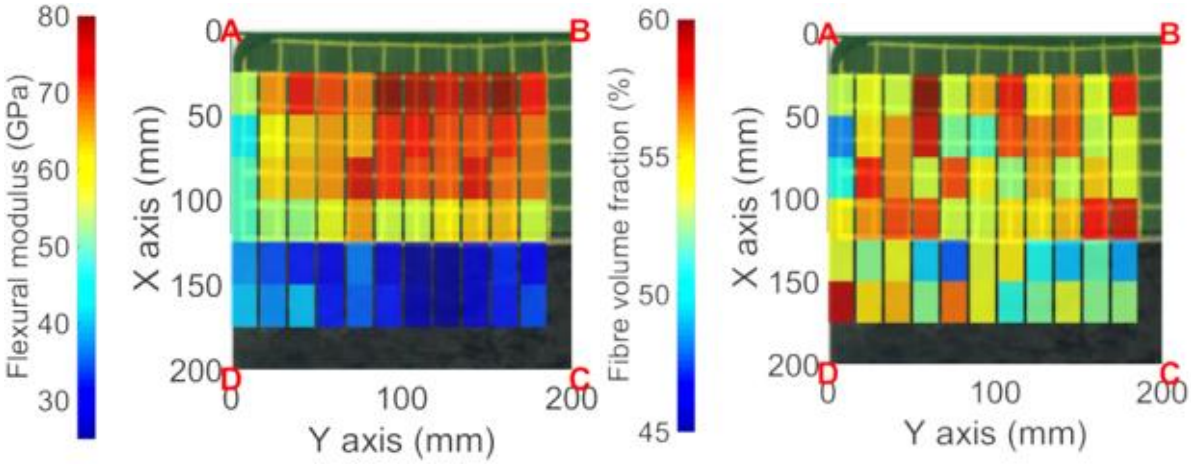

Figure 118: Localised flexural modulus of U3 0° H2 s50%.

31.82% of the pure HexMC values were lower than the manufacturer's datasheet (<30 GPa) these were where ripples were observed. At the fibre ends the mean V_f was a maximum, at 55.83% dropping to 51.60% in the HexMC. This is compared to the mean within H2 60% of V_f 55.03% and is caused by the resin within the UD bleeding out into the HexMC, resulting to a lower V_f and hence a weakness at the hybrid-HexMC interface.

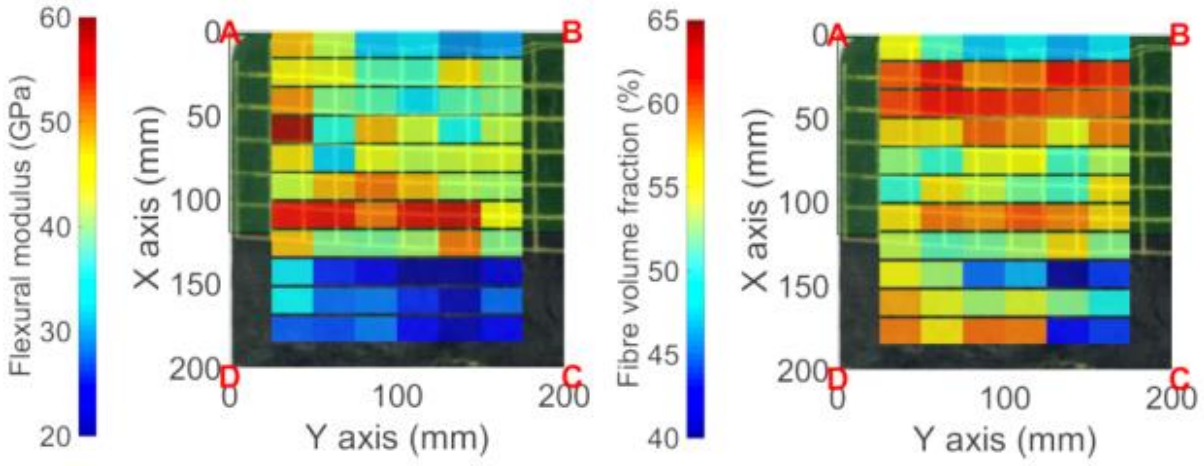

Figure 119: Localised flexural modulus and fibre volume fraction of U2 90° U1 0° H2 s50%

U2 90° U1 0° H2 s50% was significantly stiffer than pure HexMC, but with significant enhancement on flow control. Along the edge of **A→B** in Figure 119 the flexural modulus and V_f were the lowest. This was caused by the migration of the reinforcement which partially exposed the HexMC underneath and caused resin to bleed out decreasing the V_f. The properties of the HexMC were similar to those of H2 60%, and rippling was not observed.

This charge configuration has removed the effect of the stiffness being enhanced at the fibre ends from an increase in V_f as the increase from **A&D→B&C** in Figure 119 was <2%. However, there is still a trend of the HexMC V_f at the reinforcement edge being on average 5% lower and higher near the flash gap (**D**).

7.5. Distortion

Measurements of localised strain and rotation for each staged scenario are reproduced in Appendix A and summarised in Table 15. There is no discernible trend in the location of the rotation within any of the 1D staged flow scenarios. In contrast, the strains ε_{yy} in the majority of scenarios were predominately limited to the elements nearest to the flow front. This was caused by the increased level of flow from the HexMC flowing over and dragging the reinforcement; this was also observed in ε_{xx} of U3 0° H2 s50%.

The distance flowed by the prepreg, shown in Table 14, followed a similar trend to the mean rotation in Table 15. This indicates that increased flow tends to increase the rotation, which is caused from the chaotic flow of the HexMC in both the *x* and *y* directions.

The elements very rarely shrink or expand in the UD fibre direction, the greatest being by -0.05% (a slight contraction) in U3 90° H2. This can be observed in that scenario which flowed the most (ε_{yy} 0.77%) as the reinforcement shrunk and pulled away from the tool edge.

Label	Mean			S.D.		
	ε_{yy}	ε_{xx}	Rot (°)	ε_{yy}	ε_{xx}	Rot (°)
U3 90° H2	0.77	-0.05	2.51	0.37	0.04	2.00
U3 0° H2	-0.00	-0.02	8.52	0.08	0.18	7.47
U3 H2 net	-0.03	0.00	2.42	0.06	0.18	2.05
U3 90° H2 s25%	0.20	-0.01	1.70	0.13	0.03	1.38
U3 90° H2 s50%	0.20	-0.00	1.16	0.11	0.02	0.99
U3 90° H2 s75%	0.11	-0.00	1.06	0.08	0.03	0.82
U3 90° H2 D50%	0.16	-0.00	0.94	0.13	0.02	0.84
U3 0° H2 s50%	0.00	-0.01	0.72	0.03	0.04	0.64
U2 90° U1 0° H2 s50%	-0.00	-0.00	1.20	0.03	0.02	0.77

Table 15: Mean ε_{xx}, ε_{yy} and rotation (°) of staged one dimensional flow scenarios

The greatest contrast between the non-staged and staged scenarios is in the increased flow resistance (ε_{yy}) and the mean rotation, which is <1.70° compared to >2.42°.

7.6. Reinforcement staging

7.6.1. Flexural properties

The flexural modulus, E_f of the hybrids varied along the UD fibre direction. There was a general decline in E_f as the specimens were further from the UD fibre ends as the flexural specimens V_f decreased. The debulked specimen had a higher flexural modulus than non-debulked scenarios, due to the enhanced consolidation from the debulking rather than from the flow thinning the reinforcement. The 75% staged UD charge flowed less, but properties were comparable with the other non-debulked scenarios. H2 60% is the closest comparison to the flowed U3 90° H2 scenarios, as here two plies of HexMC were placed in the tool without staging or UD. However, it does not have the effects of the UD reinforcement that may change the flow behaviour of the HexMC. The V_f of the hybrids is slightly higher than in the HexMC, which is likely caused by the increase in V_f of the UD reinforcement.

Comparing the staged hybrids and the HexMC, on the right hand side of Figure 120, the mean flexural modulus of the hybrids ranged from 1.43-2.4 times that of the HexMC. From the hybrid scenarios in Table 16, it is evident that staging does not have a significant degradation on the stiffness of the hybrid. The stiffness of all the hybrids indicates that the reinforcement is enhancing the HexMC by at least 43%.

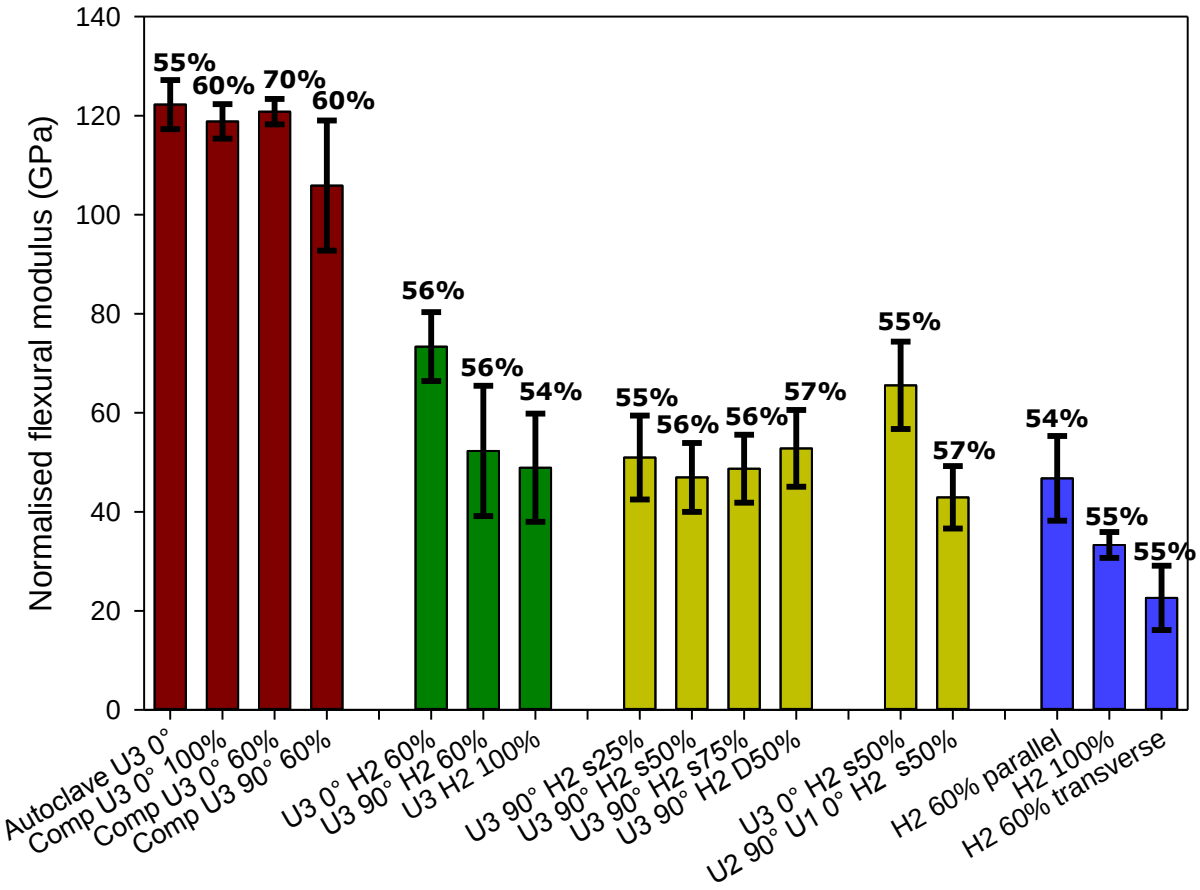

Figure 120: Comparison of normalised flexural modulus of UD, un-staged and staged hybrids and HexMC, normalised to 55% V_f.

The staged hybrids had a similar flexural modulus as the non-staged U3 90° H2 60% plaque. However, the non-staged scenario exhibited significant thinning of the UD. This was likely caused by degradation in the flexural modulus from staging, as the reinforcement has thinned less than in the non-staged scenario, and the reinforcement ratio in the staged scenarios is greater. This is more evident in the U3 0° H2 scenarios where the fibres are aligned parallel to the flow direction as there is not a large contrast in the thinning of the reinforcement, here the staged hybrid stiffness was 10.9% lower. Additionally the limited flow in the UD caused increased flow in the HexMC, increasing the HexMC fibre alignment. As the testing direction in the U3 90° hybrids was transverse to the flow direction, the properties of the HexMC section in the staged hybrids would be lower than if the UD flow as in non-staged U3 90° H2 60%.

Label	Flexural modulus (GPa) (SD)	Vf (%) (SD)	Normalised (55%) (SD)	
Autoclave U3	121.27 (2.84)	54.59 (0.73)	122.24 (4.42)	
Comp 100% U3	129.09 (2.49)	59.81 (0.63)	118.56 (3.19)	
U3 0° 60%	149.61 (4.59)	70.33 (1.50)	116.75 (2.52)	
H2 60% transverse	22.67 (6.67)	55.03 (2.36)	22.62 (6.40)	
H2 60% parallel	45.81 (7.79)	53.92 (1.77)	46.71 (7.58)	
H2 100%	33.10 (1.32)	54.79 (2.28)	33.31 (2.34)	
H2 autoclave	36.27 (8.12)	54.74 (2.50)	36.37 (7.53)	
				$\frac{\text{Hybrid}}{\text{HexMC}}$
U3 H2 autoclave	60.49 (5.13)	54.76 (0.56)	60.72 (4.76)	1.67
U3 90° H2	52.90 (13.54)	55.56 (1.63)	52.3 (12.94)	2.33
U3 0° H2	72.82 (6.92)	54.61 (1.53)	73.37 (6.82)	1.59
U3 H2 net-shape	47.81 (11.08)	53.64 (1.37)	48.91 (10.76)	1.44
U3 90° H2 s25%	51.07 (8.73)	54.75 (3.92)	51.30 (9.24)	2.25
U3 90° H2 s50%	47.82 (7.61)	56.01 (3.76)	46.95 (6.89)	2.11
U3 90° H2 s75%	49.31 (7.28)	55.87 (2.82)	48.48 (6.40)	2.18
U3 90° H2 D s50%	54.35 (8.84)	56.54 (2.57)	52.82 (7.66)	2.4
U3 0° H2 s50%	65.67 (8.81)	55.13 (2.33)	65.55 (8.71)	1.43
U2 90° U1 0° H2 s50%	44.06 (6.28)	56.59 (3.57)	42.93 (6.23)	1.94

Table 16: UD, HexMC and Hybrid scenarios flexural modulus, V_f and normalised E_f to 55% V_f, a comparison of the hybrid flexural modulus with corresponding HexMC flow scenario and estimated mean UD thickness. The final column shows the hybrid E_f over the corresponding HexMC, providing a ratio of the increased performance of hybridisation.

Whilst there is no significant change in stiffness from staging the UD plies, the real benefit is in reinforcement control which prevents migration of the UD relative to the HexMC. In addition, the increased flow resistance reduces the variation in flexural modulus, as demonstrated in Table 16.

7.6.2. Stiffness prediction

Using photogrammetry and localised V_f measurements, it was possible to calculate a theoretical flexural modulus and to compare it directly with the localised experimental modulus, as shown in Table 17. The mean theoretical flexural modulus in the staged hybrids under predicted the experimental value by up to 10%, where the UD is transverse to the flow direction (U3 90° H2). However, the analytical model over predicts by up to <2% if a ply is aligned parallel to the flow direction. This can be attributed to the flow resistance of the reinforcement increasing the flow of the HexMC and enhancing the flow induced alignment, causing a lower mean stiffness for the HexMC transverse to the flow direction as predicted by the GSA in the majority of the samples, excluding U3 0° H2 s50%.

	GSA Hybrid mean (GPa)	GSA HexMC mean (GPa)	Theoretical mean (GPa)	RMSE	$\frac{\text{Exp}}{\text{Theo}} \times 100$
U3 90° H2 60%	48.91	21.47	41.64	27.84%	117.46%
U3 0° H2 60%	75.88	47.35	71.85	12.38%	105.61%
U3 H2 100%	48.90	33.31	50.72	24.84%	96.41%
U3 90° H2 s25%	50.33	20.88	51.97	11.38%	96.84%
U3 90° H2 s50%	46.84	20.88	51.83	17.16%	90.37%
U3 90° H2 s75%	48.17	20.37	53.53	15.99%	89.99%
U3 90° H2 D50%	52.53	20.46	52.63	16.14%	99.81%
U3 0° H2 s50%	70.98	43.98	70.58	12.81%	100.57%
U2 90° U1 0° H2 s50%	42.10	20.38	41.35	14.35%	101.81%

Table 17: Comparison of theoretical and mean grid strain analysis (GSA) flexural modulus of hybrid composite normalised to 55% V_f. The GSA hybrid and HexMC mean in Table 17 is the mean flexural modulus for the specimens within the grid strain analysis (GSA); this is a direct comparison for the theoretical flexural moduli calculated from the image analysis plots in Appendix A.

It is evident in the comparison with the unstaged scenarios that the increased control of flow has improved the correlation between the theoretical and experimental modulus. As the control of flow shown in Table 15 increases the variation in element strain and rotation similarly decrease, and therefore the disagreement in theoretical and experimental flexural modulus in Table 17 also decreases.

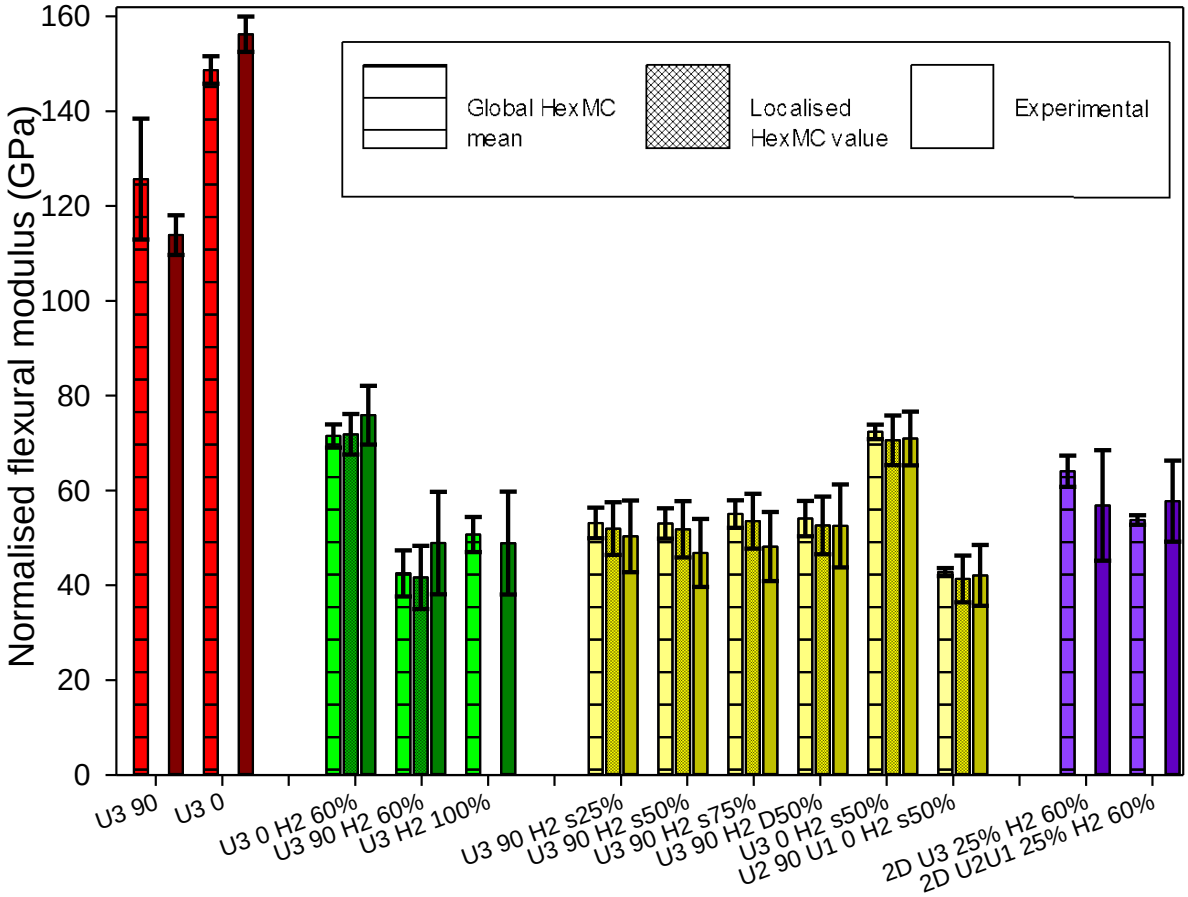

Figure 121: Global mean HexMC theoretical flexural modulus (left bars), localised HexMC theoretical (centre hatched bars) and experimental normalised (V_f 55%) modulus of UD, non-staged and staged hybrids and 2D staged hybrid scenarios within the grid strain analysis. Localised data was not available for all scenarios.

The sensitivity of the theoretical hybrid moduli on local to average HexMC stiffness for each scenario was compared with two or three bars as shown in Figure 121. The left paler, horizontal line bar in each plaque represents a global HexMC value, meaning that a single mean HexMC value was taken for the theoretical calculation. The central hatched bars represent localised HexMC

measurements, which is plotted with the normalised experimental hybrid stiffness. Some scenarios did not have local HexMC measurements so the hatched bar is not available. What can be shown is that using a global HexMC value does not cause a symmetric over or under prediction and generally the values are very close to the experimental data. However, the RMSE of the predictions to the experimental mean does deteriorate with the use of a globalised HexMC value.

	Mean (SD)			RMSE (Gpa)		
	Global	Localised	Exp	Global	Localised	±
U3 90°	125.68 (12.74)	n.d	113.86 (4.19)	18.72	n.d	n.d
U3 0°	148.69 (2.90)	n.d	156.23 (3.71)	8.1	n.d	n.d
U3 90° H2 60%	42.52 (4.86)	41.65 (6.68)	48.91 (10.80)	13.84	13.7	-0.14
U3 0° H2 60%	71.50 (2.45)	71.85(4.26)	75.88 (6.21)	8.62	9.39	0.77
U3 H2 100%	50.72 (3.69)	n.d	48.90 (10.86)	12.13	n.d	n.d
U3 90° H2 s25%	53.14 (3.22)	51.97 (5.54)	50.33 (7.57)	8.26	5.73	-2.53
U3 90° H2 s50%	53.03 (3.20)	51.83 (5.94)	46.84 (7.19)	9.91	8.04	-1.87
U3 90° H2 s75%	55.04 (2.90)	53.53 (5.80)	48.17 (7.27)	9.86	7.7	-2.16
U3 90° H2 D50%	54.08 (3.72)	52.63 (6.09)	52.53 (8.75)	9.82	8.48	-1.34
U3 0° H2 s50%	72.36 (1.51)	70.58 (5.25)	70.98 (5.66)	6.6	9.09	2.49
U2 90° U1 0° H2 s50%	42.80 (0.85)	41.35 (4.93)	42.10 (6.41)	6.44	6.04	-0.40
2D U3 25% H2 60%	64.05 (3.28)	n.d	56.85 (11.66)	11.79	n.d	n.d
2D U2U1 25% H2 60%	53.78 (1.00)	n.d	57.75 (8.56)	9.35	n.d	n.d

Table 18: Mean flexural modulus for using a global HexMC, localised compared with the experimental values and the corresponding RMSE

The stiffness was calculated using a global and localised HexMC value and is compared in Table 18. The RMSE shows increased accuracy for using localised to a global HexMC value. Using a global value for the HexMC in the theoretical stiffness calculation caused on average a slight over estimate of 2.2% compared to a localised mean stiffness. The RMSE showed a marked decrease in the U3 90° H2 staged scenarios by over 20%. This was because there was no accounting for tool edge effect on the HexMC as fibres tend to align parallel to the tool edge. The U3 0° H2 scenarios actually showed an improved prediction,

by 8% and 27%. This was caused by the same tool edge effect making the HexMC alignment more uniform across the plaque and the samples taken slightly further from the influence of the edge effect.

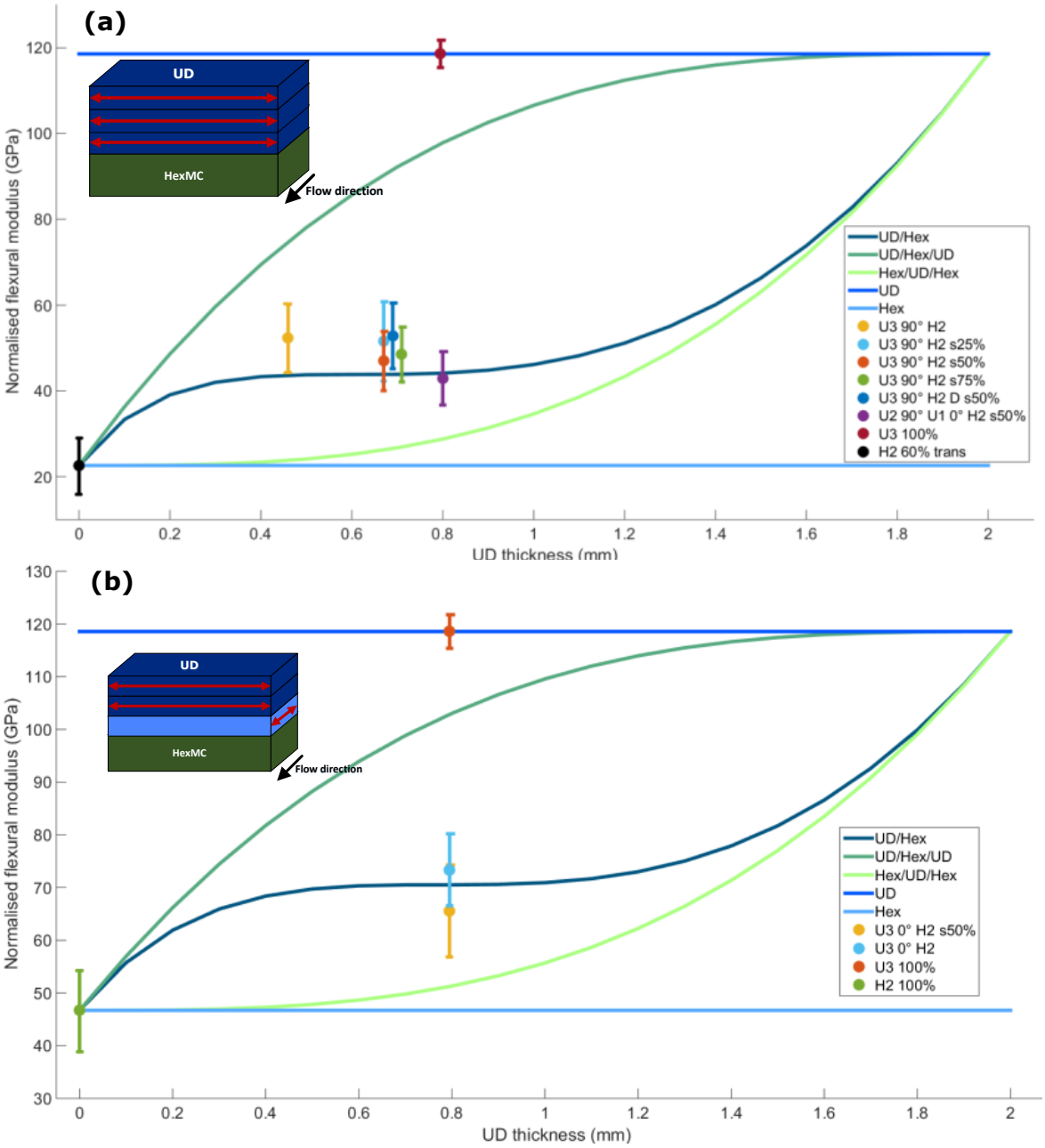

Figure 122: theoretical hybrid flexural modulus transverse and parallel to the HexMC flow direction of a 2mm specimen with increasing UD reinforcement up to 2mm with experimental plots. Normalised to V_f 55%

Different hybrid layups will lead to variation of the flexural moduli. Assuming the deflection is linear (elastic region) with respect to load, a theoretical modulus can be readily calculated. A range of different composite constructions were demonstrated: a typical sandwich construction with UD on the skin and a HexMC

core (UD/Hex/UD), the inverse (Hex/UD/Hex), and the experimental hybrid scenarios where UD is simply placed on top of HexMC (UD/Hex). This is demonstrated in a 2 mm plaque where the UD is increasing from 0 mm to 2 mm with the remaining material in the plaque is HexMC, as shown in Figure 122. The baseline for the materials were U3 100% and H2 60% transverse and parallel, depending if the bending direction is transverse (90°) or parallel (0°) to the flow direction. This figure shows the benefit of placing UD on the skin of a sandwich structure. As the UD is added, the E_f rises rapidly as the distance of the UD increases away from the neutral axis. The inverse is true where the UD is located in the core, as the stiffness is significantly enhances after the UD is >1.2 mm thick. This is where the UD increases its distance from the neutral axis and the HexMC ratio has diminished.

In sandwich structures the neutral axis (N.A) does not change with increasing UD. With hybrid UD/Hex, when increasing UD and diminishing HexMC the N.A moves towards the UD plies. Between approximately 0.4 and 0.9 mm of UD, the neutral axis does not change dramatically, <3%, as illustrated in Figure 123. This is shown in Figure 122, where E_f does not change greatly, since the N.A and second moment of area (I) are not significantly changing.

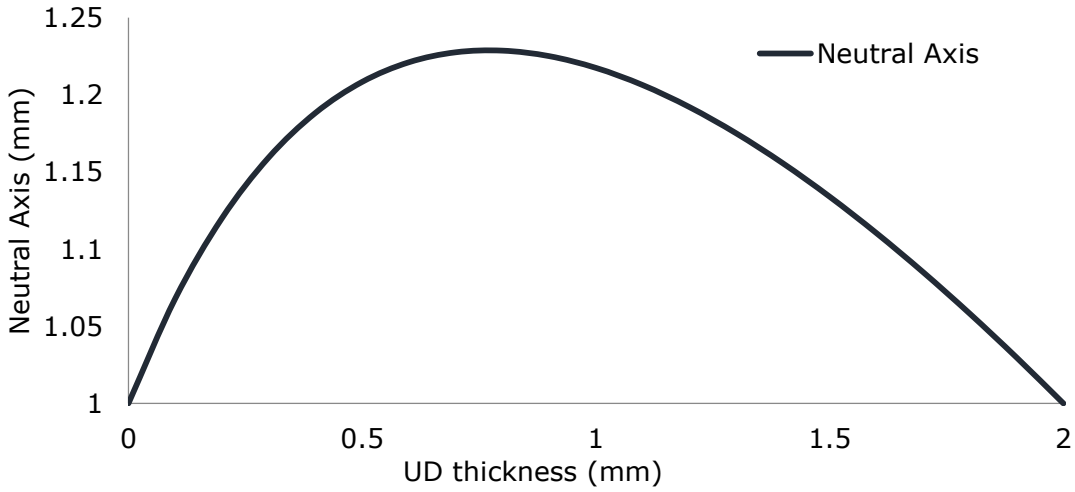

Figure 123: Neutral axis in a 2mm specimen of a hybrid structure UD/Hex from Figure 122

In U3 90° H2 there was significant flow and thinning of the UD to a mean thickness of 0.46mm compared to the other staged scenarios that ranged from 0.67-0.8 mm. Figure 122 (a) shows that there should not be a decline in the E_f as they are both within the flat theoretical region. Although almost all are above the expect modulus, it is not uncommon to observe properties of hybrid composites that are greater than expected [37, 130]. Causes for synergistic effects are still being investigated, but in this instance it was likely caused by the difference in elongation that H2 60% transverse has compared to UD. Where the HexMC fibres are aligned to the flow direction (H2 60% parallel), the elongation is similar and synergistic hybrid effects are negated [131]. This is shown in Figure 122 (b) where the experimental values are similar to the theoretical predictions. U2 90° U1 0° H2 s50% was lower than the other scenarios because of the reinforcement ply construction. The difference in properties between U3 90° H2 s50% and U2 90° U1 0° H2 s50% is 3.76 GPa (7.86%). This is a minor decline considering that a third of the reinforcement is aligned transverse to the loading direction. This emphasises the significance charge design has reducing flow while maintaining stiffness.

It is also shown in Figure 122 that flow of the HexMC does not cause significant reduction in stiffness of the UD reinforcement. It is expected that the E_f between the non-staged and staged scenarios U3 90° H2 s25-75% should have similar properties because the UD is reducing in thickness within a region where the second moment of area is not greatly changing. This graph would aid in the continuous-SMC ratio decision for a desired stiffness and in cases where the SMC would be cheaper than the reinforcement it would provide insight into the maximum stiffness gain for minimal reinforcement.

7.7. Flexural properties of Hybrid composites

Figures 124 and 126 show the mean flexural modulus and strength of UD, non-staged and staged hybrids, and HexMC respectively.

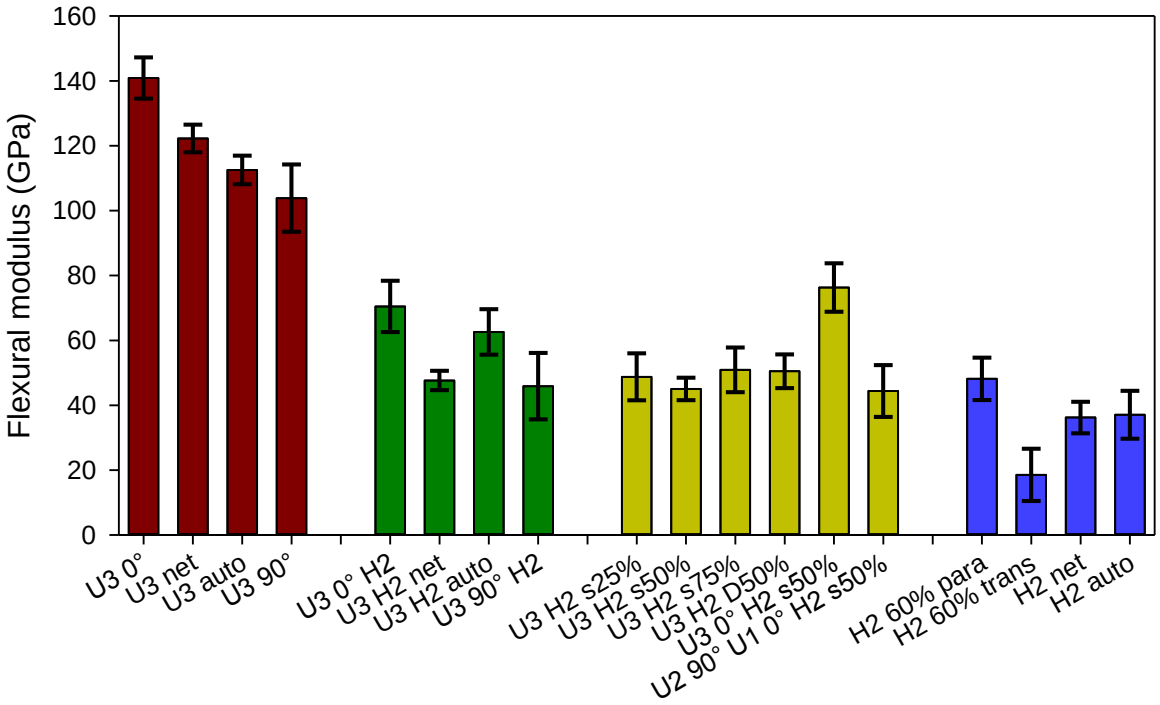

Figure 124: Flexural modulus of UD, non-staged and staged hybrids, and HexMC

The correlation between flexural modulus against strength is shown in Figure 125: the plaques that had the highest strength also had the highest modulus. The relationship is not linear as shows that the modulus increases more rapidly before the strength does. This is because the UD longitudinal fibres are carrying the load and so are able to have higher strengths; [132] whereas, the hybrids with random fibres fail earlier from local regions of weakness caused by a mixture of HexMC, fibre misalignment and local regions of low V_f.

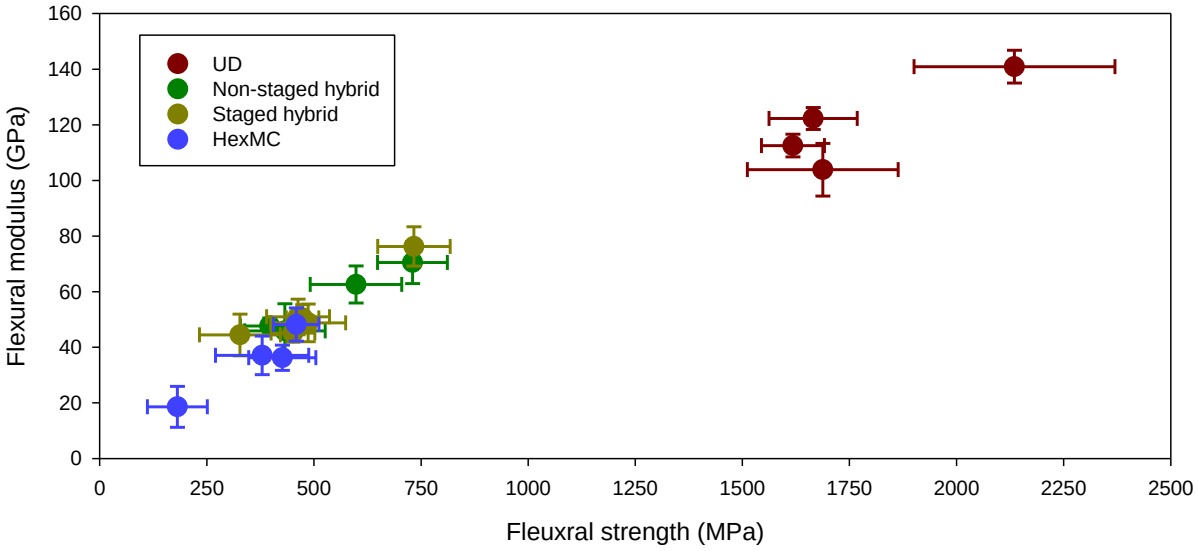

Figure 125: Flexural modulus vs flexural strength of UD, HexMC, non-staged and staged hybrids

It has been discussed previously that U3 0° had a large band of resin bleed causing a high V_f in the composite, so the highest properties were expected. Also because the flow caused misalignment in U3 90°, the stiffness was the lowest of the UD plaques. In the net-shape UD scenario, the pressure caused a higher V_f increasing the modulus by 8.6%, but only a slight increase in strength of 2.9% was observed compared to the autoclave scenario. Similarly, in the HexMC the flow induced alignment had a greater effect on the modulus compared to the strength, which were 32.9% and 7.6% higher respectively compared to the net-shape scenario.

In the hybrid scenarios where the reinforcement was aligned parallel to the flow direction, staging had minimal effect on the properties; as U3 0° H2 had a higher strength and modulus of 0.5% and 8% respectively compared to U3 0° H2 s50%. The staged hybrid had a 60% and 58% increase in strength and modulus respectively compared to HexMC (H2 60% parallel). The converse was true for the increased staging in U3 90° H2 as the staging increased the strength by between 4% to 13% and the modulus by between -2% to 11%, compared to U3 90° H2. This indicates that the staging was not affecting the flexural properties of the hybrids in either reinforcement orientation.

U2 90° U1 0° H2 s50% exhibited the largest contrast between the stiffness and strength, as the modulus was comparable with the U3 90° H2 staged scenarios being 8% lower but the strength was 29% lower. Using a single ply

perpendicular from the loading direction for flow control had minimal effect on the modulus but a significant decline in strength. This single perpendicular ply is notably weaker and once a crack is initiated, propagation quickly leads to delamination between the transverse and parallel UD interfacing plies. However still, the strength and modulus were still 81% and 139% higher respectively than the corresponding HexMC (H2 60% trans).

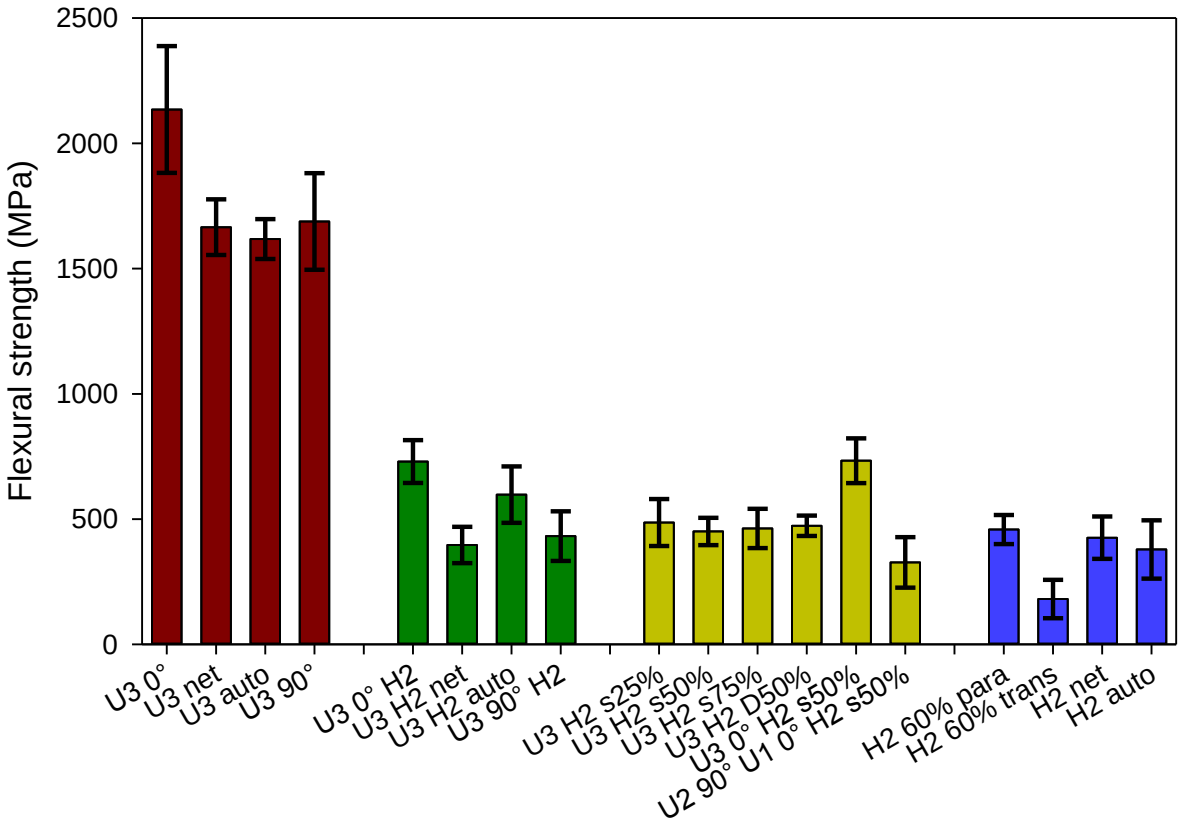

Figure 126: Flexural strength of UD, non-staged and staged hybrids, and HexMC

Comparing the hybrid plaques transverse to the flow direction, the modulus and strength were 163% and 159% higher compared to the corresponding HexMC (H2 60% trans). The hybrid scenarios had lower flexural properties than the UD, but did show a marked increase relative to the HexMC.

7.7.1. Orientation bias

The flexural modulus and strength of the hybrid composites were measured by using two different specimen configurations: with the UD plies under compression, and tension. The flexural modulus and strength of these plaques are shown in Figures 127 and 128. There was minimal stiffness difference in the orientation of hybrids as shown in Figure 127. The mean modulus of the UD under compression and tension were similar, at 54.01 GPa and 53.86 GPa, respectively. However, in terms of flexural strength there were significant differences; where the UD was aligned parallel to the flow direction the UD under compression had higher strength. The converse was true when the UD was aligned transverse to the flow direction.

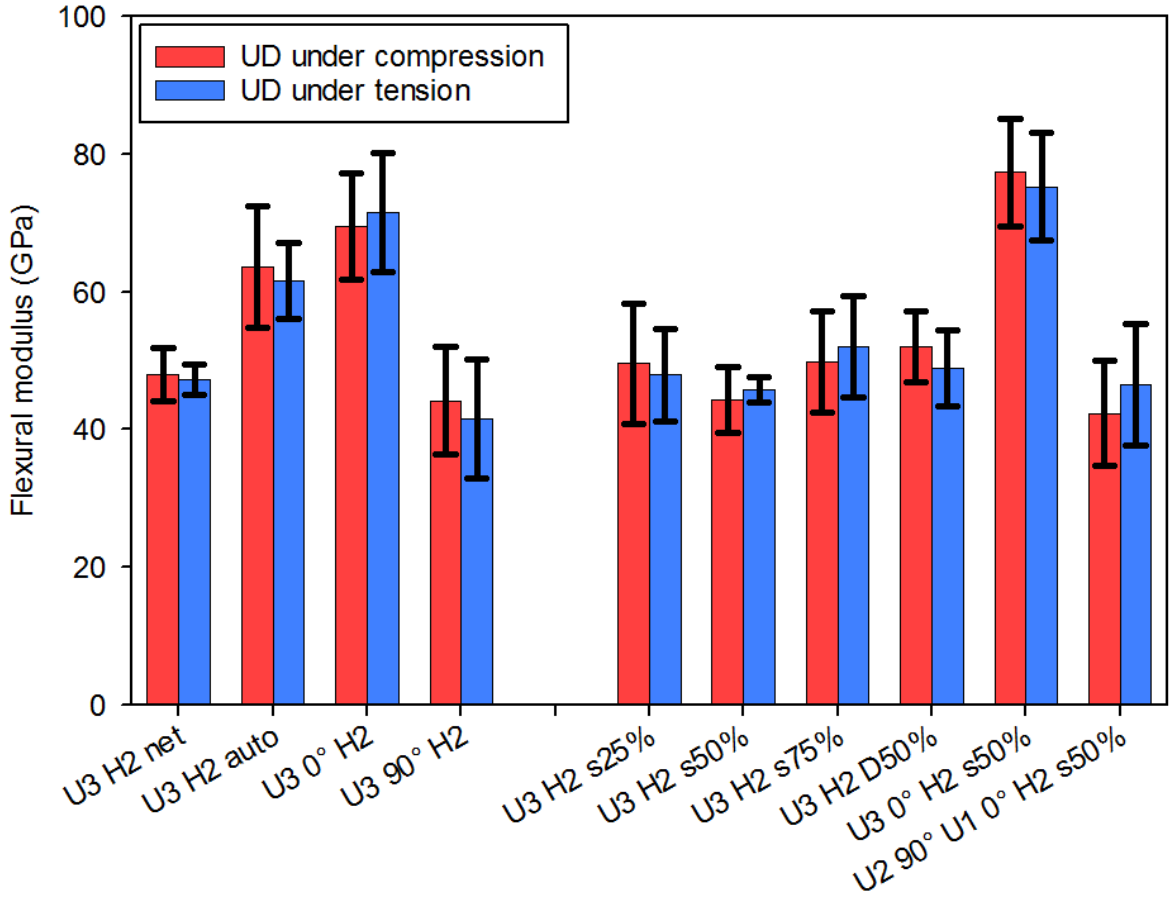

Figure 127: Flexural modulus of hybrid composites, with UD under compression (blue) and tension (red).

The fibre bundles are predominately perpendicular to the beam axis when samples were taken transverse to the flow direction, allowing cracks to readily propagate along the fibres. If the UD was under tension (HexMC under compression), the HexMC fails along the fibre bundles, followed by SMC-UD delamination. The UD then, due to the reduced thickness, bent further prior to

failure. In these scenarios, crack propagation of the HexMC occurred first if under compression, but with the UD under compression the sample tended to fail simultaneously; this is from the reduced performance of the UD under compression.

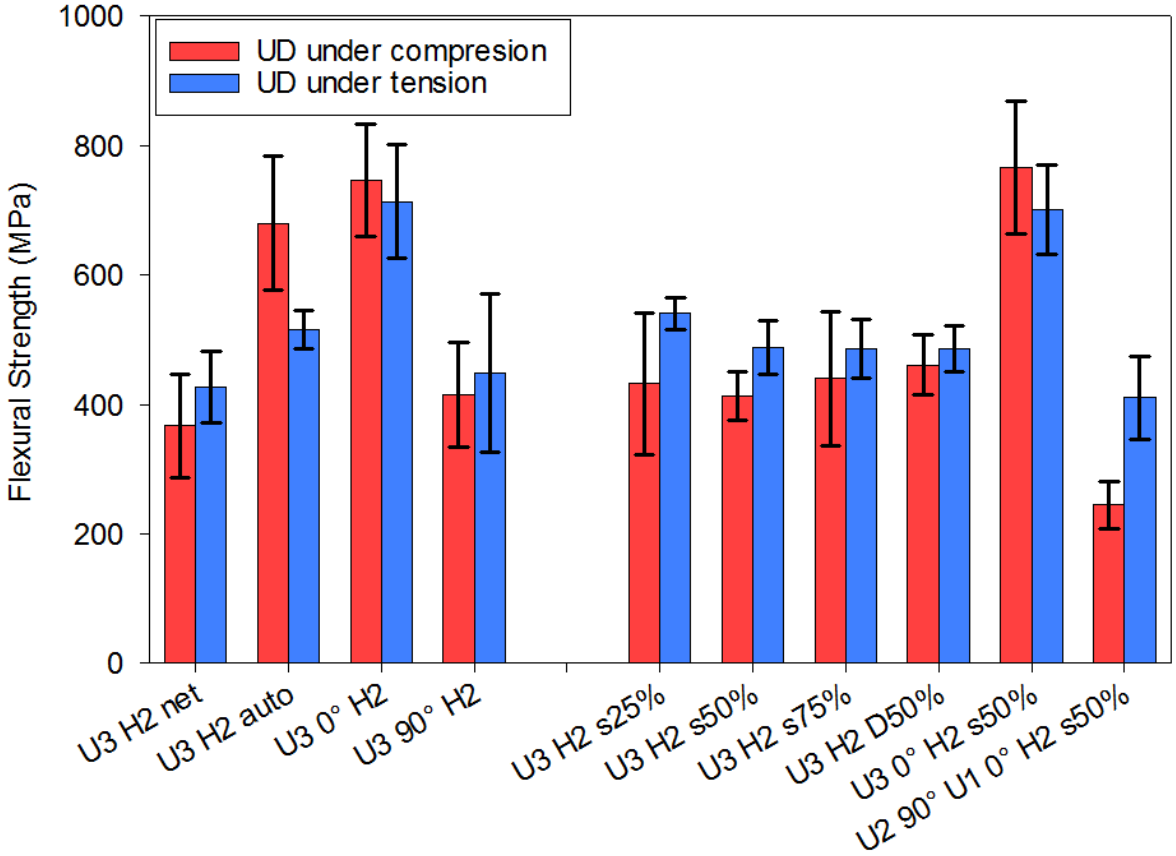

Figure 128: Flexural strength of hybrid composites, with UD under compression (blue) and tension (red)

The differences between compressive and tensile failure strength in the samples cut transverse to the flow direction were <20%, but in U2 90° U1 0° H2 s50% the difference was 40%. The UD was notably weaker under compression than under tension. With the UD under compression the ply that was transverse to the bending moment initiated failure. Once a crack is initiated, propagation is quick along the transverse fibres, which then causes delamination between the transverse and parallel plies. Where the transverse UD ply was under tension the plies bends and the HexMC under compression tends to fail first. This is similar to the staged U3 90° H2 scenarios where the majority of the samples tended to fail by HexMC compression rather than UD tension. The delamination of U2 90° U1 0° H2 s50% occurred between the 90_2 and the 0 degree ply, unlike the other scenarios, where delamination occurred between the UD and HexMC. This was

where the transverse ply initiated failure, which caused delamination of the parallel plies prior to any HexMC failure. As UD has higher properties in tension, the compressive transverse UD ply becomes the weakest part of the composite. In contrast, when the UD is under tension the performance is better and the HexMC tends to fail first under compression. This was seen in the U3 90° H2 scenarios where the UD was under tension and the HexMC failed, but when the UD was under compression there was simultaneous failure through the specimen.

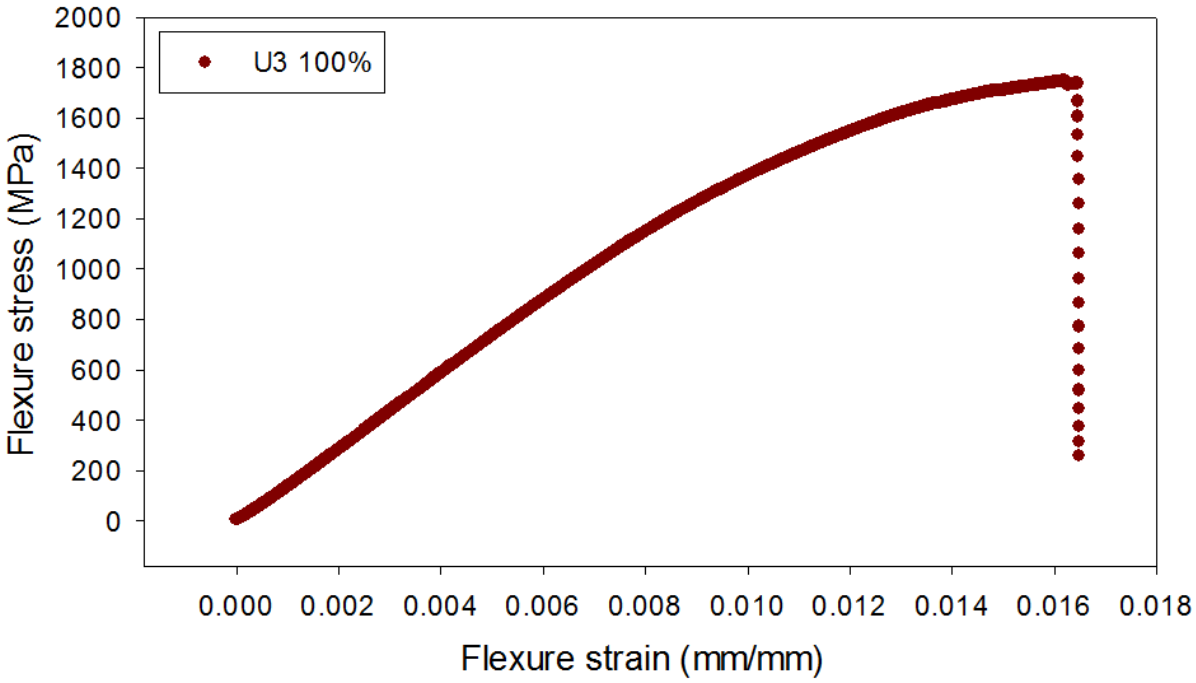

Figure 129: A typical flexural stress-strain curve for U3 100%, showing the progression of failure

U3 100%, shown in Figure 129, exhibited almost brittle failure. This was similar to the staged scenarios, as illustrated by U3 H2 s50% in Figure 130. H2 60% transverse tended to fail gradually as a series of inter-tow failures occurred, shown by the relatively flat region, which was similar in U3 90° H2. Similar findings were observed parallel to the flow direction, where HexMC and non-staged hybrids failed gradually, but staged hybrids exhibited brittle failure, comparable to UD. It would be advantageous for hybrids to fail gradually as plastic deformation absorbs energy and doesn't lead to catastrophic failure where in the automotive industry energy absorption is a desirable characteristic.

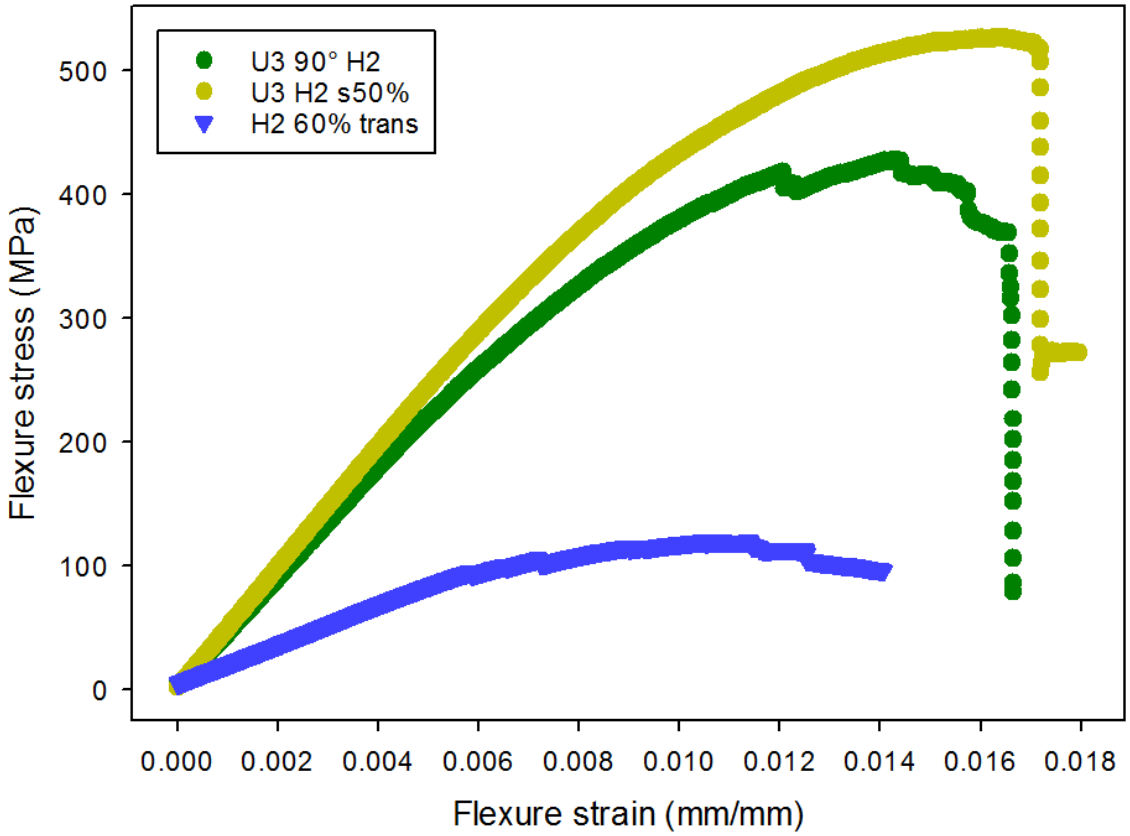

Figure 130: Typical flexural stress-strain curves of U3 90° H2, U3 H2 s50% and H2 60% trans, showing the progression of failure.

7.8. Summary

Staging the material affects the degree of cure prior to moulding and hence the flowability; however, the change in storage modulus occurs rapidly during staging. Although time consuming, the staging temperature had to be low (at ≤80 °C) for accuracy. Staging could be achieved at higher temperatures, but the change in material storage modulus will happen in <20min, making the process not repeatable. However, with heated platens and good process control, quicker staging may be possible.

Using ILSS as a method to determine a suitable degree of staging has identified that staging UD to 50% has a similar ILSS to HexMC when bonding with an un-staged material. Further staging causes the bonding strength to be lower than in HexMC. This is undesirable as the UD should be enhancing properties. Debulking the UD plies prior to staging enhanced the ILSS, as it improved the adhesion of the staged plies, as there was no tack after staging. Although debulking reduced

the flowability of the reinforcement, such a time consuming process is not possible in a production environment. Heated platens could be used to stage and provide some consolidation in a single process. In the case of a hybrid component, if the UD is required to be 3D profile, the material could be preformed at temperature, creating the desired shape and staging while providing consolidation similar to debulking.

Moulding a series of hybrid scenarios at various degrees of staging proved that partial curing combined with reinforcement design is effective at limiting the flowability of the reinforcement. This increase in flow resistance created defects in the HexMC, such as rippling and dryness on the underside, which was caused by high pressure of the tool closure, forcing the resin out of the reinforced sections.

The flexural modulus of the HexMC outside of the hybridised region was generally comparable to non-hybridised scenarios, indicating there is no significant detrimental effect of hybridisation on the HexMC properties. Although there was a noticeable V_f decline at the in-plane UD reinforcement ply drop off.

The comparison between the non-staged and staged hybrid theoretical flexural properties was higher when comparing a mean RMSE of 26.93% to 14.65%. The increased control of the reinforcement improves the accuracy of predicting the local flexural modulus. However, the difference between the mean theoretical and experimental flexural moduli were <10.01%, with a tendency to over predict when the fibres are transverse to the flow direction and under predict when both the testing and fibres are aligned in the flow direction.

The flexural modulus followed a similar trend to the flexural strength, as the highest modulus plaques tended to have the highest strength. Additionally there was no distinguishable trend for the orientation bias of the flexural modulus where the UD was under compression or tension. When testing to failure UD tended to perform better under tension if the flow direction was transverse to the beam axis. The opposite was true if the flow direction was parallel to the beam axis, where the strength was higher when the UD was under compression. This was caused by the failure mechanisms, as the material under compression,

UD or HexMC, tended to fail first. The material under tension (UD or aligned HexMC) provided the enhanced properties.

This was a one dimensional study and therefore the flow mechanisms were simplified in comparison to a complex 3D component. The next chapter will investigate two and three dimensional flow, since these studies will have scenarios where the reinforcement may ladder and migrate simultaneously.

8. Hybrid Composites – 2D & 3D flow

The one-dimensional flow studies presented in Chapters 4, 5 and 6 investigated the flow behaviour of moulding hybrid plaques, including determining the degree of distortion in the UD plies. This was a simplified flow scenario compared to a complex component, where flow can occur also out-of-plane, as in ribs. Out-of-plane movement of the moulding compound can potentially cause different types of defects which do not occur in the 1D flow studies. This chapter focuses on the 2D flow and a 3D component. The aim is to investigate whether charge design can be used to control the quality and position of the unidirectional reinforcement in the *x*, *y* and *z* directions during compression moulding of hybrid architecture components. Flow in the *X*-*Y* plane was investigated by placing the UD plies in the centre of the tool to eliminate the tool edge constraining the UD, before using a 3D tool to bring together all of the findings from the preceding studies.

8.1. Flow of reinforcement in 2D scenario

The purpose of this study is to determine if charge design would aid in the reinforcement flow resistance in a 2D scenario where it is not constrained by the tool. The reinforcement was reduced in size to minimise the effect the flow front has on the UD, as the flow front is known to be chaotic[38] and could disrupt the reinforcement edges. To investigate the 2D flow of HexMC on UD, three plies were placed centrally within the tool to enable flow of the HexMC to occur in all directions within the *X*-*Y* plane, as shown in Figure 131. The blue dotted line indicates the starting position of the HexMC, which covered 60% of the tool surface. The red dotted line indicates the initial coverage of the UD at 25%. All of the UD plies in both images were staged to 50%. Figure 131(a) shows that some distortion has occurred in the UD material transverse to the fibre direction. The central grid elements were not deformed, maintaining the 20mm x 20mm dimensions. The left and right edges of the UD plies distorted, as the HexMC material flows faster along the mid-point of these edges than in the corners. The corners of the plaque are therefore the last areas to fill due to insufficient HexMC being placed in the tool and this is shown clearly in Figure 131. Conversely, the top and bottom edges of the UD plies remain predominately straight and parallel, with only slightly narrowing at the ends as the UD fibres curved. This

implies that staging the UD plies to 50% can control the UD fibre placement when the fibres are aligned in the flow direction.

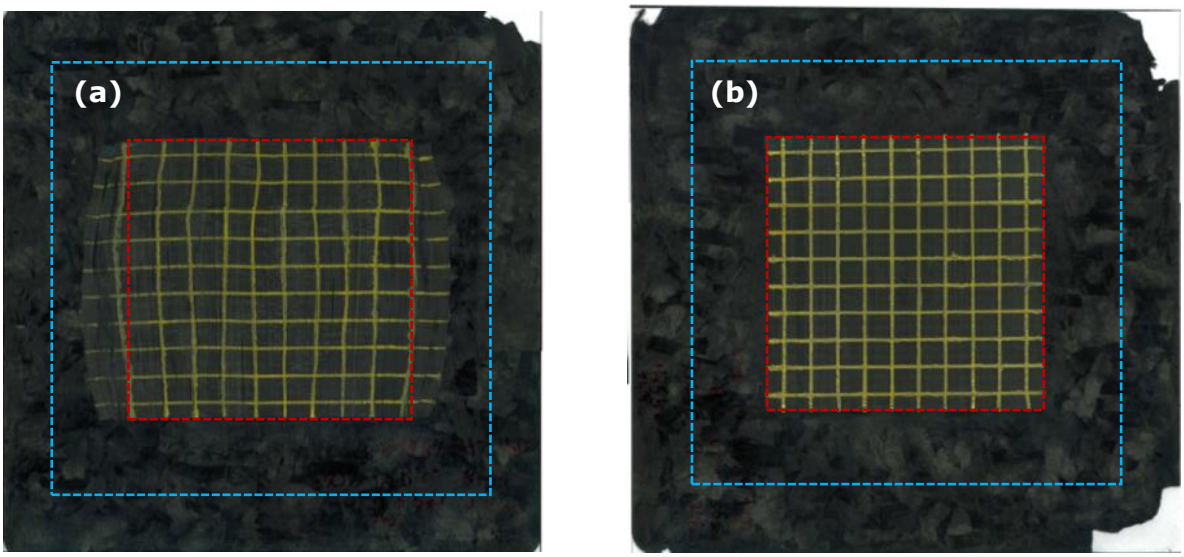

Figure 131: (a) U3 25% H2 60% s50% and (b) U2 U1 25% H2 60% s50%, 25% (red) and 60% (blue) being the UD and HexMC charge coverage respectively

Figure 131(b) demonstrates the effect of a cross-ply layup, where three plies of UD are arranged in a $90°_2/0°$ configuration. Having fibres at both 90° and 0° increases the effective stiffness of the UD ply stack in the transverse direction, compared to Figure 131(a). This increase in flow resistance prevents distortion of the UD plies in a 2D flow situation. Table 19 shows the maximum width of the reinforcement after moulding from an original width of 203 mm. There was some reinforcement flow in U2 U1 25% H2 60% s50%, of ~5.5 mm, which is a significant difference from the increase in width of 74.6 mm in U3 25% H2 60% s50%. However, no reinforcement tearing or migration was observed. The UD plies almost entirely remain within the original red dotted area, showing that a combination of resin staging and charge design can be used to control the flow and therefore distortion of the fibre architecture in hybrid plaques.

Label	Reinforcement width (percentage increase)
U3 25% H2 60% s50%	277.6 (36.7%)
U2 U1 25% H2 60% s50%	208.5 (2.7%)

Table 19: Material expansion from original with of 203mm

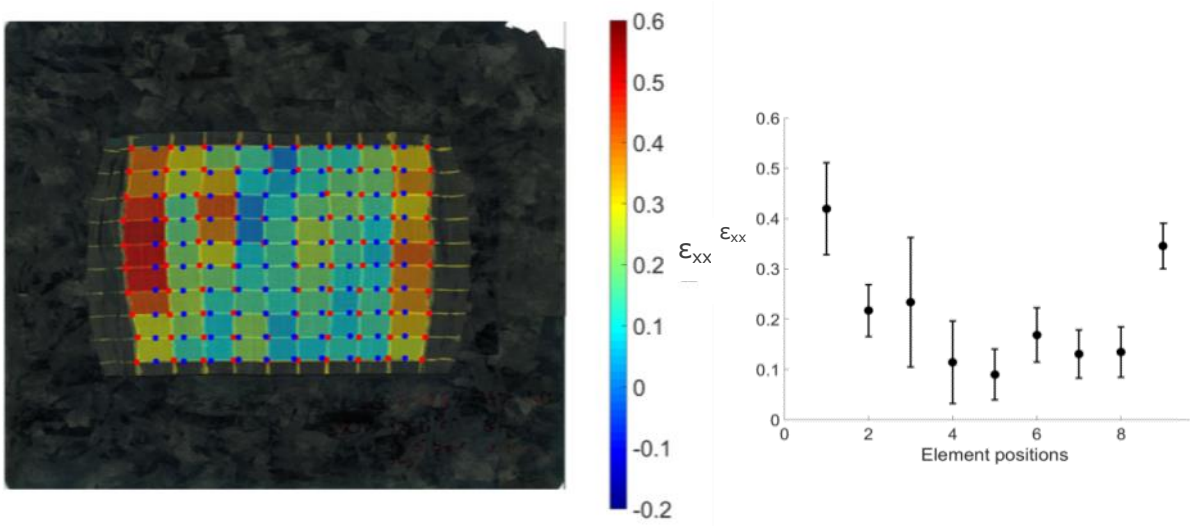

Figure 132: U3 0° 25% H2 60% ε_{xx}, with graph showing column mean of ε_{xx} highlighting the strain limited to the reinforcement edges, with a showing the vertical mean change in strain from left to right.

The strain of the elements in the x-axis of U3 0° 25% H2 60% where the UD was staged to 50% is shown in Figure 132, with a graph showing the vertical mean change from the left of the reinforcement to the right .The extension ε_{xx} of U3 0° 25% H2 60% is greatest at the left and right edges of the reinforcement, and smallest near the central element position (5 in Figure 128) with a gradual increase towards the outside. This means the flow of the HexMC was predominately affecting the edge of the reinforcement. Additionally, a minor y-direction contraction of a few millimetres was observed in the left section of the reinforcement; this was caused by a decrease in vertical length of the reinforcement as the UD bowed. The rotation shown in Figure 133, exhibited a similar trend of where the largest was predominately on the left and right edge of the reinforcement, although the means were between 2° to 0.5°, the difference is marginal and will only slightly affecting the properties of the reinforcement with regards to misalignment.

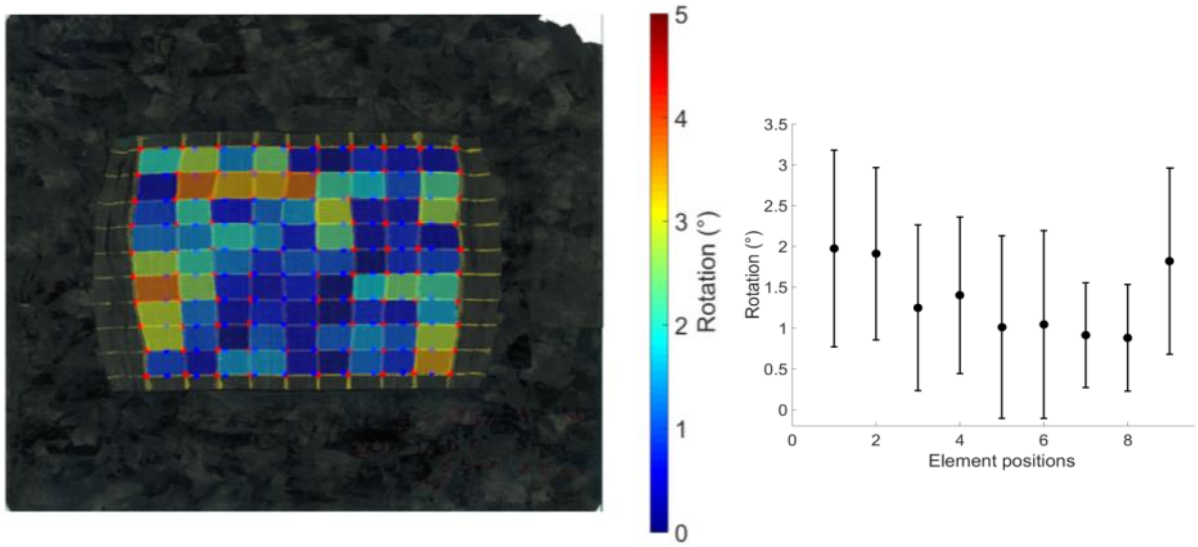

Figure 133: 2D U3 0° 25% H2 60% absolute rotation (°), with mean column element rotation (left to right)

With the UD reinforcement configuration of $90_2/0$ as opposed to 90_3, a dramatic reduction in strain and rotation was observed, as shown in Figure 134. There was no discernible migration of the reinforcement and only minor rotation and strain was measured with no geospatial trend.

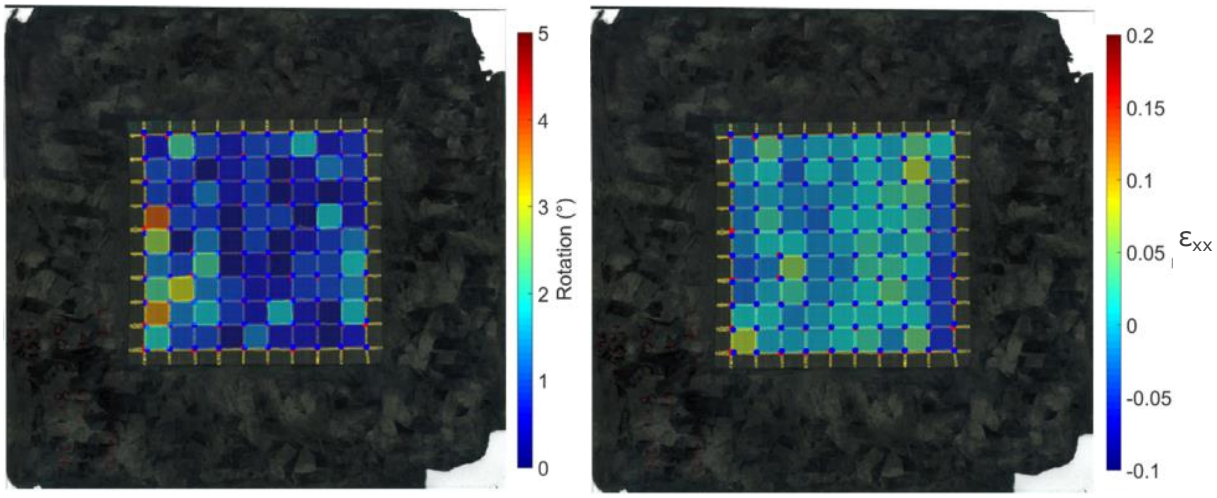

Figure 134: 2D U2 90° U1 0° 25% H2 60% absolute rotation (°) and extension (ε_{xx})

The contrast between the two 2D scenarios is highlighted by the mean and standard deviation of the rotation and extension, which is shown in Table 20. There was less distortion, rotation and variation with the $90_2/0$ reinforcement configuration. Although, the maximum rotation and ε_{yy} were the largest in U2 90° U1 0° 25% H2 60%, this was due to an anomaly in the grid detection in the

rotation where the point did not pick up exactly the grid corners. This reduction in all measures shows the enhancement ply design has had on the potential to reduce distortion and increase homogeneity in the surface of the reinforcement; thus creating a more uniform reinforcement.

Label	Mean (SD)			Max/Min		
	θ(°)	ε_{yy}	ε_{xx}	θ(°)	ε_{yy}	ε_{xx}
U3 0° 25% H2 60%	1.36 (1.05)	0.01 (0.04)	0.21 (0.13)	3.82 0	0.11 -0.1	0.53 0
U2 U1 25% H2 60%	0.92 (0.79)	0.00 (0.03)	0.00 (0.03)	3.86 0	0.01 -0.08	0.07 -0.06

Table 20: Rotation, *x* and *y* direction strain on the 2D flow scenarios

8.1.1. Localised properties of 2D flow hybrid composites

Figure 135 shows the flexural modulus and V_f of U3 90° 25% H2 60%. The top left fibre corner near **A** yielded unexpectedly low properties of E_f 16.01 GPa and V_f 22.07%. This was produced by a short shot creating a resin rich flow front. The transition region between the UD plies and the HexMC shows a reduction in V_f and stiffness, notably at the reinforcement fibre ends. The HexMC at the drop-off around the reinforcement had a V_f of 50.91%, significantly lower than the total HexMC mean of 56.15%, which included the drop-off region.

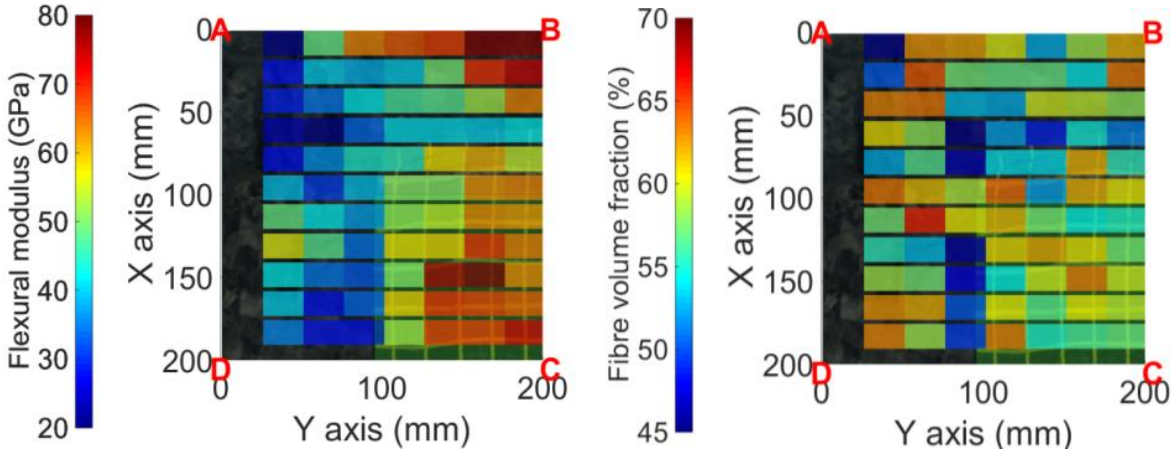

Figure 135: Flexural modulus and fibre volume fraction of U3 90° 25% H2 60%

The flexural modulus in the HexMC along **A→B** in Figure 135 was high, reaching a maximum of 81.24 GPa; this was similar to the maximum in the UD reinforced area, as shown in Table 21. The V_f was not noticeably high to account for this flexural modulus; an elevated stiffness at the edge has also been observed in the constituent materials chapter (**4**) where the fibres rotate and align parallel along the tool edge and consolidate, locally enhancing the properties. On average, the region within the UD reinforcement had a stiffness that was 44% higher than the surrounding HexMC material, but there was only a modest 2.35% increase in V_f. This suggests that the reinforcement provides significant enhancement to the HexMC while only slightly affecting the mean V_f, although there is a significant resin band around the reinforcement, which is band of weakness shown in the flexural strength.

	U3 90° 25% H2 60%				U2 U1 25% H2 60%			
Flexural modulus (GPa)	**Mean**	**max**	**min**	**SD**	**Mean**	**Max**	**min**	**SD**
within reinforcement	61.63	83.20	44.70	8.68	60.00	80.28	47.34	9.13
outside reinforcement	42.89	81.24	16.01	15.03	38.95	75.76	18.62	12.10
Fibre volume fraction (%)	**Mean**	**max**	**min**	**SD**	**Mean**	**Max**	**min**	**SD**
within reinforcement	58.50 %	63.97 %	52.24 %	3.45 %	57.09 %	59.83 %	54.48 %	1.70 %
outside reinforcement	56.15 %	66.03 %	22.07 %	7.28 %	55.62 %	65.00 %	26.90 %	6.40 %

Table 21: Properties of U3 90° 25% H2 60%

Figure 136 shows the localised flexural modulus and fibre volume fraction of U2 U1 25% H2 60%. The same HexMC edge effect in U3 90° 25% H2 60% (Figure 131) was observed in U2 U1 25% H2 60% along **A→B**. There was a noticeable decline in V_f surrounding the reinforcement, caused by resin bleeding out. However this did not lead to a reduction in flexural properties at the drop-off. A very low V_f (26.90%) and E_f were observed near region **A**, although this can be attributed to a resin rich flow front which did not carry to the tool edge and through the flash gap similar at the edge **A→B**. Excluding these regions, the average V_f of the HexMC is only 0.5% lower than that of the UD reinforcement. However, the UD reinforcement reduces the variability of the hybrid region, as

shown in Figure 136, with the standard deviation of the stiffness being lower, 9.13 GPa compared to 12.1 GPa in the HexMC. Similarly, the hybrid region had a lower variation in V_f.

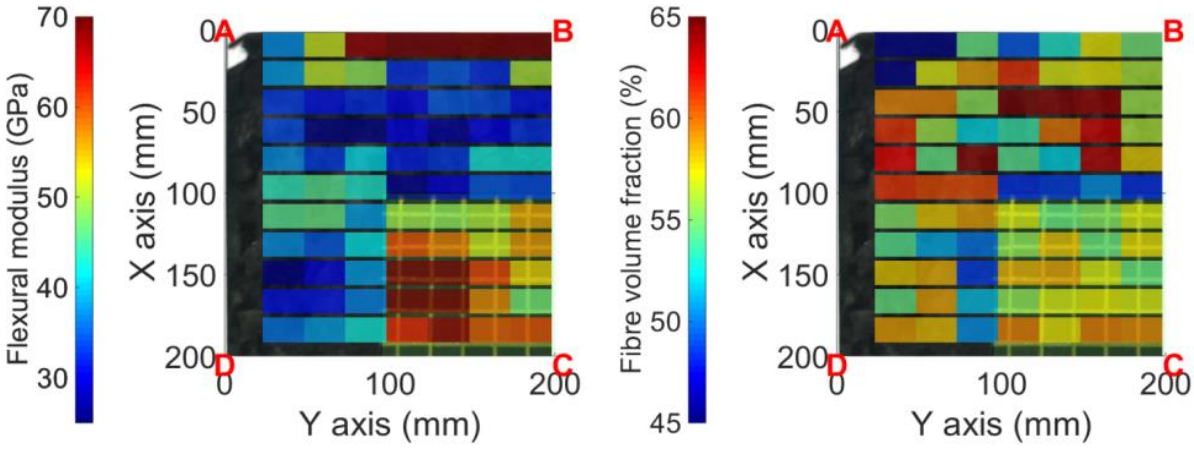

Figure 136: Flexural modulus and fibre volume fraction of U2 U1 25% H2 60%

There were regions with low stiffness within the plaque, with a minimum of 18.62 GPa in the HexMC. 7.95% of the locations were <30 GPa; these were where the testing orientation was perpendicular to the local flow direction or where fibre rippling occurred, effectively making the fibres very short. This was similar to the 1D study where the UD reinforcement exhibited a high flow resistance. U2 U1 25% H2 60% s50% exhibited two moulding defects in the HexMC region, Figure 137 shows evidence of fibre rippling and dryness on the underside of the plaque, beneath the UD material.

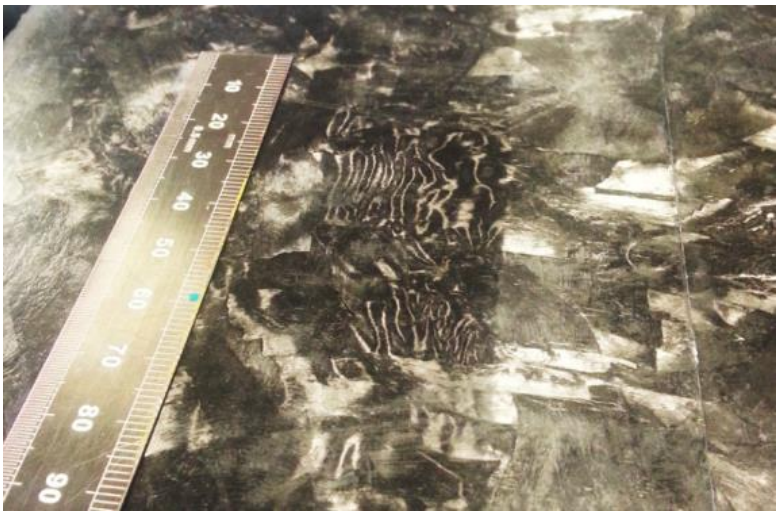

Figure 137: Ripples and dry edge on scenario U2 U1 25% H2 60% s50%

The grid strain analysis and density measurements provided a theoretical flexural modulus which was compared with the experimental results. This is shown in Figure 138 with an image showing the geospatial positions of each location. As there were no localised stiffness measurements for HexMC as in the 1D study, a single mean experimental value of 33.10 GPa for the value of HexMC was used. It is shown in Figure 138, that there is a declining agreement between the theoretical and experimental stiffness of U3 90° 25% H2 60% depending on location within the reinforcement. The local UD thinning in the reinforcement in U3 90° 25% H2 60% was accounted for in theoretical stiffness the UD by Element extension (ε_{xx}). Sample **1-8** exhibited higher deformation and increased the RMSE to 20.74% (11.79 GPa). It is likely that this reduction in properties is due to a mixture of factors such as rotation and splitting which was limited to the reinforcement edge.

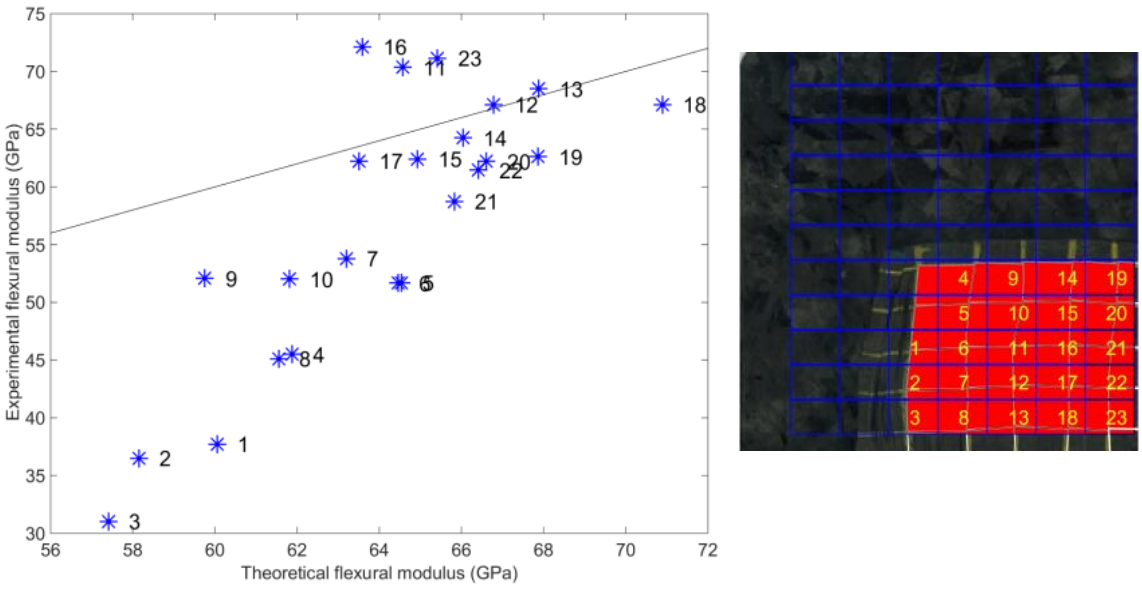

Figure 138: U3 90° 25% H2 60% s50% theoretical flexural modulus plotted against experimental with specimen location

When the reinforcement was altered from 90_3 to $90_2/0$ the flow significantly reduced, which was shown earlier in both the rotation and deformation. In U2 U1 25% H2 60%, the theoretical stiffness values were all within 3.5 GPa; as shown in the experimental over theoretical flexural modulus plot in Figure 138. The experimental stiffness exhibited higher variation in flexural moduli after normalisation to 55%, which is caused by the HexMC causing variation within the flexural specimen. It is probable that in regions **1-3** and **6**-**8** the flow caused alignment in the testing direction which enhanced the HexMC properties further.

The opposite was true along regions **10**, **15** & **20**; this can also be observed in U3 90° 25% H2 60% s50%. The 2D scenarios did not reduced the accuracy of the theoretical prediction especially in U2 U1 25% H2 60% s50% where RMSE was comparable to the 1D scenarios, at 16.18% (9.35 GPa).

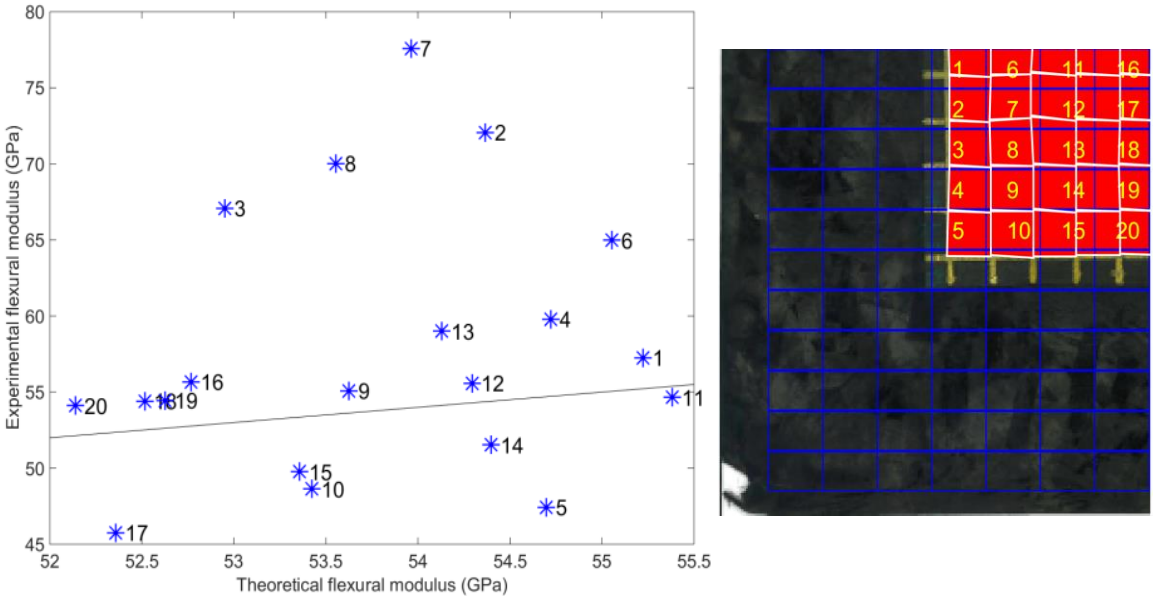

Figure 139: U2 U1 25% H2 60% s50% theoretical flexural modulus plotted against experimental with specimen location

The model has increased accuracy with increased flow control, as the mean error from the predicted values were in this case reduced from 20.74% in U3 90° 25% H2 60% s50% to 16.18% in U2 U1 25% H2 60% s50%. There have been two major issues when calculating the predicted value: the HexMC has high levels of local variability in stiffness and predicting this is difficult. As the UD distorts and flows, the prediction loses accuracy as it is not incorporating the thinning of the elements significantly. However reducing the flow of the reinforcement to negligible amounts increases the repeatability of the process (see Figure 134) allowing a manufacturer to be confident that the reinforcement is in the desired location and with less stiffness variability. To increase the model accuracy, modelling of high V_f SMC through compression moulding would be required, which would provide localised V_f and fibre orientation, effectively removing the HexMC variability.

The difference between the two 2-dimensional flow scenarios was a single ply orientation. However, the flow and rotation of the reinforcement are notably lower. The difference in stiffness between the hybrid and HexMC regions in the two scenarios were marginal of 60 GPa and 39 GPa for U2 U1 25% H2 60% s50% and 62 GPa and 43 GPa for U3 25% H2 60% s50%. It was expected that the difference would be greater as the latter had all the reinforcement plies in the testing direction. This Indicates a single transverse ply limits flow of the reinforcement enhancing the repeatability of the parts and increases the hybrid stiffness as it prevents degradation through distortion and thinning. Additionally is demonstrates that the sacrificial ply which would theoretically lower the properties as only two thirds of the reinforcement was in the beam axis has minimal effect.

8.2. 3D hybrid composites

3D components were produced to demonstrate the feasibility of manufacturing hybrid components that have a complex geometry. Three different types of plaques were produced: HexMC, non-staged hybrid and staged hybrid. A metallic insert was added to show the potential compression moulding SMCs have for high performance applications.

When placing the moulding compound a split in the plies was added at the ribs to prevent fibres bridging the rib entrance, this allowed fibre ends to fill the rib region. This is shown in Figure 140 where it can be seen that the top of the rib has multiple fibre ends.

Figure 140: Micrograph of rib and plate edge on the right

In the 3D study the UD reinforcement was placed on the flat underside of the component and on top of the towers between the ribs. Using the conclusions from the one and two-dimensional studies, 50% staging and a UD configuration of $90_2/0$ was used to minimise flow of the UD reinforcement.

The challenge in this process is that SMC charges are typically loosely assembled, using the charge mass as the main quality measure for achieving a high quality part. With a hybrid architecture component, more care has to be taken as the reinforcement needs to be placed in the desired final position. This adds complexity to the manufacturing, which risks jeopardising the simplicity of the SMC compression moulding process and therefore negating many of the advantages. The current charge has therefore been designed with this in mind, making the construction as simple as possible and straightforward to load into the tool.

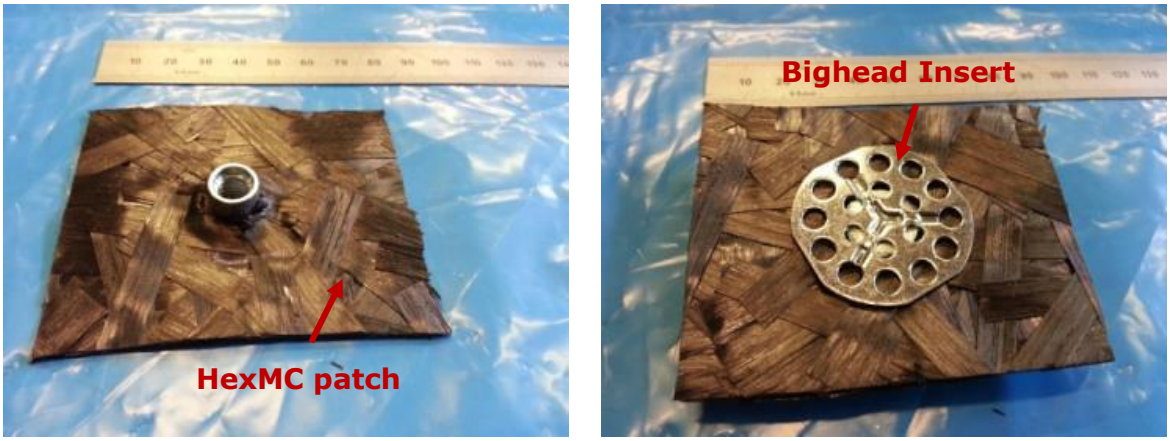

Figure 141: Patch to ensure insert was encased by the HexMC

The metallic inserts in the demonstrator components caused numerous defects, primarily because of the limited flowability of a high V_f SMC. A patch of HexMC was fitted over the top of the insert to ensure it was fully encapsulated, as shown in Figure 141, as without it there was insufficient flow. However, as the local flow is reduced and the insert is in the centre of the tool which is far from the flash gap, voids formed around the insert. Figure 142 shows an image of the cross-section of the metallic insert, highlighting the holes in the bighead fastener. It can be seen on the left and right of the insert, near the top of the thread that the fibres have flowed around the flange as they fill the cavity. This however, likely caused a similar issue to that of filling ribs, as the fibres are being trapped on the underside of the insert, preventing proper filling around the threaded section. As the fibres can no longer flow, resin bleeds into the region. Additionally it is clear from Figure 142 that fibres are unable to flow between the holes in the base plate of the insert. The resulting high pressures caused the plate to bend and the holes just filled with resin as the fibres bend towards the hole but not going through.

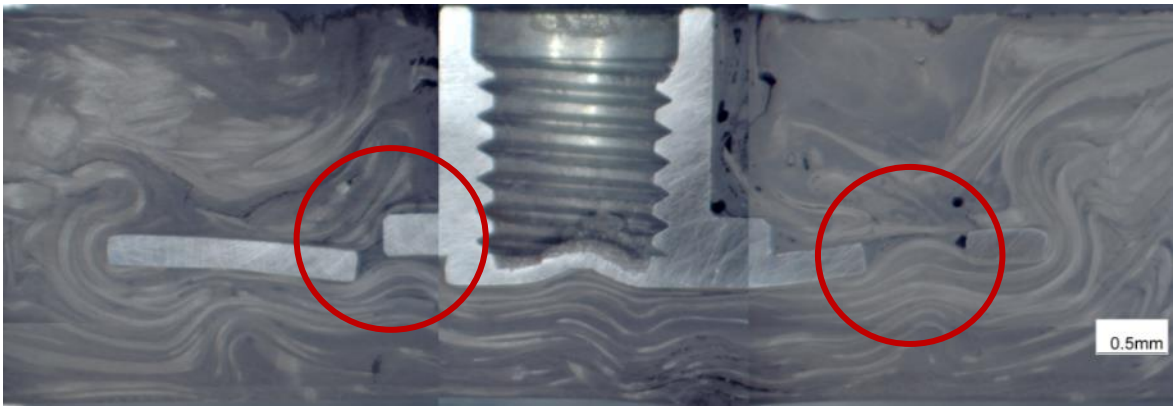

Figure 142: Micrograph of metallic insert in a hybrid plaque with HexMC patch. The highlighted areas indicate where the fibres have bent towards the holes of the insert but not gone through

The layup for the HexMC and hybrid 3D demonstrator components were the same excluding the addition of UD, enabling a direct comparison. The underside on the non-hybrid in Figure 143 has witness marks opposite the ribs caused by the HexMC. In the non-staged hybrid case in Figure 144 the HexMC dragged the UD and distorted it; this is not visible on the staged scenarios as the reinforcement is resistant to HexMC flow. On the top right and bottom left of the non-staged component ribs (Figure 144), yellow marking can be seen. This shows, the HexMC has carried the UD which flowed readily into the rib feature, which is similar to the 1D flow scenarios where there was no staging.

Figure 143: HexMC demonstrator without metallic insert

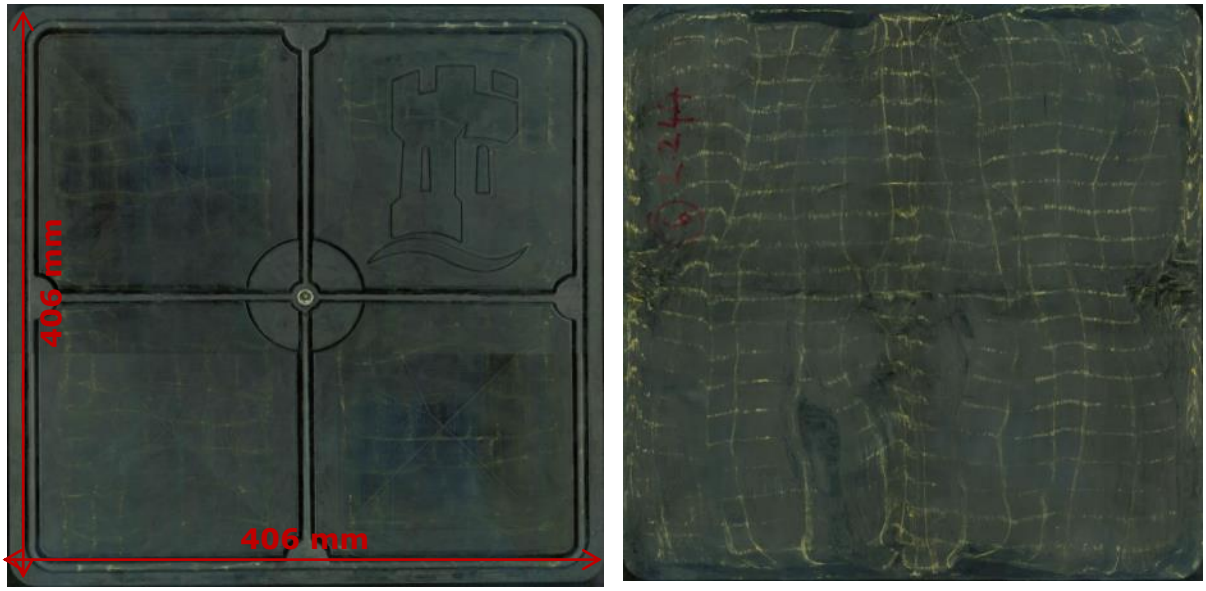

Figure 144: Hybrid composite with no staging, with bunching as the UD fibres flow together as the HexMC flows up into the rib

The flow of UD reinforcement was significant when the plies were non-staged, providing a contrast between the 3D demonstrator components. Figure 144 shows the top and bottom surfaces for the non-staged hybrid and Figure 146 shows the two surfaces for an equivalent staged hybrid component. The lines on the non-staged are less visible than the staged component. This is because the resin had a lower viscosity in the non-staged scenario and therefore flowed further, encapsulating and diluting the paint pen markings.

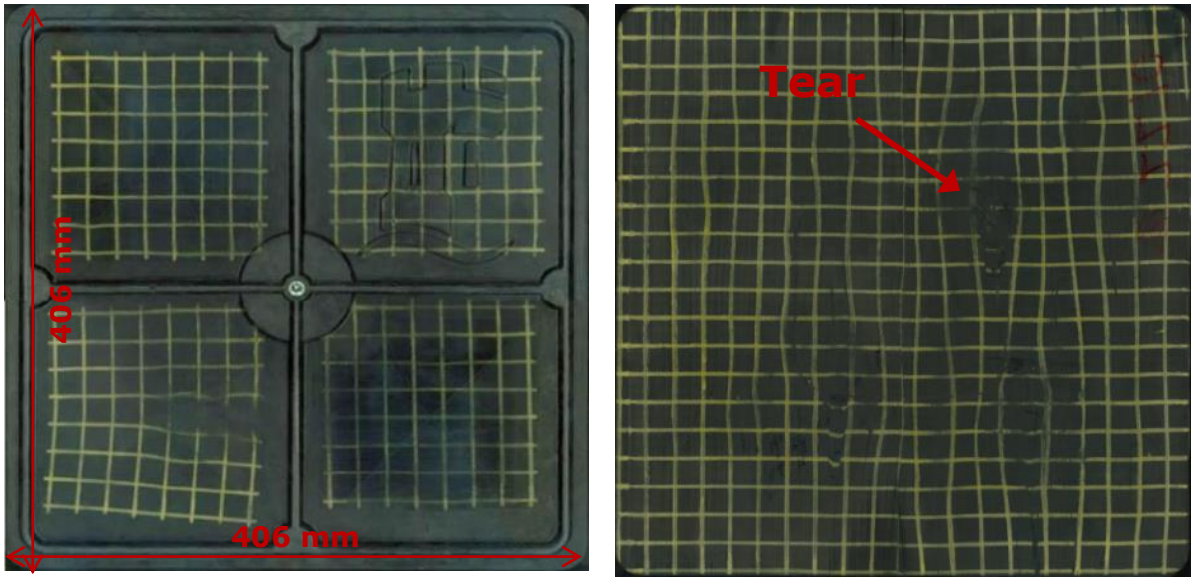

Figure 145: Staged hybrid composite top with binder, with tear as the flow of the HexMC fractures the UD plies

The Airtac binder may have adhered the UD sufficiently to the HexMC pulling the UD with it instead of flowing over. This difference may have caused the tearing of the UD, as shown in Figure 145. That said, the defects in the reinforcement shown in Figure 145 are at the thinnest sections of the component (≤2 mm). HexMC is recommended to have a minimum thickness of ~2 mm, and in these locations with 0.9mm of UD the HexMC is ~1.1 mm. To avoid tearing, the adhesive was not used, although this lead to misaligned grids as shown in Figure 146. This is because the reinforcement would slip during charge placement, which is visible in the regions between the ribs and on the underside in centre of right image in Figure 146.

Several problems occurred in the manufacture of the demonstrator, which should be considered when manufacturing a hybrid composite with staged sections. Firstly, the staged UD no longer has any tack and HexMC is a low tack moulding compound, meaning that the UD material is prone to slipping. This is especially problematic when placing a charge quickly in the hot cavity where access is limited. Secondly, in a hybrid composite it will be desirable to place the UD in a precise location but this can be difficult when there is very little to guide the location of the reinforcement.

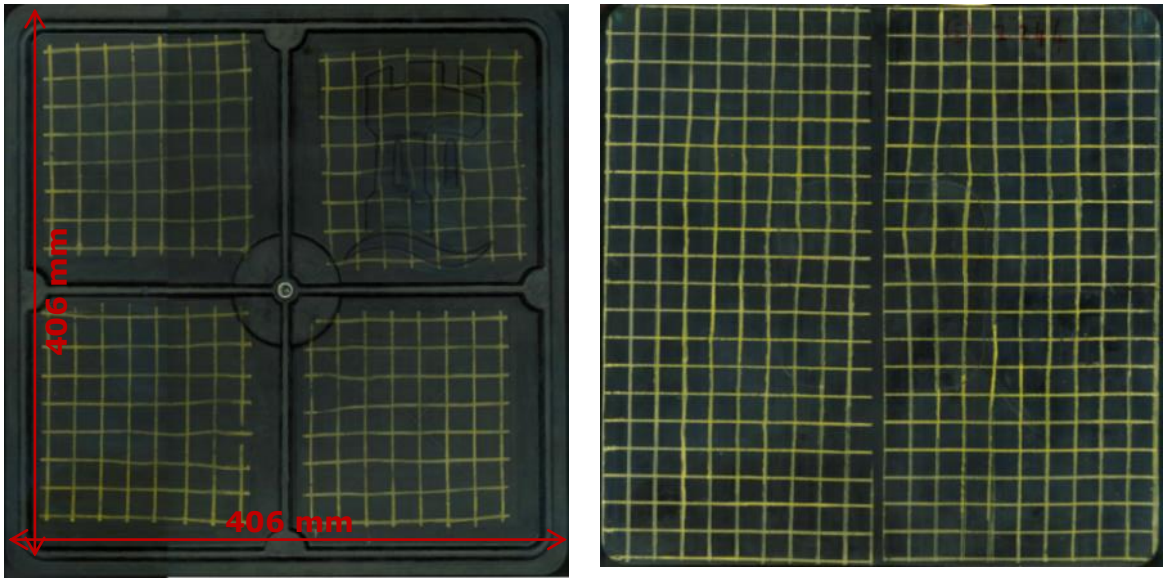

Figure 146: Staged hybrid composite top without binder

To manufacture this 3D component with sections of UD and metallic inserts several rules should be followed. The reinforcement UD should be staged to approximately 50%; any further staging and properties of the UD degrade, any less and the flow of the reinforcement is not sufficiently restricted. This has to be

done in conjunction with a sacrificial ply transverse to the reinforcing direction. UD limits the flow of the HexMC, so a higher level of charge coverage is required. Furthermore, to minimise distortion of the UD, flow of the HexMC should be kept away from the reinforcement as far as is practical. For metallic inserts, flow is required for encapsulation by the fibres and to remove voids, ideally inserts should not central in the component where flash gaps are far away, minimising the opportunity for entrapped air to escape through the flash gap and in areas of flow encouraging SMC homogenisation.

8.3. Summary

A charge configuration of one ply transverse to two other plies has been shown to significantly limit the flow of the entire reinforcement in increasingly complex scenarios. Only a few millimetres of local flow in a 2D scenario were observed on the reinforcement corners with a HexMC coverage of 60%, which is encouraging as it is recommended to have a charge coverage of 80%.

In 2D scenarios where the reinforcement can flow in both directions, a fibre volume fraction reduction was observed around the transition region between the UD reinforcement and the HexMC. Unlike in the 1D scenarios where the UD was constrained against three sides of the tool wall, the 2D reinforcement was free to migrate, but this was not observed as the friction of the reinforcement increased due to staging, which removed of the lubricating layer. Instead there was minimal flow or disruption.

When HexMC flowed into the tool edge, there was an increase in stiffness along the flash gap. This was observed again in the 2D study and provides an opportunity at the edge of components to elevate stiffness if the HexMC is designed to flow into the edge. The addition of staged reinforcement and charge design proved the potential for hybridisation for enhancing stiffness in 2D flow scenarios, justifying the case for hybridisation.

The flow of HexMC into the ribs caused the non-staged hybrid reinforcement to bunch and buckle on the underside of the rib. A similar situation occurred on the top side near the rib corners where the reinforcement was pulled into the rib.

Staging the UD prevented the reinforcement from being dragged by the HexMC into the rib features.

Handling complex charge geometries can be a challenge with staged sections as they have no tack with the HexMC. As the reinforcement will be required to be placed in its designed final location, care will be needed which is an issue as the UD sections are prone to slipping. Using a binder may cause adhesion leading to fracture of the UD fibres. Additionally, the use of metallic inserts may be more complex in hybrid composites as the presence of continuous fibres decreases the flowability of the SMC, causing it to be increasingly challenging to fully encapsulate the inserts without voids or fibre matrix separation occurring.

9. Conclusion

The aim of this research was to demonstrate the addition of continuous fibre composites and how they can improve the properties of SMCs by enhancing the local stiffness while maintaining the flowability of the SMC in order to fill complex regions of the tool.

9.1.1. Individual flow properties of discontinuous and continuous composites

Moulding the discontinuous and continuous materials together required a compromise, as each material has its own individual and recommended moulding parameters. Due to the sensitivity of moulding HexMC at low pressure, the UD was moulded at HexMC pressure. When moulding a net-shape UD plaque at this high pressure the fibre volume fraction increased through resin bleed out, but there was no apparent property degradation. However, SMCs prefer to have a degree of flow, which allowed homogenisation of the resin and fibres and also aided void removal. This was problematic as flow of unidirectional fibres caused distortion and hence property degradation. Additionally flow is desired for the SMCs to fill complex features without significant labour costs and therefore the UD reinforcement will also experience flow, in a hybrid scenario. If SMCs were prepared net-shape it would be preferable to use continuous fabrics and layup the complex geometry as the properties would be better.

There is limited literature on compression moulding of continuous fibre composites, especially where flow is expected. Therefore, research was conducted to determine the expected property degradation and flowability of UD in a one dimensional flow scenario. It was found that the flexural modulus aligned transverse to the flow direction flowed readily and only degraded by 12% compared to a net-shape plaque; however, when aligned parallel, the stiffness increased by 16% as the fibres remained aligned because there was no fibre flow and significant resin bleed.

9.1.2. One dimensional non-staged hybrid composites

Adding UD in a one dimensional flow scenario with HexMC, where the fibres were aligned transverse and parallel to the flow direction caused thinning and migration of the UD respectively. The UD in both cases became wavy, but no other defects were present. The properties on average were >44% than a pure SMC plaque. The flow of reinforcement was caused by the flow of the SMC and the lubricating layer effect, where the resin in contact with the hot tool on the surface of the UD would reduce dramatically, allowing the UD to smoothly slide over the tool face. The issue with this single shot process, where the material is put together as a single charge and placed in the tool, is that there was no control of the reinforcement. It is not practical to design a hybrid that has higher properties, but poor reliability on the final moulded reinforcement position.

9.1.3. Staging of Unidirectional prepreg

Altering the resin cure was an effective method for reducing the flowability of the prepreg to prevent the reinforcement distortion. The storage modulus was used to measure when the resin was less likely to flow as it changed from liquid to solid. The testing was conducted on prepreg since pure resin samples were not available and the aim of these tests was to measure the change of storage modulus in the prepreg for use in compression moulding. It was found that the transition from liquid to solid occurred very quickly, therefore a low temperature of 90°C was used, to improve the repeatability of the staging and provide control of the process.

As the prepreg became more staged the tack reduced, as did the ability for the resin to crosslink. Inter laminar shear strength testing was used to measure the quality of the bonding between staged and unstaged prepreg. It was found that debulking the material prior to staging enhanced the ILSS; however, this is a time consuming process and was not pursued further. It was found that staging UD to 50% was the highest degree of staging achievable while still having a comparable ILSS with HexMC.

9.1.4. One dimensional staged hybrid composites

Hybrid plaques with the UD transverse to the flow direction in one dimensional scenarios staged to 25%, 50% and 75% showed a decreasing flow from 34% to 9% compared to the non-staged scenario of 66%. Although there were sections where the UD had split, creating thin regions of resin filled bands. In addition, a region of dryness was observed on the underside following the contour of the reinforcement edge but only on the surface; this was caused by the increased pressure on the HexMC exposing dry fibres.

Where the fibres were aligned parallel (0_3) to the flow direction, migration was reduced dramatically to 6%. Conversely with a reinforcement construction of $90_2/0$ and staged to 50% flow was 9%. This is similar to all the fibres being transverse and staged to 75%. However, with such increased flow resistance rippling was observed in the HexMC just after the reinforcement ended; these were where the fibres of the HexMC became wavy through the thickness which dramatically reduced the stiffness by ~25%. The staging did not affect the flexural modulus of the hybrid, but it did provide repeatability in placing the reinforcement without migration or flow.

The flexural strength of hybrids showed that the property enhancement was more than just limited to stiffness. The properties were on average greater than 81% of pure HexMC, providing the potential for increased use in structural applications. A noticeable benefit to the hybrid was in the failure method, where the UD was under tension in bending. As the HexMC tended to fail under compression and followed by delamination between the HexMC and UD, the UD reinforcement remained intact and was able to flex further. This created a progressive failure similar to the plastic deformation in metals. This would be attractive to automotive applications where energy absorption is important as continuous fibre composites usually exhibit brittle failure.

9.1.5. Two dimensional flow properties

In the one dimensional flow scenarios it was possible to have the fibres aligned in the direction to limit the flow. In the 2D scenarios the HexMC applied flow forces in the x and y planes simultaneously; a 50% staged charge configuration of the reinforcement $90_2/0$ reduced the flow to 2.7% compared to 36.7% in 90_3.

This demonstrates the importance of charge design for controlling material flow in increasingly complex scenarios.

The HexMC demonstrator component showed perpendicular fibre aligned on the surface opposite the rib axis. This feature was also visible where there was no staging of the UD, which bunched in these regions caused from the HexMC flowing down the rib. This effect was not visible on the staged UD as the reinforcement resisted the flow of the HexMC sufficiently. This showed that staging reduced the lubricating layer effect and by adjusting the UD plies layup configuration it was possible to dramatically reduce the movement of the continuous fibres.

The main benefits of SMCs are that charge design can be simple since flow of the material can fill complex geometries that would otherwise be highly labour intensive. Adding continuous fibre to the SMC introduces some ply layup care as the reinforcement will need to be placed in the final desired position. Additionally HexMC is a low tack material while staged UD has no tack, so placing the hybrid charge in a tool where sections of the charge are susceptible to slip can be problematic. That said, using a binder in the demonstrator was a solution or alternative higher tack SMCs may stop the reinforcement slipping.

It was observed in scenarios where the hybrid was highly resistant to flow that the flowability of the HexMC reduced. This will become increasingly problematic when trying to fill complex geometries such as metallic inserts, as the SMCs will struggle to flow around the insert to fully encapsulate it. Placing the HexMC around the insert did ensure filling, but with the localised reduced flow fibre matrix separation and void content will increase since the moulding compound is not homogenising and expelling the entrapped air.

9.1.6. Three dimensional hybrid composites

The demonstrator component showed that hybridisation is feasible in complex geometry with changing wall thickness, stiffening features such as ribs and metallic inserts. However, as with all new manufacturing processes and materials, new considerations and design principles need to be considered and accounted for. Such as reinforcement ply design, minimum thickness and charge location, prepreg staging and account for loss of reinforcement tack. With such

considerations localised property enhancements shown in the 1D and 2D scenarios can be achieved to make higher performance SMC components.

9.2. Further opportunities for research

The research undertaken identified multiple opportunities for further work in two main threads, characterisation and reinforcement control.

Flow in 3D hybrid composites is complex and has caused UD fibre fracture that has not been seen in the one or two dimensional scenarios.

This study focused on localised stiffness; however, material characterisation of tensile properties has not been undertaken. It is possible that the continuous fibre plies may dominate the properties when tested in the reinforcement fibre direction. During flexural strength testing it was observed that the HexMC failed first under compression followed by delamination in the thinner UD plies, which deflected further prior to failure. This indicates that there may be some opportunities to research the enhanced energy absorption characteristics of hybrid composites.

The staged UD may have adverse effects on properties such as fatigue leading to further characterization opportunities. Additionally, forming plies after gelation could have other negative effects on the interaction between the staged and non-staged constituents.

Controlling the flow of reinforcement requires further research, as staging does decrease the flexural strength of the hybrid, and using woven or stitched fabrics may aid in the prevention of flow as well as using clamps to hold the reinforcement in place. This may allow increased flow resistance with less staging.

It was observed that debulking improved properties and reduced flow of the reinforcement, even though it was labour intensive. Increasing the staging temperature and preforming with heated platens could provide compaction similar to debulking but in significantly less time. Additionally, preforming would provide an opportunity to have the reinforcement in profiles rather than flat sections.

There are finite element analysis packages that can model the flow of SMC's, however currently at low fibre volume fractions. There is an increasing focus at increasing the fibre volume fractions in these modelled materials. This research would benefit at modelling these high V_f SMC materials that are currently being developed that have far more disruptive and limited flow capabilities with a reinforcement that can migrate and has limited flowability, which crosslinks and bleeds into the moulding compound.

Finally, where the reinforcement ends it was found that there was a resin rich region between the SMC and continuous fibre. An investigation in the joint design of the reinforcement would provide a series of guides as it was found to cause a region of weakness in the flexural strength testing.

10. References

1. F.C. Campbell, *Structural Composite Materials*. 2010: ASM International.
2. *Towards resource management, the Northern Ireland waste management strategy 2006-2010*. nd., Department of the Environment, Northern Ireland.
3. GHK, *A study to examine the benefits of the End of Life Vehicles Directive and the costs and benefits of a revision of the 2015 targets for recycling, re-use and recovery under the ELV Directive* 2006.
4. S. Piers, *The New BMW i3*. 2013, BMW UK Ltd.
5. *CES 2013 Selector*. Granta Material Intelligence.
6. P. Malnati, *Prepreg compression molding makes its commercial debut*, in *Composites World*. 2015.
7. Erbach G., *Reducing CO2 emissions from new cars*. 2014, European Parliamentary Research Service.
8. R. Kozarsky, *Carbon fibre and beyond: the $26 billion world of advanced composites*. 2011, Lux research: Boston.
9. M. H. Akonda, C. A.Lawrence, B. M. Weager *Recycled carbon fibre-reinforced polypropylene thermoplastic composites.* Composites Part A: Applied Science and Manufacturing, 2012. 43(1): p. 79-86.
10. D. Warren, *Low Cost Carbon Fiber Overview*. 2011, Oak Ridge National Laboratory: Oak Ridge, Tennessee.
11. A. Vicari, *Stronger,lighter...cheaper,better?Harnessing the power of carbon fiber*. 2013, Lux Research Inc.
12. T.L. White, F.L. Paulauskas, T.S. Bigelow, *System to continuously produce carbon fiber via microwave assisted plasma processing*. 2010: Ut-Battelle. United states.
13. Paulauskas F. L., *Advanced Oxidation & Stabilization of PAN-Based Carbon Precursor Fibers*. 2013, Oak Ridge National Laboratory.
14. S. Sikirica, *Scale Up of Novel, Low-Cost Carbon Fibers Leading to High-Volume Commercial Launch*. 2013.
15. *Commission to the council and the european parliament on the targets contained in the article 7(2)(b) of directive 2000/53/EC on end-of-life vehicle, impact assessment*. 2007, Commission of the European Communities: Brussels.
16. T. Gallone, *ICARRE 95 - Industrial Platform Demonstrator to achieve 95% recycling of the "end-of-life vehicle"*. RENAULT S.A.S.
17. M.H. Geier, *Quality Handbook for Composites Materials*. 1994, London: Chapman & hall.
18. P. Feraboli E. Peitso, F. Deleo, T. Cleveland, *Characterization of Prepreg-Based Discontinuous Carbon Fiber/Epoxy Systems.* Journal of Reinforced Plastics and Composites, 2009. 28(10): p. 1191-12-14.
19. S. Mazumdar, *Composite Manufacturing: Materials, Product, and Process Engineering*. 2001: CRC Press.
20. B.T. Astrom, *Manufacturing of Polymer Composites*. 1997, London: Chapman & Hall.
21. P. Feraboli, F. Gasco, B. Wade, S. Maier, R. Kwan, A. Masini, L. De Oto, M. Reggiani, *Lamborghini "Forged Composites" Technology for the Suspension Arms of the Sesto Elemento*, in *American Society of Composites*. 2011: Montreal

22. M. Arce, M. Tuttle, *Certification of Discontinuous Composite Material Forms for Aircraft Structures*, in *Joint Advanced Materials and Structures* 2014: Seattle.
23. CompositesWorld, *Lucintel estimates global sheet molding compound market, 2014-2019*, in *CompositesWorld*. 11/29/2014.
24. P. Feraboli, E. Peitso, F. Deleo, T. CLeveland, M. Graves, P. Stickler, *Characterization of Discontinuous Carbon Fiber/Epoxy Systems for Aerospace Applications: Part I*, in *Technical Conference of American Society for Composites*. 2007. p. 2253-2274.
25. D. Burn, *Thermoplastic Adhesion to random Carbon Fibre Composites*. 2016.
26. S. Ringenbach, J. Richeton, J. Coulton, *Hyundai's breakthrough front bumper crash beam*, in *JEC Composites*. Aug 2015. p. 39-41.
27. P.J. Dufton, *Lightweight Thermoset Composites: Materials in Use, Their Processing and Applications*. 2000, Rapra Industry Analysis report series: Shawbury,Shropshire.
28. S. Das, *The cost of automotive polymer composites: a review and assessment of DOE's light weight materials composites research*. 2001, Oak Ridge National Laboratory: Oak Ridge, Tennessee.
29. P.E. Degarmo, J.T. Black, R.A. Kohser, *Materials and Process in Manufacturing* ed. 11th. 2011: John Wiley & Sons.
30. D.E. Davenport, R. Petrovich, G. Sutton, *Low Pressure Resin Transfer Molding for Cost Effective Aircraft Quality Structures.* Society for the Advancement of Material and Process Engineering 2007.
31. R. Chaudhari, M. Pick, O. Geiger, D. Schmidt, P. Elsner, F. Henning, *Compression RTM - A new process for manufacturing high volume continuous fiber reinforce composites*, in *International CFK-Valley Stade Convention*. 2011, Fraunhofer ICT: Stade.
32. Goodship V., *A Practical Guide to Injection Moulding*. Vol. Shrewsbury. 2004: Rapra Technology ltd.
33. L. Orgeas, P.J.J. Dumont, *Sheet moulding compounds*. 2012.
34. A.M. Grillet, A.C.B Bogaerds, G.W.M. Peters, F.P.T Baaijens, *Numerical analysis of flow mark surface defects in injection molding flow.* Journal of Rheology, 2002. 46: p. 651-669.
35. T.D. Papathanasiou, D.C. Guell, *Flow-induced alignment in composite materials*. 1997, Cambridge: Woodhead Publishing Limited.
36. C. Lee, C. Tucker, *Flow and Heat Transfer in Compression Mold Filling.* Journal of Non-Newtonian Fluid Mechanics, 1986. 24: p. 245-264.
37. Fu Shao-Yun,Mai Yiu-Wing,Lauke BerndandYue Chee-Yoon, *Synergistic effect on the fracture toughness of hybrid short glass fiber and short carbon fiber reinforced polypropylene composites.* Materials Science and Engineering: A, 2002. 323(1–2): p. 326-335.
38. Odenberger P. T.,Andersson H. M.andLundström T. S., *Experimental flow-front visualisation in compression moulding of SMC.* Composites Part A: Applied Science and Manufacturing, 2004. 35(10): p. 1125-1134.
39. M.R. Barone, D.A. Caulk, *Kinematics of Flow in Sheet Molding Compounds.* Polymer Composites, 1985. 6(2): p. 105-109.
40. N.E.J. Olsson T.S. Lundström, K. Olofsson, *Design of experiment study of compression moulding of SMC.* Plastics, Rubber & Composites, 2009. 38(9-10): p. 426-431

41. N.E.J. Olsson, T.S. Lundström, K. Olofsson, *compression moulding of smc: coupling between the flow and the local void contents* in *International Conference on Composite Materials*. 2009: Edinburgh.
42. S. Y. Kim, Y. T. Im, *Three-dimensional thermo-viscoplastic analysis of compression molding of sheet molding compounds with fiber volume fraction prediction.* Journal of Materials Processing Technology, 1997. 63(1–3): p. 631-636.
43. E. Schmachtenberg, D. Lippe, K. Skrodolies, *Faser/Matrix-Entmischung während des Fließpressens von SMC.* Journal of Plastics Technology, 2005.
44. *Manufacturing Techniques for Polymer Matrix Composites (PMCs)*, ed. K.H. S. Advani. 2012: Woodhead Publishing.
45. *Comprehensive Composite Materials*. 2000.
46. B A. Davis, P J. Gramann, T.A. Osswald, A.C. Rois, *Compression Molding*. 2003: Hanser.
47. J.H. Jeong, K.T. Kim , Y.T. Im, *Plane-strain compression molding analysis of sheet molding compounds in flat and cross-sectional T-shape molds.* Journal of Materials Processing Technology, 1996. 57(3–4): p. 320-331.
48. A. London-Hurtado, T.A. Osswald, J.P. Hernandez-Ortız, *Modeling the behavior of fiber suspensions in the molding of polymer composites.* Journal Reinforced Plastics & Composites, 2011. 30: p. 781-790.
49. K. L. Smith, N.P. Suh, *An approach towards the reduction of sink marks in sheet molding compound.* Polymer Engineering & Science, 1979. 19(12): p. 829-834.
50. M. Rabinovich, K.L. Olsavsky, B. Leach, M. Cabrera-Rios, J.M. Castro, *Sheet molding compound characterization using spiral flow.* Journal of Applies Polymer Science, 2008. 109(4): p. 2465-2471.
51. D.M. Lasell, *Part and Mold Design Guidelines for the High Volume Compression Molding of Carbon Fiber Reinforce Epoxy*. 2012, Think Composites L.L.C.
52. K. Mason, *Compression molding with structural carbon SMC* in *Composites World*. 1/1/2005.
53. Londoño-Hurtado, A. Hernandez-Ortiz, J. Pablo, T. A. Osswald,, *Mechanism of fiber–matrix separation in ribbed compression molded parts.* Polymer Composites, 2007. 28(4): p. 451-457.
54. S. H. Jo, E. G. Kim *Effect of product geometry on fiber orientation of compression-molded rib type products.* Journal of Materials Processing Technology, 2002. 130–131: p. 156-160.
55. K.T. Kim, Y.T. Im *Experimental study on physical properties of compression molded SMC parts under plane strain condition.* Composite Structures, 1996. 35(2): p. 131-141.
56. H.G. Kia, *Sheet Molding Compound Materials: Science & Technology*. 1993: Hanser Gardner.
57. J. Xu, J. Kim , Ho Ted, L.L. James, *Compression molding of sheet molding compounds in plate-rib type geometry.* Polymer Composites, 1993. 14(1): p. 51-58.
58. S.K.Christensen, B. Hutchinson, E.M. Sun, T.A. Osswald *Fiber-Matrix Separation in Ribbed SMC and BMC Parts*, in *Society of Plastics Engineering*. 1997: Toronto. p. 782-789.

59. Fan Jyh-Dar, L. L. James,J. Kim , Y.T. Im, *Cure analysis of sheet molding compound in molds with substructures.* Polymer Engineering & Science, 1989. 29(11): p. 740-748.
60. A.A. Arifin, W. Wang, T. Matsubara, *Experimental investigation on the compression and crush responses of cross-ply laminates with 0° plies of unidirectionally arrayed chopped strand.* Composites Part B: Engineering, 2016. 98: p. 182-193.
61. I. Taketa, T. Okabe, H. Matsutani, A. Kitano, *Flowability of unidirectionally arrayed chopped strands in compression molding.* Composites Part B: Engineering, 2011. 42(6): p. 1764-1769.
62. R.E Shalin, *Polymer Matrix Composites*. 2012, London: Chapman & Hall.
63. T.G Mezger, *The Rheology Handbook*. 2011: Vincentz Network.
64. J. M. Laza, C. A. Julian, E. Larrauri, M. Rodriguez, L. M. Leon, *Thermal scanning rheometer analysis of curing kinetic of an epoxy resin: 2. An amine as curing agent.* Polymer, 1999. 40(1): p. 35-45.
65. M.L. Costa, E.C. Botelho, J.M.F. de Paiva, M.C.Rezende, *Characterization of Cure of Carbon/Epoxy Prepreg Used in Aerospace Field.* Materials Research, 2005. 8(3): p. 317-322.
66. W.Stark, M. Jaunich, J. McHugh, , *Carbon-fibre epoxy prepreg (CFC) curing in an autoclave analogue process controlled by Dynamic Mechanical Analysis (DMA).* Polymer Testing, 2013. 32(8): p. 1487-1494.
67. M. Hargis, B.P. Grady, L. Aktas, K.R. Bomireddy, S. Howsman, M.C.Altan, T. Rose, H. Rose, *Calorimetric and Rheological Measurements of Three Commercial Thermosetting Prepreg Epoxies.* Journal of Composite Materials 2005. 40(10): p. 873-897.
68. M. Hayaty M.H. Beheshty, M. Esfandeh, *A new approach for determination of gel time of a glass/epoxy Prepreg.* Journal of Applies Polymer Science, 2011. 120: p. 1483-1489.
69. K.D. Potter, *Understanding the Origins of Defects and Variability in Composites Manufacture*, in *International Conference on Composite Materials*. 2009: Edinburgh.
70. J. Sloan, *High-speed press cure for high-speed racers*, in *Composites World*. 2011.
71. Akiyama Koichi, *Development of PCM technology*. 2011, Mitsubishi Rayon Co. Ltd.
72. H.N. Dhakal, Z.Y. Zhang, R. Guthrie, J. MacMullen, N. Bennett, *Development of flax/carbon fibre hybrid composites for enhanced properties.* Carbohydrate Polymers, 2013. 96(1): p. 1-8.
73. Min-Seok Sohn Xiao-Zhi Hu, *Processing of carbon-fibre/epoxy composites with cost-effective interlaminar reinforcement.* Composites Science and Technology, 1998. 58(2): p. 211-220.
74. S. A.Hitchen, R. M. J. Kemp, *Development of novel cost effective hybrid ply carbon-fibre composites.* Composites Science and Technology, 1996. 56(9): p. 1047-1054.
75. Y.X Li, X. J. Choy, C. L.,Guo, Z. Zhang, *Compressive and flexural behavior of ultra-high-modulus polyethylene fiber and carbon fiber hybrid composites.* Composites Science and Technology, 1999. 59(1): p. 13-18.

76. J. P.Nunes, A. S.Pouzada, C. A. Bernardo, *The use of a three-point support flexural test to predict the stiffness of anisotropic composite plates in bending.* Polymer Testing, 2002. 21(1): p. 27-33.
77. P.K. Mallick, *Effect of Fiber Misorientation on the Tensile Strength of Compression Molded Continuous Fiber Composites.* Polymer Composites, 1986. 7(1): p. 14-18.
78. J. Wulfsberg, A. Herrmann, G. Ziegmann, G. Lonsdorfer, N. Stöß, M. Fette, *Combination of Carbon Fibre Sheet Moulding Compound and Prepreg Compression Moulding in Aerospace Industry.* Procedia Engineering, 2014. 81: p. 1601-1607.
79. D. Bond, L.T. Harper, T. A. Turner, N. A. Warrior, *Full-Field Strain Measurement of Notched Discontinuous Carbon Fibre Composites*, in *International Conference on Composites Materials*. 2009: Edinbrugh.
80. P. Feraboli, E. Peitso, T. Cleveland, P.B. Stickler, J.C. Halpin, *Notched behavior of prepreg-based discontinuous carbon fiber/epoxy systems.* Composites Part A: Applied Science and Manufacturing, 2009. 40(3): p. 289-299.
81. D. Emerson, D. Grauer, B. Hangs, M. Reif, F. Henning, A. Martsman, S.T. Jespersen, *Uising Unidirectional Glass Tapes to Improve Impact Performance of Thermoplastic Composites in Automotive Applications*, in *12th Annual Automotive Composites Conference and Exhibition*. 2012: Troy, MI. p. 85-97.
82. *Lightweight strategy for the automotive industry*, in *The magazine of the Business Unit Composites, Presses and more composites*. 2015. p. 4-34.
83. G. Gardiner, *Wet compression molding*, in *CompositesWorld*. 02/01/2016.
84. B.Hangs, R. Jauch, F. Henning, D. Grauer, S. Jespersen, A. Martsman, *Co-compression molding of tailored continuous-fiber-inserts and inline-compounded long-fiber-thermoplastics*, in *SPE ACCE 2012*. 2012, Fraunhofer: Troy, MI.
85. A. Sasaki, T. Hayashi, K. Akiyama, *Flexural Behavior of CF/PP Hollow Beam Made by Continuous and Discontinuous UD Tape*, in *European Conference on Composite Materials*. 2012: Venice,Italy.
86. T. Matsuo, K.Takayama, J. Takahashi, S.Nagoh, K. Kiriyama, T. Hayashi, *Design and Manufacture of Anisotropic Hollow Beam Using Thermoplastics Composite*, in *International Conference on Composite Materials*. 2013: Montreal, Canada. p. 696-703.
87. S. Lambour, *Hybrid thermoplastic technology: Get a finished complex part in one step, saving weight and costs*, in *SAMPE* 2015: Amiens.
88. Composites JEC, *Over-moulded organo-sheets: heavily filled parts by the millions*, in *JEC Composites*. 2013. p. 22-27.
89. O. Westphal O. Calme, M. Crepin, F. Ribour, *Hybrid thermoplastic technologies: Advanced lightweight solutions for industry*, in *SAMPE*. 2015: Amiens.
90. K. Mäntyjärvi, J. Tulonen, T. Saarnivuo, J. Porter, J. A. Karjalainen, *Grid Patterns by Laser for Forming Strain Analysis* International Journal of Material Forming, 2008(1): p. 249-252.
91. K.Hariharan, S.Suresh, *Comparison of Optical Strain Analysis and Circular Grid Analysis in Sheet Metal Forming*, in *Society of Automotive Engineers International*. 2007.

92. W. Boesemann, R. Godding, H. Huette, *Photogrammetric Measurement Techniques for Quality Control in Sheet Metal Forming*, in *International Archives of PHtogrammetry and Remove Sensing*. 2000: Amsterdam. p. 48-55.
93. W Buerzle, E. Mazza, *On the deformation behavior of human amnion.* Journal of Biomechanics, 2013. 46(11): p. 1777-1783.
94. F. Ozturk, M. Dilmec, M. Turkoz, R.E. Ece, H.S. Halkaci, *Grid Marking and Measurement Methods for Sheet Metal Formability*, in *International Conference and Exhibition on Design and Production of Machines and Dies/Molds*. 2009: Aydin,Turkey.
95. P. Dumont, L. Orgéas, S.Le Corre, D. Favier, *Anisotropic viscous behavior of sheet molding compounds (SMC) during compression molding.* International Journal of Plasticity, 2003. 19(5): p. 625-646.
96. G.F. Nino, O.K.Bergsma, H. E.Bersee, A. Beukers, *Influence of Fiber Orientation on Mechanical Performance for Thermoformed Composites*, in *International Conference on Composite Materials*. 2007: Kyoto, Japan.
97. K. Vanclooster, S. V. Lomov, I. Verpoest, *Experimental validation of forming simulations of fabric reinforced polymers using an unsymmetrical mould configuration.* Composites Part A: Applied Science and Manufacturing, 2009. 40(4): p. 530-539.
98. T.A. Martin, G.R. Christie, D. Bhattacharyya, *Composite sheet forming*, ed. D. Bhattacharyya. 1997: Elsevier Science.
99. H.E.N Bersee, S. Lindstedt, G.Nino, A. Beukers, *Diaphragm Forming of THermoset Composites*, in *16th International Conference on Composite Materials*. 2006: Kyoto,Japan.
100. C.M. O'Bradaigh, R.B. Pipes, *Issues in Diaphragm Forming of Continuous Fiber Reinforce Thermoplastic Composites.* Polymer Composites, 1991. 12(4): p. 246-256.
101. S.G. Pantelakis, E.A. Baxevani, *Optimization of the diaphragm forming process with regard to product quality and cost.* Composites: Part A, 2002. 33: p. 459-470.
102. S. V. Lomov, P.h Boisse, E. Deluycker, F. Morestin, K. Vanclooster, D. Vandepitte, I. Verpoest, A. Willems, *Full-field strain measurements in textile deformability studies.* Composites Part A: Applied Science and Manufacturing, 2008. 39(8): p. 1232-1244.
103. M. P. F. Sutcliffe S. L. Lemanski, A. E. Scott,, *Measurement of fibre waviness in industrial composite components.* Composites Science and Technology, 2012. 72(16): p. 2016-2023.
104. *Quality Control for Composite Production*, m.v.s. Apodius, Editor. 2015: Aachen, Germany.
105. B.S-Y Fu, B. Lauke, Y. W. Mai, *Science and Engineering of Short Fibre Reinforced Polymer Composites*. 2009: Elsevier.
106. J.D. Buckley, D.D. Edie, *Carbon-Carbon Materials and Composites*. 1993, New Jersey: Noyes Publications.
107. BS EN ISO 14125:1998+A1:2011 Fibre-reinforce plastic composites — Determination of flexural properties.
108. Mujika F., *On the difference between flexural moduli obtained by three-point and four-point bending tests.* Polymer Testing, 2006. 25(2): p. 214-220.
109. D. Richerson, W. E. Lee, *Modern Ceramic Engineering: Properties, Processing, and Use in Design*. 3 ed. 2005: CRC Press.

110. N. Venkateshwaran, A. Elayaperumal, G. K. Sathiya *Prediction of tensile properties of hybrid-natural fiber composites.* Composites Part B: Engineering, 2012. 43(2): p. 793-796.
111. J. Mirbagheri, M. Tajvidi, I. Ghasemi, J. Hermanson, *Prediction of the Elastic Modulus of Wood Flour/Kenaf Fibre/Polypropylene Hybrid Composites.* Iranian Polymer Journal, 2007. 16: p. 271-278.
112. S.Y. Fu, B. Lauke, E. Mader, C.Yue, X. Hu, Y.Mai, *Hybrid effects on tensile properties of hybrid short-glass-fiber-and short-carbon-fiber-reinforced polypropylene composites.* Journal of Materials Science, 2001. 36: p. 1243-1251.
113. M. Guen, R. Newman, Alan Fernyhough, G. Emms, M, Staiger, *The damping-modulus relationship in flax-carbon fibre hybrid composites.* Composites Part B, 2016. 89: p. 27-33.
114. A. Dorigato, A Pegoretti, *Flexural and impact behaviour of carbon/basalt fibers hybrid laminates.* Journal of Composite Materials, 2014. 48: p. 1121-1130.
115. F.L. Matthews, R.D. Rawlings, *Composite Materials: Engineering and Science*. 1999: Elsevier.
116. J.N. Reddy, A. Miravete, *Practical Analysis of Composite Laminates*. 1998: CRC Press.
117. C.T. Herakovich, *Mechanics of Fibrous Composites*. 1998: John Wiley & Sons.
118. R.D. Adams, M.R. Maheri, *Dynamic Flexural Properties of Anisotropic Fibrous Composite Beams.* Composites Science and Technology, 1994. 50: p. 497-514.
119. Corp. Hexcel, *HexPly® M77/38%/UD300/SGL-50K - product datasheet*. 09/2011 version: a.
120. Corp. Hexcel, *HexMC® Moulding Concept Carbon Epoxy HexMC®/ C / 2000 / R1A*. 03/2005.
121. Loctite, *Loctite Frekote 700-NC, data sheet*. 01/2015.
122. M.L. Costa, S. Frascino, M. de Almeida, M.C. Rezende, *The influence of porosity on the interlaminar shear strength of carbon/epoxy and carbon/bismaleimide fabric laminates.* Composites Science and Technology, 2001. 61: p. 2101-2108.
123. P. Olivier J. P. Cottu , B. Ferret *Effects of cure cycle pressure and voids on some mechanical properties of carbon/epoxy laminates* Composites 1995. 26(7): p. 509-515.
124. K.J. Bowles, S. Frimpong, *Relationship Between Voids and Interlaminar Shear Strength of Polymer Matrix Composites*, in *36th International SAMPE Symposium and Exhibition*. 1991, NASA: San Diego.
125. S. Dai, P.R. Cunningham, S. Marshall, C. Silva, *Influence of fibre architecture on the tensile, compressive and flexural behaviour of 3D woven composites.* Composites Part A: Applied Science and Manufacturing, 2015. 69: p. 195-207.
126. *Composite Material Handbook MIL 17 Guidelines for Characterization of Structural Materials*. 2002: U.S. Department of Defense.
127. Logan D.L., *A First Course in the Finite Element Method, SI Version*. 5 ed. 2012.
128. R.C Lam, J.L Kardos, *The permeability and compressibility of aligned and cross-plied carbon fiber beds during processing of composites.* Polymer Engineering & Science, 1991. 31(14): p. 1064-1070.

129. K. Johanson, L. T. Harper, M. S. Johnson, N. A. Warrior, *Heterogeneity of discontinuous carbon fibre composites: Damage initiation captured by Digital Image Correlation.* Composites Part A: Applied Science and Manufacturing, 2015. 68: p. 304-312.
130. Ary Subagia, I. D. G. Kim, Yonjig Tijing, Leonard D. Kim, Cheol Sang Shon, Ho Kyong, *Effect of stacking sequence on the flexural properties of hybrid composites reinforced with carbon and basalt fibers.* Composites Part B: Engineering, 2014. 58: p. 251-258.
131. Swolfs Yentl,Verpoest IgnaasandGorbatikh Larissa, *Maximising the hybrid effect in unidirectional hybrid composites.* Materials & Design, 2016. 93: p. 39-45.
132. B. Strong, *Fundamental of Composites Manufacturing: Materials Methods, and Applications*, ed. SME. 2008.

11. Appendix A

The following appendix provides additional information of the theoretical prediction flow for the one dimensional staged scenarios and their corresponding strain and rotation surface plots. Which shows the trend that staging and charge design reduces both the element strain and the rotation.

U3 90° H2 s25%

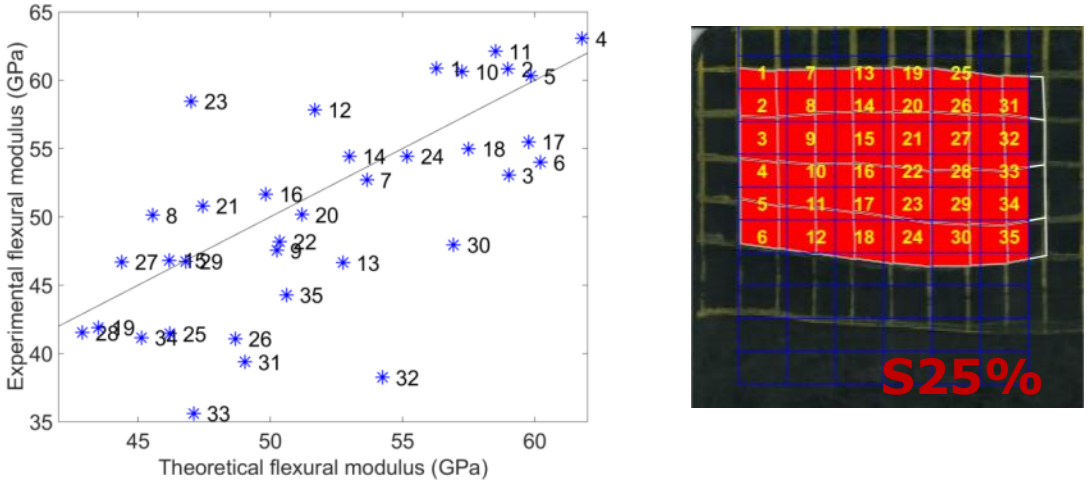

Figure 147: Experimental flexural modulus plotted against theoretical of U3 90° H2 s25%

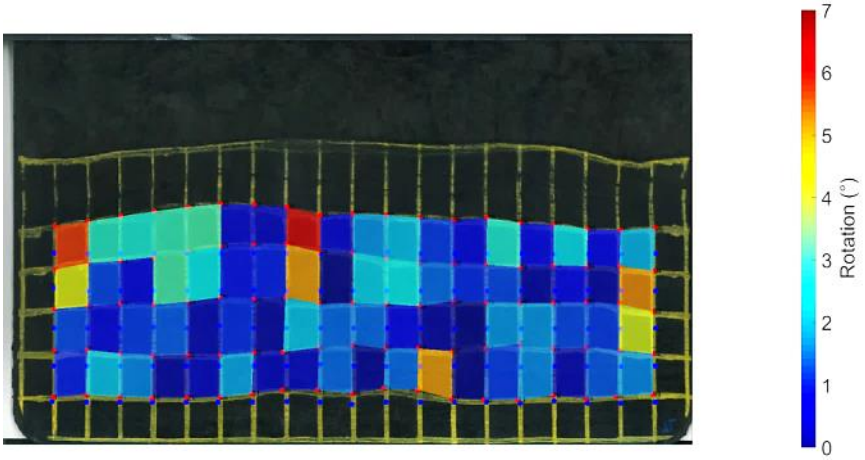

Figure 148: Absolute rotation of U3 90° H2 s25%

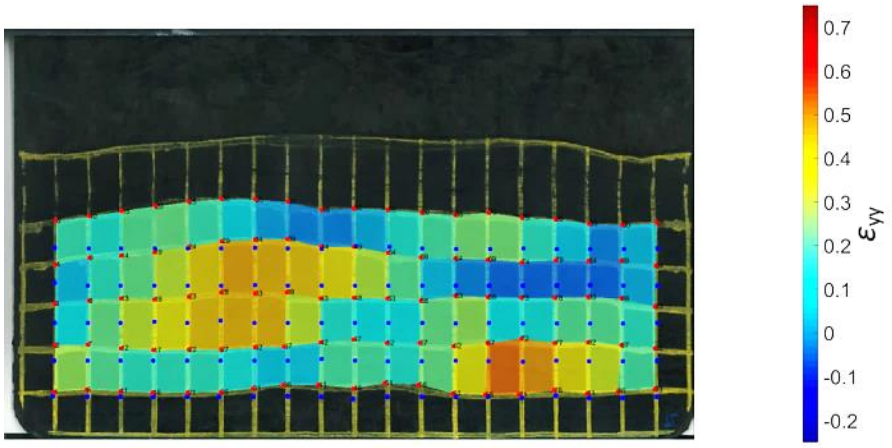

Figure 149: ε_{yy} of U3 90° H2 s25%

U3 90° H2 s50%

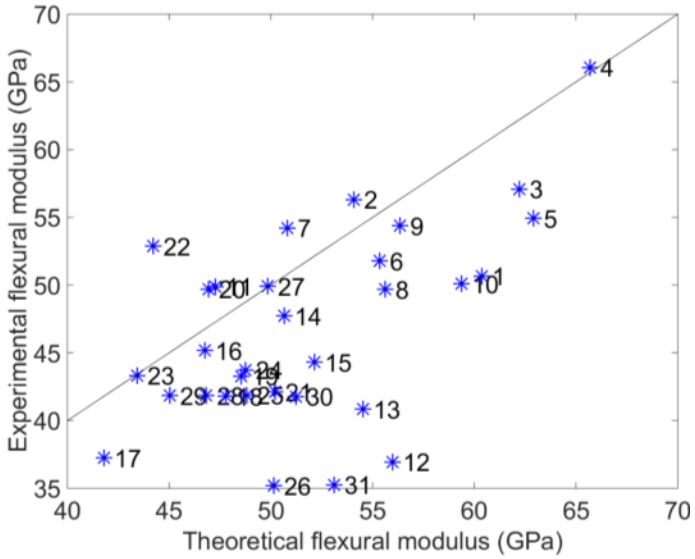

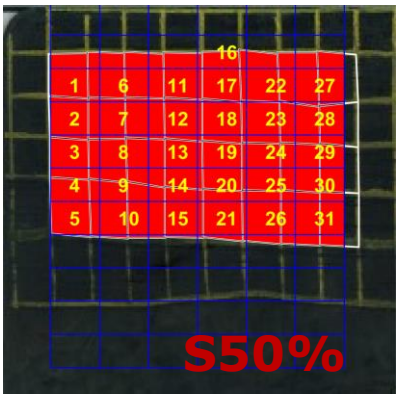

Figure 150: Experimental flexural modulus plotted against theoretical of U3 90° H2 s50%

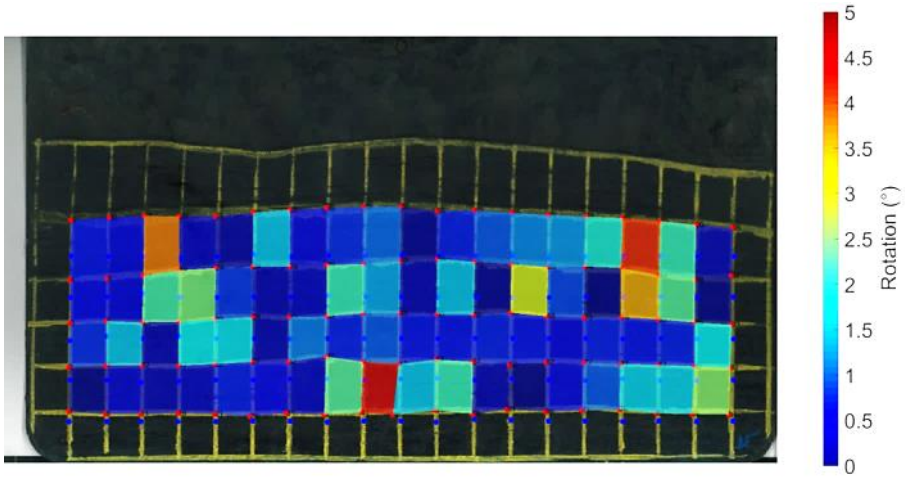

Figure 151: Absolute rotation of U3 90° H2 s50%

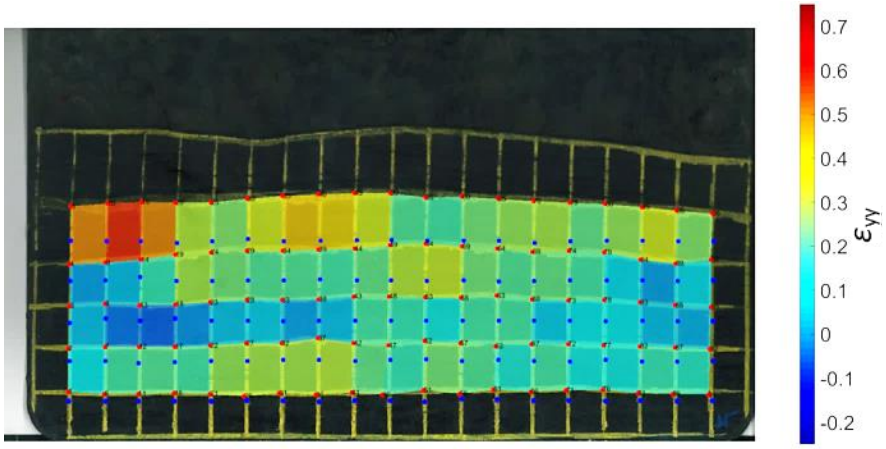

Figure 152: ε_{yy} of U3 90° H2 s50%

U3 90° H2 s75%

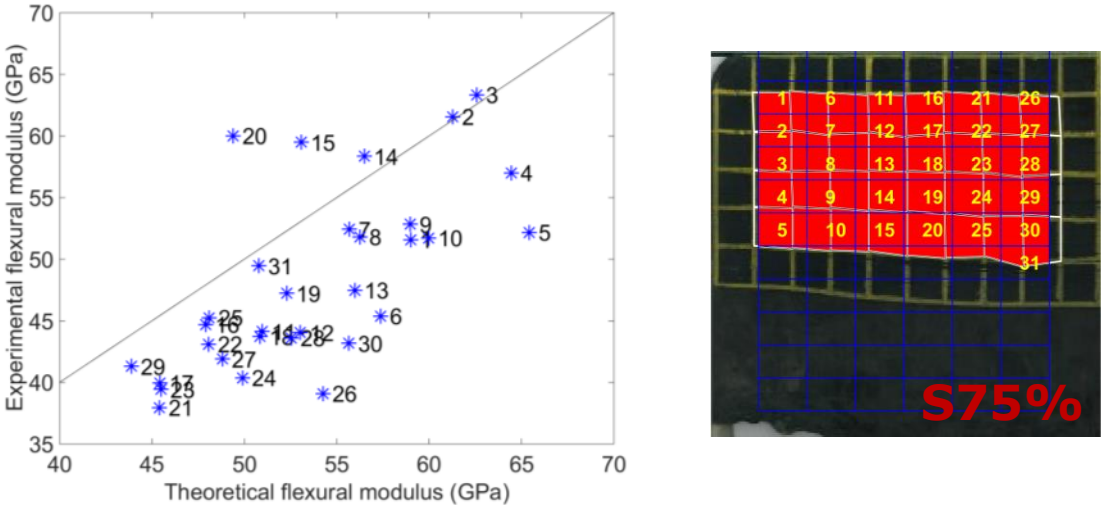

Figure 153: Experimental flexural modulus plotted against theoretical of U3 90° H2 s75%

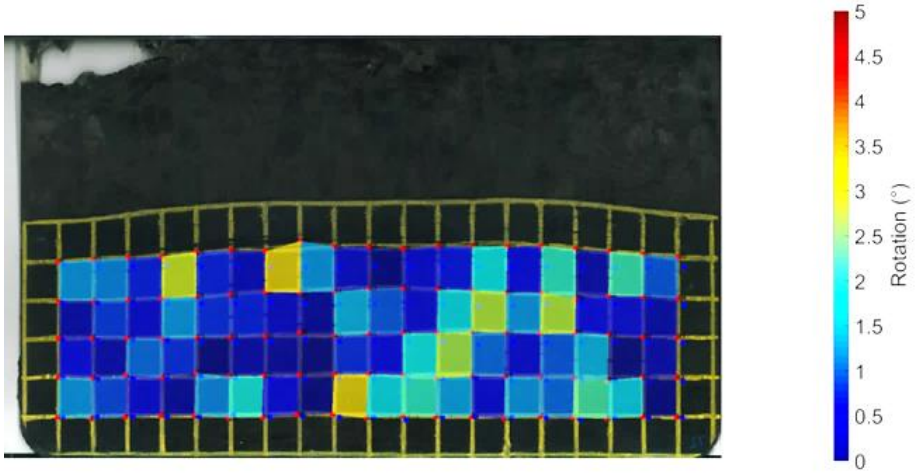

Figure 154: Absolute rotation of U3 90° H2 s75%

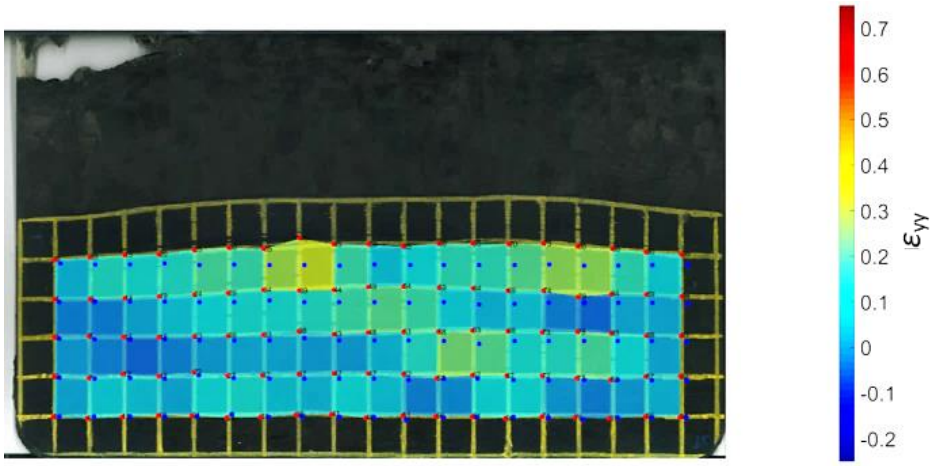

Figure 155: ε_{yy} of U3 90° H2 s75%

U3 90° H2 D50%

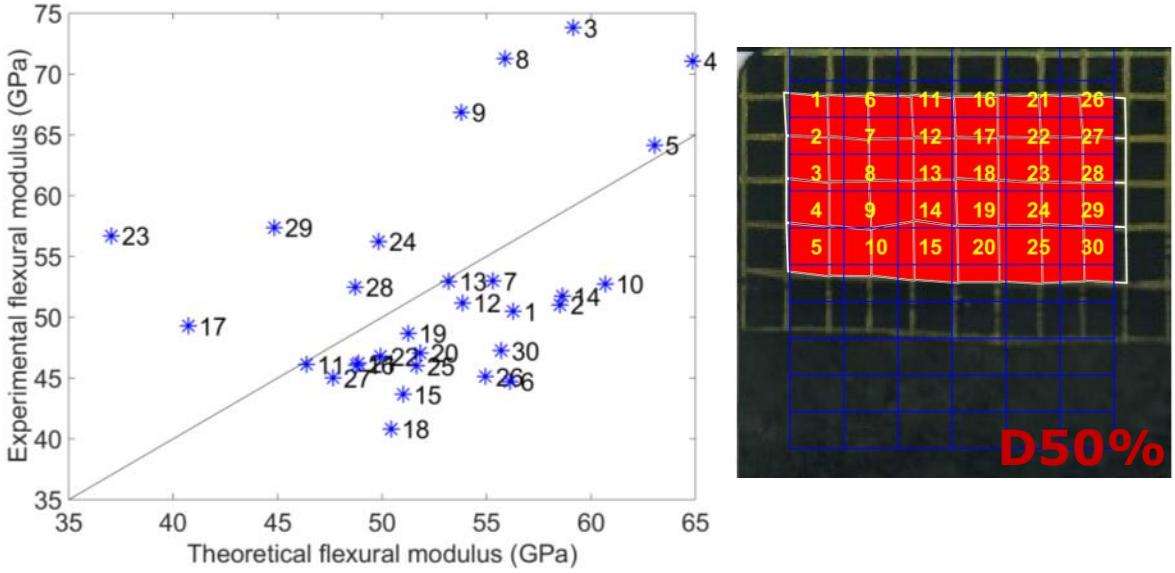

Figure 156: Experimental flexural modulus plotted against theoretical of U3 90° H2 D50%

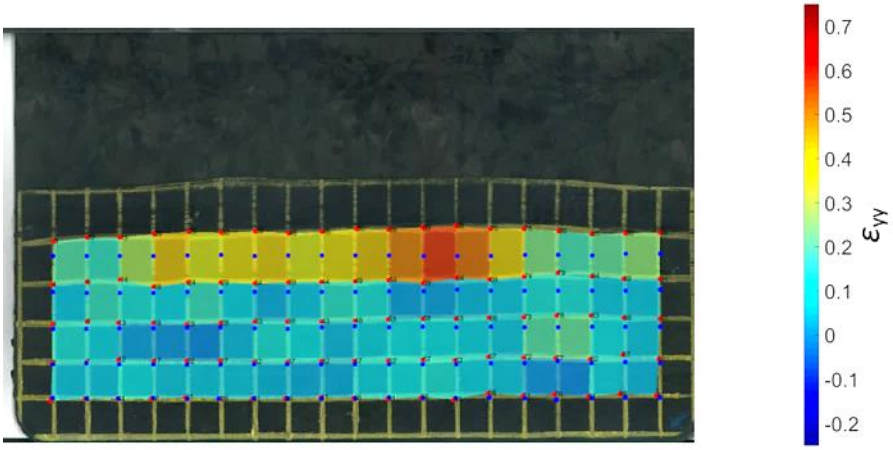

Figure 157: ε_{yy} of U3 90° H2 D50%

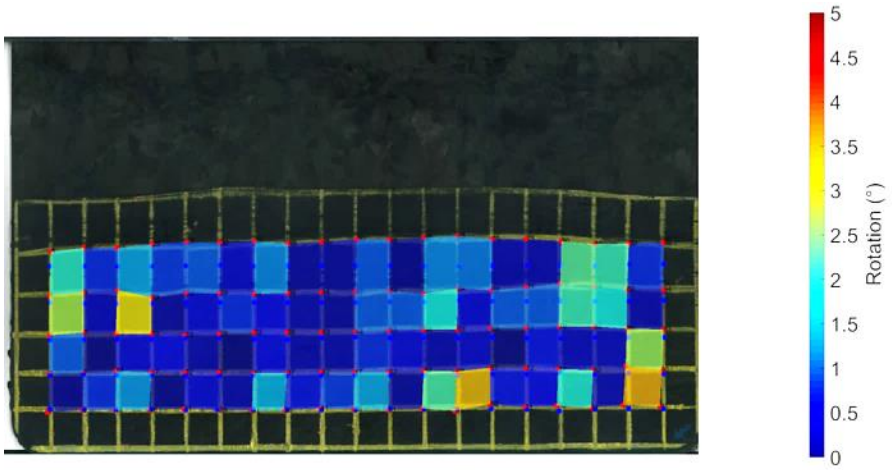

Figure 158: Absolute rotation of U3 90° H2 D50%

U3 0° H2 s50%

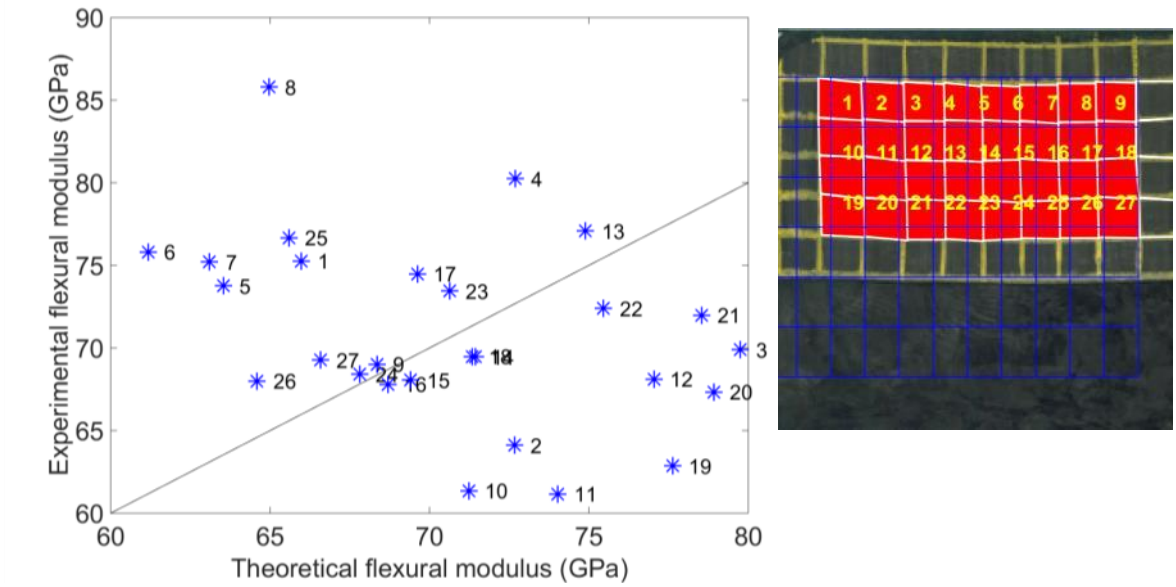

Figure 159: Comparison of U3 0° H2 s50% experimental and theoretical flexural modulus with point location

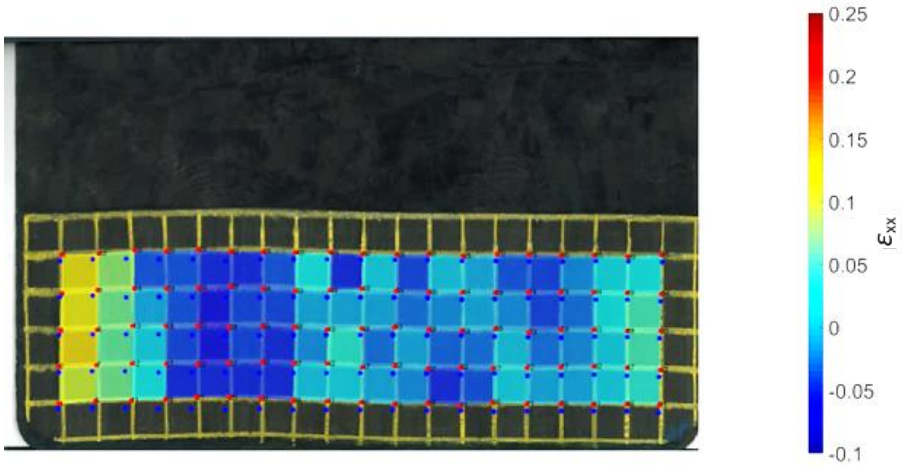

Figure 160: ε_{xx} of U3 0° H2 s50%

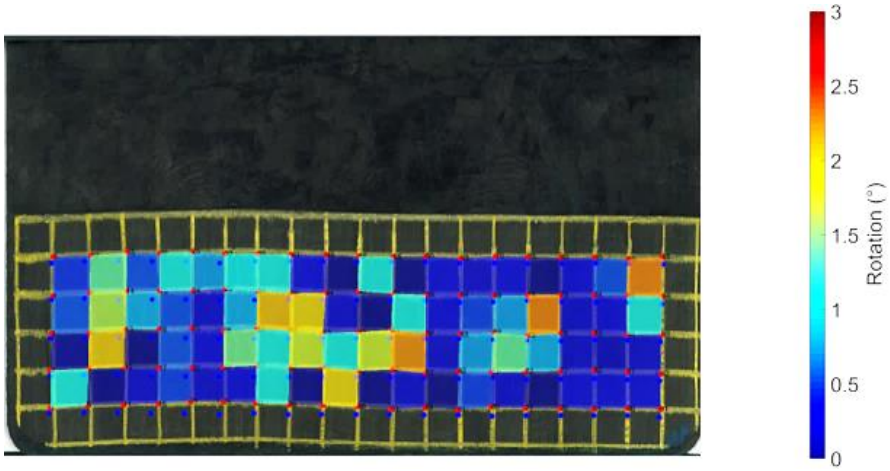

Figure 161: Absolute rotation of U3 0° H2 s50%

U2 90° U1 0° H2 s50%

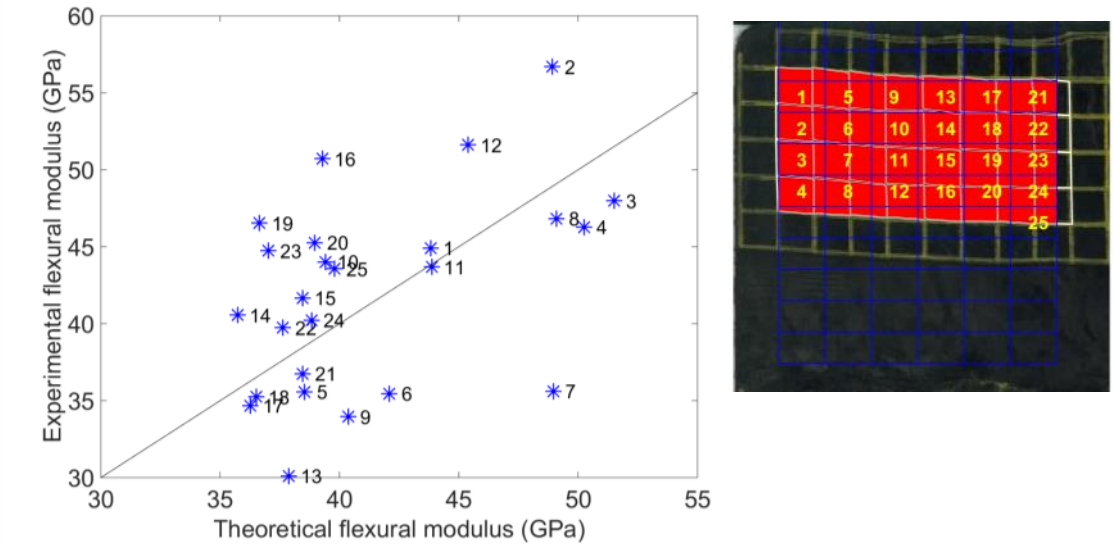

Figure 162: Comparison of U2 90° U1 0° H2 s50% experimental and theoretical flexural modulus with point location

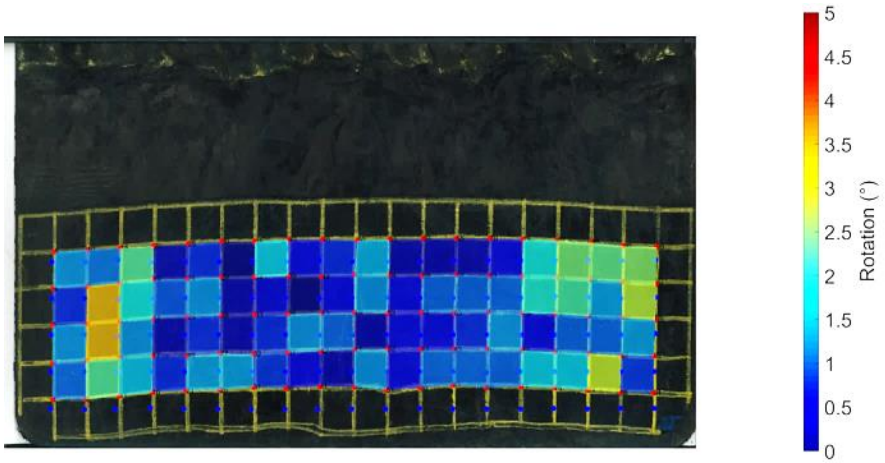

Figure 163: Absolute rotation of U2 90° U1 0°H2 s50%

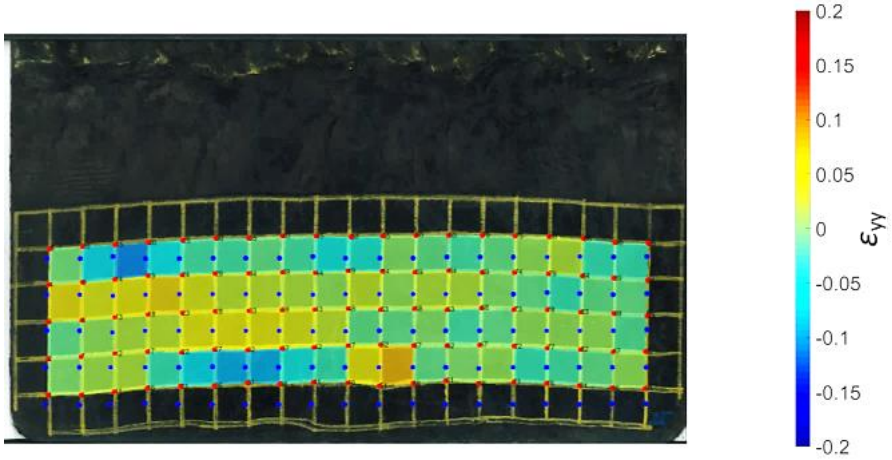

Figure 164: ε_{yy} of U2 90° U1 0°H2 s50%

12. Appendix B: Publications

D.M. Corbridge, L.T. Harper, D.S.A. De Focatiis, N.A. Warrior, Compression Mould of Hybrid Fibre Architectures for Structural Automotive Applications, SAMPE Europe, Amiens, 2015

D.M. Corbridge, L.T. Harper, D.S.A. De Focatiis, N.A. Warrior, Compression Moulding of Composites with Hybrid Fibre Architectures, Composites: Part A, 2017, 95, 87-99